Chemistry of meso-meso linked porphyrin arrays(Dissertation_全文)

AUTHOR(S):

Aratani, Naoki

Chemistry of *meso-meso* Linked Porphyrin Arrays

Naoki Aratani

学位申請論文

Chemistry of *meso-meso* Linked Porphyrin Arrays

メゾ−メゾ結合ポルフィリン多量体の化学

荒谷直樹
Naoki Aratani
2005
Organic Chemistry of Molecular Assembly
Department of Chemistry
Graduate School of Science
Kyoto University

Preface

The studies on the Thesis were carried out under the guidance of Professor Dr. Atsuhiro Osuka at the Department of Chemistry, Graduate School of Science, Kyoto University for 7 years since 1998.

The research on this Thesis suggests that the porphyrin arrays the author synthesized provide key tools for bridging the gap between "bottom-up" synthetic methods and "top-down" fabrication. Collectively, this work provides an important milestone for the preparation of sub-micro scale discrete organic molecules and the fabrication of molecular-based materials, hence contributing to device applications significantly.

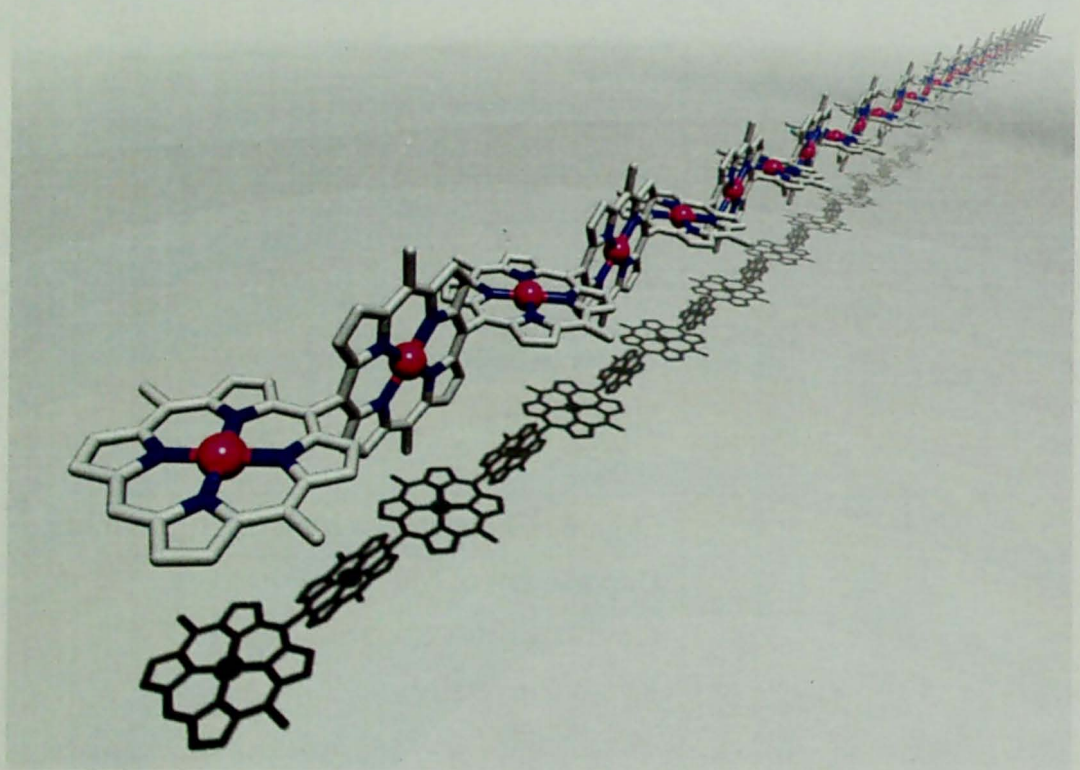

Contents

Chapter 1. General Introduction

In this Chapter, the background and brief review of the chemistry of *meso-meso* linked porphyrin arrays and the overview of this Thesis are described.

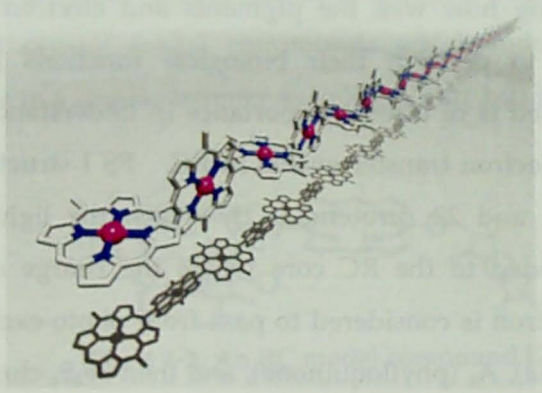

1-1. Background

The fascinating three-dimensional structures of photosynthetic reaction centers (RCs) of cyanobacterial photosystems PS I and PS II determined by the X-ray crystallography are clearly demonstrating how well the pigments and electron carriers are arranged within protein matrix to perform their biological functions [1-3]. The structural information thus provided is of utmost importance in understanding the mechanism of the initial energy and electron transfer events in RC. PS I structure has been found to contain 96 chlorophylls and 22 carotenoids by which the light energy is efficiently harvested and then guided to the RC core where the charge separation is achieved quantitatively. An electron is considered to pass from photo-excited chlorophyll dimer P700 to cofactors A_0 (Chl*a*), A_1 (phylloquinone), and then Fe_4S_4 clusters. In the PS II RC, the initial electron transfer is taking place from photo-excited P680 to pheophytin, and then to Q_A, that is essentially the same as that in purple bacteria reaction center (PbRC) [4-7]. In contrast to PS I, the light harvesting in PbRC is achieved through the separate membrane-intrinsic light-harvesting complexes (LH1 and LH2) [8].

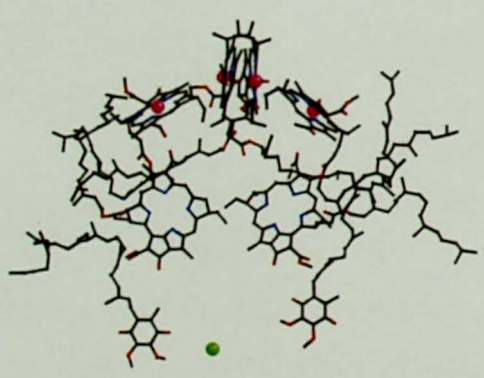

Chart 1-1. An image of the *Rhodobacter sphaeroides* RC together with its cofactors [6].

Both of PS I and PbRC constitute well-organized supramolecular systems in which the chromophores are held at fixed distances and orientations relative to one another [4-12]. It is evident that the well-defined geometries are crucial for efficient and ultrafast energy and electron transfers in the natural systems. Thus, a variety of chemical artificial models consisting of multi-porphyrins have been explored in order to understand the mechanisms being operative in the photosynthetic systems as well as to duplicate the light harvesting and charge separating functions [13-17].

Many researchers have continued the synthetic approach toward photosynthetic RCs by synthesizing a variety of electron acceptor linked porphyrin compounds and multi-porphyrin arrays to realize the coupled light-harvesting energy-transfer and charge-separating multi-step electron-transfer reactions in a single molecule, preferably by way of the reaction sequence that is similar to that in the natural RCs [13-16]. Osuka *et al.* has developed several model compounds which indeed realized a long-lived charge-separated state in a similar manner as in RC (Chart 1-2) [18-20].

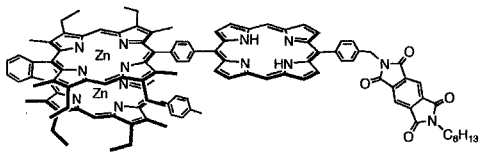

Chart 1-2. An RC model compound [20].

1-2. Discovery of *meso-meso* Linked Porphyrin Arrays

The word *Porphyrin* is derived from the Greek *porphura* meaning purple, and all porphyrins are intensely colored. The two sites of positions on the porphyrin periphery are referred to as *meso* and *β*. (Chart 1-3).

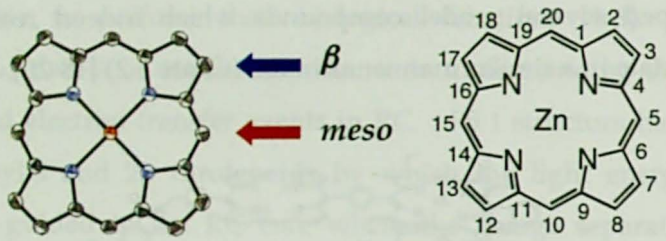

Chart 1-3. Molecular structure

History of *meso-meso* Linked Porphyrin Arrays

A variety of 1,4-phenylene bridged diporphyrins with varying the energy gap of the photo-induced charge separation were synthesized by Osuka's group [19]. In order to elucidate the electron transfer behaviors in the Marcus top region, a strongly electron deficient porphyrin as the electron acceptor was needed. An attempt to prepare *meso*-nitrated porphyrin from 5,15-diaryl Zn^{II} porphyrin $\mathbf{Z_0 1}$ by using Baldwin's conditions ($AgNO_2$, I_2 [21]) was planned. The nitration proceeded nicely to give nitrated porphyrin **1** in 90% yield, along with serendipitous formation of a bis-porphyrin linked by a single bond between *meso* positions (Scheme 1-1). This interesting side product $\mathbf{Z_0 2}$ was formed only in 10% yield. These products were hard to separate on a silica gel column but were found to be nicely separated by means of size-exclusion chromatography (SEC). This was the starting point of chemistry of *meso-meso* linked porphyrins in Osuka's lab [22].

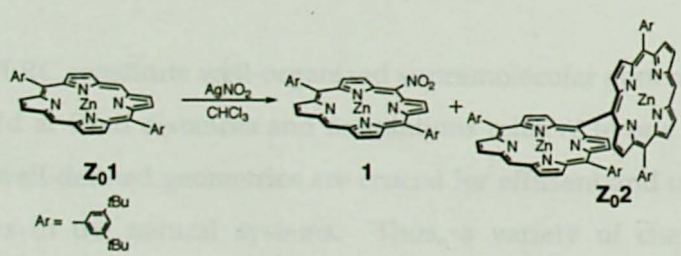

Scheme 1-1. Reaction of Zn^{II} 5,15-diarylporphyrin with $AgNO_2$.

The formation of $\mathbf{Z_0 2}$ can be understood in terms of the initial one-electron oxidation

of $\mathbf{Z_01}$ followed by the nucleophilic attack of NO_2^- ion. The similar mechanism for the formation of $\mathbf{Z_02}$ through the nucleophilic attack of a neutral molecule of reaction of $\mathbf{Z_01}$ on the cation radical of $\mathbf{Z_01}$ was thought. Thus, $AgPF_6$ bearing non-nucleophilic anion for the oxidation of $\mathbf{Z_01}$ was employed, gaving only *meso-meso* linked porphyrin oligomers [22]. Typically, the reaction of $\mathbf{Z_01}$ with 0.5 equiv. of $AgPF_6$ in $CHCl_3$ for 5 h followed by a preparative size exclusion chromatography (SEC) gave $\mathbf{Z_02}$ in 25% yield, $\mathbf{Z_03}$ in 4% yield, and highly oligomer along with recovery of $\mathbf{Z_01}$ (47%) (Scheme 1-2). The coupling reaction of $\mathbf{Z_02}$ under analogous conditions afforded $\mathbf{Z_04}$ in 23% yield. The similar coupling reaction of 5,10,15-triarylporphyrins with a single free *meso*-position gave diporphyrins in higher yields (65–95%) under the forcing conditions with $AgPF_6$ and I_2 [23].

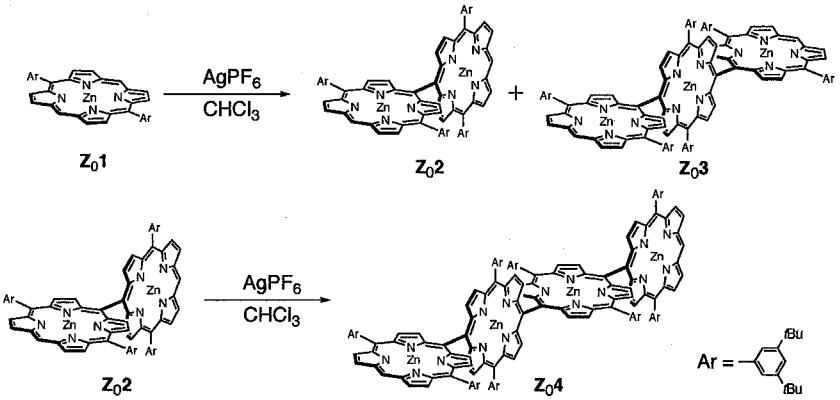

Scheme 1-2. Ag^I-promoted *meso-meso* coupling reaction of Zn^{II} 5,15-diarylporphyrin.

Independently at the same time, the syntheses of *meso-meso* linked porphyrin arrays *via* other routes were reported. Segawa *et al.* reported the synthesis of a *meso-meso* linked diporphyrin (4% yield) and a triporphyrin (0.5% yield) in low yields by acid-catalyzed [2+2] condensation reaction of a *meso*-formylated porphyrin with dipyrromethane [24], and Smith *et al.* reported the synthesis of analogous *meso-meso* linked diporphyrin with 1,1,2,2-tetra(5-formyl-2-pyrrolyl)ethene as a key intermediate (Scheme 1-3) [25].

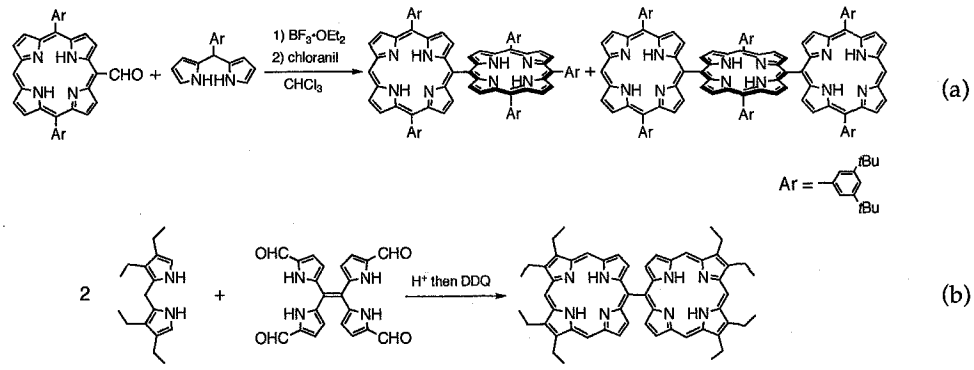

Scheme 1-3. Synthetic scheme of *meso-meso* linked porphyrin oligomers *via* (a) *meso*-formyl porphyrin [24] and (b) tetrapyrrolylethene [25].

Ag^I-promoted oxidative coupling reaction has the advantages of easy-handling and relatively high yielding. After discovery of Ag^I salt method, several groups reported *meso-meso* coupling reaction by using other oxidants, including thallium(III) trifluoroacetate [26], 2,3-dichloro-5,6-dicyano-1,4-benzoquinone (DDQ) [27], and NBS [28]. The anodic electrochemical oxidation method [29] is useful, since the oxidation potentials can be best tuned for the porphyrins which are hardly or only slowly coupled in the reaction with $AgPF_6$, providing its applicability to a wider range of substrates.

Development of Giant Porphyrin Arrays

On the other hand, in the last two decades, covalently and noncovalently linked multi-(metallo)porphyrin arrays have been extensively explored for their numerous applications in molecular devices; for example, photoactive species, sensors, nonlinear optical devices, and other [13,30,31]. Recent efforts in this field have produced a variety of covalently linked porphyrin arrays, which include linear [32], cyclic [33-35], dendritic [36], stacked [37], starbursts [38], and other fascinating three-dimensional arrangements [39,40]. In addition, the preparation and characterization of monodisperse giant molecules with precise structure and precise size have attracted considerable interest in light of their potential applications to the nascent field of molecular electronic devices [41-43]. It still remains a great synthetic challenge to explore a discrete, finite functional supramolecule with a well-defined structure. Recent progress in the field of synthetic and analytic techniques has allowed the synthesis of porphyrin arrays consisting of six or more porphyrins. However, most of these syntheses needed lengthy multi-step reactions and/or low yielding procedures and were often hampered by poor solubility, difficult separations, and demanding characterizations. Therefore, high solubilities, easy

separations, and reliable characterizations of the arrays are of prime importance to explore a larger molecular system.

Here, Ag^{I}-promoted *meso-meso* coupling reaction of 5,15-diaryl Zn^{II}-porphyrins has several advantages; 1) the *meso-meso* coupling regioselectivity is quite high, 2) the porphyrin arrays posses essentially the same linear rod-like shape, 3) the porphyrin arrays are highly soluble presumably due to orthogonal conformations arising from steric hindrance around the *meso-meso*-linkage, 4) the separation of the coupling products is easy by recycling preparative GPC-HPLC chromatography as a result of large difference in molecular weight, and finally 5) the long coupling products still bear two free *meso*-positions available for next reaction.

With these backgrounds, the author has launched a challenging project to repeat this *meso-meso* doubling reaction to make exceedingly long molecules until no further reaction occurs!

1-3. Overview of This Thesis

Through recent extensive synthetic efforts, the molecular lengths of linear monodisperse π-conjugated oligomers have now reached a range over 10 nm. Synthesis of an extremely long discrete molecule is indeed a challenge and the author embarked on the synthesis of long *meso-meso* linked porphyrin oligomers. This Thesis deals with author's synthetic approach towards extremely long porphyrin arrays on the basis of Ag^{I}-promoted coupling reaction, which hopefully enlarges the range of discrete rod-like molecules that can be manipulated by conventional techniques and should provides an important milestone for the fabrication of molecular-based materials, hence contributing to device applications significantly. Here, as mentioned in the former section, the high solubility is crucial for the manipulations of long porphyrin arrays. The *meso-meso* linked porphyrin arrays are favorable for the high solubility owing to the orthogonal conformation that suppresses π-π stacking. But this is not sufficient, since ones encountered a serious solubility problem at the stage of $\mathbf{Z_0 8}$. In order to circumvent the solubility problem, a more soluble substrate, Zn^{II} bis(3,5-dioctyloxylphenyl)porphyrin **Z1**, was employed.

In Chapter 2, the investigation on synthesis of giant porphyrin arrays attempted using a stepwise doubling approach on the basis of Ag^{I}-promoted coupling reaction starting from **Z1** is described [44]. These porphyrin arrays provide key tools for bridging the gap between "bottom-up" synthetic methods and "top-down" fabrication.

In Chapter 3, the physical properties of *meso-meso* linked giant porphyrin arrays were described [45]. These arrays are appearing owing to the unprecedented giant molecular size, the expected simple rod-like molecular shape, and the repeated regular arrangement of porphyrin rings in a close proximity.

In Chapter 4, synthesis of *meso-meso* linked hybrid porphyrin arrays by Pd-catalyzed cross-coupling reaction was reported [46]. In order to explore more diverse structures of *meso-meso* linked porphyrin arrays, Pd-catalyzed Suzuki-Miyaura coupling reaction in a manner complementary to Ag^{I}-promoted oxidative coupling of porphyrins was developed. This strategy is useful for the preparations of hybrid porphyrin arrays with definite composition and unique molecular shape.

The directly *meso-meso* linked porphyrins are expected to enable highly efficient energy transfer and electron transfer reactions owing to the very close proximity of the neighboring porphyrins. These properties are also interesting in view of a potential use

as photonic molecular wire. In Chapter 5, an artificial energy transfer model system is mentioned [47]. This system comprises of an energy donating *meso-meso* linked Zn^{II} porphyrin array and an energy accepting 5,15-bisphenylethynylated Zn^{II} porphyrin linked *via* a 1,4-phenylene spacer.

The author also exploited an effective synthetic route, through which Zn^{II} porphyrin arrays can be fabricated with a thiol-protected aryl group to provide terminal-thiolated long porphyrin arrays *via* terminal-brominated porphyrin arrays by bromination with N-bromosuccinimide and subsequent Pd-catalyzed Suzuki-Miyaura arylation. In Chapter 6, the investigation on synthesis and properties functionalized Zn^{II} porphyrin arrays are described [48].

Chapter 2. Synthesis of *meso-meso* Linked Porphyrin Arrays [44]

In this Chapter, synthesis and characterization of giant porphyrin arrays are described.

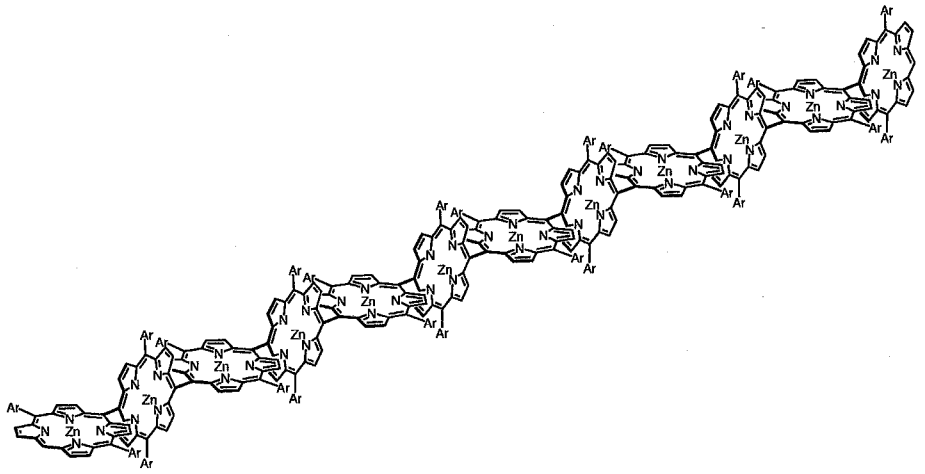

2-1. Introduction

In the last two decades, remarkable progress has been made in the synthesis of electrochemically and/or photochemically active oligomeric and polymeric materials, which leads to exploration of new molecular architectures, better understanding of their properties, and practical applications in electronic and optical devices [41,42,49,50]. Among these, poly(arene)s represented by poly(*p*-phenylene)s (PPP) [51], poly(pyrrole)s [52], and poly(thiophene)s [53] occupy a central position because of their increased conductivities upon doping and a close proximity to commercialization. PPP is one of the most typical π-conjugated polymers. Whereas the neutral form of PPP is an insulator with a low conductivity around 10^{-12} Scm^{-1}, its conductivity is suddenly enhanced into the metallic level with values around 500 Scm^{-1} upon doping with I_2 or AsF_5 [54]. Even though both the theories and calculations on the ideal polymers have been explored [55], experiments on *monodisperse* oligomers, where no ensemble averaging is needed, can provide more direct and insightful information and are thus of great importance. In this connection, the synthesis of *monodisperse* macromolecular rods of precise length and constitution has attracted keen attention in light of their potential application as molecular-scale electronics, optical devices, solar energy conversion, and so forth, since such discrete oligomers can also offer a good opportunity for systematic studies on structure-property relationships that will be useful for predicting specific information on the electronic, photonic, and morphological properties.

Through recent extensive synthetic efforts, the molecular lengths of linear monodisperse π-conjugated oligomers have now reached a range over 10 nm. As to oligo-*p*-phenylene, up to 16 *p*-phenylene rings were covalently connected by the repetitive approach by Hensel and Schlüter [56], who also synthesized a cyclotetraicosaphenylene on the basis of the same strategy [57]. However, these cyclic oligomers cannot perform an efficient π-conjugation because of distortion from planarity and the local resonance stabilization within each aromatic ring. Meier *et al.* synthesized monodisperse oligo(1,4-phenylene-ethenylene)s up to 12-mer as a more planar π-conjugated oligomer [58]. Tour *et al.* developed an approach to grow molecular systems by iterative divergent/convergent method, which resulted in the synthesis of phenylethynyl 18-mer bearing protected thiol groups for the connection on the gold electrodes [59]. This method, when combined with the solid-phase synthesis, furnished block-alternating 23-mer consisting of oligo(1,4-phenylene-ethynylene)s and oligo(2,5-thiophene-

ethynylene)s, whose molecular length reached about 160 Å [60].

On the other side, oligo- and poly-thiophenes have been actively exploited for molecular devices such as organic conductive materials, electroluminescence (EL) devices, organic light emissive diodes (OLED), field effect transistors (FET), and so forth [61]. Roncali *et al.* reported the synthesis and characterization of monodisperse soluble oligothienylenevinylenes with chain lengths up to 10 nm [62]. Tanaka *et al.* prepared a thiophene-based polymer with a small band gap by using a nonclassical-thiophene as a building block [63]. A series of long discrete oligothiophene molecules were synthesized by Otsubo and co-workers, which culminated in the synthesis of a discrete 96-mer [64]. Yet it still remains as a great synthetic challenge to explore a discrete functional molecule with well-defined structures far beyond these achievements.

Among a number of molecular modules as a construction element of supramolecular rods, porphyrins are one of the most attractive building blocks, since they offer a variety of desirable features such as rigid planar geometry, high stability, intense electronic absorption and emission, small HOMO-LUMO energy gap, and flexible tunability of their optical and redox properties by appropriate metallation [30]. As a matter of fact, extensive efforts have been made on the preparations of porphyrin arrays with a view to use them for realization of various functional units and molecular devices [31]. However, these studies have been often hampered by poor solubility, difficult separation, and demanding characterization, which are intrinsic for covalently linked large porphyrin arrays.

In 1997, Osuka's group has reported Ag^{I}-promoted *meso-meso* coupling reaction of a 5,15-diaryl Zn^{II}-porphyrin [22]. This reaction has following advantages; 1) the regioselectivity of the *meso-meso* coupling reaction is always quite high, 2) the molecular length grows rapidly at a rate of 2^n, where n is the number of iterations, 3) the porphyrin array products are highly soluble owing to orthogonal conformations, which allows the easy manipulation of very long porphyrin arrays, 4) the separation of the coupling products is easy on a recycling preparative GPC-HPLC chromatography as a result of a large difference in the molecular weights of the porphyrin products, and finally 5) the long coupling products still bear two free *meso*-positions that are available for the next reaction as long as the porphyrin array is soluble in the reaction solvent. Taking advantage of these features, the author synthesized a series of *meso-meso* linked porphyrin arrays up to its 128-mer that had been, at that time, the longest man-made discrete molecule [44]. In this respect, further extension of this synthetic strategy is challenging

of its own.

In this Chapter, the synthesis of much longer *meso-meso* linked porphyrin arrays **Z*n*** (where *n* represents the number of porphyrins, Chart 2-1) is reported. This series of arrays is particularly attractive in respect of linear rod-like structure, ample electronic interaction between neighboring porphyrins, and unprecedented giant molecular size. These properties are interesting as a photonic molecular wire, since 1) the large Coulombic interactions between the neighboring porphyrins are favorable for rapid excitation energy hopping, and 2) each porphyrin unit retains its individual character presumably because of the orthogonal geometry, thus preventing the formation of energy-sink.

In the present study, the author isolated a *meso-meso* linked porphyrin 1024-mer, which is, to the best of his knowledge, the longest (ca. 850 nm = 0.85 μm) monodisperse rod-like man-made molecule that has a molecular formula of $C_{65536}H_{83970}N_{4096}O_{4096}Zn_{1024}$. [65]

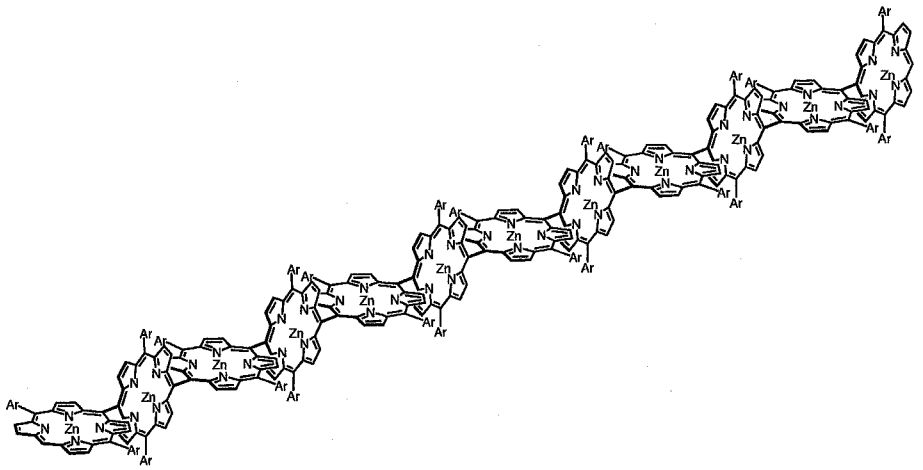

Chart 2-1. *meso-meso* linked porphyrin arrays **Z12.**

2-2. Synthesis and Separation

meso-meso Coupled porphyrin oligomers were prepared by the Ag^{I}-promoted oxidative coupling reaction. One of the key advantages of this synthetic strategy is high solubility of long porphyrin products even in its 128-mer stage, which allowed for its isolation and characterization. Synthesis of zinc(II) 5,15-bis(3,5-dioctyloxyphenyl) porphyrin (**Z1**) is shown in Scheme 2-1. 3,5-Dihydroxybenzoic acid (**2**) was esterified in methanol with a catalytic amount of conc. H_2SO_4 to form methyl 3,5-dihydroxylbenzoate (**3**). Alkylation of the ester **3** was performed by a Williamson type reaction to give methyl 3,5-dioctyloxybenzoate (**4**), which was reduced with $LiAlH_4$ to 3,5-dioctyloxy benzyl alcohol (**5**). 3,5-Dioctyloxybenzaldehyde (**6**) was obtained by oxidation of **5** with PCC in CH_2Cl_2. The porphyrin **Z1** was prepared from **6** and bis(2-pyrryl)methane (**7**) [66] in 44% yield under the standard conditions [67].

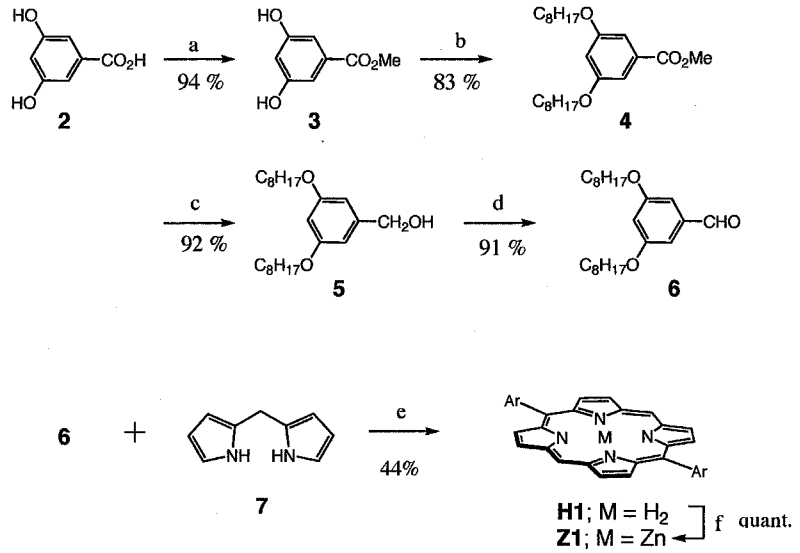

Scheme 2-1. Synthetic scheme of **Z1**. Ar = 3,5-dioctyloxyphenyl. Conditions: (a) H_2SO_4, MeOH, (b) $C_8H_{17}Br$, acetone, K_2CO_3, (c) i) $LiAlH_4$, THF; ii) H_2O, (d) PCC, CH_2Cl_2, (e) i) TFA, CH_2Cl_2; ii) DDQ, (f) $Zn(OAc)_2$, CH_2Cl_2, MeOH. .

Chain elongation strategy is quite simple, by repeating dimerization reactions from **Z1** to **Z2**, **Z2** to **Z4**, **Z4** to **Z8**, **Z8** to **Z16**, **Z16** to **Z32**, **Z32** to **Z64**, and **Z64** to **Z128** (Scheme 2-2). The reaction of **Z1** with 1.2 equiv. of $AgPF_6$ at 30°C in $CHCl_3$ for 10 h followed by preparative SEC (size exclusion chromatography) gave **Z2** (22-27%), **Z3** (3-6%), **Z4** (2%), and a small amount of higher oligomers along with the recovery of **Z1** (50-55%). In each step, dimerized, trimerized, and tetramerized compounds were obtained constantly in

20-30%, ~13%, and ~6% yields, respectively, along with the recovery of starting materials (50-55%). Use of purified $CHCl_3$ as the reaction solvent and keeping the reaction temperature strictly at 30°C were crucial to attain constant results, since the coupling reaction of **Z1** was sensitive to additives and temperatures. Addition of small amounts (0.5-3%) of *N,N*-dimethylformamide (DMF), *N,N*-dimethylacetamide (DMA), hexamethylphosphoramide (HMPA) accelerated the reaction to give poly(Zn^{II} porphyrinylene) [68], while addition of small amounts of amine results in complete retardation of the coupling reaction [69]. Slight heating at 40–50°C also accelerated the coupling reaction to provide a wider range of large porphyrin arrays in an uncontrollable manner.

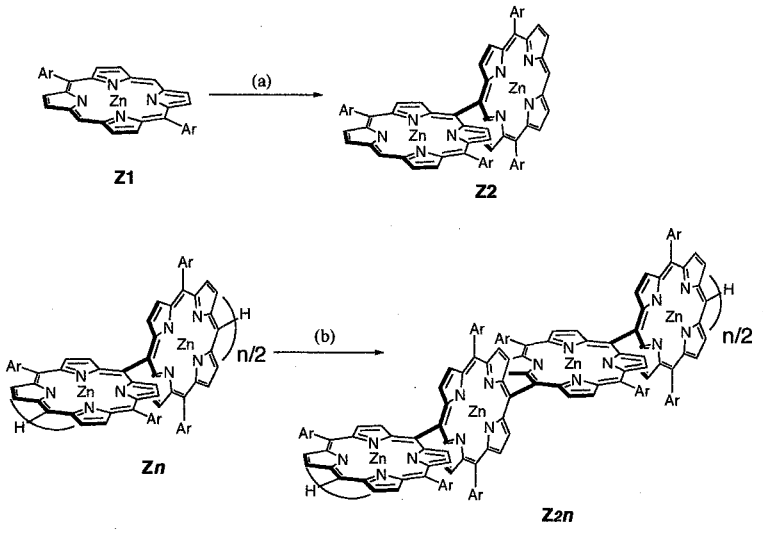

Scheme 2-1. Synthetic scheme of **Z*n***. Ar = 3,5-dioctyloxyphenyl. Conditions: (a) $AgPF_6$, $CHCl_3$, 30°C, (b) $AgPF_6$, $CHCl_3$, room temperature.

The use of recycling preparative GPC-HPLC was crucial for the isolation of porphyrin products. Figure 2-1 shows GPC-HPLC chromatographs (column conditions; JAI-GEL 5H-AF, 4H-AF, and 3H-AF with THF) of the reactions of **Z1**, **Z2**, **Z4**, and **Z8** (Figure 2-1a), **Z16**, **Z32**, and **Z64** (Figure 2-1b). The coupling products were nicely separated over GPC-HPLC in all cases after several recycling separations owing to large differences in molecular weight, thus allowing isolation of pure long porphyrin arrays. In each step, strict separation of doubling product is crucially important for further chain elongation, since even a small contamination will lead to serious problem in longer array. During many repeated preparations, he also isolated **Z3**, **Z5**, **Z6**, **Z7**, **Z10**, **Z12**, **Z20**, **Z24**, **Z40**, **Z48**, **Z80**, **Z96**, and **Z192**, and accumulated more than 100 mg of **Z128**.

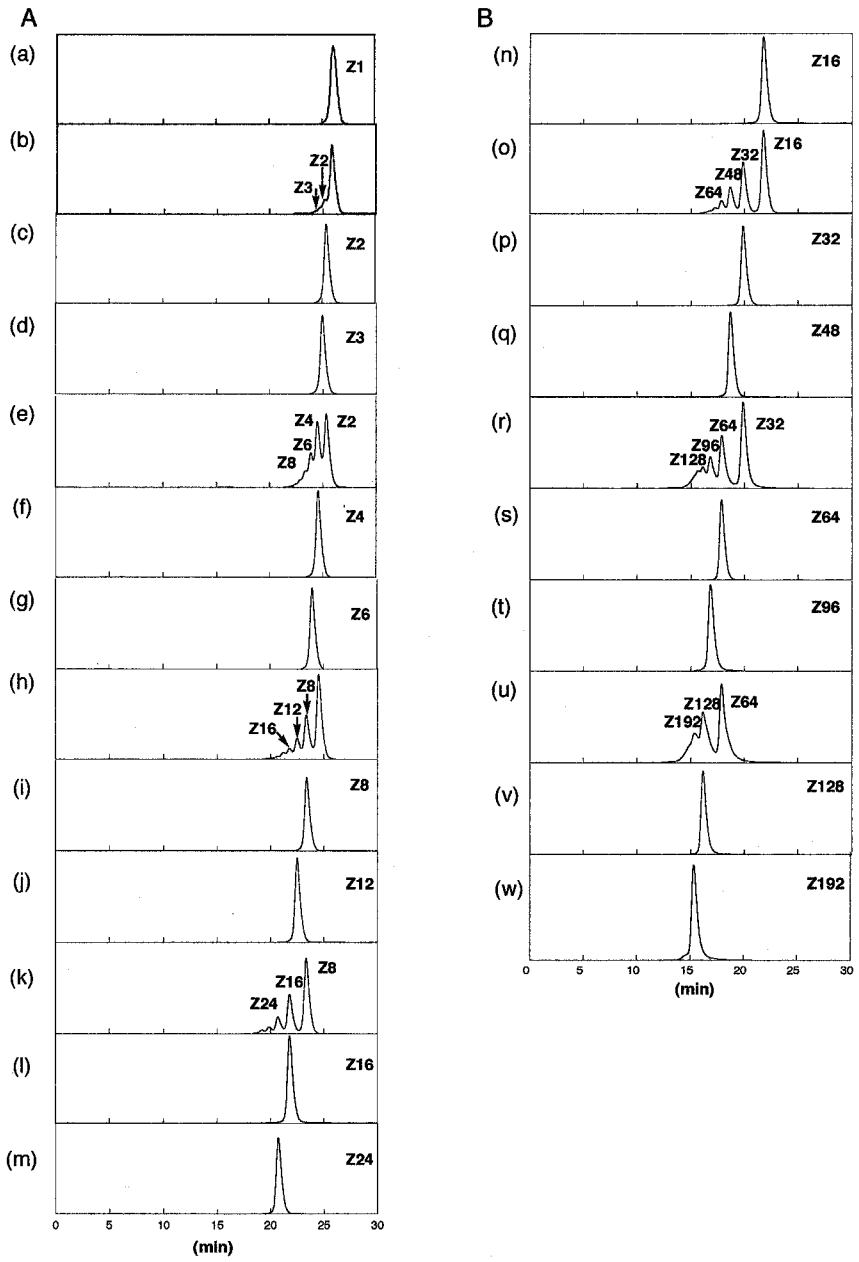

Figure 2-1. GPC-HPLC chromatograms of Ag^{I}-promoted coupling reaction detected by absorbance at 413 nm. Each chromatogram is normalized to the maximum intensity.

A; the reaction from **Z1** (a-d), from **Z2** (e-g), from **Z4** (h-j), and form **Z8** (k-m); (a) **Z1**, (b) after 9 h, (c) purified **Z2**, (d) purified **Z3**, (e) after 8 h, (f) purified **Z4**, (g) purified **Z6**, (h) after 4 h, (i) purified **Z8**, (j) purified **Z12**, (k) after 8 h, (l) purified **Z16**, and (m) purified **Z24**.

B; the reaction from **Z16** (n-q), from **Z32** (r-t), and from **Z64** (u-w); (n) **Z16**, (o) after 9 h, (p) purified **Z32**. (q) purified **Z48**, (r) after 8 h, (s) purified **Z64**, (t) purified **Z96**, (u) after 11 h, (v) purified **Z128**, and (w) purified **Z192**. GPC setup is the combination of JAI-GEL 5H-AF, 4H-AF, and 3H-AF.

Additionally, **Z*n*** can be transformed into the corresponding free-base porphyrin arrays **H*n*** in good yields, which can in turn be metallated with a variety of metal ions to give metallated *meso-meso* linked arrays (Cu^{II}, Ni^{II}, and Pd^{II} etc.).

The **Z128** array has a molecular length of ca. 106 nm in its linear form but is sufficiently soluble in THF and $CHCl_3$. Thus, the coupling reaction of **Z128** was attempted, although the coupling reaction of such an extremely long molecule should be entropically very unfavorable because of only two reactive free *meso*-positions. **Z128** was reacted with 12 equiv. of $AgPF_6$ in $CHCl_3$ for 11 h at room temperature and the reaction mixture was analyzed by GPC-HPLC, which indicated the formation of **Z256**, **Z384**, and **Z512** (Figure 2-2). These large porphyrin arrays were actually isolated by the preparative recycling GPC-HPLC; **Z256** (26%), **Z384** (11%), and **Z512** (4%). Isolated arrays elute at 14.8 min (**Z256**), 14.1 min (**Z384**), and 13.6 min (**Z512**) on the present column setup.

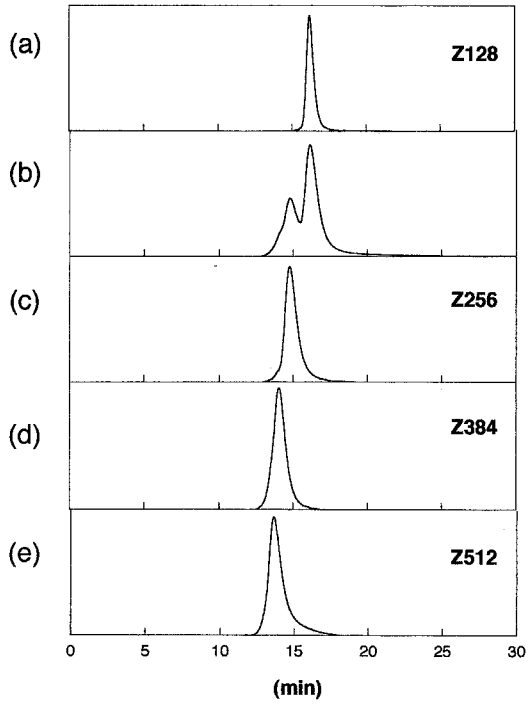

Figure 2-2. GPC-HPLC chromatograms of the reaction from **Z128**. (a) **Z128**, (b) reaction mixture of **Z128**, (c) purified **Z256**, (d) purified **Z384**, and (e) purified **Z512**. GPC setup is the combination of JAI-GEL 5H-AF, 4H-AF, and 3H-AF.

Finally, the author examined the coupling reaction of **Z256** under the similar conditions, which afforded **Z512**, **Z768**, and **Z1024** as judged from the GPC-HPLC chart of

the reaction mixture (Figure 2-3, we used different analytical column setup in order to get better separation for larger arrays; JAI-GEL 5H-AF, and 4H-AF, with THF. The preparative column GPC showed clearer separation; Figure 2-4.). Separation of these reaction products turned out to be considerably difficult because of their retention times are quite close to the exclusion limit. But after repeated recycling separations over the preparative GPC-HPLC, the author isolated **Z512** (13%), **Z768** (5%), and **Z1024** (2%). The isolated long arrays exhibit the retention times of 9.9, 9.6, and 9.5 min for **Z512**, **Z768**, and **Z1024**, respectively. The longest molecule of **Z1024** has a molecular length of 0.85 μm in its linear form and a molecular formula of $C_{65536}H_{83970}N_{4096}O_{4096}Zn_{1024}$.

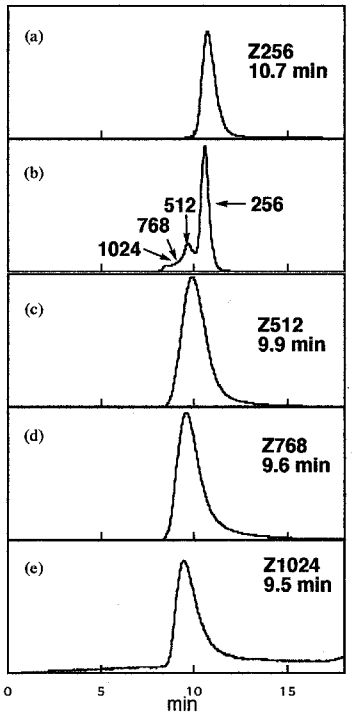

Figure 2-3. GPC-HPLC chromatograms of the reaction from **Z256**. (a) **Z256**, (b) reaction mixture of **Z256**, (c) purified **Z512**, (d) purified **Z768**, and (e) purified **Z1024**. GPC setup is the combination of JAI-GEL 5H-AF and 4H-AF.

While **Z128** can be stored in a refrigerator for a long time without serious deterioration and can be manipulated essentially in a similar manner to normal small organic compounds, the manipulations of the larger arrays (**Z256**, **Z384**, **Z512**, **Z768**, and **Z1024**) are more difficult, since freshly separated samples are reasonably soluble but change to insoluble material upon storage even in a refrigerator in the dark. Once these porphyrin arrays become insoluble, it was very difficult to redissolve them in common

organic solvents. This tendency becomes more serious upon increase in the array size.

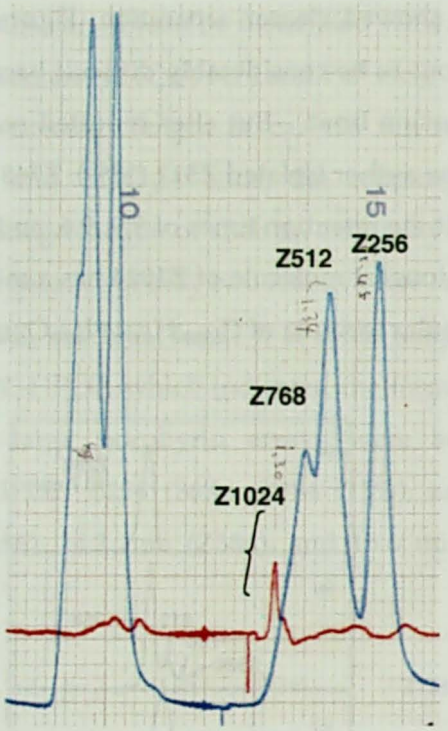

Figure 2-4. GPC-HPLC chromatograms of the reaction from **Z256**.

It may be a big question how two giant molecules can find two reacting sites (the end *meso*-positions) for each other in the reaction. Considering the large size of the porphyrin arrays, the coupling reaction must be entropically very unfavorable. Despite this situation, the coupling reactions proceed to give even longer products. One possible explanation may be pre-association of porphyrin arrays in $CHCl_3$, which might bring two or more porphyrin arrays parallel with their ends closely.

2-3. Characterization of *meso-meso* Linked Porphyrin Arrays

2-3-1. Molecular Weight Analysis of *meso-meso* Linked Porphyrin Arrays

The molecular weights of these porphyrin arrays were strictly determined by matrix-assisted laser desorption ionization/time of flight (MALDI-TOF) method up to **Z128** and the results are summarized in Table 1. The mass spectra of **Z64**, **Z96**, and **Z128** reveal the parent peaks at 6632, 99050, and 130295, respectively, along small dicationic peaks, clearly indicating their clean monodispersity (Figure 2-4). Unfortunately, however, the parent ion peaks of higher porphyrin arrays could not be detected for > **Z128**.

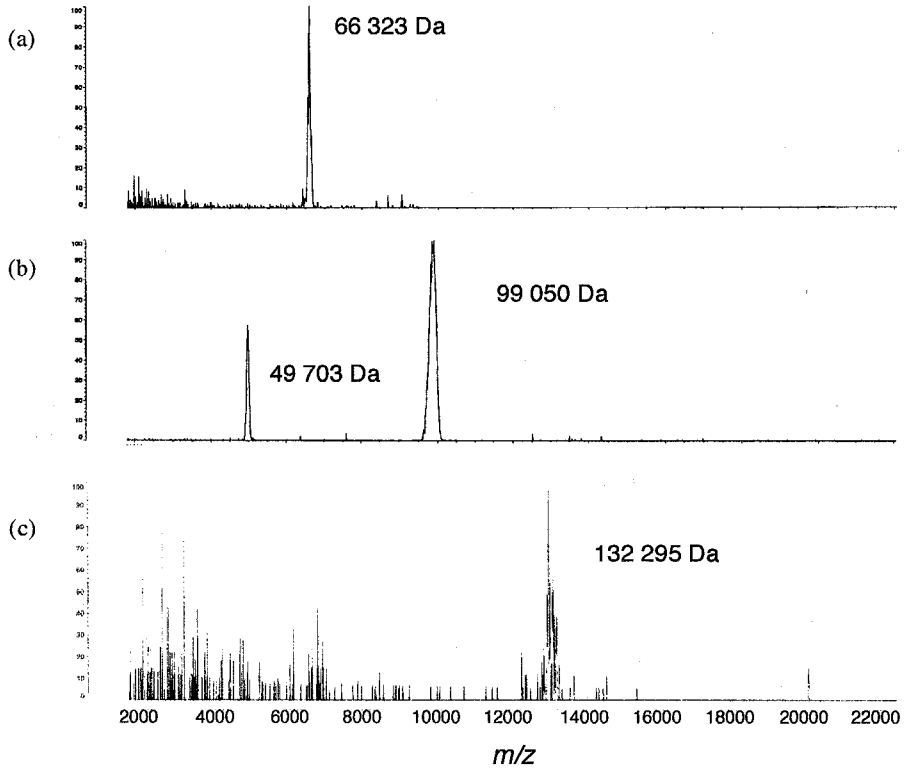

Figure 2-4. MALDI-TOF mass spectra (9-nitroanthracene was used as a matrix). (a) **Z64**, (b) **Z96**, and (b) **Z128**.

Another information on the monodispersity of the separated porphyrin arrays was given from their GPC-HPLC eluting features, since all the isolated porphyrin arrays exhibit clear elution bands in GPC-HPLC charts whose retention times show a good continuous relationship *versus* the actual molecular weights, similar to the relationship of polystyrene standards *versus* the actual molecular weights. **Zn** and polystyrene

standards elute in a similar manner against their molecular weights in a region of log*Mw* < 4, while **Zn** elute much faster than polystyrene standards of the same molecular weight in a region of log*Mw* > 4 and this discrepancy becomes more significant with increasing molecular weight (Figure 2-5a). Figure 2-5b demonstrates a good continuous relationship of the actual molecular weights versus analytical GPC molecular weights estimated with respect to polystyrene standards.

Table 1. Compounds list. Observed and calculated Molecular weight and GPC retention times.

compound	molecular formula	M_c [a]	M_o [b]	retention time[c] (min)
Z1	$C_{64}H_{84}N_4O_4Zn$	1 037	1 036	26.1
Z2	$C_{128}H_{166}N_8O_8Zn_2$	2 075	2 076	25.4
Z3	$C_{192}H_{248}N_{12}O_{12}Zn_3$	3 114	3 112	24.9
Z4	$C_{256}H_{330}N_{16}O_{16}Zn_4$	4 146	4 145	24.5
Z5	$C_{320}H_{412}N_{20}O_{20}Zn_5$	5 186	5 183	24.2
Z6	$C_{384}H_{494}N_{24}O_{24}Zn_6$	6 222	6 214	23.9
Z7	$C_{448}H_{576}N_{28}O_{28}Zn_7$	7 259	7 253	23.6
Z8	$C_{512}H_{658}N_{32}O_{32}Zn_8$	8 296	8 286	23.4
Z10	$C_{640}H_{822}N_{40}O_{40}Zn_{10}$	10 369	10 351	22.9
Z12	$C_{768}H_{986}N_{48}O_{48}Zn_{12}$	12 443	12 416	22.5
Z16	$C_{1024}H_{1314}N_{64}O_{64}Zn_{16}$	16 590	16 566	21.8
Z20	$C_{1280}H_{1642}N_{80}O_{80}Zn_{20}$	20 736	20 769	21.2
Z24	$C_{1536}H_{1970}N_{96}O_{96}Zn_{24}$	24 884	24 465	20.7
Z32	$C_{2048}H_{2626}N_{128}O_{128}Zn_{32}$	33 178	33 292	19.9
Z40	$C_{2560}H_{3282}N_{160}O_{160}Zn_{40}$	41 470	41 177	19.2
Z48	$C_{3072}H_{3938}N_{192}O_{192}Zn_{48}$	49 764	49 497	18.7
Z64	$C_{4096}H_{5250}N_{256}O_{256}Zn_{64}$	66 350	66 323	17.8
Z96	$C_{6144}H_{7874}N_{384}O_{384}Zn_{96}$	99 527	99 050	16.8
Z128	$C_{8192}H_{10498}N_{512}O_{512}Zn_{128}$	132 709	130 295	16.1
Z192	$C_{12288}H_{15746}N_{768}O_{768}Zn_{192}$	199 052	d	15.3
Z256	$C_{16384}H_{20994}N_{1024}O_{1024}Zn_{256}$	265 416	d	14.8
Z384	$C_{24576}H_{31490}N_{1536}O_{1536}Zn_{384}$	398 122	d	14.1
Z512	$C_{32768}H_{41986}N_{2048}O_{2048}Zn_{512}$	530 830	d	13.6
Z768	$C_{49152}H_{62978}N_{3072}O_{3072}Zn_{768}$	796 242	d	d
Z1024	$C_{65536}H_{83970}N_{4096}O_{4096}Zn_{1024}$	1 061 658	d	d

(a) Calculated molecular weight. (b) MALDI-TOF mass detected molecular weight.

(c) GPC-HPLC analysis (JAIGEL-5H-AF, 4H-AF, and 3H-AF columns in series).

(d) Not determined.

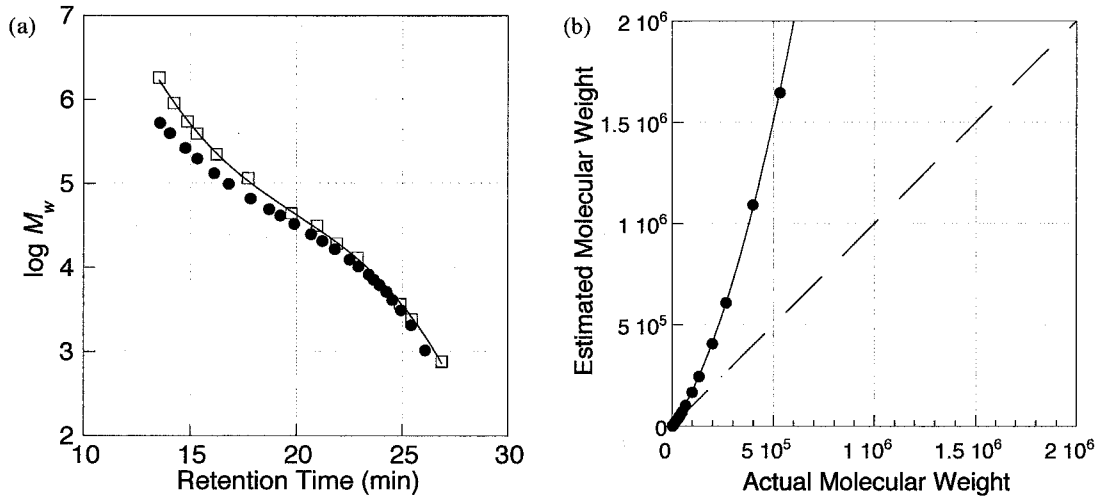

Figure 2-5. (a) Relationship of the retention time versus log *Mw*. ●; Zn, □; standard polystyrene. (b) *Mn* determined by GPC relative to polystyrene standards versus actual molecular weights of **Z*n***.

The **Z*n*** series is a rare example of a set of exactly discrete homologous chain molecules covering a very wide range of molecular size (from 1,000 to 1,000,000 Da). Thus this series provides a nice opportunity to examine the relationship of hydrodynamic volume *versus* molecular shape. As shown in Figure 2-5b, the molecular weights of **Z*n*** measured using polystyrene standards are much larger than the actual values. Particularly in the case of **Z512**, the estimated *Mw* is about three times larger than the actual *Mw*. This is in line with the previous reports that the molecular weights of rod-like molecules, when estimated by GPC against random coil polystyrene standards, are considerably inflated relative to the actual values [70]. These results thus indicate that **Z*n*** do not take random coil conformation like the polystyrene standards but rather take rod-like conformation in solution as a whole. This relationship may provide important information on the hydrodynamic volume of one dimensional rod-like molecules at molecular size up to $Mw = 5 \times 10^5$ Da and is actually quite useful in estimating the weight average molecular weights of large poly(porphyrinylene)s [68].

2-3-2. ^{1}H-NMR Spectra of *meso-meso* Linked Porphyrin Arrays

^{1}H NMR spectra of **Z1**, **Z2**, **Z3**, **Z4**, **Z5**, **Z6**, **Z7**, and **Z8** taken in $CDCl_3$ at room temperature were shown in Figure 2-6. Assignments were performed through comprehensive ROESY experiments (the designation of the protons was given in Figure 2-7). In the spectrum of **Z1**, a singlet for the *meso*-protons (H^m) appears at 10.31 ppm and two doublets for the β-protons appear at 9.43 (H^1) and 9.26 (H^2) ppm. The spectrum of **Z2** exhibits a singlet for H^m at 10.38 ppm and two doublets for the outer β-protons at 9.49 (H^1) and 9.28 (H^2) ppm and two doublets for inner β-protons at 8.82 (H^3) and 8.10 (H^4) ppm, which are characteristic of a *meso-meso* linked diporphyrin. The inner β-protons are lying in the shielding region of the neighboring porphyrin. Similarly, the spectrum of **Z3** exhibits a singlet for H^m, two doublets for H^1 and H^2 and four doublets for the inner β-protons H^3, H^4, H^5, and H^6. The ^{1}H NMR spectra of **Z1~Z8** clearly indicate totally symmetric structures with straight rod-like conformations.

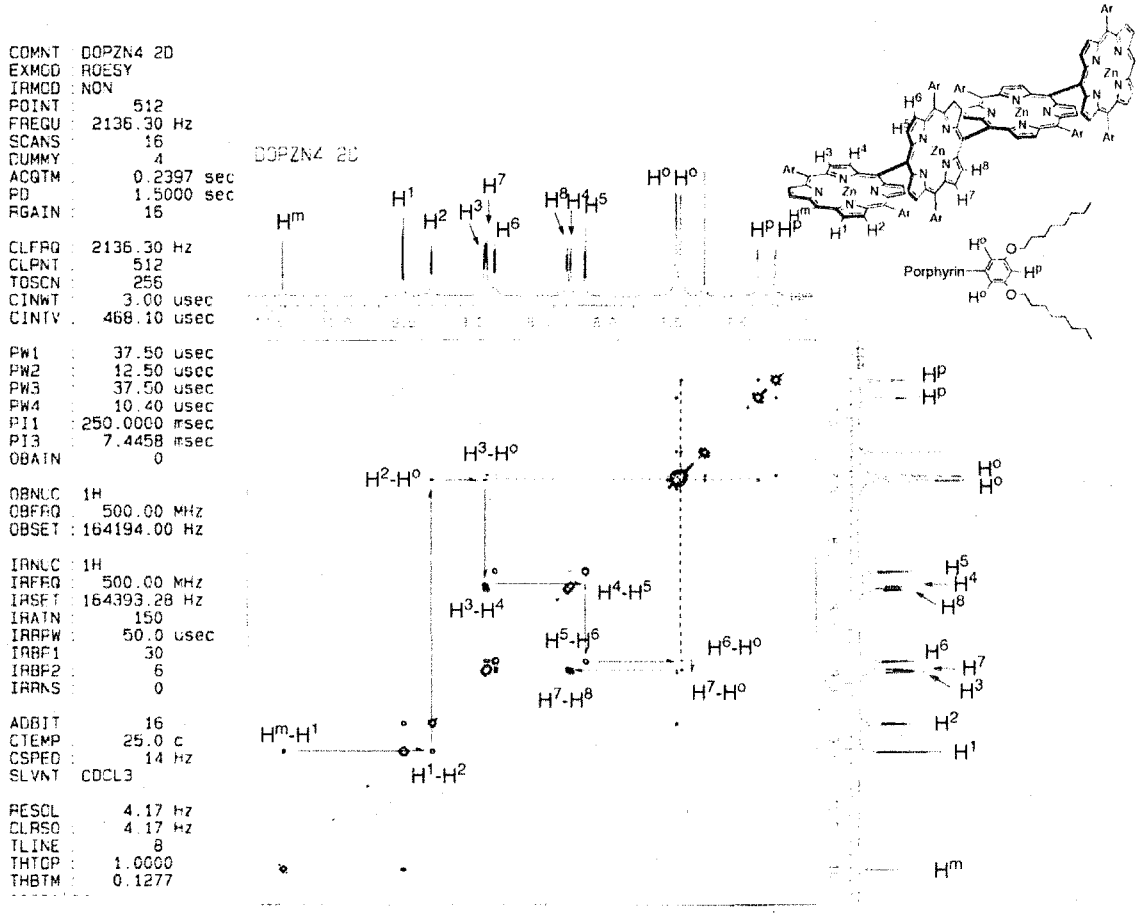

Figure 2-7. ROESY spectum of **Z4** in $CDCl_3$ at rt.

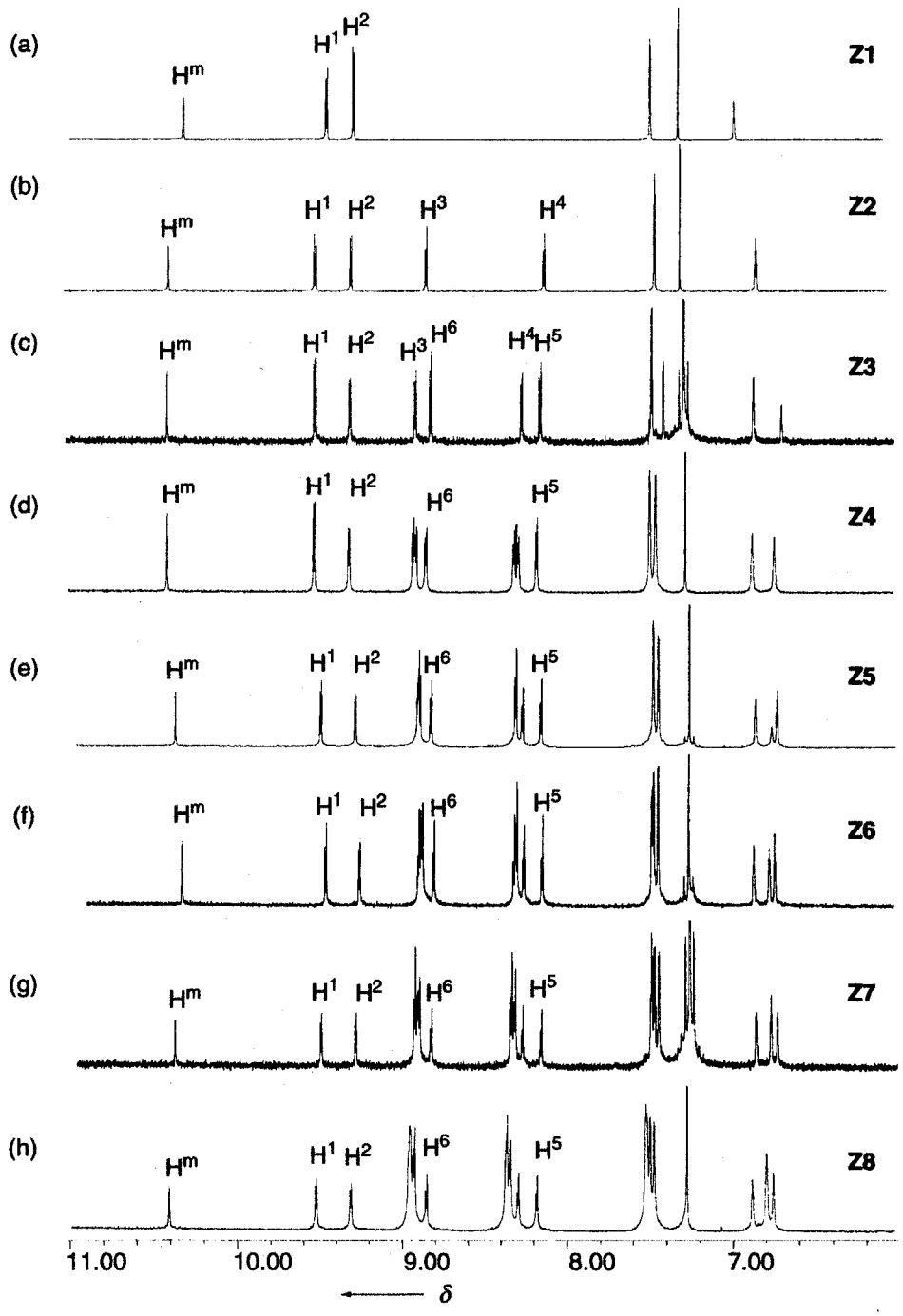

Figure 2-6. ^{1}H-NMR spectra in $CDCl_3$, (a) **Z1**, (b) **Z2**, (c) **Z3**, (d) **Z4**, (e) **Z5**, (f) **Z6**, (g) **Z7**, and (h) **Z8**.

The ^{1}H NMR spectra of **Z16**, **Z32**, **Z64**, and **Z128**, taken in $CDCl_3$ at room temperature were shown in Figure 2-8. Similar to these, the array **Z256** also displays relatively well-resolved ^{1}H NMR spectrum, in which H^m appears as a singlet at 10.42 ppm and H^1

and H^2 appear as two doublets at 9.53 and 9.31 ppm (Figure 2-9).

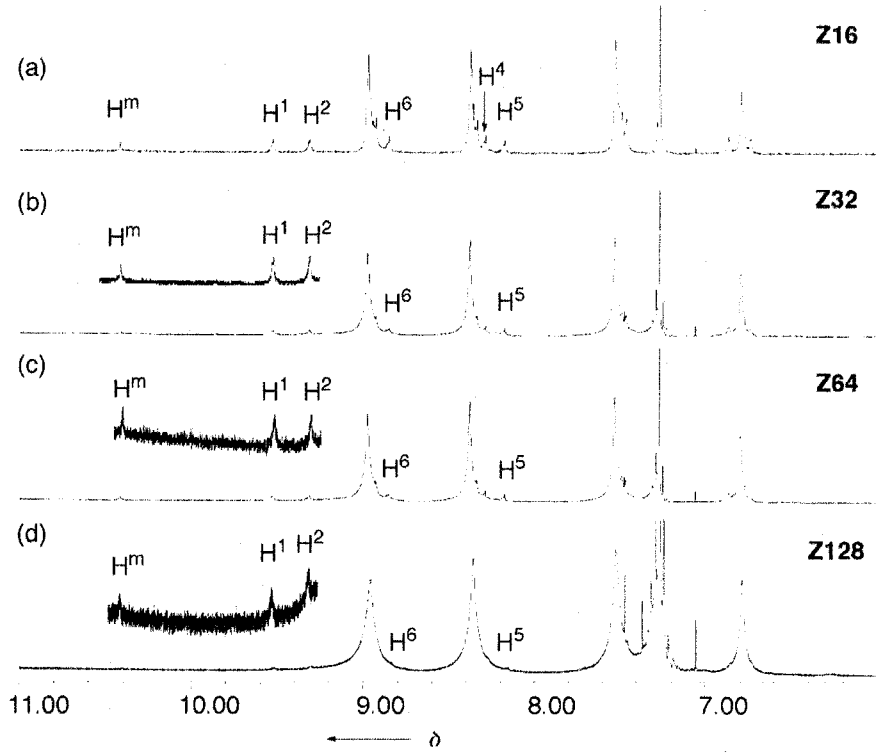

Figure 2-8. ^{1}H-NMR spectra in $CDCl_3$, (a) **Z16**, (b) **Z32**, (c) **Z64**, and (d) **Z128**.

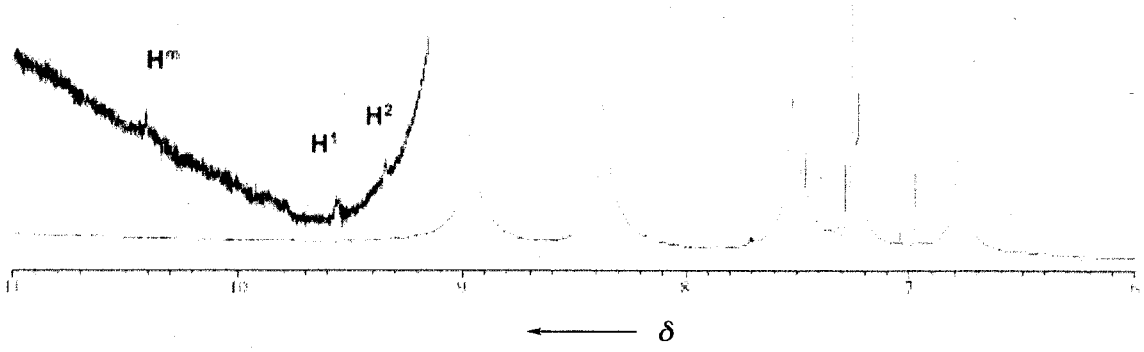

Figure 2-9. ^{1}H-NMR spectra of **Z256** in $CDCl_3$.

It is worthy to note that H^m, H^1 and H^2, and many inner β-protons (H^3-H^8, etc.) appear at nearly the same chemical shifts for all the arrays, indicating no significant aggregation of the arrays under these rather concentrated ^{1}H NMR conditions.

The free base porphyrin arrays **H*n*** show similar ^{1}H NMR spectra (Figure 2-10). The

porphyrin inner-NH protons appear at –3.15 ppm for **H1**, while –2.44 for **H2**, -1.65 (2H) and –2.40 (4H) for **H3**, and –1.62 (4H), and –2.39 (4H) for **H4**, and –1.57 (4H), -1.60 (4H), and –2.38 (4H) for **H6**. Thus those in the inner porphyrins are shifted to lower field, reflecting the ring current of neighboring and close porphyrins.

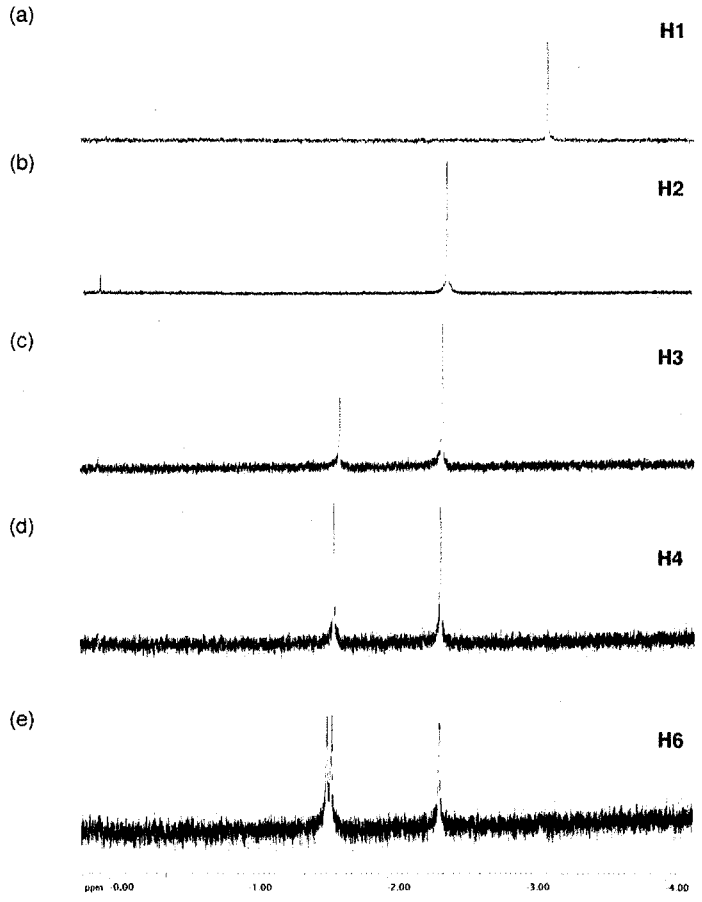

Figure 2-10. ^{1}H-NMR spectra from -4.00 to 0.00 ppm, (a) **H1**, (b) **H2**, (c) **H3**, (d) **H4**, and (e) **H6**.

2-3-3. Single-crystal X-ray Diffraction Analysis

The molecular structure of 5,15-bis(3,5-dioctyloxyphenyl)porphyrin **H1** was determined by X-ray crystal analysis (Figure 2-11). The porphyrin rings show rather planar structures with small deviations (0.023 Å for **H1**) from the mean planes consisting of 24 core atoms.

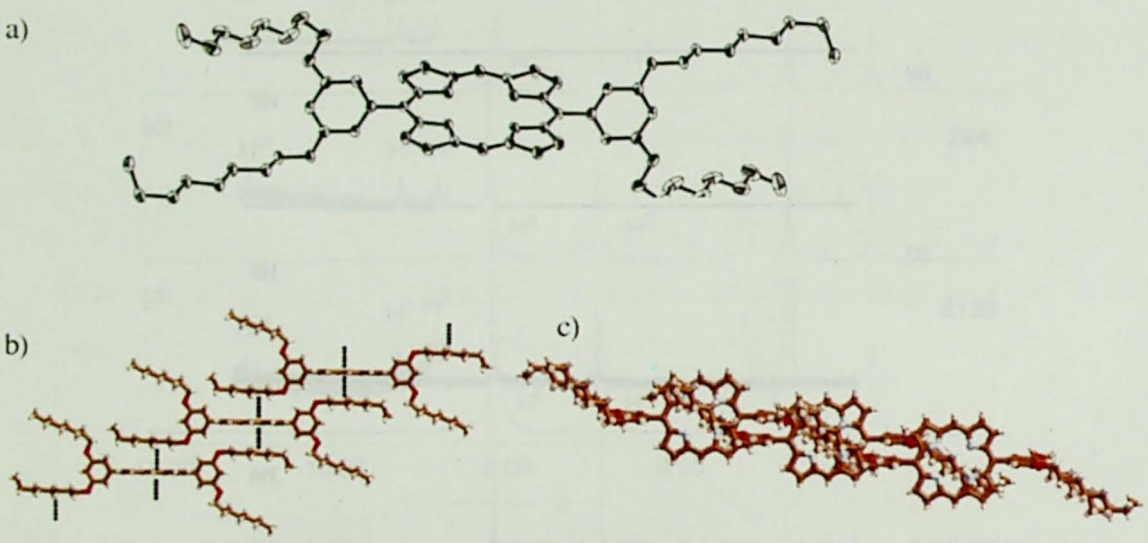

Figure 2-11. Crystal structure of **H1**. (a) The ORTEP drawing with thermal ellipsoids at 50% probability. Hydrogen atoms are omitted for clarity. Crystal packing structure; (b) side view and (c) top view.

Single crystals of **Z2** were obtained from a THF/*iso*-propanol solution although unfortunately the diffraction data were not suitable for analysis [71]. Through many attempts to make single-crystals of *meso-meso* coupled porphyrin arrays, the single crystals suitable for X-ray structure analysis were obtained for triporphyrin $\mathbf{Z_P3}$ (all aryl substituents of porphyrin array are phenyl group) as the first crystal structure of a *meso-meso* linked triporphyrin (Figure 2-12). In the solid-state, the triporphyrin $\mathbf{Z_P3}$ displays a straight and orthogonal structure with dihedral angles between the directly linked porphyrins of 88.3° and *meso-meso* bond lengths of 1.51(1) Å. This bond length is within a range of a typical C–C single bond.

The packing structures provide information on molecular interactions in the solid

state. In the crystal structure of **H1**, both faces of each porphyrin are covered by the octyloxy side chains of the neighboring porphyrins in a parallel manner with a distance of ca. 3.5 Å (Figure 2-11b). Interestingly, the non-interacting octyloxy side chains on the opposite side take an oblique orientation with respect to the porphyrin plane. These structural features suggest week C-H π interaction between the porphyrin π-plane and parallel octyloxy side chain [72], which leads to the formation of infinite one-dimensional network (Figure 2-11c). On the other hand, the porphyrin trimer $\mathbf{Z_P3}$ takes one-dimensional network with different structural motifs, in which orthogonally-linked triporphyrin subunits are nicely packed with week C-H π interaction between the porphyrin π-plane and aromatic C-H. Distance between the mean plane and phenyl *p*-carbon is estimated to be ca. 3.23 Å (Figure 2-12c).

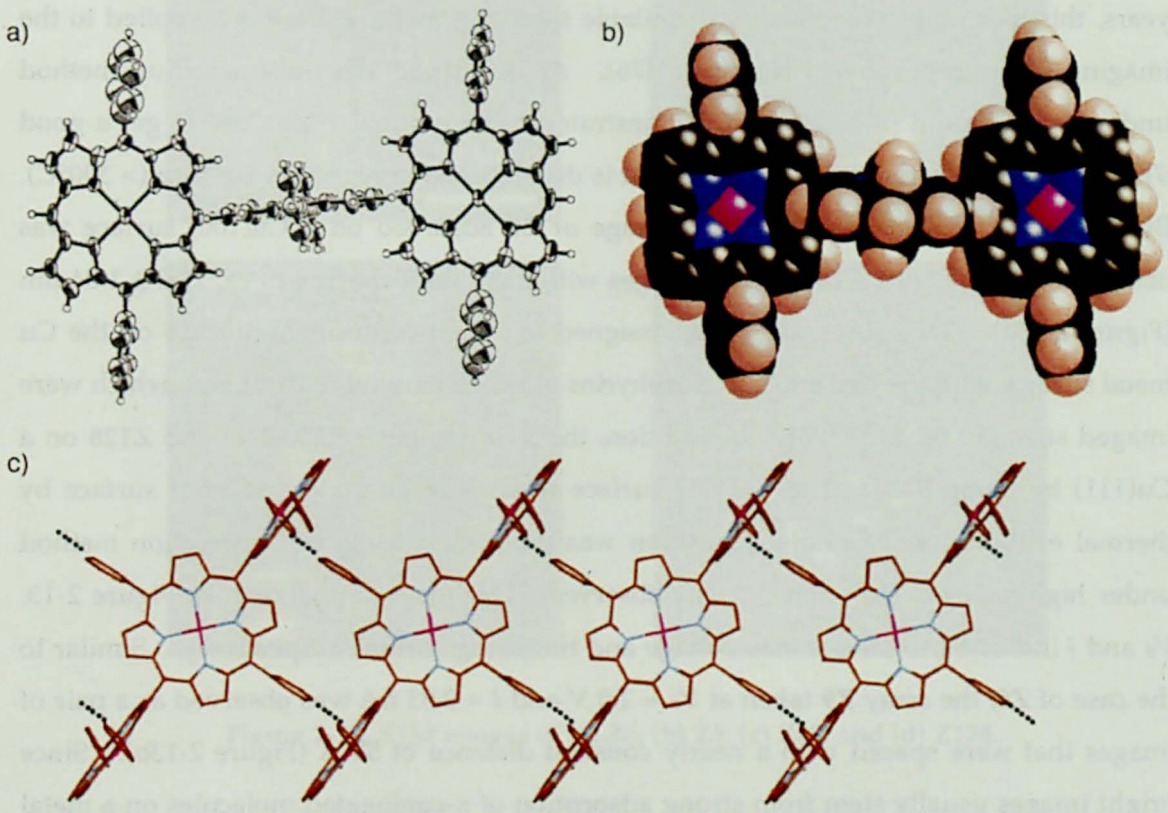

Figure 2-12. Crystal structure of Z_P3. (a) The ORTEP drawing with thermal ellipsoids at 50% probability. Solvent molecules are omitted for clarity. (b) The space filling drawing. (c) Crystal packing structure.

2-3-4. Structure investigation by Scanning Tunneling Microscopy (STM) and Atomic Force Microscopy (AFM)

Achieving direct access to single molecule has become a growing area of contemporary interdisciplinary research since the discovery of STM in 1982 [73]. Accordingly, the detection of molecular shape with a certain molecular size by means of STM has become more and more feasible [74]. Even atomic force microscopy (AFM) may be effective to produce a molecular shape and/or packing pattern of a big molecule with sufficient size. Research in this area has also aimed at the engineering of single molecules and/or atoms at the exploration of molecular properties on an individual nonstatistical basis. In 1996, IBM research group succeeded in the observation of the STM image of tetrakis(3,5-di-*t*-butylphenyl)porphyrin Cu(II) complex [75]. In recent years, this technique, combined with suitable sampling method, has been applied to the imaging of large porphyrin oligomers [76]. Among these, the pulse injection method under high vacuum [77] has been demonstrated to be particular effective to get a good STM image of a large porphyrin array that is decomposed at high temperature (> 300°C). By employing this method, the STM image of **Z6** adsorbed on a Cu(100) surface was observed, which consists of two dot images with a constant spacing of ca. 2.00 ± 1.04 nm (Figure 2-13a). This observation was assigned to a bent conformation of **Z6** on the Cu metal surface with the two end Zn^{II} porphyrins attached parallel to the metal, which were imaged strongly by STM [78]. In addition, the STM images of **Z9**, **Z48**, and **Z128** on a Cu(111) by using STM. The Cu(111) surface was made on a cleaved mica surface by thermal evaporation. Sample deposition was performed using pulse injection method under high vacuum (10^{-6} mbar). The observed STM images are shown in Figure 2-13. *Vs* and *I* indicate the sample bias voltage and tunneling current, respectively. Similar to the case of **Z6**, the array **Z9** taken at $Vs = 2.0$ V and $I = 0.03$ nA was observed as a pair of images that were spaced with a nearly constant distance of 55 Å (Figure 2-13b). Since bright images usually stem from strong adsorption of π-conjugated molecules on a metal surface, the bright pair-wise images may be assigned to the adsorption of the two end porphyrins with their planes parallel to the metal. Thus it may be suggested that **Z9**, similar to **Z6**, takes a bent conformation with the intervening porphyrins being detached from the metal surface. This assignment suggests conformational flexibility of *meso-meso* linked porphyrins. This feature is highlighted by the STM images of **Z48** and **Z128**. Among many unclear images that may arise from significant entanglement or aggregation,

a clear image of a single molecule **Z48** taken at *Vs* = 2.0 V and *I* = 0.03 nA was obtained, which displays a severely bent conformation on the plane of the metal surface (Figure 2-13c). Importantly, the molecular length of **Z48** is estimated to be 43.5 nm from this STM image, which is exactly the predicted molecular length of **Z48** (40.0 nm), which provided a strong support for its discrete structure. The author also obtained a clear image for a single molecule **Z128** taken at *Vs* = 0.5 V and *I* = 0.05 nA (Figure 2-13d), which also shows a snake-like largely bent structure with a molecular length of 117 nm that again matches well with its predicted molecular length (106.9 nm).

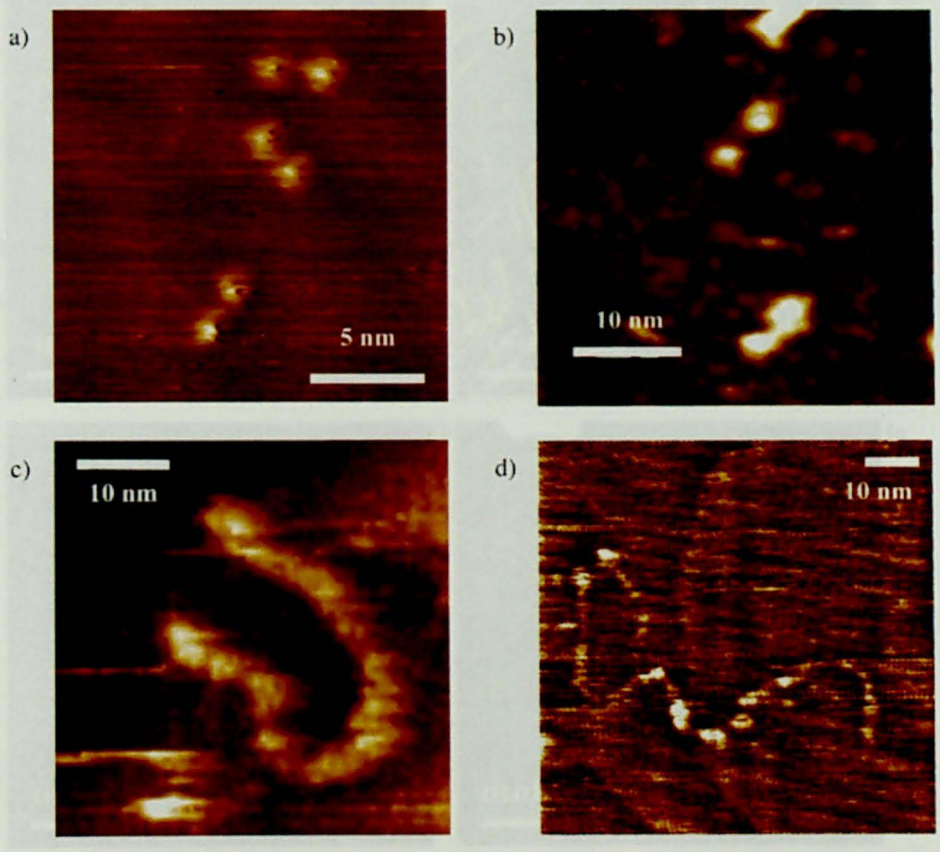

Figure 2-13. STM images of (a) **Z6**, (b) **Z9**, (c) **Z48**, and (d) **Z128**.

The detection of long porphyrin arrays on a single molecular level has also been attempted by means of an atomic force microscopy (AFM) technique on the highly oriented pyrolytic graphite (HOPG) substrate. In these experiments, a very dilute solution of porphyrin array in $CHCl_3$ was spread onto freshly cleaved HOPG surface, which was followed by a slow evaporation of the solvent. Figure 2-14a displays the tapping-mode AFM images of **Z96**, in which **Z96** molecules are aligned along the graphite

crystal lattice. It is interesting to note that many **Z96** molecules are observed as extending wire-like shape with nearly the same molecular length of 87.3 ± 14.5 nm. In the next step, single molecules of **Z256** and **Z512** were observed on the clean sapphire $Al_2O_3(0001)$ surface (Figure 14b-d). The single molecules were well dispersed, showing clear zig-zag shape with molecular length that is fully consistent with the structures. The molecular lengths observed by scanning probe microscopy with the number of porphyrin units *N* are plotted in Figure 2-15.

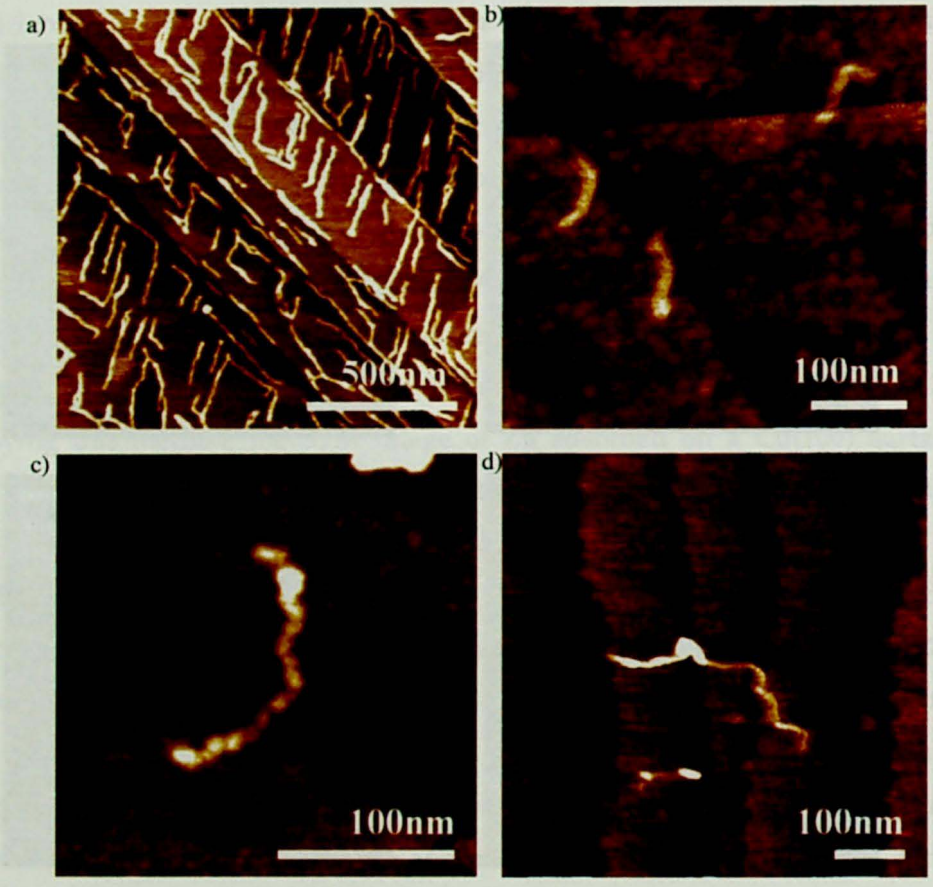

Figure 2-14. AFM images of (a) **Z96** on HOPG, (b) **Z96**, (c) **Z256**, and (d) **Z512** on sapphire.

But its largely bent structure was somewhat unexpected, since a 10,20-*meso*-*meso* direct connection of porphyrins was thought to result in a more stiff linear rod-like structure. A similar bent and more winding structure was detected for **Z128** under the comparable conditions. It is thus conceivable that conformation flexibility of **Z*n*** may be also substantially large in solution and become larger with increasing molecular size. The observed roughly straight structures of **Z96** on HOPG may stem from its favorable interaction with the graphite crystal lattice, hence suggesting that the conformational

flexibility of the porphyrin arrays depends on the environments.

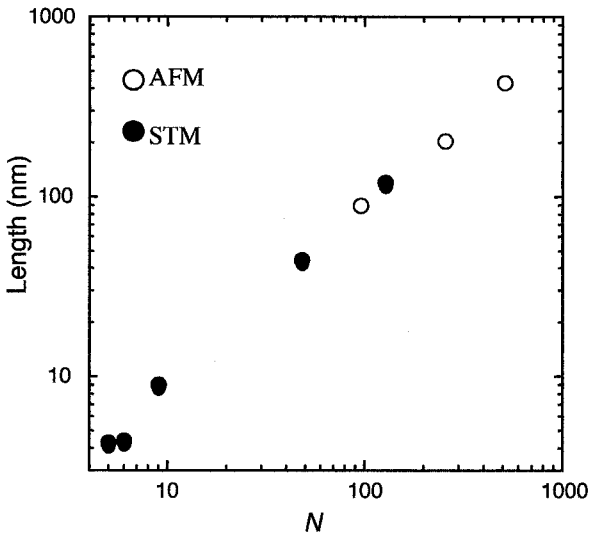

Figure 2-15. Relationship between the number of porphyrin unit (*N*) and the observed molecular length.

2-4. Summary

The iterative dimerization strategy has proven to be effective for the preparations of very long *meso-meso* linked Zn^{II} porphyrin arrays. Although the same starting monomer **Z1** can be polymerized under the slightly activated reaction conditions to macromolecules with dispersed molecular weight, the step-wise doubling strategy with strict purification of each doubling product allowed for the discrete preparation of gigantically long molecules in an unprecedented manner. Crucial to this success is the high regio-selectivity of the Ag^{I}-promoted oxidative coupling. In the reaction of **Z*n***, the author did not observe formation of any products that have other connectivity. Equally important is the high solubility of **Z*n*** despite their large molecular weights, which allows for the manipulation of these large molecules. The author noted, however, marked differences in solubility and stability between the arrays up to **Z128** and those longer than **Z128**. **Z128** can be stored for a long time without any serious chemical changes, while **Z256**, for example, tends to become insoluble material upon storage in the solid state for several months. This insoluble **Z256** is hardly dissolved to organic solvents, precluding analyses by GPC or UV-vis measurement.

Another advantage of this doubling strategy is evidently a large difference in the molecular weights among a reactant and products that becomes larger as the reactant array becomes larger, thus making the separation of coupling products relatively easy over the preparative GPC-HPLC. Despite this advantage, the separation of extremely long molecules such as **Z512** and **Z1024** needed recycled separations over the GPC many times. Lastly, the long arrays such as **Z128** and **Z256** still have a self-coupling reactivity that is enough to produce even longer arrays for a reaction time comparable to those of the shorter arrays.

Chapter 3. Physical Properties of *meso-meso* Linked Porphyrin Arrays

In this Chapter, photophysical, electrochemical, morphological properties of giant porphyrin arrays are described.

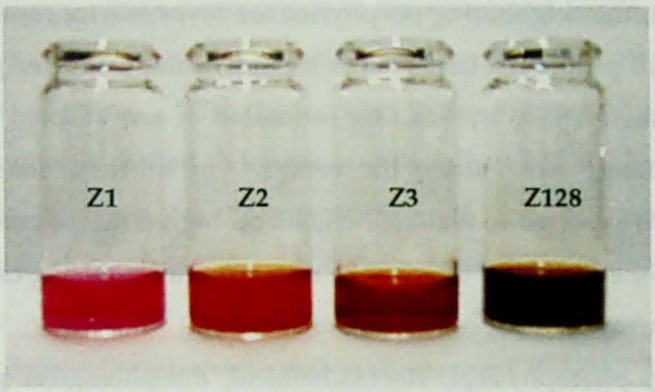

3-1. Introduction

The long *meso-meso* linked porphyrin arrays have the following properties: 1) on the basis of the linear molecular shape the whole molecular length can be easily predicted by the number of porphyrins (8.35 Å per one porphyrin unit), 2) the large Coulombic interactions between the neighboring porphyrins are favorable for rapid excitation-energy transmission, 3) each porphyrin unit retains its individual character presumably due to the orthogonal geometry, thus minimizing formation of any stacked energy sink which will disrupt the energy flow along the arrays. In other words, *meso-meso* linked porphyrin arrays are expected to realize the fast and high-efficient energy transfer over a long distance down the array and thus can be utilized as a promising candidate for energy transfer functional arrays in molecular photonic devices.

In this Chapter, photophysical, electrochemical, morphological properties of giant porphyrin arrays are described.

3-2. Photophysical Properties of *meso-meso* Linked Porphyrin Arrays [45]

3-2-1. Absorption Spectra of *meso-meso* Linked Porphyrin Arrays

The absorption spectra of the directly *meso-meso* linked Zn^{II} porphyrin arrays normalized at ca. 413 nm, which corresponds to the split Soret bands at high energy, are shown in Figure 3-1. The *meso-meso* coupled porphyrin arrays displayed split Soret bands due to exciton coupling. With the increase in the number of porphyrin units, the Soret band at low energy is shifted to longer wavelength, while the Soret band at shorter wavelength remains nearly at the same wavelength (ca. 413 nm), resulting in a progressive increase in the splitting energy. The relative intensities of split Soret bands also depend on the number of porphyrins; the intensity of longer wavelength bands becomes increasingly stronger relative to that at shorter wavelength. On the other hand, the spectral changes in the Q-band region are modest with gradual red-shift and increase in intensity.

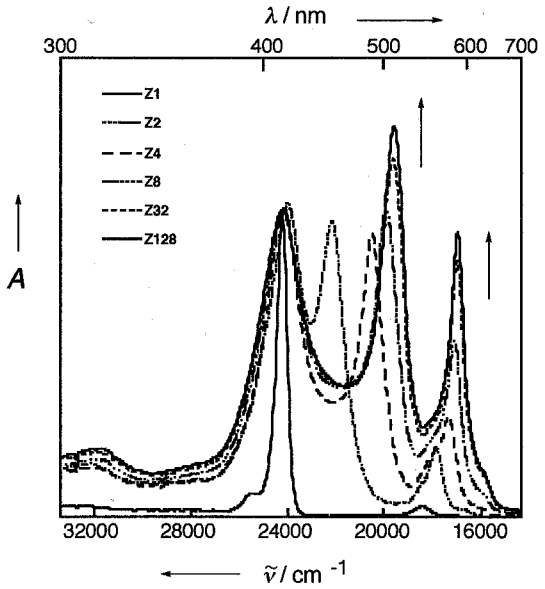

Figure 3-1. Absorption spectra of **Z1**, **Z2**, **Z4**, **Z8**, **Z32**, and **Z128** taken in THF.

The systematic spectral changes of the Soret bands can be explained by the simple point-dipole exciton coupling theory developed by Kasha [79]. In simple monomer, they are approximately degenerate (E_u in D_{4h}), but in porphyrin oligomers they couple differently. The Soret band of Zn^{II} porphyrin has two perpendicular components of B_X and B_Y as depicted in Figure 3-2. In the case of **Z2**, only B_X transitions are parallel, and

other dipole interactions should be zero for an averaged perpendicular conformation of **Z2** which has been predicted to be the most stable on the basis of AM1 calculation and has been confirmed by its X-ray crystal structure [70,80]. Unperturbed Soret transitions observed at ca. 413 nm for all the arrays (**Z2** to **Z128**) suggest an orthogonal conformation *vice versa*. Transitions are allowed to the lower energy of the two B_X states and the two unperturbed transitions B_Y and B_Z. Thus, the Soret band of **Z2** is split into a red-shifted B_X component and unperturbed B_Y, B_Z components. These interpretations coincide with the observed spectra of these arrays in solution.

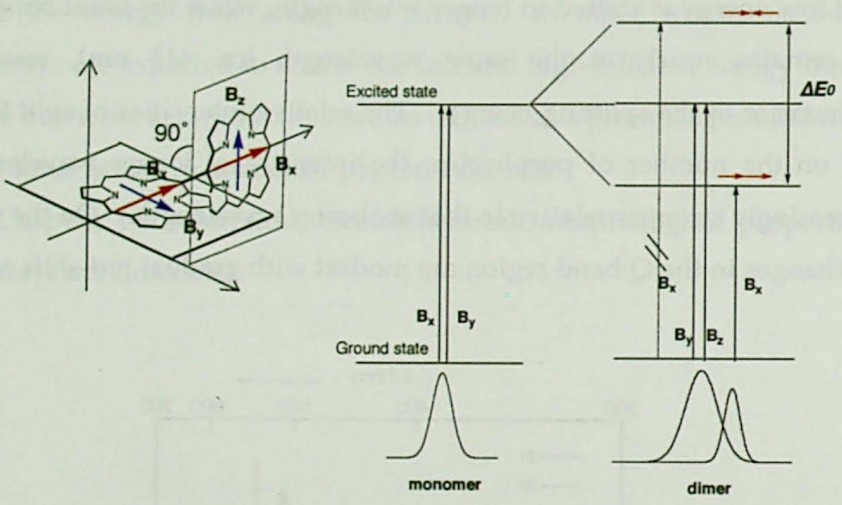

Figure 3-2. Schematic energy level diagram for *meso-meso* linked Zn^{II} porphyrin.

The Coulombic interaction energy (E) depends on the magnitude of the transition dipole moments as well as the distance as written by Eq. (1),

$$E = \frac{1}{4\pi\varepsilon_0}\left[\frac{\mu_1 \cdot \mu_2}{R^3} - 3\frac{(\mu_1 \cdot r)(\mu_2 \cdot r)}{R^5}\right] \qquad (1)$$

$$= \frac{|\mu_1||\mu_2|}{4\pi\varepsilon_0 R^3}\left(1 - 3\cos^2\theta\right) \qquad (2) \quad \text{(when to dipoles are parallel)}$$

where μ_i is the transition dipole moment of molecule *i*, *r* the position vector linking the centers of two molecules, *R* the center-to-center chromophore distance, and , and θ is angle between polarization axes and the line of molecular centers. Then, the following equation predicts the relationship of the exciton coupling energy of the neighboring

porphyrin units, ΔE_0, ($\theta = 0$, $\mu_1 = \mu_2 = \mu$)

$$\Delta E_0 = (-E) - E = \frac{\mu^2}{\pi\varepsilon_0 R^3} \qquad (3)$$

The total splitting energy (ΔE) for larger linear arrays should be given by Eq. (4) when the excitonic interactions between non-nearest neighbor porphyrins are negligible owing to the substantial distance,

$$\Delta E = 2\ \Delta E_0 \cos[\pi/(N+1)] \qquad (4)$$

Here N represents the number of chromophores. The exact value of ΔE is not known because the transition to the highest energy excitonic state is forbidden. Therefore, the splitting energy ΔE can be taken to be twice the value of the difference in energy between the red shifted B_X band and the unperturbed $B_{Y,Z}$ band. When ΔE data were plotted to Eq. (4), a nice straight line with a slope of $\Delta E_0 = 4250$ cm^{-1} was obtained (Figure 3-3). The observed linear relationship indicates that the absorption spectral shapes are actually influenced by the number of porphyrins and the constituent porphyrins are regularly aligned in the same arrangement in solution. On this basis, these arrays in the ground state are believed to consist of repeating individual chromophores with substantial electronic interactions.

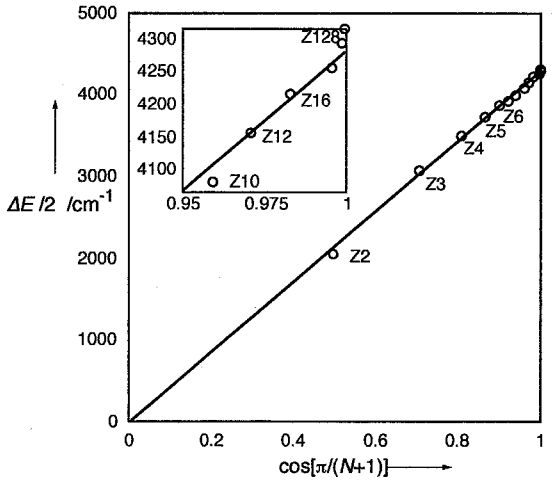

Figure 3-3. Plot of ΔE versus $2\cos[\pi/(N+1)]$.

Table 2. Absorption spectral data of *meso-meso* linked porphyrin arrays in THF

compound	absorption peaks (log ε)[a] / nm ($M^{-1}cm^{-1}$)
Z1	413.0 (5.81), 543.0 (4.34)
Z2	418 (5.43), 452 (5.40), 560 (4.78)
Z3	414 (5.57), 476 (5.51), 571 (4.95)
Z4	414 (5.64), 488 (5.61), 576 (5.15)
Z5	415 (5.71), 494 (5.69), 580 (5.31)
Z6	414 (5.77), 498 (5.77), 582 (5.45)
Z7	414(5.83), 500 (5.82), 583 (5.54)
Z8	414 (5.87), 502 (5.87), 585 (5.63)
Z10	414 (5.95), 505 (5.97), 586 (5.75)
Z12	414 (6.02), 507 (6.05), 587 (5.86)
Z16	414 (6.11), 508 (6.14), 587 (5.98)
Z32	414 (6.41), 509 (6.49), 588 (6.34)
Z64	414 (6.70), 510 (6.80), 589 (6.66)
Z128	414 (7.00), 511 (7.10), 589 (6.96)
Z256	414 (7.30), 511 (7.40), 589 (7.26)
Z384	414 (7.48), 511 (7.58), 589 (7.44)
Z512	414 (7.60), 511 (7.70), 589 (7.56)

The absorption spectra of long Zn^{II} porphyrin arrays are reminiscent of water-soluble porphyrin J-aggregate, which exhibit sharp and red-shifted peaks below the Q- and B-bands in aqueous solution at room temperature [81]. The J-aggregates are characteristic of a sharp absorption band below the transition band of monomers. Intermolecular interaction between dipole moments cause the coherent delocalization of excitons over an aggregate. Thus the exciton split low-energy Soret band can be represented by the head-to-tail arrangement of the B_X transition dipoles as depicted in Figure 3-2. On the other hand, according to the four-orbital model [82], the strength of the Q(0,0) transition is dictated by the energy difference between $a_{1u}(\pi) \rightarrow e_g(\pi^*)$ and $a_{2u}(\pi) \rightarrow e_g(\pi^*)$ one-electron promotions and is thus strongly influenced by the relative energies of the $a_{1u}(\pi)$ and $a_{2u}(\pi)$ HOMOs (*vide infra*). The intensity of the Q(1,0) band does not

change significantly among metalloporphyrins because this band primarily gets intensity *via* vibronic borrowing from the strong Soret band. In Zn^{II} porphyrin monomer, the Q(1,0) band is dominant. The Q-bands of the porphyrin arrays become enhanced and sharper as the number of porphyrin units increases (Figure 3-1). Since the Q(1,0) bands of Zn^{II} porphyrins gain their intensities *via* vibronic coupling from the B bands, the enhanced Q-bands of the porphyrin arrays may be assigned due to increased vibronic coupling mainly contributed by the decreased energy gap between the exciton split low-energy B- and Q-bands in the porphyrin arrays. The sharp exciton split B- and Q-bands are consistent with the view of the electronic transitions of porphyrin J-aggregates. The orientations of the transition dipoles for low-energy exciton split B- and Q-bands are the same, which is along the long axis of the porphyrin arrays as shown by the positive anisotropy values in the fluorescence excitation anisotropy spectra for these two transitions. Ohta *et al.* reported that the transition moment of the exciton split band is aligned along the long axis of the linked porphyrin arrays (**Z2-Z4**) from the electro-absorption experiment, which revealed that Stark effect of monomeric band is considerably different from the exciton split band [83]. Relatively broad B-bands at ca. 413 nm with a negative anisotropy value, which has the characteristic of the monomeric Soret transition, in turn, can be understood to suggest that there exist the conformational heterogeneities with respect to dihedral angle distribution at the *meso-meso* linkage.

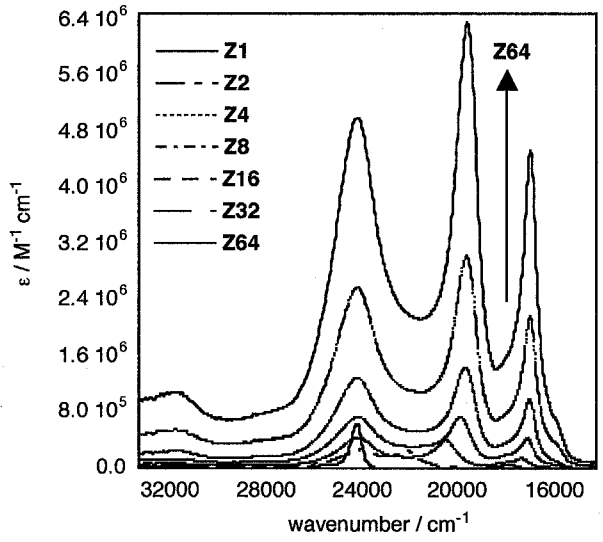

Figure 3-4. Absorption spectra of **Z1** - **Z64** with molecular coefficient (THF).

3-2-2. Fluorescence Spectra of *meso-meso* Linked Porphyrin Arrays

The steady-state fluorescence spectra of the arrays according to the relative intensity scale are displayed in Figure 3-5. **Z1** exhibits two-peak emission (584 and 633 nm) characteristic of Zn^{II} porphyrin and **Z2** exhibits a red-shifted and broader fluorescence spectrum. The fluorescence spectra of longer arrays are observed in nearly the same region as the two bands at ca. 15600 cm^{-1} (640 nm) and ca. 15000 cm^{-1} (667 nm). The relative fluorescence quantum yields determined with respect to $\Phi_F = 0.03$ of Zn^{II} TPP [84] increase up to **Z16** and then decrease with the increase of the number of porphyrin units (Table 2). The decreased fluorescence quantum yields of longer porphyrin arrays > **Z16** indicate that each porphyrin unit in the array cannot act as an individual fluorophore.

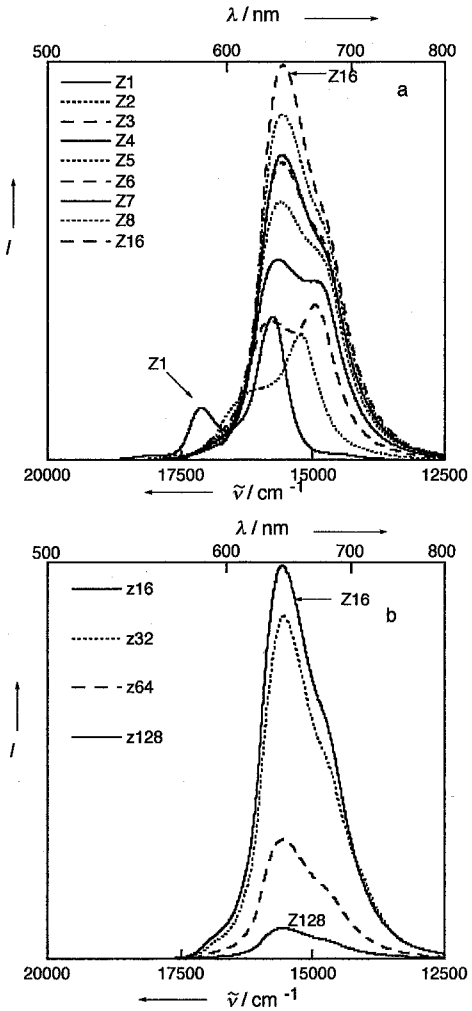

Figure 3-5. The fluorescence spectra of ***Zn*** taken after excitation of a THF solution at 413 nm with the absorbance adjusted at 0.20. (a) **Z1-Z8** and **Z16**, (b) **Z16**, **Z32**, **Z64**, and **Z128**.

As shown in Figure 3-6, the total fluorescence intensity is dropped from **Z128** to **Z256** but not so much changed from **Z256** to **Z512**.

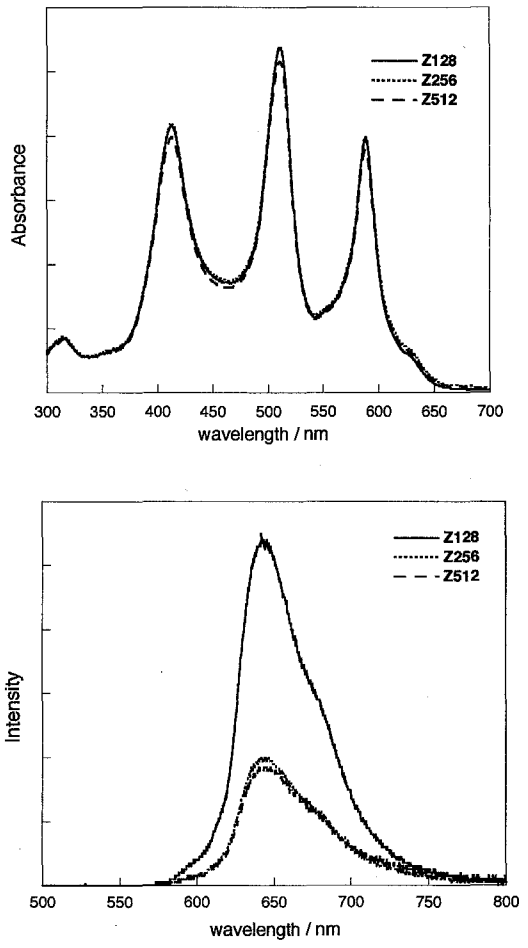

Figure 3-6. (a) UV-vis and (b) fluorescence spectra of **Z128**, **Z256**, and **Z512** in THF.

The author also measured the fluorescence lifetimes of the porphyrin arrays by using time-correlated single photon counting method (Table 2). The fluorescence decays of ***Zn*** also show a similar trend to the fluorescence quantum yields. As the porphyrin array becomes longer, the average fluorescence lifetimes of ***Zn*** decrease consistently up to **Z512**. In the shorter arrays than **Z16**, the fluorescence decays exhibit single exponential behavior. On the other hand, as the array becomes longer than **Z16**, the fluorescence temporal profiles start to show double exponential decay in which the contribution by the fast decay component increases gradually as the array becomes longer up to **Z512** (Table 3).

After the formation of the vibrationally ground S_1-state, the relaxation processes decaying to the ground state appear as fluorescence decays with the lifetime of 2.64 ns in

the monomeric porphyrin **Z1**. As the number of porphyrin units increases in the arrays, the fluorescence lifetimes gradually decrease to exhibit asymptotic feature. The fluorescence decay becomes nonexponential in longer arrays especially above **Z32**, which may be probably ascribed to the increased heterogeneity in conformers. The overall photoexcitation dynamics occurring in these porphyrin arrays are summarized in Table 3.

Table 3. Summary of fluorescence data.

model	$\Delta E(cm^{-1})$ [a]	Φ_F [b]	τ_{avg}(ns) [c]	τ_1(ns,%) [d]	τ_2(ns,%) [e]	r [f]
Z1	-	0.022	2.64			0.008
Z2	2060	0.034	1.83			0.03
Z3	3176	0.044	1.72			0.05
Z4	3692	0.055	1.65			0.16
Z6	4104	0.066	1.59			0.21
Z8	4283	0.074	1.55			0.29
Z12	4434	0.080	1.52			0.31
Z16	4499	0.088	1.50			0.31
Z24	4557	0.083	1.43	1.49(95.4)	0.14(4.6)	0.27
Z32	4569	0.062	1.40	1.48(92.8)	0.33(7.2)	0.24
Z48	4595	0.058	0.93	1.47(61.1)	0.08(38.9)	0.20
Z64	4595	0.033	0.51	1.47(31.2)	0.08(68.8)	0.17
Z96	4615	0.031	0.50	1.45(27.7)	0.14(72.3)	0.13
Z128	4615	0.012	0.49	1.42(21.8)	0.22(78.2)	0.12
Z256	4615	0.012	0.40	1.05(28.8)	0.14(71.2)	0.12
Z512	4615	0.006	0.26	0.92(17.7)	0.12(82.3)	0.12

It should be noted that the fluorescence decay profiles depend on the probe wavelength especially in **Z256** and **Z512** (Figure 3-7). Specifically, as the probe wavelength is moved towards red, the overall fluorescence decays become slower in **Z256** and **Z512**. In shorter arrays, however, the fluorescence decays do not show the probe wavelength dependence. This feature indicates that the excitation energy migration occurs from the initially excited shorter porphyrin oligomer segments to the longer ones, which is commonly observed in the photoexcitation dynamics of polymers.

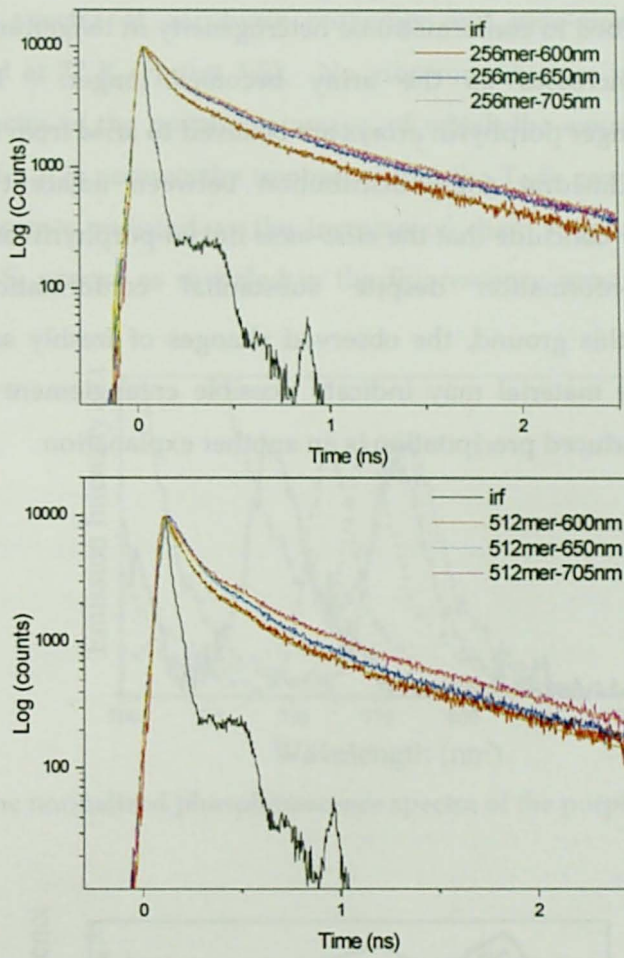

Model / λ(nm)	256mer (ns, %)	512mer (ns, %)
600	1.04(25%) + 0.138(75%)	0.965(16%) + 0.124(84%)
650	1.06(27%) + 0.144(73%)	0.902(14%) + 0.114(86%)
705	1.07(31%) + 0.148(69%)	0.940(20%) + 0.114(80%)
τ_{ave}	0.40	0.26

Fugure 3-7. Fluorescence decay profiles for **Z256** and **Z512**.

A plot of the molecular extinction coefficient of **Z*n*** *versus* the number of porphyrins (*n*) indicates a linear summation behavior in absorption intensity as the array becomes longer. On the other hand, in longer arrays than **Z16**, the fluorescence quantum yields

gradually decrease and the contribution by the short component became larger, exhibiting a good correlation with a decrease in fluorescence quantum yield. These spectroscopic data have been ascribed to conformational heterogeneity in longer arrays and the degree of heterogeneity increases as the array becomes longer. The conformational heterogeneities in longer porphyrin arrays are believed to arise from bending of the main chain as well as dihedral angle distribution between adjacent porphyrin planes. Collectively, we may conclude that the *meso-meso* linked porphyrin arrays take a roughly linear rod-like conformation despite substantial conformation flexibility and heterogeneity. On this ground, the observed changes of freshly separated long array samples to insoluble material may indicate possible entanglement of the main chain. Usual aggregation-induced precipitation is an another explanation.

3-2-3. Triplet States of *meso-meso* Linked Porphyrin Arrays [85]

Phosphorescence spectra of porphyrin monomer and *meso-meso* linked porphyrin arrays were observed at 77 K (Figure 3-8). No vibronic structure was observed in the phosphorescence spectra of the porphyrin arrays, of which the emission maximum was gradually red shifted. It is noteworthy to observe that the T_1–S_0 energy difference of the porphyrin arrays becomes reduced as the increase of chain length in contrast to the invariance of the S_1–S_0 energy as revealed in the fluorescence spectra of the porphyrin arrays.

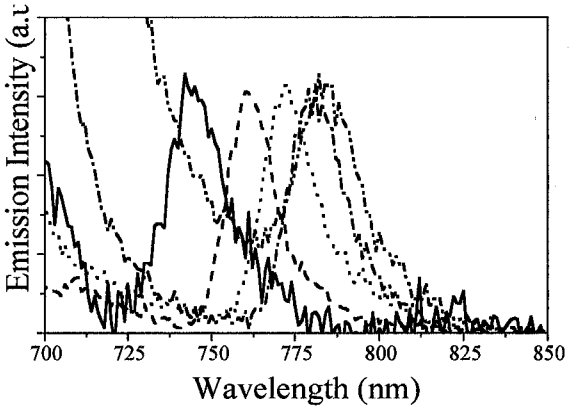

Figure 3-8. The normalized phosphorescence spectra of the porphyrin arrays.

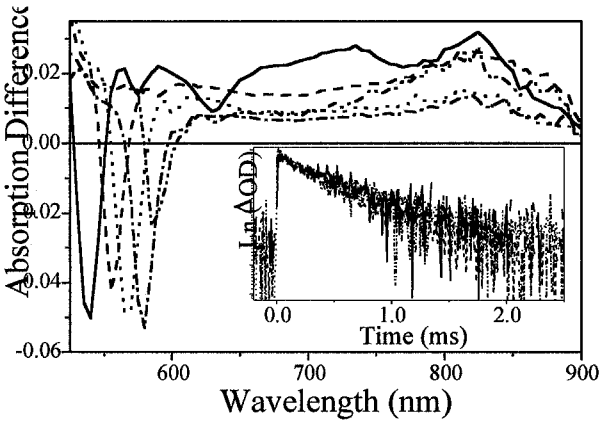

Figure 3-9. The T-T absorption spectra of the porphyrin arrays in toluene; **Z1**(—), **Z2**(---), **Z3**(····), **Z6**(-·-·-) and **Z12**(-·-·-·-). Inset shows the normalized decay profile of the T-T absorption at 825 nm.

The triplet-triplet (T-T) absorption spectra of porphyrin monomer and *meso-meso* linked porphyrin arrays were observed at the time delay of 5 μs (Figure 3-9). The T-T

absorption spectrum of **Z1** showed a characteristic feature arising from the $^3(\pi,\pi^*)$ states of Zn^{II} porphyrins. In the triplet state absorption spectrum of **Z1**, the author could also observe the dual-bands feature in the near-IR region having maxima at 735 and 825 nm, respectively, which correspond to the energy difference of ca. 1480 cm^{-1}. This energy is similar to that of vibronic transition progression normally found in the emission from the $^1(\pi,\pi^*)$ and $^3(\pi,\pi^*)$ states of metalloporphyrins. On the contrary, the triplet absorption spectra of the porphyrin arrays (**Z2**, **Z3**, **Z6**, and **Z12**) were almost the same without any vibronic structures (Figure 3-9).

The triplet states of the porphyrin monomer and *meso-meso* linked porphyrin arrays have almost the same lifetime of around 670 μs, while the S_1 state lifetimes were reduced as the number of porphyrin units was increased, meaning the S_1-states are largely sensitive to the perturbation of electronic configurations by the linkage of porphyrin moieties. These results indicate that the triplet state relaxation of the directly-linked porphyrin arrays is governed mainly by the spin conversion processes (spin orbit coupling) rather than energy gap law. Some photophysical data of triplet state of Zn^{II} porphyrin arrays are summarized in Table 4.

Table 4. Photophysical properties of triplet state of Zn^{II} porphyrin arrays.

compound	[a]$\lambda_{p,max}$ (nm)	[b]$\lambda_{T\text{-}T,max}$ (nm)	[c]τ_T (μs)
Z1	743	825	632
Z2	760	820	689
Z3	773	825	673
Z6	781	830	661
Z12	785	825	675

[a]The peak wavelength of the phosphorescence.

[b]The peak wavelength of the T-T absorption.

[c]Triplet state lifetime measured by T-T absorption at 825 nm.

The triplet state absorption spectrum of Zn^{II} porphyrin is generally composed of two bands; one lies in the visible wavelength region and the other in the near-infrared region. While the near-infrared absorption in the triplet state corresponds to the transition

between two states with singly excited configurations [$a_{1u}(\pi),e_g(\pi*) \rightarrow a_{1u}(\pi),b_{2u}(\pi*)$ or $a_{2u}(\pi),e_g(\pi*) \rightarrow a_{2u}(\pi),b_{1u}(\pi*)$], the visible absorption is known as due to the transition from the lowest excited state with singly excited configuration to the higher excited state with doubly excited configurations [$a_{1u}(\pi),e_g(\pi*)$ or $a_{2u}(\pi),e_g(\pi*) \rightarrow a_{1u}(\pi),a_{2u}(\pi),e_{g2}(\pi*)$]. The $T_1 \rightarrow T_n$ absorption spectra exhibited by Zn^{II} porphyrin arrays are similar to the $T_1 \rightarrow T_n$ absorption spectrum observed for **Z1** monomer, suggesting that $T_1 \rightarrow T_n$ transition generates a $^3(\pi,\pi*)$ excited state closely related to the singly excited configuration in near IR region. It suggests that the triplet state excitation is essentially localized on one porphyrin macrocycle, and the triplet states have a lifetime time similar to that of the parent porphyrin monomer.

3-2-3. Fluorescence Excitation Anisotropy Spectra of *meso-meso* Linked Porphyrin Arrays

In order to obtain information on the relative orientation between absorption and emission dipoles of the porphyrin arrays, the fluorescence excitation anisotropy spectra were measured (Figure 3-10). The fluorescence excitation polarization of **Z1** is nearly 1/7 regardless of the excitation wavelength, which is typical when both absorption and emission oscillators are degenerate and polarized in the same plane. In **Z*n***, however, negative anisotropy values in the fluorescence excitation anisotropy spectra around at 413 nm were observed, and the limiting negative anisotropy value of approximately –0.1 in the arrays indicated a relatively large angle displacement between the absorption and emission dipoles upon photoexcitation at 413 nm, though this value is still smaller than the orthogonal orientation anisotropy value of –0.2. On the other hand, the positive anisotropy values from 450 to 500 nm, which corresponds to the low-energy Soret band. The anisotropy values above ~450 nm for **Z*n*** become larger and reach the maximum at **Z16** and then decrease in the longer arrays. The maximum anisotropy value of ~0.3 above ~450 nm in **Z16**, which is still slightly smaller than 0.4 for perfect in-plane orientation between absorption and emission dipoles, indicates a nearly parallel alignment between absorption and emission dipoles upon photoexcitation at the low-energy exciton split Soret and Q-bands. These features indicate that the overall geometries of Zn remain as linear form as Zn is shorter than **Z16** and start to deviate from a linearity in overall geometry for > **Z16**.

The fluorescence anisotropy decay, $r(t)$, offers detailed information on the diffusive motions of the chromophores [86-88]. The $r(t)$ exhibits multiexponential decay rates due to anisotropic rotations with respect to asymmetric molecular axis in the porphyrin arrays. The overall anisotropy decay rate is summarized in Table 2, which indicates that the overall decay rate of the longer array becomes slower.

Porphyrin monomer is a disk-like molecule and one may expect the in-plane rotations to be much easier than the out-of-plane rotations. The out-of-plane motion requires the displacement of solvent molecules. The in-plane rotations probably require less displacement of the solvent and are expected to be more rapid. Thus, upon increasing the number of porphyrin molecules, these oligomers become non-symmetric and one can expect unequal rotational rates in specific directions: the molecular rotation perpendicular to the long axis should experience more restriction from the surrounding solvent

molecules but the in-plane rotational contributions to the overall rotational diffusion motion is less influenced by the increase of chain length (Table 2).

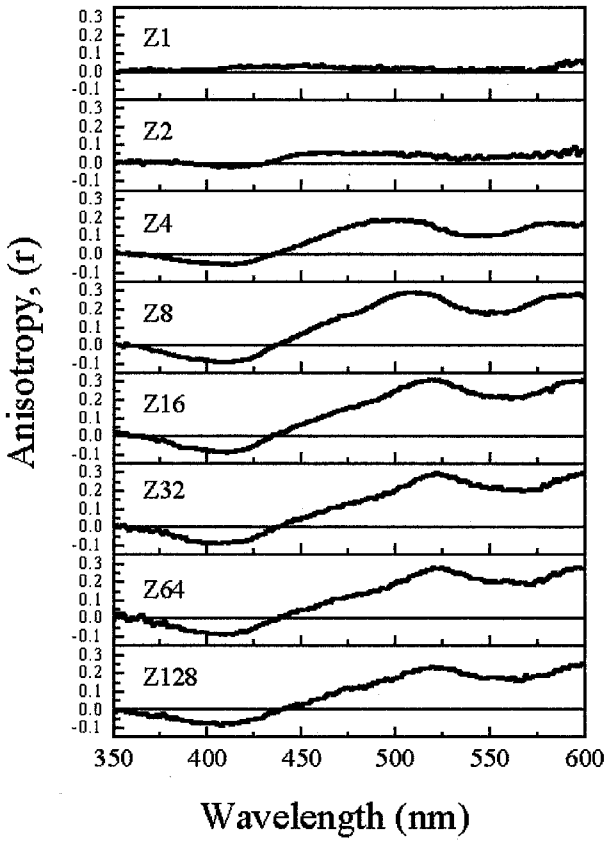

Figure 3-10. A series of steady-state fluorescence excitation anisotropy spectra of ***Zn*** in THF.

3-2-4. Coherent Length of the Porphyrin Arrays

In low-dimensional molecular assemblies like J-aggregates and photosynthetic antenna system, the exciton delocalization length has been the central issue, featuring the number of molecules over which the exciton's wavefunction is spread [89,90]. The length is determined by the competition between the intermolecular excitation transfer interactions and static disorder imposed by the environment (random solvent shift). The excited state of the ideal aggregate with neither static nor dynamic energy fluctuations is delocalized over the full aggregate, at least as far as the wavelength of the light is longer than the physical dimensions of the aggregate. In real systems, however, there is always some static disorder of single-molecule energies (spectral inhomogeneity) and/or intermolecular couplings. This leads to a distribution of molecular energies that tend to localize the elementary excited state of the system, and hence the effective aggregate size N does not correspond any longer to the physical size of the system. Furthermore, at room temperature, the molecular energies and interactions are subject to random fluctuations caused by the solvent bath. This dynamic disorder will further localize the excited state.

In order to estimate the coherent length in the porphyrin arrays investigated in this work, the natural radiative lifetimes are plotted in Figure 3-11 as a function of the number of porphyrin units in the arrays according to the relationship of $\tau_0 = \tau / \Phi$ where τ_0, τ and Φ are natural radiative lifetimes, fluorescence lifetimes and fluorescence quantum yields of the porphyrin arrays, respectively [91,92].

Since the natural radiative lifetime is expected to be proportional to the exciton coherent length (N units), the crossing point value of approximately 4-6 porphyrin units in this plot seems to be the best estimation of the coherence length in these porphyrin arrays. This coherence length seems similar or slightly longer than that in LH1 and LH2 complexes, which has been estimated to be about four bacteriochlorophyll units. A slightly longer coherence length in linear porphyrin arrays is probably due to the covalent direct linkage between the adjacent porphyrins with a shorter center-to-center distance of ~ 8.4 Å as compared with longer center-to-center distance of ~ 20 Å between the nearest neighboring bacteriochlorophyll units embedded in protein matrix in LH1 and LH2 antenna complexes. Despite these situations, it is interesting to note that each porphyrin in the arrays behaves as an individual separate chromophore.

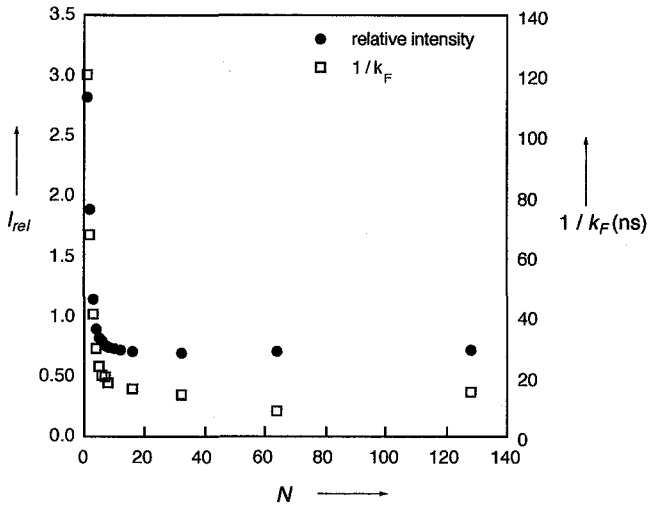

Figure 3-11. Plots of the inverse of k_F (□) and the relative fluorescence intensity (●) of two peaks versus the number of porphyrins (N).

3-2-5. Other Decay Processes of the Porphyrin Arrays

Like the exciton-exciton annihilation in the J-aggregates, the initial fast decay components of 1-4 ps time constants observed in longer porphyrin arrays under the high photoexcitation density are believed to arise from the same process (Figure 3-12). The initial fast decay components become increasingly manifest in longer porphyrin arrays than **Z8** with an increase in the photoexcitation density. In the case of shorter porphyrin arrays than **Z4**, however, the temporal profiles remain relatively unchanged upon increasing the photoexcitation density, indicating that the exciton delocalization length is longer than four porphyrin units. The subsequent decay/rise components of approximately 20-30 ps time constants are believed to arise from the conversion of nonorthogonal S_1-state conformers to a perfectly orthogonally arranged emitting state of the porphyrin arrays. The contribution by the conformational heterogeneity of this series of samples to these processes is not so significant as indicated by the relatively small amplitudes of these components in the porphyrin arrays. But such contribution becomes larger as the number of porphyrin units in the arrays increases. This feature indicates that the conformational heterogeneity with respect to dihedral angle between the adjacent porphyrins become more manifest in longer porphyrin arrays.

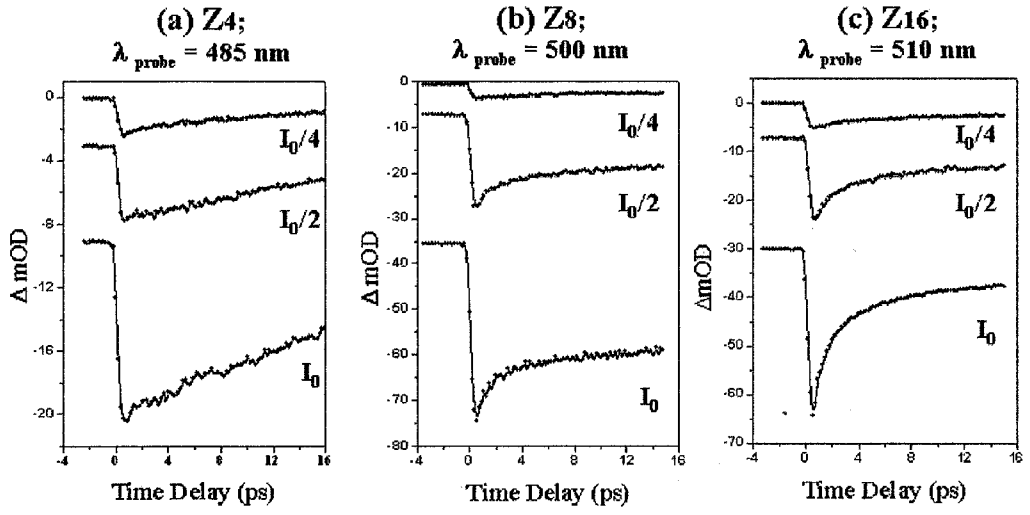

Figure 3-12. Photoexcitation density dependence on the transient absorption decay profiles for (a) **Z4**, (b) **Z8**, and (c) **Z16**.

3-3. Electrochemical Properties of *meso-meso* Linked Porphyrin Arrays

The one electron oxidation potentials of the Zn^{II} *meso-meso* linked porphyrin arrays are also an important parameter for their functions as well as for understanding the mechanism of the Ag^{I}-promoted *meso-meso* coupling. Therefore, the electrochemical properties, particularly the one-electron oxidation potentials, were studied by cyclic voltammetry (CV) in dry $CHCl_3$ containing 0.1 M tetrabutylammonium tetrafluoroborate (n-Bu_4NBF_4) as a supporting electrolyte. At the present stage, waves associated with electrochemical reduction could not be measured precisely in our hands. The cyclic voltammograms of the Zn^{II} porphyrin arrays are shown in Figure 3-13.

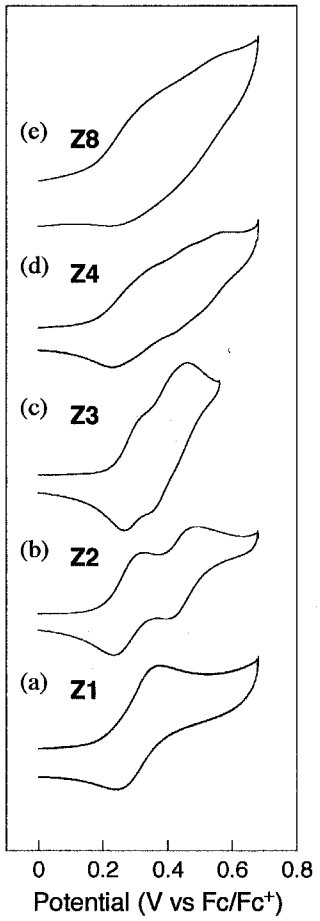

Figure 3-13. Cyclic Voltammograms (vs Fc/Fc^+) for the oxidation of (a) **Z1**, (b) **Z2**, (c) **Z3**, (d) **Z4**, (e) **Z8** in $CHCl_3$ using Pt working electrode and 0.1 M n-Bu_4NBF_4 as a supporting electrolyte.

The monomer **Z1** undergoes a reversible first oxidation at 0.31 V versus

ferrocene/ferrocenium, while two reversible oxidation waves at 0.28 and 0.43 V in **Z2** are detected, which have been assigned as split first oxidation waves (one electron per porphyrin) as judged from the results of other electronically coupled diporphyrins. This split one-electron oxidation for each Zn^{II} porphyrin should arise from the influence of a positive charge of first generated Zn^{II} porphyrin cation radical. E_{OX1} of **Z2** was similar to E_{OX1} of **Z1**, indicating the HOMO in **Z2** is close to that in **Z1**, while E_{OX2} was slightly higher than E_{OX1} of **Z1**. The one-electron oxidation potential of **Z3** was detected at 0.29 V but the first oxidation potential waves of **Z4** and **Z8** could not be peaked out clearly. Despite the poorly resolved voltammograms, it is possible to assign the first one-electron oxidation around 0.3 V for **Z4** and **Z8**. Therefore, it may be concluded that these Zn^{II} porphyrin arrays ***Zn*** have nearly the same first one-electron oxidation potentials that are independent of the number of the porphyrin rings. These data support one's predicted reaction mechanism. Thus, the Ag^{I} promoted oxidation might occur at each porphyrin array with the equal probability so that the coupling reactions proceed smoothly at all stages.

3-4. ESR Spectra of *meso-meso* Linked Porphyrin Arrays

When a Zn^{II} 5,10,15,20-tetraphenylporphyrin is oxidized to its radical cation, the corresponding a_{2u} orbital becomes a magnetic orbital (Figure 3-14) [93]. High *meso-meso* coupling regio-selectivity observed for *meso-meso* coupling observed for zinc(II) 5,15-diarylporphyrins may be related with their favorable a_{2u} HOMO in which the electron density at the *meso* carbons is much larger than at the β-pyrrole carbons (Figure 3-14). Thus, when $\mathbf{Z_0 1}$ is oxidized to the radical cation, the corresponding a_{2u} orbital becomes the magnetic orbital. Such a cation radical will be attacked by a neutral Zn^{II} porphyrin molecule at its *meso*-position, which is in this case the most nucleophilic site. To experimentally confirm their orbital characteristics, the EPR detection of the cation radicals of $\mathbf{Z_0 1}$ by using a simple two-electrode cell for EPR measurements [94] was examined. At a potential of 1.6 V to the counter electrode, electrooxidation proceeded to give the ESR spectrum at g = 2.0055 assignable to the cation radical of $\mathbf{Z_0 1}$ that was coupled with four equivalent nitrogens with a_N = 1.5 G (Figure 3-15). This indicated that one electron was removed from a_{2u} orbital in $\mathbf{Z_0 1}$.

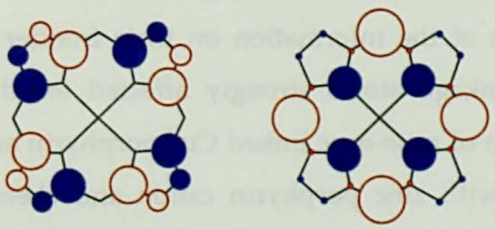

Figure 3-14. Schematic presentation of the two HOMOs, a_{1u} and a_{2u}, of the D_{4h} porphyrin ring.

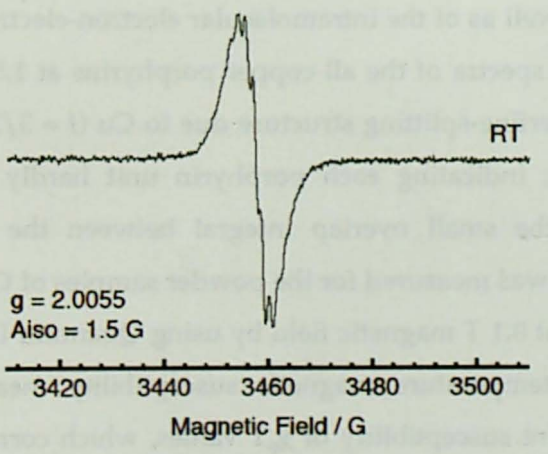

Figure 3-15. ESR spectra of $\mathbf{Z_0 1}$ cation radical formed by electrochemical oxidation.

From a mechanistic point of view, the anodic electrochemical oxidation is of particular interest, since the coupling regio-selectivity was found to vary depending upon the central metal ion.

In sharp contrast to the Zn^{II} porphyrins, Cu^{II}, Pd^{II}, and Ni^{II} 5,15-diarylporphyrins afforded the corresponding *meso-β* directly linked diporphyrins exclusively [95,96]. Interestingly, these porphyrins have been known to favor the a_{1u} HOMO in which the *meso* carbons become four nodes, resulting in larger electron density at the *β*-pyrrole carbons relative to the *meso* carbons (Figure 3-14). Therefore, the results from the electrochemical oxidation reactions are in line with the proposed mechanism involving the initial one-electron oxidation of metalloporphyrin followed by nucleophilic attack of a neutral metalloporphyrin at the *meso* carbons.

On the other hand, spin correlation in π-conjugated molecules has recently merited attention in the field of spin chemistry [97,98]. To achieve a ferromagnetic interaction between the radicals in π-conjugated molecular systems, the molecular topology is widely adopted into their molecular design. Recently Segawa *et al.* show that the π-polyradical of directly *meso-meso* linked and *meso-β* linked Zn^{II} porphyrin oligomers were generated by chemical oxidation, which resulted in the spin allinment [99]. These experiments are also intriguing in terms of the information on their frontier orbital, since the overlap integral between the linkage atoms strongly affected for their electronic interaction. Thus the spin correlation of *meso-meso* linked Cu^{II} porphyrin arrays **C*n***, which are totally *iso*-electronic structure with zinc porphyrin cation and chemically stable and easy to handle but are not the same frontier orbital, was checked. **C*n*** were synthesized from corresponding free base porphyrin arrays. Figure 3-16 shows the ESR spectra and SQUID of **C2**-**C5**. The ESR spectroscopy provides definitive information about the electronic structure as well as of the intramolecular electron-electron interactions in these compounds. The ESR spectra of the all copper porphyrins at 1.5 K were observed as a single peak with a hyperfine-splitting structure due to Cu (I = 3/2, g = (2.08171, 2.08171, 2.18900), a_{cu} = 214 G), indicating each porphyrin unit hardly penetrates each other probably because of the small overlap integral between the Cu porphyrins. The magnetic susceptibility was measured for the powder samples of **C*n*** with the temperature range from 2 to 300 K at 0.1 T magnetic field by using Quantum Design MPMS-7 (Figure 3-16). The variable temperature magnetic susceptibility measurements revealed a temperature-independent susceptibility of $\chi_p T$ values, which corresponds to the $S = n \times 1/2$, being consistent with the independent porphyrin structure at their ground states.

Consequently, in contrast to the case of the zinc porphyrin π-cation radical, complete localization of unpaired electron is observed in the copper porphyrin arrays, suggesting that the strength of the intrapoprhyrin electronic interaction is controllable by central metals and redox states.

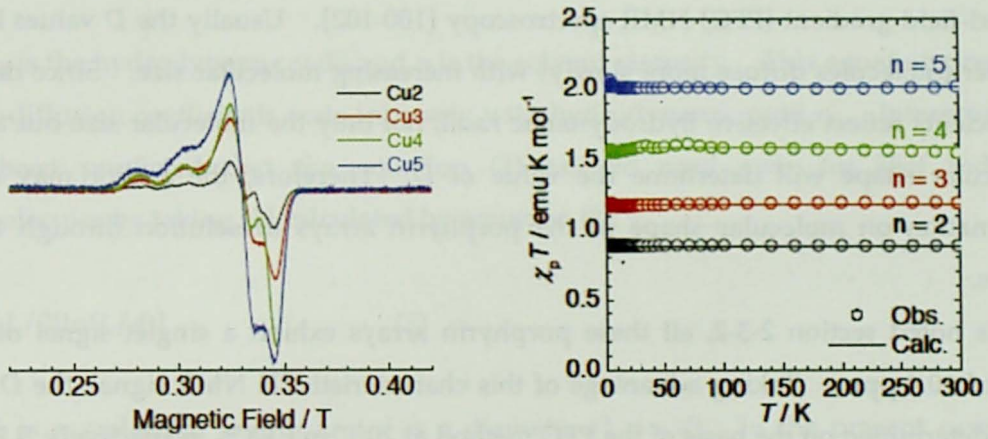

Figure 3-16. (a) ESR spectra of C2-C5 at 1.5 K. (b) The magnetic susceptibility measured by SQUID.

3-5. Conformational Investigation by means of Pulsed-Field-Gradient (PFG) NMR Spectroscopy

To get information on the molecular motion of *meso-meso* linked Zn^{II} porphyrin arrays in solution, the self-diffusion coefficients (*D*) were measured on the basis of the pulsed-field gradient (PFG) NMR spectroscopy [100-102]. Usually the *D* values become smaller (molecules diffuse more slowly) with increasing molecular size. Since diffusion coefficients reflect effective hydrodynamic radii, not only the molecular size but also the molecular shape will determine the value of *D*. Therefore, the author may acquire information on molecular shape of the porphyrin arrays in solution through their *D* values.

As noted section 2-3-2, all these porphyrin arrays exhibit a singlet signal of H^m at around 10.4 ppm. Taking advantage of this characteristic ^1H NMR signal, the *D* values were determined on the basis of the PFG method at 20°C in $CDCl_3$, respectively, 9.7×10^{-10} m^2/s for **Z3**, 3.4×10^{-10} m^2/s for **Z8**, 1.3×10^{-10} m^2/s for **Z20**, 1.2×10^{-10} m^2/s for **Z24**, and 8.3×10^{-11} m^2/s for **Z48**. Thus, it has been actually shown that the *D* values become smaller with increasing molecular length (Figure 3-17).

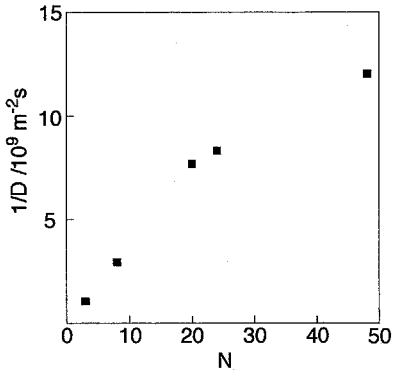

Figure 3-17. Self-diffusion coefficients *D* versus the number of porphyrin units.

The information of the porphyrin arrays in solution may be gained from their self-diffusion coefficients (*D*). The Stokes-Einstein equation relates *D* to molecular parameters:

$$D = k_B T / f \qquad (1)$$

where k_B is the Boltzmann constant, T is the absolute temperature, and f is the frictional coefficient, a measure of the forces that retard molecule's motion. For a spherical particle the frictional coefficient is given by

$$f = 6\pi\eta r_H \qquad (2)$$

where r_H is the hydrodynamic radii and η is the solvent viscosity. This equation predicts that self-diffusion coefficients scale inversely with hydrodynamic radii r_H. Interestingly, it has been predicted that the equation (2) can be used even for stiff rod-like macromolecules by taking rH calculated by equation (3):

$$r_H = L/2[\ln(L/d)] \qquad (3)$$

where L is a molecular length and d is a diameter ($L >> d$). In the present case, the molecular length of ***Zn*** can be precisely predicted by the number of porphyrins, provided their linear rod-like conformations in solution. Given d = 10 Å, the D value leads to estimation of effective L = 170 Å for **Z20** and 192 Å for **Z24**. This estimated is consistent with the calculated structures.

The rotational correlation time of the molecule (θ) is given by

$$\theta = \eta V/\mathrm{RT} \qquad (4)$$

where R is the gas constant and V is the volume of the rotating unit. And the rotational correlation time is also related to the diffusion coefficient by $\theta = (6D)^{-1}$. Since the rotational diffusion time τ_{rot} is the rotational correlation time per molecule, τ_{rot} is given by

$$\tau_{rot} = \eta V/k_B\mathrm{T} \qquad (5)$$

Because the rotational diffusion time can be measured by the fluorescence anisotropy decay, we also can obtain similar information on the self-diffusion processes of ***Zn*** in solution to PFG NMR measurements. As a consequence, as the array becomes longer, the slower fluorescence anisotropy decay times were observed mainly due to an increase in molecular hydrodynamic volume caused by an increase in the total length of ***Zn***.

3-6. Summary

The directly linked porphyrin arrays up to 1024 porphyrin units connected together linearly were successfully isolated and their photophysical properties depending upon the length of the arrays were investigated by various time-resolved laser spectroscopic methods. Characteristically, ***Zn*** exhibit large splitting of Soret bands due to strong exciton coupling. With increase in the number of porphyrins, the low-energy Soret band is shifted to longer wavelength, while the high-energy Soret band remains at nearly the same position, resulting in a progressive increase in the splitting energy. The observed Soret band splitting can be well described by exciton coupling theory. The energy differences between high- and low-energy Soret bands become larger as the array becomes longer, showing asymptotic feature (ΔE = ~4250 cm^{-1}). On the other hand, the band shifts in the Q-bands are not so significant, but showing a gradual increase in their intensities. A plot of the molar extinction coefficients of ***Zn*** as a function of the number of porphyrin units exhibits a good linear correlation, indicating the higher absorptivity as the array becomes longer. In other words, each porphyrin moiety in the array acts as an independent light absorbing unit.

The directly-linked porphyrin arrays would be the closest artificial light harvesting array to the natural photosynthetic organisms, providing that these arrays are the most suitable synthetic molecular modules for the realization of molecular photonic devices based on the porphyrin arrays. In the fabrication of molecular photonic devices, the rigid rod-like structure should be useful because the implementation of such molecules can be done in a more predictable manner. From a viewpoint of functional requirements, the arrays should have the very regular pigment arrangements which allow a facile incoherent hopping but does not result in the alteration of photophysical properties of the individual pigment leading to formation of so-called energy sink. In these respects, the present *meso-meso* linked porphyrin arrays are ideal, since they maintain the orthogonality between the adjacent porphyrin units, and consequently the conformational heterogeneity should be minimized. Overall, the regularly arranged porphyrin arrays with ample electronic interactions will be promising as a light-harvesting photonic wire by transmitting singlet excitation energy rapidly over the array. The initial exciton migration process has revealed by measuring the ultrafast anisotropy dynamics. The internal conversion process is accompanied by the incoherent energy hopping processes as evidenced by a large change in the anisotropy value at the initial stage of the transient

absorption spectra.

Chapter 4. New Synthetic Method of *meso-meso* Linked Porphyrin Arrays by Using Palladium-Catalyzed Suzuki-Miyaura Coupling Reaction [46]

In this Chapter, a new synthetic method of *meso-meso* linked porphyrin arrays of a variety of compositions and connectivities by Pd-catalyzed cross-coupling reaction in a complementary manner to Ag^{I}-promoted oxidative coupling was roported.

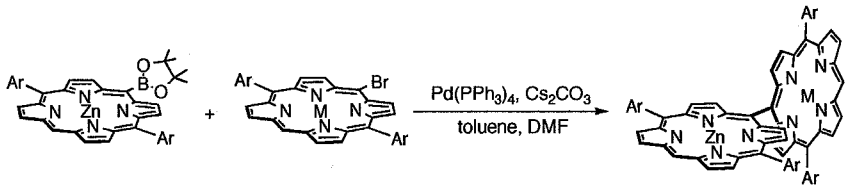

4-1. Introduction

Covalently linked multi-porphyrinic molecules have been attracting continuous attention in relation to the understanding and duplication of electron and/or energy transfer in the natural photosynthetic systems as well as the development of novel functional materials [103]. Among these, *meso-meso* linked porphyrin arrays possess an unique position, in that they are directly linked and are favorable for achieving rapid energy- and electron-transfer reactions owing to a short center-to-center distance (ca. 8.4 Å), large Coulombic interaction, and a nearly orthogonal conformation that minimizes conjugation of neighboring porphyrins, making a state-to-state dynamic energy- and/or electron-transfer process feasible without causing serious electronic delocalization [104].

Ag^{I}-salt promoted oxidative *meso-meso* coupling reaction of 5,15-diaryl Zn^{II} porphyrins has been shown to be particularly effective in making homogenous porphyrin arrays, which was highlighted by the synthesis of a discrete 1024-mer with ca. 1,000,000 Da molecular weight and 0.8 μm molecular length in its straight form. Unfortunately, however, this method is not applicable to the preparation of heterometal-mixed diporphyrins such as Zn^{II} free-base diporphyrin **ZH**, which was therefore prepared in 6% yield from partial metallation of bis free-base porphyrin **H2** (Scheme 4-1) [104]. The low yield was mainly due to nonselective metallation and very similar chromatographic eluting properties of **H2, ZH,** and **Z2.**

Therefore, the author deveroped a new synthetic method of *meso-meso* linked porphyrin arrays of a variety of compositions and connectivities by using Pd-catalyzed cross-coupling reaction in a complementary manner to Ag^{I}-promoted oxidative coupling. This strategy results in the preparation of a varaiety of porphyrin arrays.

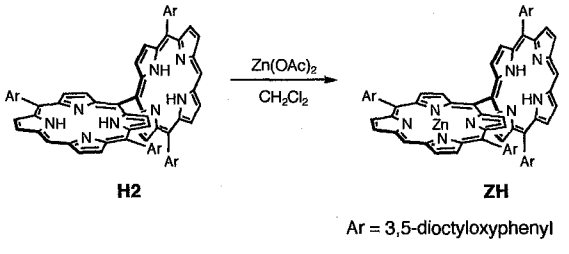

Scheme 4-1. Partial metalation synthesis of Zn^{II} free-base diporphyrin **ZH.**

4-2. Pd-catalyzed Cross-Coupling Reaction for the Formation of *meso-meso* Linked Porphyrin Arrays

Scheme 4-2 shows Pd-catalyzed coupling strategy for the synthesis of *meso-meso* coupled hybrid porphyrin arrays. Porphyrin boronate **8** was prepared in 90% yield from *meso*-bromoporphyrin **9** by coupling with pinacol borane [67b,105]. Cross-coupling of **8** and **9** was carried out in a mixture of toluene and DMF in the presence of a catalytic amount (~10mol%) of $Pd(PPh_3)_4$ and 1.5 equiv. of Cs_2CO_3 at 80°C under an inert atmosphere to give **ZH** in 54% yield. In marked contrast to the partial metallation route, isolation of **1** was easy on a size-exclusion chromatography (SEC) owing to a molecular weight difference between the diporphyrin product and the starting materials. The Zn^{II}-free base hybrid **ZH** thus prepared exhibited the identical properties with the diporphyrin product prepared from the partial metallation of **H2**. Similarly, Zn^{II}-Ni^{II} hybrid diporphyrin **ZN** was prepared in 57% yield.

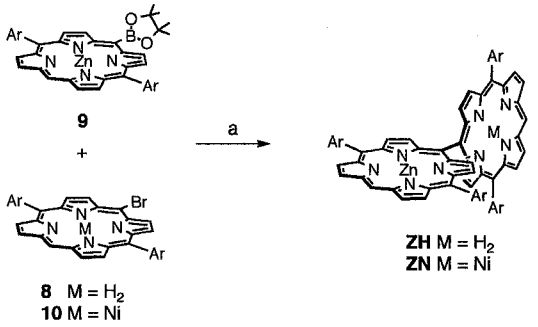

Scheme 4-2. Cross-coupling synthesis of **ZH** and **ZN**. Reaction conditions: (a) $Pd(PPh_3)_4$, Cs_2CO_3, toluene, DMF, 80°C, 3 h, Ar = 3,5-dioctyloxyphenyl.

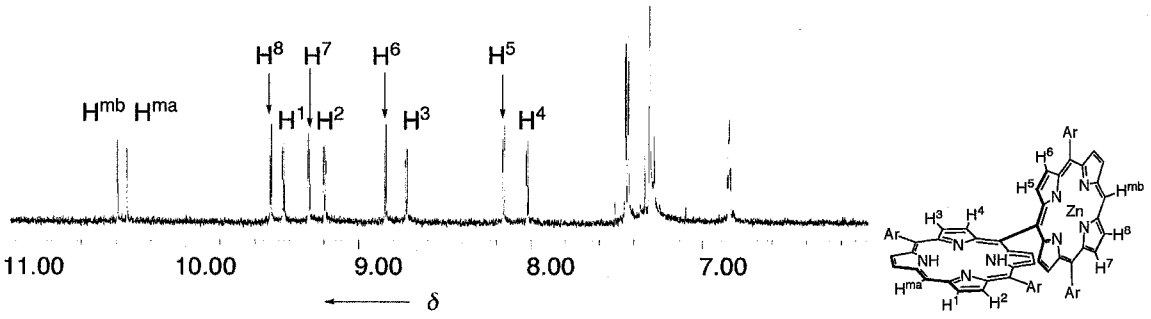

Figure 4-1. ^1H NMR spectrum of **ZH** in $CDCl_3$.

Linear and bent hybrid triporphyrin arrays **13** and **16** were prepared by the coupling

reactions of **11** with **12** and **15** [35g,106] in 45 and 46% yields, respectively (Scheme 4-3). Virtually no scrambling of metallated porphyrin sites during the coupling reaction is notable, since this method allows the synthesis of porphyrin arrays with metallated sites in a predictable manner, which are quite useful for the studies on photo-induced energy and/or electron transfer reactions [103].

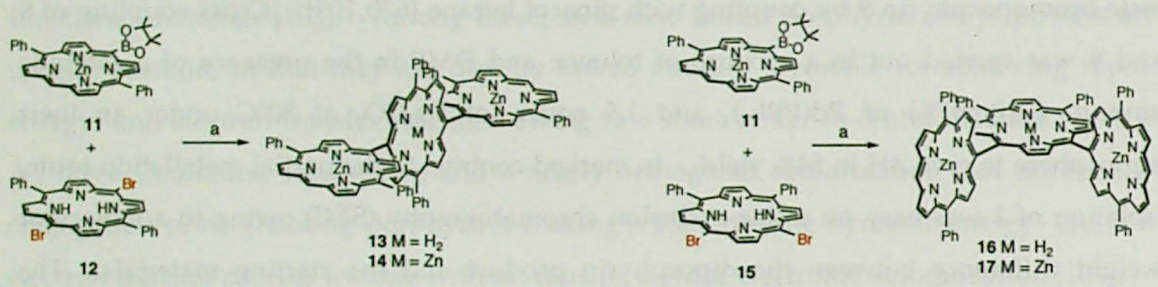

Scheme 4-3. Synthesis of linear and bent hybrid triporphyrin arrays **13** and **16**. Reaction conditions: (a) $Pd(PPh_3)_4$, Cs_2CO_3, toluene, DMF, 80°C, 3 h.

Taking advantage of no scrambling of this coupling, *meso,meso'*-dibromo Zn^{II} porphyrin hexamer **Z6Br$_2$** was reacted with free base porphyrin boronate **18** under the same conditions to give porphyrin octamer **19** (11%) and heptamer **20** (32%) (Scheme 4-4). The products **19** and **20** displayed the parent mass at m/z = 8167 (Calcd for $C_{512}H_{662}N_{32}O_{32}Zn_6$ = 8169) and 7198 (Calcd for $C_{448}H_{578}N_{28}O_{28}Zn_6$ = 7196), respectively, by the MALDI-TOF mass measurements. Analysis of their ^{1}H-NMR spectra revealed the location of free base porphyrins as shown in the Scheme 4-4.

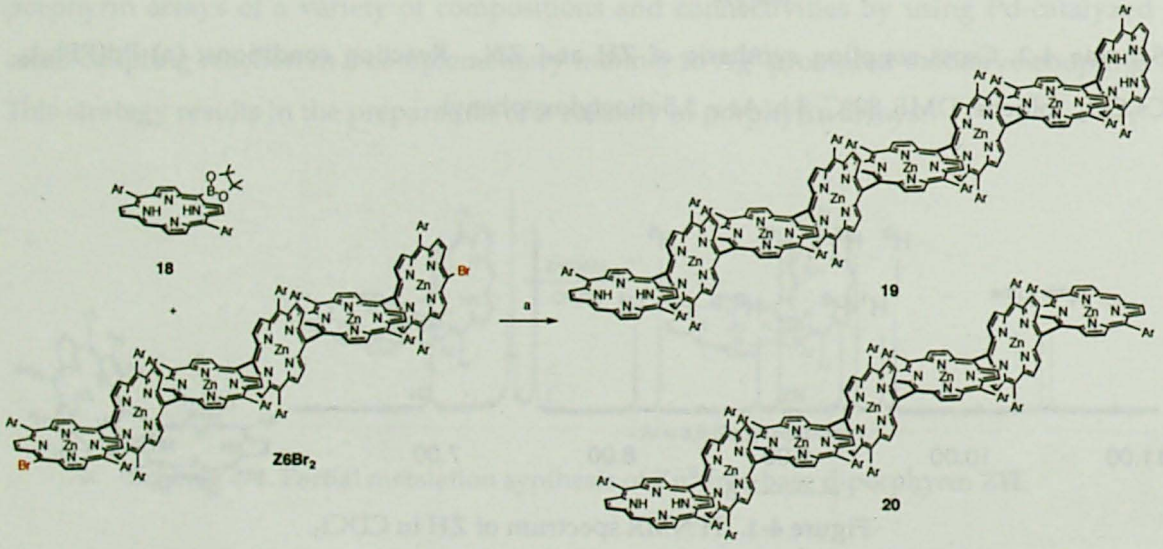

Scheme 4-4. Synthesis of terminal-demetalated long porphyrin arrays **19** and **20**. Reaction conditions: (a) $Pd(PPh_3)_4$, Cs_2CO_3, toluene, DMF, 80°C, 5 h, Ar = 3,5-dioctyloxyphenyl.

After the pioneering work of Sanders and Anderson in 1989 [35e], several cyclic porphyrins have been reported [35], in which each porphyrin is connected by covalent bonds. However, the linkages are only limited to aryl- or alkynyl-based *meso*-groups. Therefore, the electronic interaction between the neighbouring chromophores in the ground state remains small. With the aim of creating a highly electronic interactive cyclic porphyrin arrays, the author applied Pd-catalyzed coupling raction.

The synthetic route is shown in Scheme 4-5. An important key intermediate, 5,10-bis(3,5-dioctyloxyphenyl)porphyrin was prepared in 8% yield [106]. Coupling reactions were performed to 5,10-diaryl-15-bromoporphyrin and 5,15-diboronylated-10,20-dihexyl zinc (II) porphyrin with $Pd(PPh_3)_4$, affording *anti*- and *syn*-triporphyrin. After bromination of *syn*-triporphyrin by NBS, 5,15-diboronated-10,20-dihexylporphyrin was again reacted to give cycloporphyrin 8-mer. Separation of the octamer was successfully achieved using preparative gel permeation chromatography. The simple pattern of ^{1}H-NMR peaks and the absence of *meso* proton peak support the cyclic structure having D_{4h} symmetry (*vide infra*).

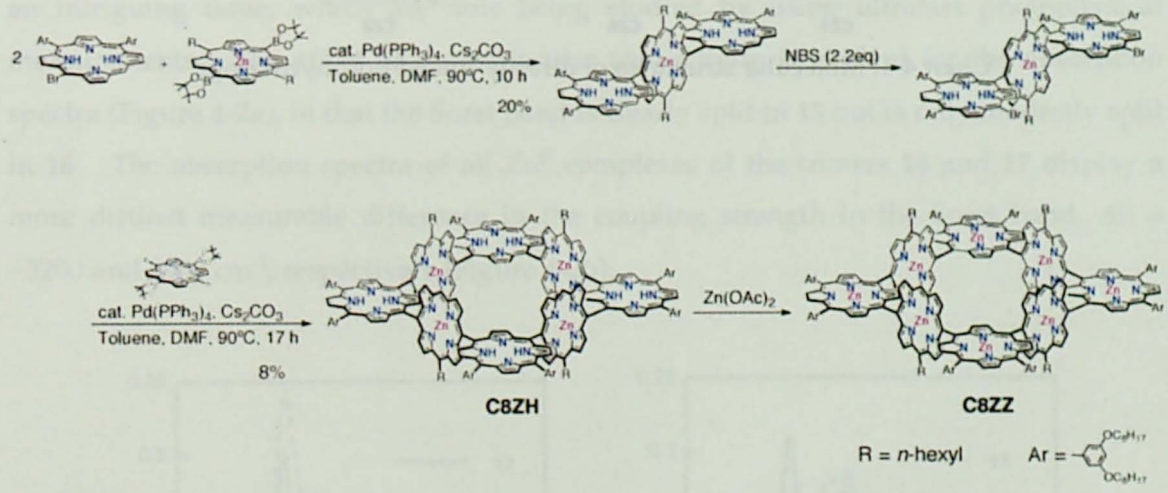

Scheme 4-5. Synthesis of cyclic porphyrin arrays **C8ZH** and **C8ZZ**. R = hexyl. Ar = 3,5-dioctyloxyphenyl.

In the course of this project, when 5,10-diaryl-15-boronated zinc (II) porphyrin and 5,15-dibromo-10,20-dihexylporphyrin (free-base bromide and zinc(II) complex boronated in reverse) was reacted, homo coupling reaction of 5,10-diaryl-15-bromo zinc (II) porphyrin was performed, providing 5,10-diary Zn^{II} porphyrin dimer (Scheme 4-6). This serendipitous formation hit on a good idea of directly *meso-meso* linked porphyrin rings **CZ4**, **CZ6**, and **CZ8** that respectively comprise of four, six, and eight porphyrins which

finally synthesized in a stepwise manner from a 5,10-diaryl zinc(II) porphyrin building block (Chart 4-1) [107].

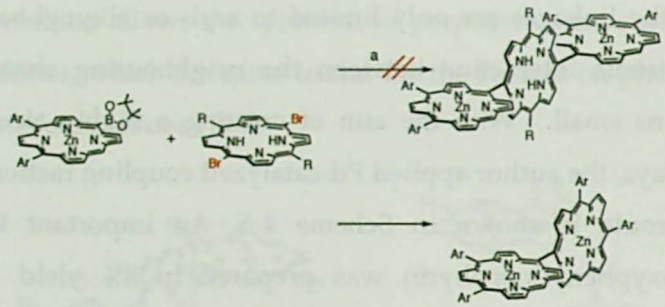

Scheme 4-6. Reaction conditions: (a) $Pd(PPh_3)_4$, Cs_2CO_3, toluene, DMF, 80°C, 5 h. R = hexyl. Ar = 3,5-dioctyloxyphenyl.

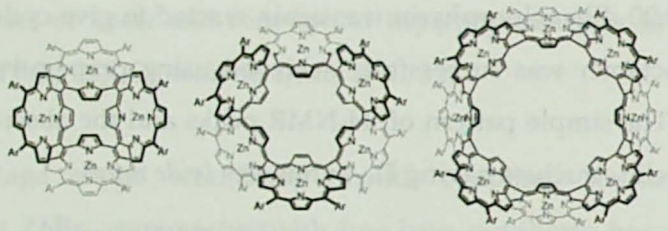

CZ4 CZ6 CZ8

Chart 4-1. Molecular structures of directly-linked porphyrin rings

4-3. Photophysical Properties of Unique Shaped *meso-meso* Linked Porphyrin Arrays

The absorption spectrum of **ZH** is given by a sum of the spectra of Zn^{II}-Zn^{II} dimer (**Z2**) and free-base — free-base dimer (**H2**) rather than the sum of the spectra of Zn^{II} monomer and free-base monomer, indicating that electronic state of *meso-meso* linked porphyrin is strongly perturbed by the exciton coupling not only in the S_2-state but also in the S_1-state. Here, it is noteworthy that in spite of the direct *meso-meso* linkage the excited Zn^{II}-porphyrin and free base porphyrin can be treated as an individual separate state owing to orthogonal conformation, thus allowing an extremely rapid state-to-state energy transfer in **ZH** in THF.

The similar energy transfer is also suggested for both **13** and **16**, since the fluorescence emission is coming only from the free-base porphyrin even upon irradiation at 556 nm that corresponds to the predominant excitation of the peripheral Zn^{II}-porphyrins. The effect of the molecular connectivity, e.g. *straight versus bent*, on the energy transfer rate is an intriguing issue, which are now being studied by using ultrafast photophysical measurements. The effect of the molecular connectivity is evident for the absorption spectra (Figure 4-2a), in that the Soret band is clearly split in **13** but is only modestly split in **16**. The absorption spectra of all Zn^{II} complexes of the trimers **14** and **17** display a more distinct measurable difference in the coupling strength in the Soret band, ΔE = ~3200 and 2400 cm^{-1}, respectively (Figure 4-2b).

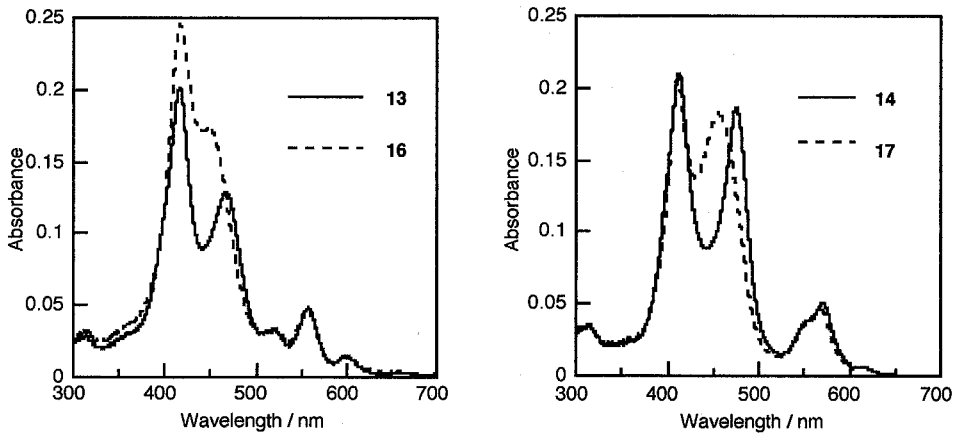

Figure 4-2. UV-vis spectra of linear and bent-shaped porphyrin arrays in THF.

It is appropriate to place two transition dipole moments of each porphyrin unit as

shown in Figure 4-3. It is expected that the exciton coupling of three transition dipoles ($M_{X1}+M_{X2}+M_{X3}$) is possible but the other interactions should be zero in **14**, while the degenerate two exciton couplings ($M_{X1}+M_{X2}$ and $M_{Y2}+M_{Y3}$) are possible but the other interactions should be zero in **17**. Non-interacting transition dipoles would result in unperturbed Soret band at the same position as the porphyrin monomer. It is likely that the ratio of interacting (parallel) to noninteracting (perpendicular) components is reflected on the relative oscillator strength of split Soret bands.

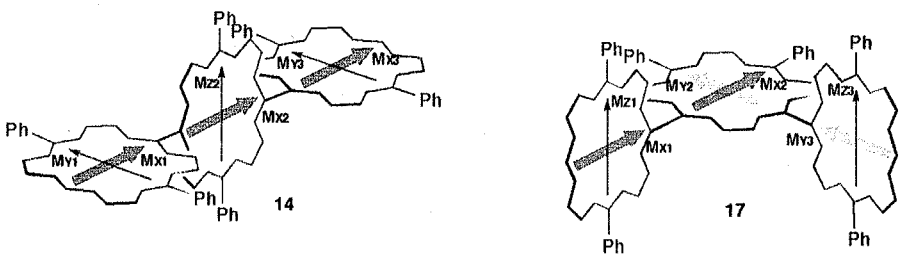

Figure 4-3. Schematic representations of transition moments in the linear- and bent-shaped porphyrin trimers.

In the steady-state fluorescence spectra of **19** and **20** in THF, the fluorescence emissions come predominantly from the free base porphyrin in both cases, indicating the efficient energy transfer from the photo-excited Zn^{II}-porphyrin array to the free base porphyrin end (Figure 4-4). These properties are interesting in light of the use as a photonic molecular wire, since the excitation energy widely captured by a Zn^{II}-porphyrin array is efficiently transmitted uni-directionally to a free base porphyrin.

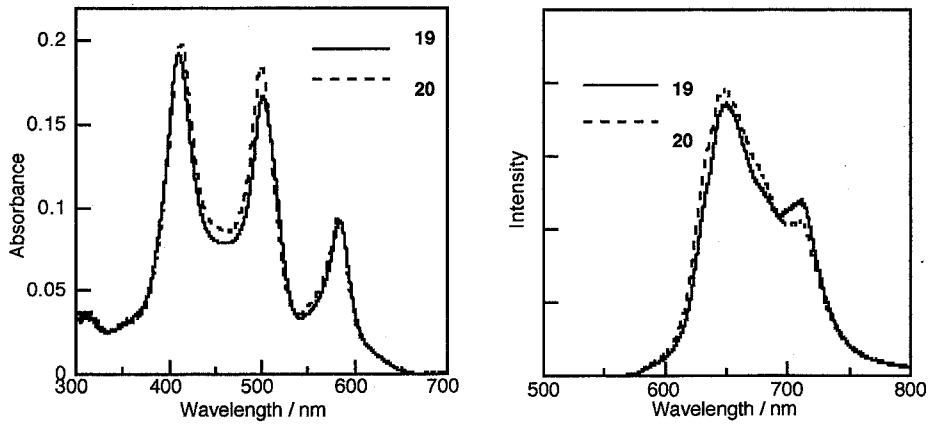

Figure 4-4. UV-vis and fluorescence spectra of *meso-meso* linked zinc(II)-free base hybrid porphyrin long arrays in THF. (a) UV specta of **19** and **20**, and (b) Fluorescence spectra of **19** and **20**upon excitation at 411 nm.

4-4. Challenge to the Giant Conjugated Molecular Ring

Cyclic molecular structures have attained considerable interest as size- and shape-persistent objects [108]. The synthetic strategies are usually based on modular approaches, such as acetylene scaffolding [109] and other repetitive reaction sequences, for example, Suzuki coupling steps to give macrocyclic oligophenylenes [110]. The shape-persistent cyclic oligophenylene rings consisting of 24 phenylene rings with a diameter of about 3 nm from Schlüter and co-workers [110], and the macrocyclic porphyrin hexamer with a diameter of about 4.6 nm from Gossauer and co-workers [35cd] are known to date. Structures with fully conjugated π systems as the periphery are particularly promising candidates, as persistent currents depend on the coherence of the electron wavefunction over the whole ring.

Only few examples of cycles with fully conjugated periphery, such as the cyclic oligothiophenes reported by Bäuerle and co-workers [111], the cyclo[8]pyrrole reported by Sessler and co-workers [112], and the giant molecular cycle with a diameter of about 12 nm, which has acetylene-connected *para*-thiophene and *para*-benzene rings [113], are known to date.

On the other hand, very small cyclic metallic structures (≅ 1 μm) are known to support persistent currents at low temperate by the coherence of electron wavefunctions over the whole ring [114]. However, persistent currents periodic in the enclosed flux have not been observed for organic molecules to date [113]. The macrocyclic model compound has to fulfill certain requirements in size and conjugation. As the magnetic flux Φ, given by the product of the enclosed surface πr^2 multiplied by the magnetic field B ($\Phi = \pi r^2 B$), has to be in the order of the magnetic flux quantum ($\Phi_0 = he^{-1}$) to observe a full oscillation (h being Planck's constant and e being the elementary charge), the radius r needed can be estimated from Equation (1), with B in Tesla.

$$r = \sqrt{\frac{h}{eB\pi}} \qquad (1)$$

The largest static magnetic fields currently available are about 30–40 T. The required radius of a molecular ring structure which may allow the monitoring of a full oscillation of the magnetization in these magnetic fields is according to Equation (1) to be about **6 nm**.

Here, the STM images of **Z48** and **Z128** on the copper substrate (Figure 2-13) make ones imagine that two end porphyrins could be connected by some method to form the huge rings.

Firstly, cyclization reaction of linear oligomers by Ag^{I} method was examined under the high dilute conditions. Unfortunately this attempt was unsuccessful.

The second trial is shown in Scheme 4-7. Two terminal bromo porphyrin **Z48Br$_2$** and boronated porphyrin was reacted with Pd catalyst. After 1 week, new peak appeared in the GPC chart, then isolated (Figure 4-5). The MALDI-TOF mass spectrum exhibits 49 porphyrin components (Figure 4-6) and, in the ^{1}H NMR no *meso* protons were observed (Figure 4-7).

In order to confirm the molecular structure, the STM measurement is currently undergoing.

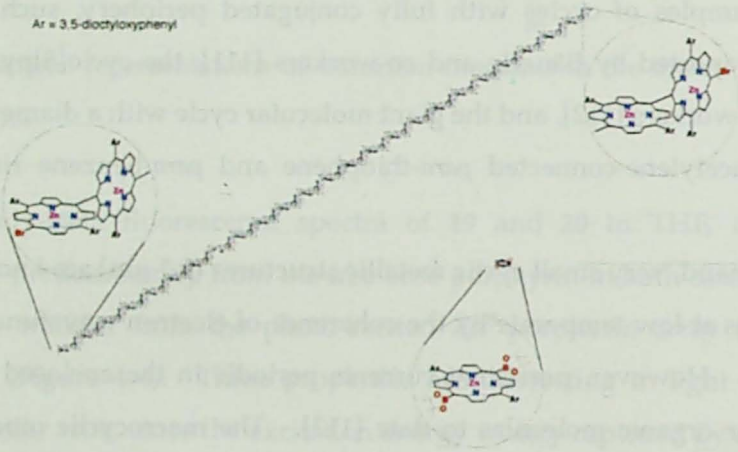

Scheme 4-7. Synthetic scheme of cyclic porphyrin 49-mer.

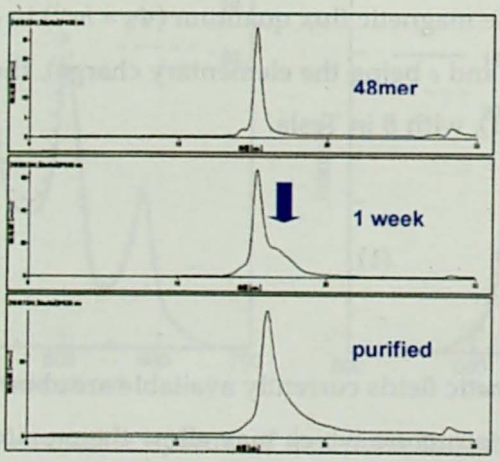

Figure 4-5. Reaction profile traced by GPC.

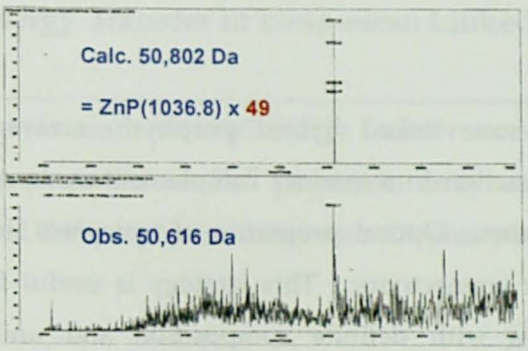

Figure 4-6. MALDI-TOF mass spectrum of isolated product.

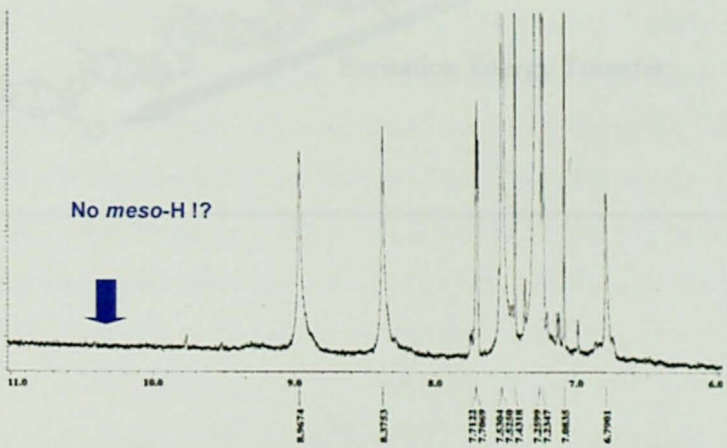

Figure 4-7. ^{1}H NMR spectrum of isolated product.

This compound is expected to have radius of 6.5 nm, fulfilling requirements in size to indicate persistent currents periodic (Figure 4-8).

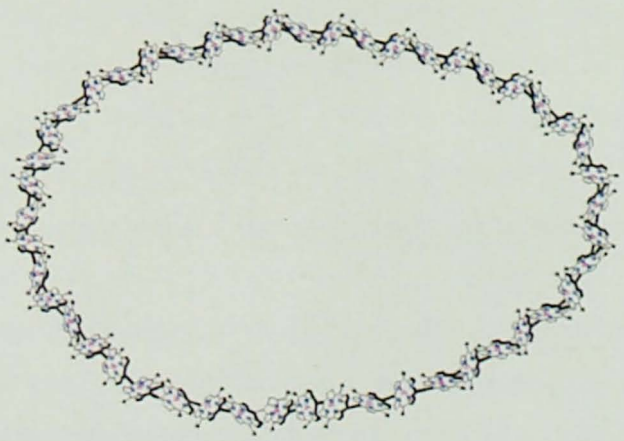

Figure 4-8. A possible structure of isolated product.

4-5. Summary

In conclusion, *meso-meso* linked hybrid porphyrin arrays can be prepared by Pd-catalyzed coupling reaction in a manner complementary to Ag^{I}-promoted oxidative coupling of Zn^{II}-porphyrins. Optical properties of *meso-meso* linked triporphyrins are indeed sensitive to their connectivity. This strategy is useful for the preparations of hybrid porphyrin arrays with definite composition and unique molecular shape, including huge porphyrin rings.

Chapter 5. Excited Energy Transfer in *meso-meso* Linked Porphyrin Arrays[47]

In this Chapter, investigation on a artificial energy transfer model system comprising of an energy donating *meso-meso* linked Zn^{II} porphyrin array and an energy accepting 5,15-bisphenylethynylated Zn^{II} porphyrin linked *via* a 1,4-phenylene spacer is reported. .

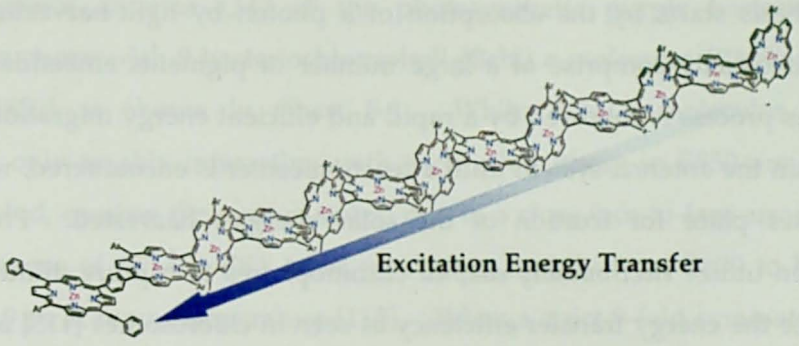

5-1. Introduction

Multi-chromophoric systems based on the porphyrins have attracted an intense attention in relation to the elucidation of the electron and energy transfer in the natural photosynthetic systems as well as the development (or exploration) of molecular devices.

Photosynthesis starts by the absorption of a photon by light-harvesting (antenna) complexes that usually comprise of a large number of pigments embedded in protein matrices. This process is followed by a rapid and efficient energy migration over many pigments within the antenna system until a reaction center is encountered, where charge separation takes place for fixation of the solar energies harvested. Photosynthetic organisms often utilize *electronically coupled* chromophores to capture dilute sunlight as well as enhance the energy transfer efficiency as seen in chlorosomes [115] and LH1 and LH2 in bacterial antenna systems, and phycobilisomes in cyanobacteria and red algae [116]. In these cases, photosynthetic pigments form aggregates whose excitation leads to the formation of excitons with quantum-mechanical coherence extending over many chromophores.

Chart 5-1. X-ray crystal structure of purple bacterial Light-Harvesting Complex II [8].

As mentioned in Chapter 1, numerous artificial molecular architectures based on porphyrins have been explored with the aim of achieving efficient and directed energy transfer. Although some of these studies help understand light-harvesting and energy-transfer phenomena at the molecular level, there is only a limited number of reports on the energy transfer system involving a strongly coupled array of donor or acceptor [117]. Strong electronic coupling (exciton coupling) leads to the alteration of the

absorption and emission properties, hence affecting the EET efficiency. More importantly, unless forming a stacked non-fluorescent energy sink, an electronically coupled array of chromophores may be favorable for the light harvesting antenna function owing to faster EET and a larger absorption cross-section. Such effects have been only scarcely tested in structurally well-defined synthetic models.

The peripheral antenna LH2 of the photosynthetic purple bacteria forms two wheel-like structures with 9 bacteriochlorophyll (Bchl) *a* molecules (B800) and 18 Bchl *a* molecules (B850) as shown in Chart 5-1. While Bchl *a* molecules in B800 are electronically only weakly interacting with each other, those in B850 are electronically strongly coupled, causing the exciton states, due to a close face-to-face arrangement with a Mg-Mg distance of 8.7 Å. EET takes place very rapidly from B800 to B850 within a time of 0.7~0.9 ps at room temperature [118]. When a strict 9-fold symmetry is assumed for B850, optically allowed is only the second lowest exciton state with the lowest exciton state becoming dipole-forbidden [119]. In this situation, it would be difficult to explain the very rapid energy transfer from B800 to B850 within a framework of Förster mechanism, which allows EET only between optically allowed states. The energy-accepting optically allowed state in B850 is located too low from the energy donating B800 state. This optically forbidden lowest exciton state in B850 may be involved in the subsequent EET to LH1 as an energy donor. Recently, Sumi proposed a revised Förster formula for EET that occurs between a donor and an acceptor in a situation where at least one of them is an exciton holding aggregate of chromophores [119]. When the physical size of aggregate is not much smaller than the average donor-acceptor distance, as found quite commonly in natural photosynthetic systems, individual chromophores retain their transition dipoles against the EET partner, even if their overall sum is nearly zero due to the dipole-forbidden nature of an exciton state. This revised formula has explained the rapid EET from B800 to B850 in a satisfactory manner [120].

In this Chapter the author reports the synthesis and EET processes of covalently-linked donor-acceptor systems, **Zn*n*A**; n = 1, 2, 3, 6, 12, and 24, as shown in Schemes 5-1, in which a 5,15-bisphenylethynylated porphyrin acceptor is linked *via* a 1,4-phenylene spacer at the end *meso*-carbon of a *meso-meso* linked Zn^{II} porphyrin array.

Meso-meso linked porphyrin arrays have two free *meso*-positions, which are used for the attachment of the energy-accepting unit. One of the interesting key features is the direct *meso-meso* linkage, which gives rise to substantially large electronic coupling but the

resultant orthogonal conformation of the neighboring porphyrins disrupts the electronic π-conjugation. These properties should be favorable for achieving efficient energy transfer along the array. In addition, the restricted linear geometry of *meso-meso* linked porphyrin arrays avoids the formation of a stacked dimeric energy sink that might disrupt the energy-transfer flow along the array. The linear geometry is also interesting with regard to the topological effect on antenna function [121]. With this background, the excitation energy transfer in **Z*n*A** was examined.

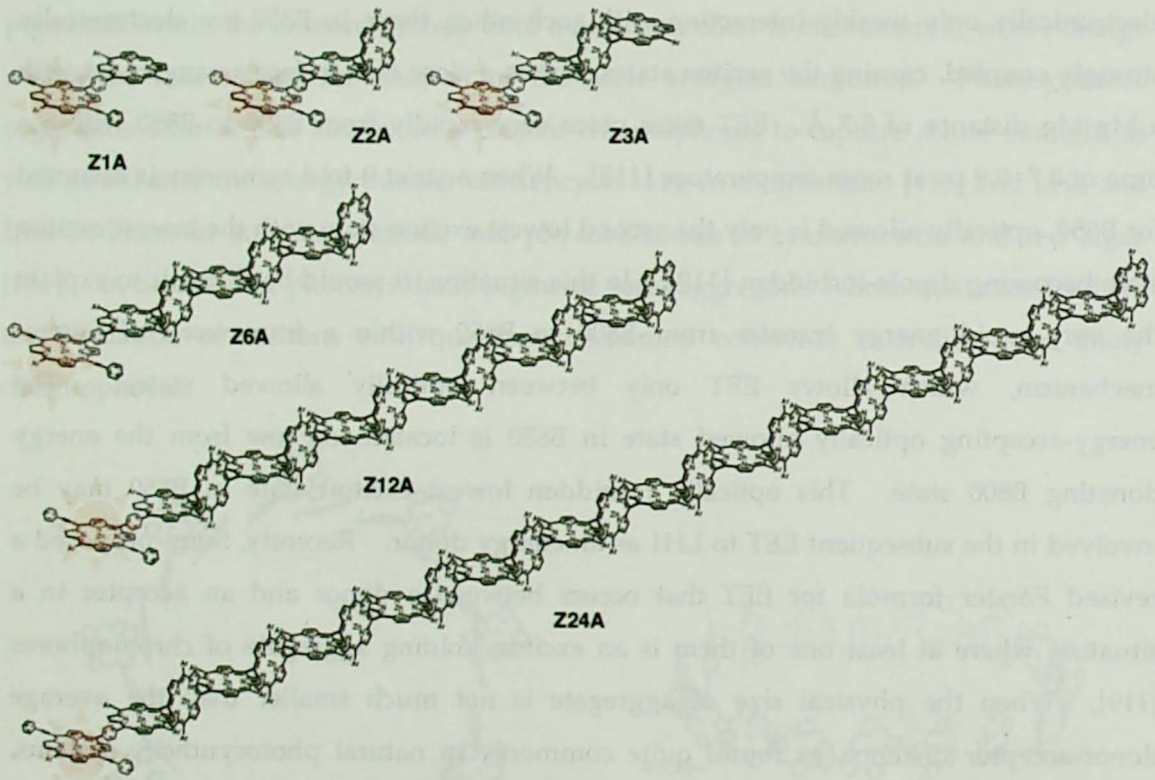

Scheme 5-1. Molecular structures of **Z1A**-**Z24A**. Ar = 3,5-dioctyloxyphenyl.

5-2. Molecular Design and Synthesis

Scheme 5-2 shows the synthetic route. *p*-(4,4,5,5-Tetramethyl-1,3,2-dioxaborolan-2-yl)-benzaldehyde was prepared in 92% yield by pinacol protection of 4-formylphenyl-boronic acid. The porphyrin boronate **21** was prepared in 13% yield from the acid catalyzed condensation of 3,5-dioctyloxybenzaldehyde and the protected boronate with 2.0 equiv. 2,2'-dipyrromethane followed by oxidation with 3 equiv DDQ. Subsequent bromination of **21** with 2.2 equiv. NBS followed by zinc(II) metallation yielded Zn^{II} dibromoporphyrin **22** in 92% yield. Sonogashira coupling of the porphyrin **22** with an excess of phenylacetylene (bis(triphenylphosphine) palladium(II) chloride and CuI, triethylamine / toluene, at 50°C, for 3 h) [122,123] gave 5,15-bisphenylethynylated boronate Zn^{II} porphyrin **23** in 64% yield.

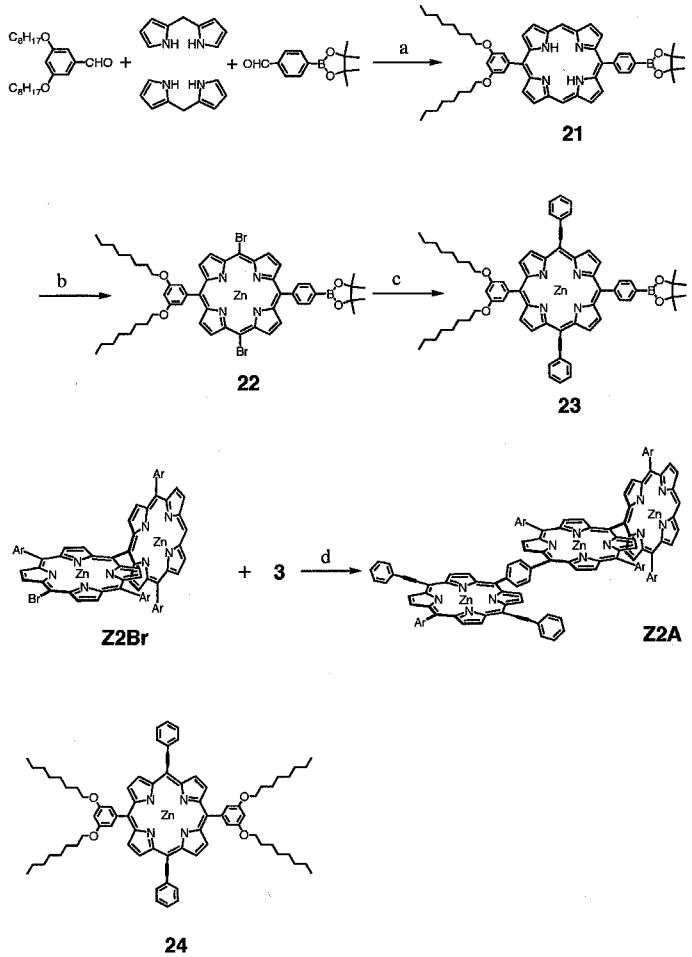

Scheme 5-2. Synthesis of **Z2A**. Ar = 3,5-dioctyloxyphenyl. Conditions: (a) i) TFA, ii) DDQ, 13%; (b) i) $Zn(OAc)_2$, ii) NBS, pyridine, CH_2Cl_2, 92%; (c) phenylacetylene, CuI, $PdCl_2(PPh_3)_2$, triethylamine, toluene, 64%; (d) $Pd(PPh_3)_4$, Cs_2CO_3, DMF, toluene, 76%.

Meso-meso linked Zn^{II} porphyrin arrays **Z2**, **Z3**, **Z6**, **Z12**, and **Z24** were synthesized by the usual Ag^{I}-promoted coupling of 5,15-diaryl Zn^{II} porphyrin **Z1**. Controlled NBS bromination of **Z1**, **Z2**, **Z3**, **Z6**, **Z12**, and **Z24** gave a mixture of *meso*-bromo- and *meso,meso'*-dibromo Zn^{II} porphyrins.

Finally, Suzuki cross-coupling reaction of the porphyrin **23** with **Z1Br**, **Z2Br**, **Z3Br**, **Z6Br**, **Z12Br**, and **Z24Br** (10 mol% $Pd(PPh_3)_4$, 3 equiv Cs_2CO_3, DMF/toluene, at 80°C, for 4 h) gave models **Z1A**, **Z2A**, **Z3A**, **Z6A**, **Z12A**, and **Z24A** in 10~77% yields [46,124,125]. These model compounds have *meso-meso* linked Zn^{II} porphyrin arrays as the energy donor and a 5,15-bisphenylethynylated Zn^{II} porphyrin as the energy acceptor. The latter has been shown to act as an energy acceptor owing to its red-shifted Q band and hence favorable spectral overlap for the energy transfer from *meso-meso* linked porphyrin array.

Models **Z*n*A** were difficult to separate over the usual silica gel column but were obtained in a pure form by using the recycling preparative GPC-HPLC. In the case of **Z24A**, as many as 16 recycling over our GPC-HPLC setup enabled the isolation of pure **Z24A** in 28% (Figure 5-1).

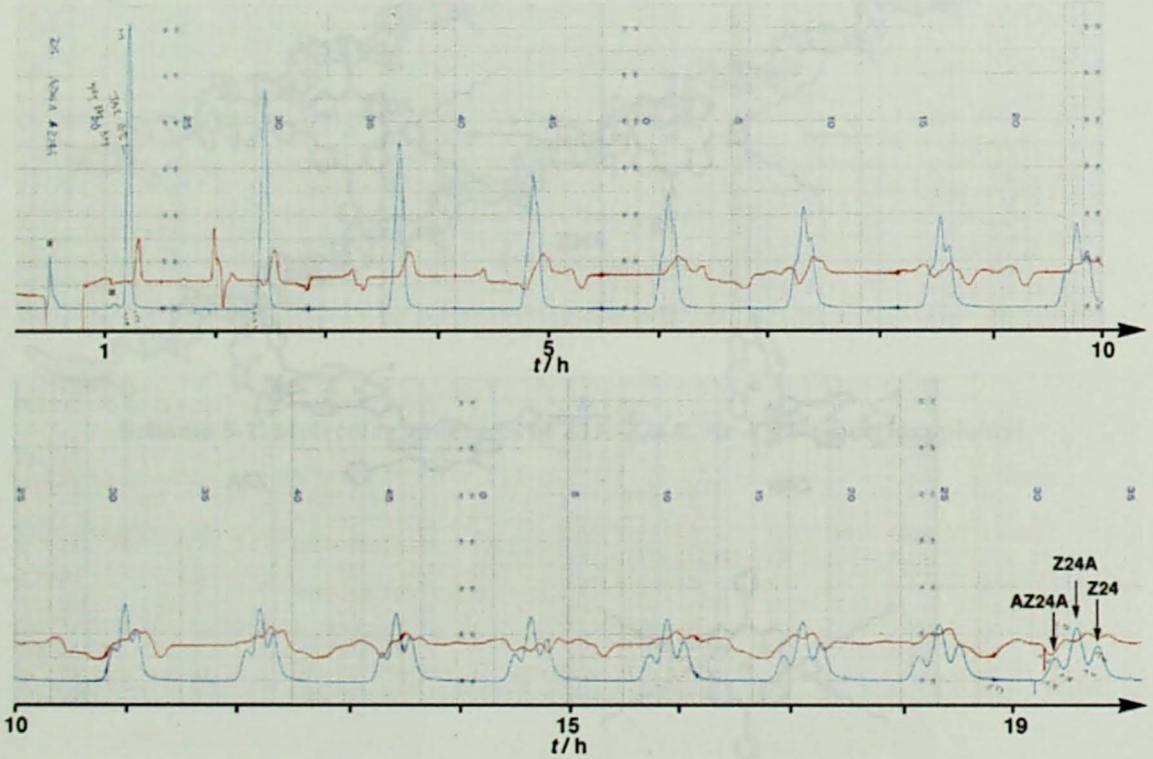

Figure 5-1. The recycling GPC-HPLC chromatogram of the reaction mixture to separate **Z24**, **Z24A** and **AZ24A**. The blue line indicates the UV signal detected at 413 nm. *inpurities.

5,15-Bisphenylethynyl-10,20-bis(3,5-dioctyloxyphenyl) Zn^{II} porphyrin **4** was prepared

as a reference molecule [123]. All new compounds were fully characterized by ^{1}H NMR spectra, FAB or MALDI-TOF mass spectroscopy, UV-vis absorption spectroscopy, and GPC analysis. Among these, the long porphyrin arrays **Z12A** and **Z24A** contain 13 and 25 porphyrin units in a linear fashion with a molecular length of 113 and 217 Å, respectively. The corresponding parent ions were clearly detected at m/z = 13423 (calcd for $C_{832}H_{1044}N_{52}O_{50}Zn_{13}$, 13423.9) and m/z = 25862 (calcd for $C_{1600}H_{2028}N_{100}O_{98}Zn_{25}$, 25865.1) in the MALDI-TOF mass spectra (Figure 5-2).

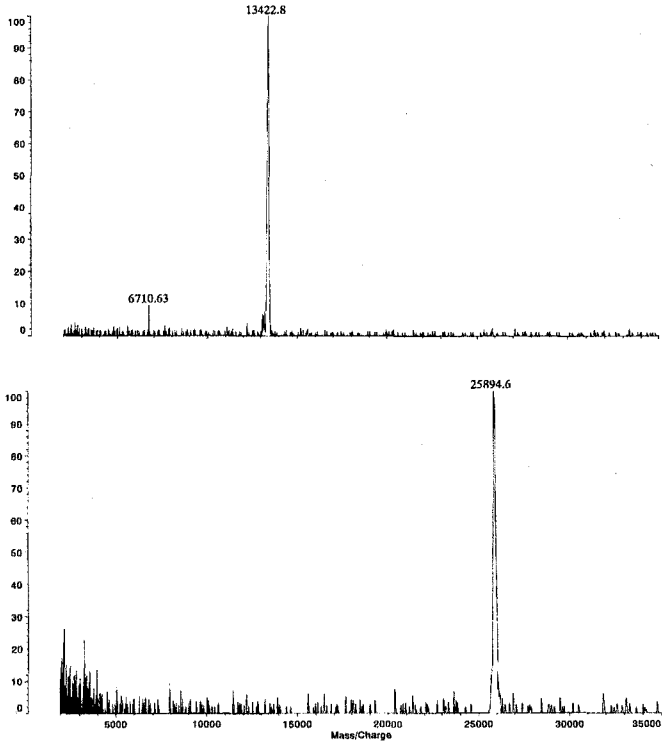

Figure 5-2. MALDI-TOF mass spectra of **Z12A** (upper) and **Z24A** (lower) recorded in positive ion mode with 9-nitroanthracence as matrix.

5-3. Steady-State Spectroscopy

Figure 5-3 shows the absorption spectra of **Z1A**, **Z2A**, **Z3A**, **Z6A**, **Z12A**, and **Z24A** in THF, along with those of 1:1 mixtures of acceptor-free *meso-meso* linked porphyrin arrays (**Z1**, **Z2**, **Z3**, **Z6**, **Z12**, and **Z24**) and the porphyrin **24**. In line with Chapter 3-2, the exciton-split Soret bands of the *meso-meso* linked porphyrin arrays are observed at 417-423 nm and at > 466 nm. The Soret bands of the bisphenylethynylated Zn^{II} porphyrin are observed constantly at 448 nm. The Q-bands of the *meso-meso* linked porphyrin arrays are observed at 550~588 nm with progressive intensification and red-shift upon the increase of the number of porphyrins, while the Q-bands of the bisphenylethynylated Zn^{II} porphyrin are observed at 649 nm. Comparisons of the respective absorption spectra revealed that the absorption spectra of **Z*n*A** in the Q-band region are essentially given by the sum of the spectra of *meso-meso* linked porphyrin arrays **Z*n*** and **24**, indicating that electronic interactions in the ground state are weak. On the other hand, there are some differences in the Soret-bands region, which are caused by the exciton coupling between the **Z*n*** and the 5,15-bisphenylethylanted Zn^{II} porphyrin part owing to the large transition moments of the Soret bands ($S_0 \rightarrow S_2$). It is interesting to note that a selective photoexcitation of the *meso-meso* linked porphyrin arrays is possible at 550-560 nm.

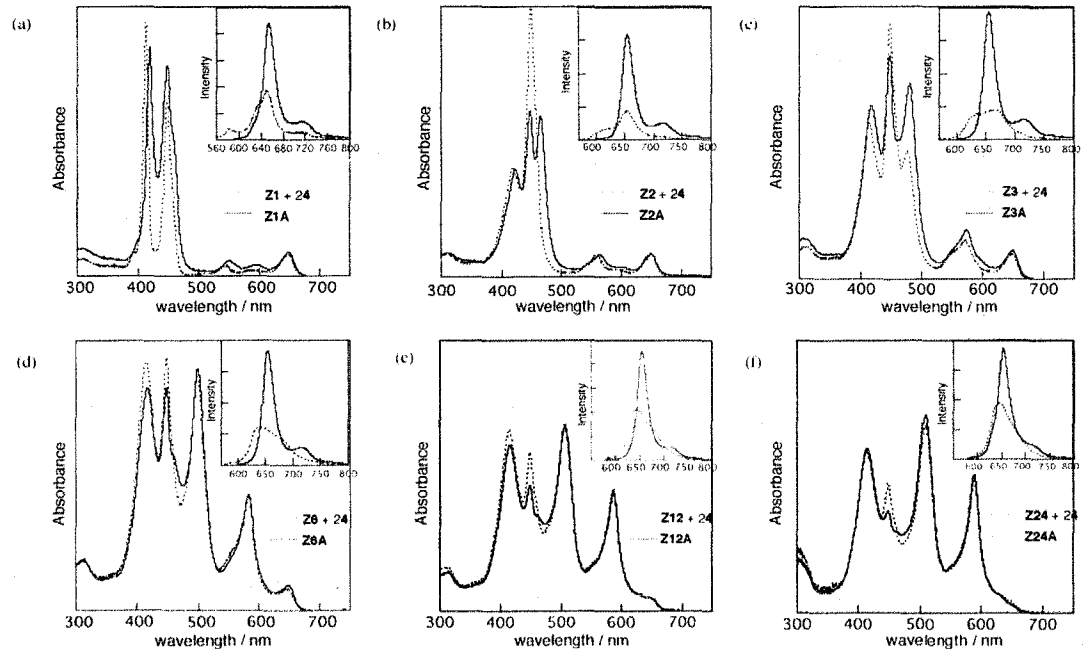

Figure 5-3. Absorption and fluorescence spectra of (a) **Z1A**, (b) **Z2A**, (c) **Z3A**, (d) **Z6A**, (e) **Z12A**, and (f) **Z24A**. Fluorescence spectra (shown in insets) were taken for excitation at their Q-bands. Solid lines are for **Z*n*A** and broken lines are for 1:1 mixtures of **Z*n*** and **24**.

The steady-state fluorescence spectra of **Z1A–Z24A** are shown in the insets of Figure 5-3, along with those of 1:1 mixtures of acceptor-free *meso-meso* linked porphyrin arrays (**Z1**, **Z2**, **Z3**, **Z6**, **Z12**, and **Z24**) and the porphyrin **24**. Upon photoexcitation at 550-560 nm corresponding to a selective excitation at the *meso-meso* linked porphyrin array, 1:1 mixtures of *meso-meso* linked Zn^{II} porphyrin arrays and **24** exhibit the fluorescence predominantly from the *meso-meso* linked Zn^{II} porphyrin arrays. The models **Z1A-Z12A** exhibit the fluorescence predominantly coming from the bisphenylethynylated Zn^{II} porphyrin moiety, indicating the efficient, nearly quantitative EET processes. The fluorescence of **Z24A** comes mainly from the acceptor moiety but also partly from the long donor porphyrin array (Figure 5-4). Here, it is noted that the donor emissions are completely overlapping the Q-band of the energy-accepting unit, being favorable for the rapid EET.

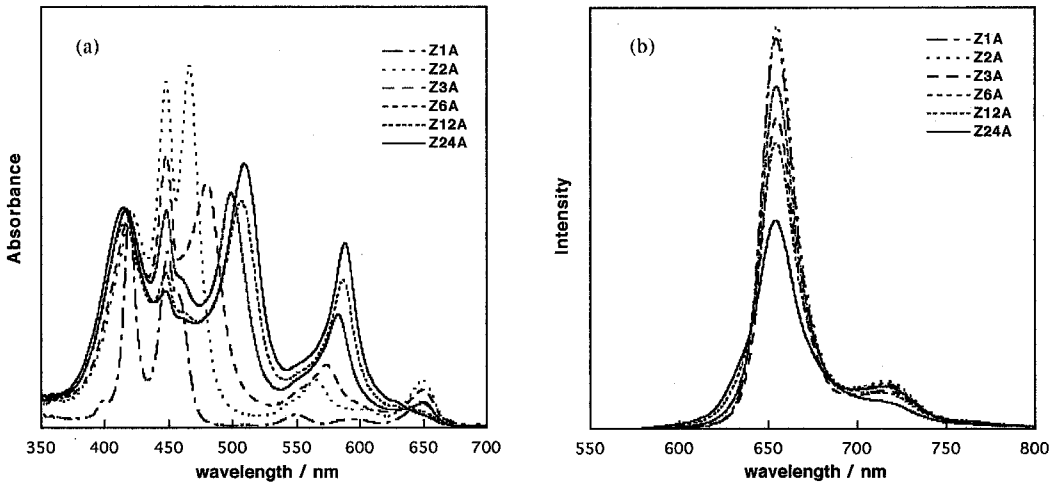

Figure 5-4. (a) Absorption and (b) fluorescence spectra of **Z*n*A**. The emission was taken for excitation at the top of Soret band (ca. 420 nm).

Figure 5-5a shows the comparison of the absorption spectra of **Z1A–Z24A** at the same concentration (9×10^{-8} M). At this dilute concentration, there is no serious aggregation, since the absorbance reflects the number of the porphyrins in the molecule. It is evident that the extensive exciton coupling within the *meso-meso* linked porphyrin array gives rise to a larger cross section between 350 and 650 nm. This spectral feature is favorable for light harvesting antenna function. Figure 5-5b compares the steady-state fluorescence taken for excitation at 508 nm, where the **Z1A** model has practically no absorbance and **Z12A** and **Z24A** have the large absorbance due to the exciton coupling. In **Z2A–Z12A**,

the incident light at this wavelength (508 nm) is efficiently delivered to the end energy acceptor, since the resultant fluorescence intensification is parallel to the increase in the absorbance at 508 nm. But the fluorescence intensity of **Z24A** is somewhat less than a value expected from its absorbance, indicating that the intramolecular EET is also efficient but not quantitative.

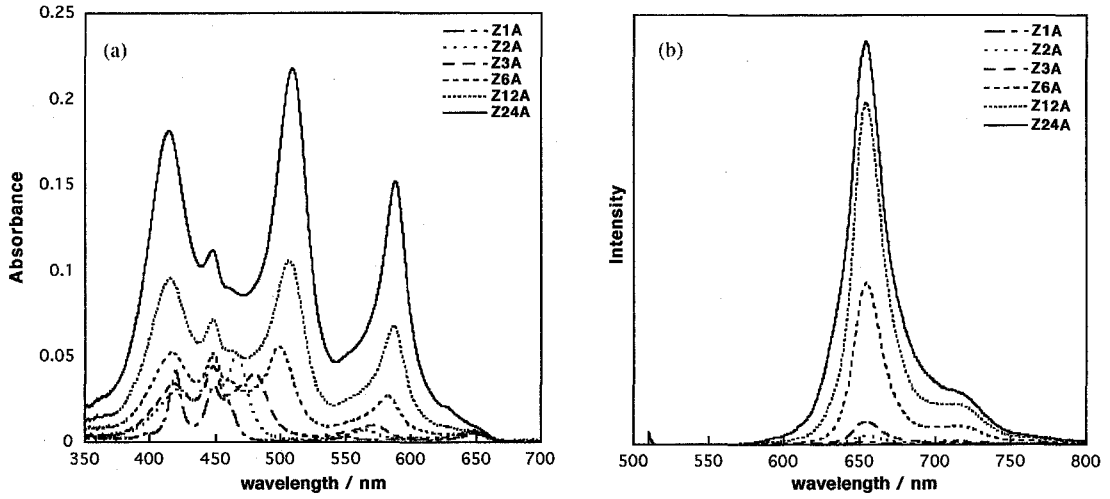

Figure 5-5. (a) Absorption and (b) fluorescence spectra of **Z1A–Z24A** at 9 x 10-8 M in THF. Fluorescence spectra were taken for excitation at 508 nm.

5-4. Transient Absorption Spectra

The transient absorption spectra of **Z1A, Z2A, Z3A, Z6A, Z12A** and **Z24A** were taken by the selective S_1-excitation of the *meso-meso* linked porphyrin arrays at the Q-bands (Figure 5-6). The transient absorption spectrum of **Z1A** at 2-ps delay time indicated a bleaching around 420 nm due to the depletion of the *meso-meso* linked porphyrin array (energy donor), which decayed quickly with $\tau = 1.6$ ps (Figure 5-7a). Along this spectral change, a new bleaching at 650 nm due to the depletion of the bisphenylethynylated Zn^{II} porphyrin (energy acceptor) was observed to be growing with $\tau = 2.5$ ps (Figures 5-6a and 5-7a). Therefore, these two spectral changes indicate the efficient intramolecular EET from the *meso-meso* linked porphyrin array to the bisphenylethynylated Zn^{II} porphyrin.

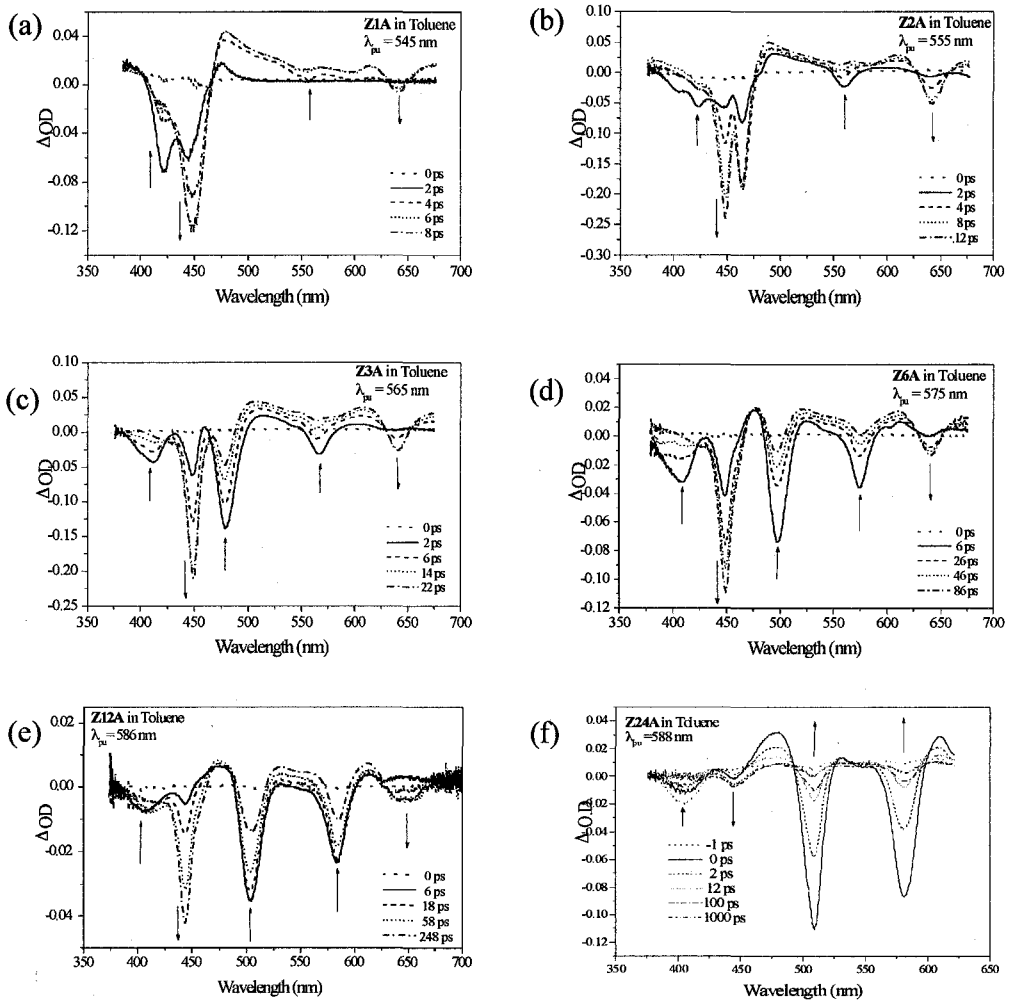

Figure 5-6. Transient absorption and fluorescence spectra of (a) **Z1A**, (b) **Z2A**, (c) **Z3A**, (d) **Z6A**, (e) **Z12A**, and (f) **Z24A**.

Essentially the similar transient absorption spectra and temporal profiles were observed for **Z2A, Z3A, Z6A, Z12A** , and **Z24A** (Figures 5-6 and 5-7). On the basis of these data, the EET rate constants have been determined for **Z2A** (3.3 ps)$^{-1}$, **Z3A** (5.5 ps)$^{-1}$, **Z6A** (21 ps)$^{-1}$, **Z12A** (63 ps)$^{-1}$, and **Z24A** (108 ps)$^{-1}$.

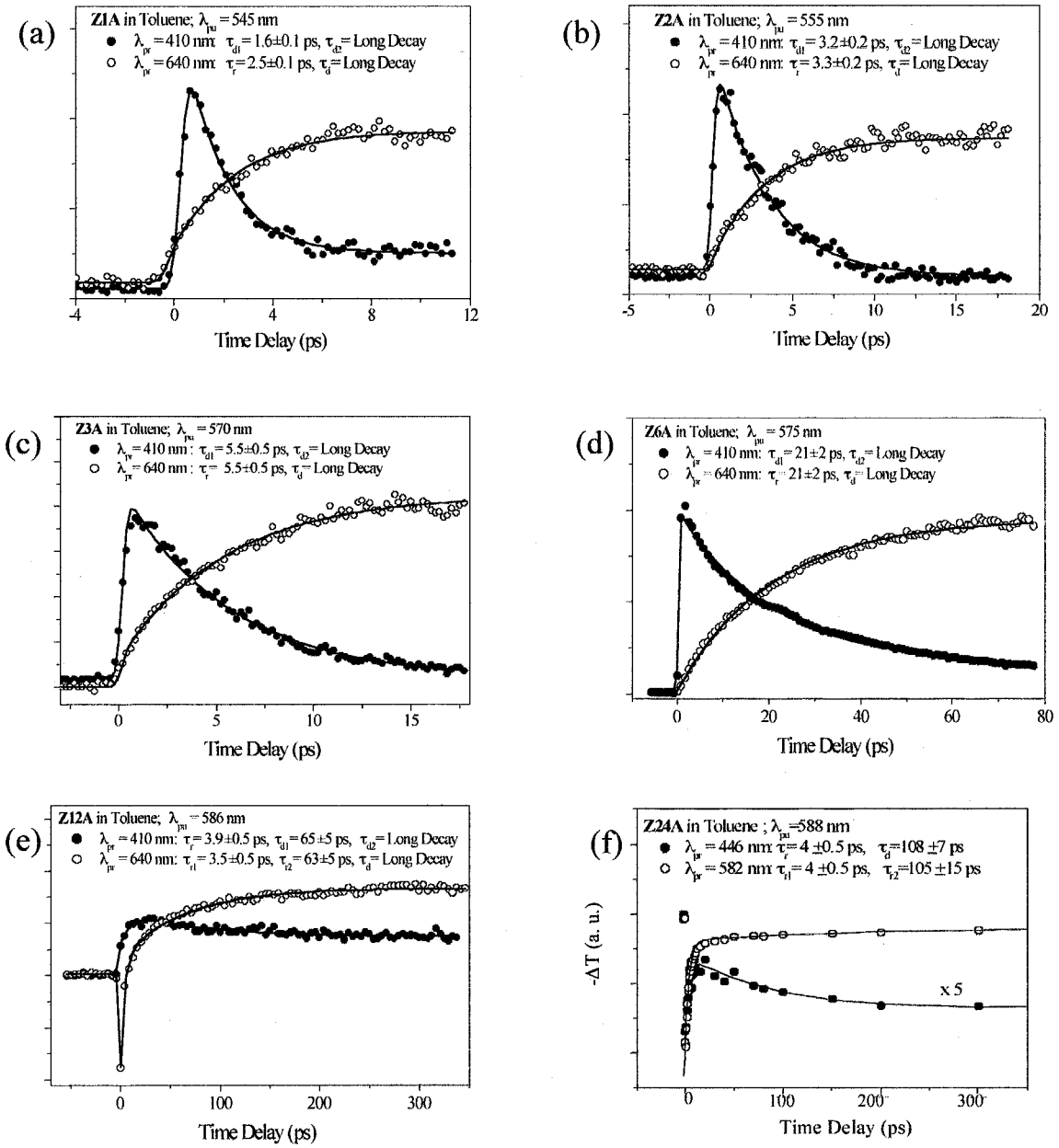

Figure 5-7. Temporal time-profiles of the transient absorption spectra of (a) **Z1A**, (b) **Z2A**, (c) **Z3A**, (d) **Z6A**, (e) **Z12A**, and (f) **Z24A**.

5-5. Transient Absorption Anisotoropy Decay Analysis

The femtosecond transient absorption anisotropy decay measurements for **Z1A**, **Z2A**, **Z3A**, and **Z6A** were also measured (Figure 5-8). The transition dipole of the S_1-state of the *meso-meso* linked porphyrin array donor has been shown to align along the long molecular axis, and that of the lowest S_1-state of the 5,15-bisphenylethynyl Zn^{II} porphyrin acceptor has been considered to align along the 5,15-direction. Therefore, in **Z2A**, **Z3A**, and **Z6A**, the key transition dipole moments of the donor and acceptor are placed in an orthogonal arrangement in their lowest excited states. Accordingly, a large anisotropy change is expected during the energy transfer processes. The anisotropy dynamics of **Z1A** probed at 480 nm exhibits only a rapid decay with τ = 0.2 ps. In the case of **Z2A**, at 470 nm prove wavelength, we observed an initial rapid anisotropy decay with τ = 0.2 ps, followed by an anisotropy rise with τ = 3.3 ps (Figure 5-8b). The time constant of the anisotropy rise matches nicely with the EET rate constant. The author observed similar behaviors both for **Z3A** and **Z6A**; a rapid anisotropy decay with τ = 0.2 ps followed by an anisotropy rise with τ = 5.5 ps in **Z3A**, and a rapid anisotropy decay with τ = 0.2 ps followed by an anisotropy rise with τ = 21 ps in **Z6A**, respectively (Figures 5-8c and d). The fast anisotropy decay with τ = 0.2 ps indicates coherent coupling time, while the observed anisotropy rise with slower time constants can be ascribed to the intramolecular energy transfer.

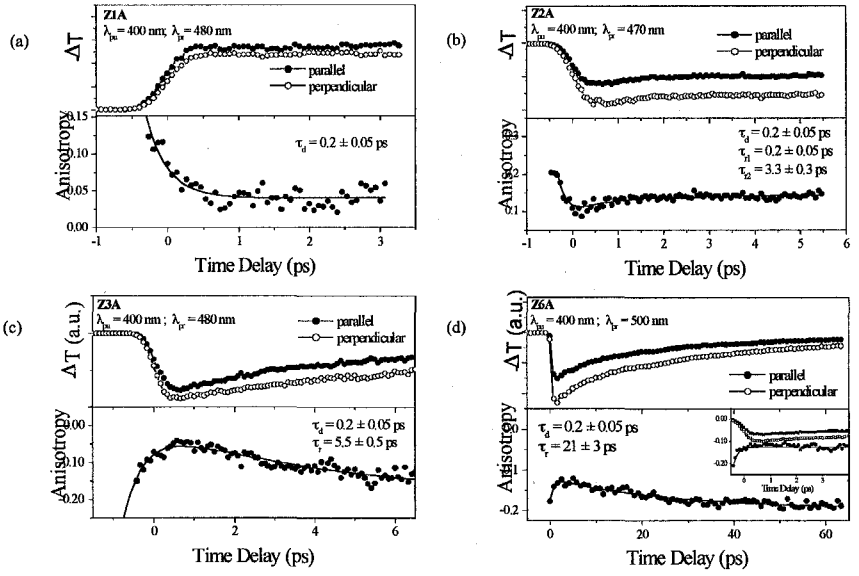

Figure 5-8. Femtosecond transient absorption anisotropy decays of (a) **Z1A**, (b) **Z2A**, (c) **Z3A**, and (d) **Z6A**.

5-6. Theoretical Studies

The intramolecular EET events in **Z1A–Z24A** have been confirmed by the steady-state fluorescence measurements and the transient absorption measurements. The exciton coupling within the *meso-meso* linked Zn^{II} porphyrin arrays causes the alteration and extension of the absorption spectral shape, which are quite favorable for the light harvesting antenna function. Captured light energy is then delivered efficiently to the energy-accepting site in all the models **Z1A–Z24A**. The EET is almost quantitative in **Z1A**, **Z2A**, **Z3A**, **Z6A**, and **Z12A** but is not quantitative but efficient in **Z24A** as judged from Figure 5-3. Large electronic interaction between the directly *meso-meso* linked neighboring porphyrin must be responsible for the EET.

The anisotropy decay measurements have indicated that the present EET processes are accompanied by a large change in the direction of the transition dipole moment. In the case of **Z1A**, the anisotropy decay dynamics become complicated mainly due to the fact that a broad absorption band around 450 nm is not solely due to the acceptor Soret band but due to a mixture with the exciton split Soret band arising from excitonic interactions between donor and acceptor. Thus, even in the magic angle detection at 460 nm upon photoexcitation of **Z1A** at 400 nm, rise and decay components due to the simultaneous participation of donor and acceptor bleaching recoveries in the energy transfer process were observed. In the case of **Z2A**, similar phenomena especially at 470 nm probe wavelength were observed, which contains a contribution from the exciton split Soret band between donor and acceptor. This process should be sensitive to the probe wavelength because the exciton split Soret band and the Soret band of acceptor are overlapped at around 450 nm in the case of **Z1A**. At 480 nm probe, the contribution from the exciton split Soret band becomes reduced. The anisotropy dynamics of **Z1A**, probed at 480 nm, contains the initial rise due to the fast equilibrium between B_X and B_Y polarizations of the donor part followed by a relatively slow energy transfer process with τ = ~2 ps. The initial anisotropy decay of **Z6A** has also been assigned to the fast equilibrium between B_X and B_Y polarizations, which reflects the coherent coupling time in preparing a large dipole (coherently coupled one) along the long axis of the array, while a slow anisotropy rise with τ = ~21 ps can be assigned to the EET, because the time constant agrees with the EET rate constant, $(21\ ps)^{-1}$, and the donor and acceptor dipole moments are arranged orthogonal to each other. Similar behaviors in **Z2A** and **Z3A** were observed.

In the next step, the author considers the dependence of the EET rate constant upon the number of the porphyrins in the array.

Table 1. Observed and calculated EET rate constants

model	R (Å)[a]	k_{obs}^{-1} (ps)[b]	k_N^{-1} (ps)[c]	k_N^{-1} (ps)[d]	k_N^{-1} (ps)[e]
Z1A	12.7	2.5 ± 0.1	—	—	—
Z2A	16.9	3.3 ± 0.2	6.9	5.0	3.4
Z3A	21.0	5.5 ± 0.5	20	7.5	5.9
Z6A	33.6	21 ± 2	160	15	23
Z12A	58.6	63 ± 5	2300	30	70
Z24A	109	108 ± 7	49000	60	163

[a] Center to center distances between the donor and the acceptor.

[b] EET rate constants measured by the transient absorption spectra.

[c] EET rate constants calculated by eq. 7.

[d] EET rate constants calculated by eq. 8.

[e] EET rate constants calculated by eqs. 13 and 14 for L = 4.

Exciton Model

First, let me consider that excited states on the porphyrin array are excitons, and their quantum-mechanical wave functions extend coherently over the entire array. Such exciton states are formed due to ample inter-porphyrin EET interactions which, as the first approximation, can be regarded as brought about by the electrostatic interaction between transition dipoles at neighboring porphyrins in the array. Participating in the interaction at each porphyrin is a component with a transition dipole parallel to the array axis in the doubly-degenerate S_1 transitions. When the array is composed of N porphyrins, the lowest exciton state on the array can be represented by

$$|d\rangle = \sqrt{\frac{2}{N+1}} \sum_{n=1}^{N} sin\left(\frac{\pi}{N+1} n\right) |n\rangle \qquad (1)$$

where $|n\rangle$ represents a state of the array that the nth porphyrin therein is excited with a transition dipole parallel to the array while all the other porphyrins are unexcited. The energy eigenvalue of $|d\rangle$ is given by

$$E_d = E_0 + 2\Delta\cos\,[\pi/(N+1)] \qquad (2)$$

where E_0 represents the excitation energy of the S_1 transition of a single porphyrin, and Δ represents the EET interaction between neighboring porphyrins in the array. The total transition dipole of this donor state $|d\rangle$ is parallel to the array axis with a magnitude

$$\sqrt{\frac{2}{N+1}}\sum_{n=1}^{N} sin\left(\frac{\pi}{N+1}n\right)\mu = \sqrt{\frac{2}{N+1}}\cot\left(\frac{\pi}{2N+2}\right)\mu \qquad (3)$$

where μ represents the magnitude of the S_1 transition dipole of a single porphyrin.

Next, the author considers the acceptor state of the EET at the 5,15-bisphenylethynyl porphyrin. The attachment of phenylacethylene moieties at 5 and 15 positions breaks the two-fold degeneracy of the S_1 transitions at the acceptor porphyrin in such a way that the component with a transition dipole parallel to the 5,15 direction becomes the lowest excited state. EET from the donor takes place with energies of its fluorescence spectrum as long as it overlaps the absorption spectrum of the acceptor. In the present case, the fluorescence spectrum of the porphyrin-array donor covers completely the absorption spectrum of the acceptor porphyrin in the energy region of its S_1 transitions, as mentioned earlier. In this situation, it seems reasonable to consider that the acceptor state for the EET is a mixture of the S_1 component with the 5,15-transition dipole and the other component with the perpendicular 10,20-transition dipole. The 5,15-transition dipole is perpendicular to the long molecular axis of the porphyrin-array donor, while the 10,20-transition dipole is parallel to it. Since all the porphyrins in the array have a transition dipole parallel to the array axis in the donor state for the EET, they do not interact with the former at the acceptor porphyrin at least in the transition-dipole approximation. Therefore, the author considers that the observed rapid EET from the donor to the acceptor takes place *via* the S_1 component with the 10,20-transition dipole at the acceptor porphyrin.

The traditional theory on the EET rate constant is Förster's one [126], which considers that EET arises by the electrostatic interaction between transition dipoles at the donor and the acceptor. In the present problem, the donor is regarded as the tightly-bound entire porphyrin array with a single total transition dipole of eq. 3 parallel to the array axis and located at the center of the array. Its EET interaction with the 10,20-transition dipole on the acceptor porphyrin is given by $[2/(N+1)]^{1/2}\cot[\pi/(2N+2)](R_1/R)^3J$ where R represents the distance from the acceptor porphyrin to the center of the porphyrin array, and R_1 and

J represent respectively the distance and the EET coupling in **Z1A** for $N = 1$. Förster's formula is given by the lowest (i.e., second-order) perturbation in the EET interaction, that is, by Fermi's Golden Rule. The rate constant for the EET obtained is given by

$$k_N = \frac{4\pi J^2}{\hbar(N+1)}\left(\frac{R_1}{R}\right)^6 \cot^2\left(\frac{\pi}{2N+2}\right)\int I_a(E)L_N(E)dE \qquad (4)$$

where $I_a(E)$ and $L_N(E)$ represent respectively the absorption spectrum of the acceptor porphyrin and the fluorescence spectrum of the array of N porphyrins as the donor, both being normalized as

$$\int I_a(E)dE = \int L_N(E)dE = 1 \qquad (5)$$

In eq. 4, it has been assumed that the absorption spectrum of the S_1 component with the 5,15-transition dipole and that of the other component with the perpendicular 10,20-transition dipole on the acceptor porphyrin can be regarded as similar to each other in the energy range covered by the fluorescence spectrum of the porphyrin-array donor, both being approximated as proportional to $I_a(E)$.

The value of J is concerned with the actual degree of mixture of the S_1 component with the 10,20-transition dipole in the acceptor state. Instead of actually calculating the degree of the mixture, let him be content with estimating J as an effective EET coupling from the observed value of k_1, since J is practically more useful. For $N = 1$, eq 4 reduces to

$$k_1 = \frac{2\pi}{\hbar}J^2\int I_a(E)L_1(E)dE \qquad (6)$$

Here, k_1 = (~2.5 ps)$^{-1}$, and also $\int I_a(E)L_1(E)dE$, called Förster's overlap integral, to be (~2500 cm^{-1})$^{-1}$ were observed. These values enable us to derive $J \approx 29$ cm^{-1} from eq. 6.

Dependence of the EET rate constant on the number (N) of porphyrins in the donor-array manifests itself most purified in the ratio of k_N/k_1, which is given by

$$\frac{k_N}{k_1} = \frac{2}{N+1}\left(\frac{R_1}{R}\right)^6 \cot^2\left(\frac{\pi}{2N+2}\right)\frac{\int I_a(E)L_N(E)dE}{\int I_a(E)L_1(E)dE} \qquad (7)$$

In k_N of eq 4, both the effective EET coupling J in **Z1A** and Förster's overlap integral have some ambiguities arising from the approximation for $I_a(E)$ mentioned below eq 5. The ratio of k_N/k_1 does not include J, and also the ratio of Förster's overlap integrals at the right-hand end of eq 7 is nearly independent on N with a magnitude of about 1.0 except for $N = 3$ where it is about 0.87. Therefore, the N dependence of k_N/k_1 can be used as a check of theories for EET.

The center-to-center distance R between the donor and the acceptor was estimated by the CPK models, being listed in Table 1. For $k_1 = (\sim 2.5\ \text{ps})^{-1}$, this equation 7 gives $k_2 = (\sim 6.9\ \text{ps})^{-1}$, $k_3 = (\sim 20\ \text{ps})^{-1}$, $k_6 = (\sim 160\ \text{ps})^{-1}$, $k_{12} = (\sim 2.3\ \text{ns})^{-1}$, and $k_{24} = (\sim 49\ \text{ns})^{-1}$. These values are too small in comparison with the observed ones, as shown also in Table 1. The author sees thus that the observed data cannot be described by Förster's theory. The rate constant with the R^{-6} dependence therein decreases too rapidly with R to reproduce the observed data.

Origins of inapplicability of Förster's theory mentioned above can be found in its two assumptions that excited states on the porphyrin array are excitons which extend coherently over the entire array, and that the entire array can be regarded as a single suprachromophore with a single transition dipole in the calculation of the EET rate constant. Concerning the first assumption, it is very difficult to consider that the coherence length of an exciton extends over the entire array for long models **Z12A** and **Z24A**.

Independent Chromophore Model

As a limit for breaking the first assumption, let me consider that excited states on the porphyrin array have no coherence among porphyrins. In this limit, an excitation is localized at a single porphyrin in the array, and it carries correctly a single transition dipole. Considering further the weak-coupling limit in the EET, excitations on the porphyrin array are regarded as maintained in thermal equilibrium in the course of EET from the donor to the acceptor. Since each porphyrin in the array has the same excitation energy, an excitation can be found at each porphyrin with the same probability given by $1/N$ in thermal equilibrium. An excitation found at the $n = 1$ porphyrin can be transferred to the acceptor porphyrin with a probability k1 given by eq 6, and that found at the $n = 2$ porphyrin can be transferred with a probability $k_1(R_1/R_2)^6$ where R_2 represents the center-to-center distance between the $n = 2$ porphyrin in the array and the acceptor

porphyrin. Since $(R_1/R_2)^6$ = ~0.049, neglect of EET from an excitation found at the n = 2 porphyrin and also from that found at remoter porphyrins for n ≥ 3 is possible. Therefore, the rate constant for EET to the acceptor porphyrin from the donor array composed of N porphyrins is given by

$$k_N = k_1/N \qquad (8)$$

For k_1= (~2.5 ps)$^{-1}$, this equation 8 gives k_2 = (~5.0 ps)$^{-1}$, k_3 = (~7.5 ps)$^{-1}$, k_6 = (~15 ps)$^{-1}$, k_{12} = (~30 ps)$^{-1}$, and k_{24} = (~60 ps)$^{-1}$. These values are not very bad but differ considerably from the observed EET rate constants (Table 1).

Coherent Model

Let him check the second assumption in Förster's formula that the entire porphyrin array can be regarded as a single suprachromophore with a single transition dipole in the calculation of the EET rate constant. In reality, individual porphyrins coupled coherently with each other in the donor state of eq 1 on the array carry well-defined transition dipoles whose vectorial sum gives the total transition dipole of eq 3 appearing in Förster's formula of eq 4. These individual transition dipoles $[2/(N+1)]^{1/2}\sin[\pi n/(N+1)]\mu$ for n = 1, 2, · · ·, N at each porphyrin in the donor array interact with the transition dipole at the acceptor porphyrin with different strengthes because of differences in the interaction distance. Interaction of the nth porphyrin in the array is given by $[2/(N+1)]^{1/2}\sin[\pi n/(N+1)](R_1/R_n)^3J$, where R_n represents the center-to-center distance between the nth porphyrin in the array and the acceptor porphyrin, and J represents the effective EET coupling between the n = 1 porphyrin in the array and the acceptor porphyrin in eq 6. Taking into account the interaction of these transition dipoles with the acceptor transition dipole, he gets the correct total interaction strength for EET between the porphyrin-array donor and the acceptor porphyrin, as

$$V_N = J\sqrt{\frac{2}{N+1}}\sum_{n=1}^{N} sin\left(\frac{\pi}{N+1}n\right)\left(\frac{R_1}{R_n}\right)^3 \qquad (9)$$

Since $(R_1/R_2)^3$ = ~0.22 and $(R_1/R_3)^3$ = ~0.081, terms at least for n = 2 and 3 in the summation on the right-hand side cannot be neglected in comparison with the term for n = 1. On the basis of Fermi's Golden Rule, the rate constant for the EET caused by V_N of

eq 9 is given by

$$k_N = \frac{2\pi}{\hbar} V_N^2 \int I_a(E) L_i(E) dE \qquad (10)$$

It must be taken into account also here that the coherence length of an exciton in the donor array is not as long as the entire array at least for **Z12A** and **Z24A**, because of decoherence disturbances increasing in number with the array length. Therefore, let me consider that the lowest exciton state on the array can cover coherently at most L porphyrins. Accordingly, it is only when $N \leq L$ that we can use eq 10 with eq 9 for describing the rate constant of the EET. When $N > L$, an exciton with the coherence length L can be found at $N - L + 1$ locations on the array composed of N porphyrins, with the same energy given by eq 2 for $N = L$ therein. Considering the weak-coupling limit in the EET, excitations on the porphyrin array are regarded as maintained in thermal equilibrium in the course of EET from the donor to the acceptor. In thermal equilibrium, each exciton state can be realized with the same probability given by $1/(N - L + 1)$. An exciton found at the location nearest to the acceptor porphyrin transfers its excitation energy to the acceptor with a probability k_L given by eq 10 for $N = L$ therein. An exciton found at the location next nearest to the acceptor porphyrin transfers its excitation energy with a probability k_L' given by eq 10 with V_N therein changed into

$$V_N' = J\sqrt{\frac{2}{N+1}} \sum_{n=1}^{L} \sin\left(\frac{\pi}{N+1} n\right) \left(\frac{R_1}{R_{n+1}}\right)^3 \qquad (11)$$

instead of V_L for k_L. Since k_L' has only a magnitude on the order of $(R_1/R_2)^6$ (= ~0.049) times as small as k_L, it is possible to neglect EET from an exciton found at the next-nearest location, and also excitons found at remoter locations even if they exist. Therefore, the rate constant for EET to the acceptor porphyrin from the array composed of N porphyrins was obtained, as

$$k_N = k_L/(N - L + 1), \text{ for } N > L. \qquad (12)$$

As mentioned previously, the N dependence of the ratio k_N/k_1 can be used as a check of theories for EET. It is given by

$$\frac{k_N}{k_1} = \frac{2}{N+1}\left[\sum_{n=1}^{N} sin\left(\frac{\pi}{N+1}n\right)\left(\frac{R_1}{R_n}\right)^3\right]^2 \frac{\int I_a(E)L_N(E)dE}{\int I_a(E)L_1(E)dE}, \text{ for } N \le L \quad (13)$$

and

$$k_N/k_1 = (k_L/k_1)/(N - L + 1), \text{ for } N > L. \quad (14)$$

It is notable here that eq 8 is a special case of eq 14 for $L = 1$.

The coherence length L has been estimated to be about 4 on the present porphyrin array.

The coherent length (L) in S_1-state of *meso-meso* linked Zn^{II} porphyrin array has been estimated to be ~5 on the basis of the equation developed by Knoeter [127]; $L = \sqrt{\frac{3\pi^2|\Delta E_0|}{\gamma}} - 1$ by letting $|\Delta E_0| = 270$ cm^{-1} and $\gamma = 236$ cm^{-1}. The coupling strength $|\Delta E_0|$ of ~ 275 cm^{-1} was estimated from the ratio of the absorption coefficients of Soret and Q bands in monomer (~1/16). In this estimation, the author considered only the dipole-dipole interaction between porphyrin moieties and may neglect the coupling originated from the through-bond effect. In this work, the coupling strength (V) of ~ 570 cm^{-1} by plotting the peak positions of Q bands and fitting to the equation of $E_k = E_0 + 2V\cos\left(\frac{\pi}{N+1}\right)$ was obtained. The empirical formula developed by Kakitani [128]; $L = 1.38 + 1.33\frac{V}{\gamma}$ seems to be more applicable in our porphyrin array system because this model is based on the one-dimensional linear array system and deals with the steady-sate exciton coherent length. A detailed studies on the energy relaxation dynamics of *meso,meso'*-dibrominated Zn^{II} porphyrin array also predicts L = ~4 [129].

When $L = 4$ and k_1 = (~2.5 ps)$^{-1}$, these equations 13 and 14 give k_2 = (~3.4 ps)$^{-1}$, k_3 = (~5.9 ps)$^{-1}$, k_6 = (~23 ps)$^{-1}$, k_{12} = (~70 ps)$^{-1}$, and k_{24} = (~163 ps)$^{-1}$. These values are in good agreement with the observed ones except the longest model **Z24A** (Table 1). Therefore, this approach seems most suitable in reproducing the observed rate constants of EET from the porphyrin array to the acceptor porphyrin. Ones thus understand that the excited states of the *meso-meso* linked Zn^{II} porphyrin arrays are excitons extending over a number of porphyrins even in the S_1-states. The behavior of **Z24A** has not been fully understood at the present stage. Increased conformational heterogeneity may be one of causes for

this discrepancy.

If the center-to-center distance R_1 between the $n = 1$ porphyrin in the donor array and the acceptor porphyrin was much larger than the total length ΔR of the donor array composed of N porphyrins, differences among R_n's could be neglected on the right-hand side of eq 9. Accordingly, all the R_n's could be approximated by the distance R between the acceptor porphyrin and the center of the porphyrin-array donor. Thereby, eq 10 would reduce to eq 4 that can be obtained by Förster's formula. In reality, however, R_1 (= ~12.7 Å) is not much larger than ΔR (= ~8.3 Å) even for $N = 2$, and eq 10 gives the k_N value much different from eq 4, the difference becoming enormous when N becomes larger. Such a difference can be regarded as a size effect of the donor and/or the acceptor for EET, where at least one of them is a molecular aggregate whose excited states are excitons, and simultaneously the physical size of the aggregate is not much smaller than the average donor-acceptor distance. In this situation, Förster's formula is not correct in a sense that it deviates from the rate constant of EET derived correctly from the lowest (i.e., second-order) perturbational expansion in the EET coupling between the donor and the acceptor, although Förster's formula itself is also second order in the coupling. Such a formula that is correct in the weak-coupling limit has been presented by Sumi. It may be called a revised Förster formula. It has successfully been applied to EET in the antenna system of photosynthesis where the situation mentioned above can widely be found. In fact, the rate constant of eq 10 with eq 9 for the present problem corresponds to a special case in the general formula for the rate constant of EET given in Ref. [119].

In the present models, the acceptor porphyrin is connected with the adjacent porphyrin (**P1**) through a 1,4-phenylene spacer with the center-to-center distance R_1 = ~12.7 Å. **P1** is naturally the edge porphyrin in the donor array. Additional attachment of the second porphyrin (**P2**) to **Z1A** leads to **Z2A** that has a center-to-center donor-acceptor distance of R_2 = ~21.0 Å. In such situations, the EET interaction between two molecules might have to be calculated more appropriately than by the transition-dipole approximation. For example, it might be calculated by the so-called mono-pole approximation [130] with correct account of the spatial extension of the wave functions in the excited states of the molecules, or by taking into account also electron-exchange effects. In these cases, the $(R_1/R_n)^3$ dependence of the terms for $n \geq 2$ in the summation on the right-hand side of eq 9 might be a little revised. After such a revision, these terms for $n \geq 2$ should still retain magnitudes not negligible in comparison

with the first term therein. This situation is essential in reproducing the N dependence of the observed EET rate constant by k_N of the revised Förster's formula eq 10 with eq 9. On the contrary, eq 8 obtained by completely neglecting the spatial coherence of the exciton state gives k_N considerably smaller than the observed ones, mainly because it has been approximated in eq 8 to be only the $n = 1$ porphyrin in the donor array that takes part in EET to the acceptor porphyrin.

5-7. Summary

A series of *meso-meso* linked Zn^{II} porphyrin arrays bearing a 5,15-bisphenylethynylated Zn^{II} porphyrin were prepared for the examination of EET systems involving a strongly coupled array of donor or acceptor. In all the model compounds including **Z24A**, the efficient intramolecular EET processes have been proven by the steady-state fluorescence measurement and as well as the time-resolved transient absorption spectroscopy and ultrafast anisotropy decay measurements. The EET is almost quantitative in **Z1A** to **Z12A** but is competitive in **Z24A**. Long-distance, yet efficient EET processes are realized through the exciton states whose coherence is extended over several porphyrin pigments in the meso-meso linked Zn^{II} porphyrin arrays, as such in the natural photosynthetic light harvesting systems such as chlorosomes, LH1, and LH2. This strategy is very useful for the design of efficient artificial EET systems in the future. For these EET systems involving an aggregate, Sumi's revised Förster formula has been demonstrated to be useful for the analysis. These results may encourage further application of *meso-meso* linked porphyrin arrays for even longer EET and directed EET from a well defined donor to an acceptor over an extremely long distance, since such a long array is now available in a discrete form. Finally, advantages of strongly coupled arrays of chromophores in antenna function should be emphasized in terms of fast EET and large absorption cross-section unless forming an energy-wasting sink.

Chapter 6. Fabrication of *meso-meso* Linked Porphyrin Arrays toward the Nano Scale Science

In this Chapter, investigation on reactivity of the end free *meso*-positions of the *meso-meso* linked porphyrin arrays and complete conversion into *meso*-mercaptophenyl porphyrin arrays are described.

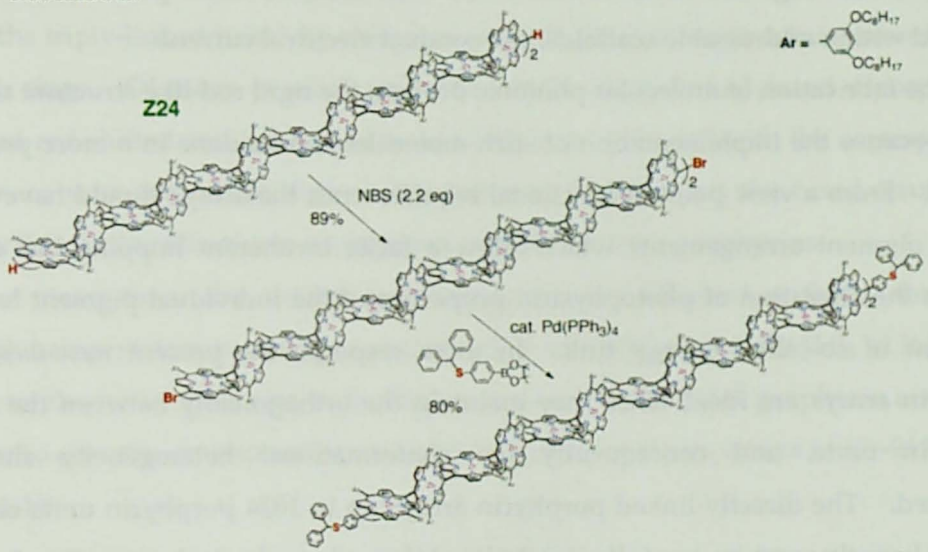

6-1. Introduction

During the past decade, π-conjugated oligomers investigated as advanced materials for electronic and photonic applications have attracted ever-increasing interests from both academic and industrial researchers. In recent years, interdisciplinary groups of chemist, physicists, and engineers demonstrated that individual or small packets of molecules, mounted within addressable scaffolds, can conduct electrical currents.

In the fabrication of molecular photonic devices, the rigid rod-like structure should be useful because the implementation of such molecules can be done in a more predictable manner. From a view point of functional requirements, the arrays should have the very regular pigment arrangements which allow a facile incoherent hopping but does not result in the alteration of photophysical properties of the individual pigment leading to formation of so-called energy sink. In these respects, the present *meso-meso* linked porphyrin arrays are ideal, since they maintain the orthogonality between the adjacent porphyrin units, and consequently the conformational heterogeneity should be minimized. The directly linked porphyrin arrays up to 1024 porphyrin units connected together linearly were successfully isolated and their photophysical properties depending upon the length of the arrays were investigated by various time-resolved laser spectroscopic methods. It is noteworthy that the energy transfer rate of $(\sim 0.55\ ps)^{-1}$ in the directly linked porphyrin dimer is quite similar to that from B800 to B850 in LH2 complexes ($(\sim 0.65\ ps)^{-1}$). Considering this fact, the directly-linked porphyrin arrays would be the closest artificial light harvesting array to the natural photosynthetic organisms, providing that the directly-linked porphyrin arrays are the most suitable synthetic molecular modules for the realization of molecular photonic devices based on the porphyrin arrays. Overall, the regularly arranged porphyrin arrays with ample electronic interactions will be promising as a light-harvesting *photonic* wire by transmitting singlet excitation energy rapidly over the array [131].

On the other hand, the creation of electronically π-conjugated porphyrin arrays in which the porphyrin π-electronic systems merge to form large supramolecular chromophores is also an attractive target in light of their remarkable photophysical and electrochemical properties [132]. Such conjugated porphyrin arrays are thus of interest in view of their potential use as a conducting electronic wire. The central issue is definitely to increase the electronic interaction between the constituent porphyrins in the arrays. The degree of the electronic interactions can be evaluated from red-shifted

absorption band arising from the decreased optical HOMO-LUMO gap. In the course of studies on the *meso-meso* coupling reactions, treatment of 5,10,15-triaryl substituted Ni^{II} porphyrin with tris(4-bromophenyl)aminium hexachloroantimonate (p-$BrC_6H_4)_3NSbCl_6$ (BAHA) in $CHCl_3$ led to the formation of *meso-β* doubly linked diporphyrins [133,134]. Further oxidation of *meso-meso* linked Cu^{II} diporphyrin with BAHA in C_6F_6 led to the formation of *meso-meso* 2*β*-*β* triply-linked diporphyrins [135]. X-ray crystallography revealed the triply-linked fused diporphyrins adopt highly planar structures over the two porphyrin rings. Of many peculiar properties of the triply-linked fused diporphyrins, the Q-band red-shifted and intensified band at 996 nm compared with the corresponding porphyrin or *meso-meso* singly linked diporphyrins indicate that the fused structure is very favorable for the effective π-conjugation over the entire diporphyrins.

In the mean time, the similar transformation was achieved without observable peripheral halogenation by using a combination of DDQ and $Sc^{III}(OTf)_3$ [136]. This synthetic method was applicable to the higher *meso-meso* linked Zn^{II} porphyrin arrays (up to 12-mer) to give the corresponding completely fused porphyrin arrays in 62~91% yields (Scheme 6-1).

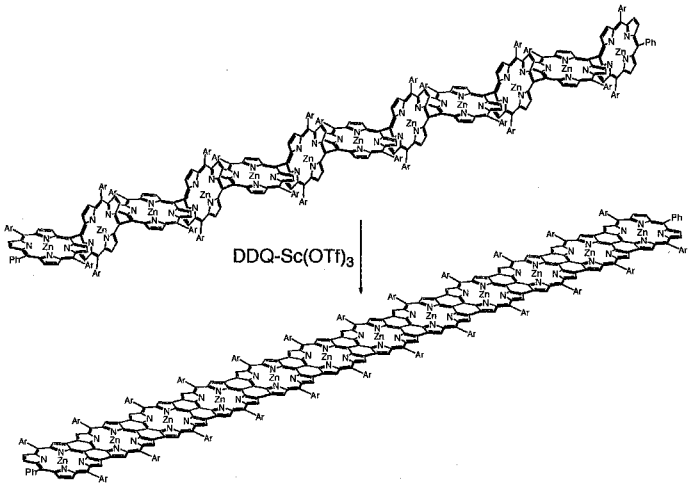

Scheme 6-1. Synthesis of porphyrin tape 12-mer.

The produced completely fused porphyrin arrays have planar tape-shaped structures, and display the extremely red-shifted absorption bands, reflecting the extensively π-conjugated electronic systems over the array. Most notably, the lowest energy electronic absorption bands become increasingly red-shifted and intensified upon the increase of the number of the porphyrins, and are reaching into the infrared frequency. Eventually, the longest fused array, 12-mer, exhibits a lower lying electronic excitation

band with a peak around 3500 cm^{-1}. Up to this stage, there is no detectable ECL (effective conjugation length) effect. It is interesting to note that the intensities of C-H stretching bands were weakened upon the coverage of the electronic absorption band with respect to other uncovered IR frequency. Detailed studies on the interactions of electronic and vibrational excitations may provide interesting information of so-called vibronic coupling relationship. It may be suggested that Born-Oppenheimer approximation is no longer valid for these long porphyrin tape molecules.

Totally, triply-linked fused porphyrins made from *meso-meso* linked porphyrins exhibit properties associated with an extremely delocalized π-electronic system as a consequence of their planar structure enforced by the fused connections. The extremely small HOMO-LUMO gaps, the exceedingly low oxidation potentials, and the long flat molecular shapes of the higher porphyrin tapes encourage their potent use as the *electronic* molecular wire [131]. This promising reaction strongly encourages the creation of a perfect molecular wire in which an electron can be transmitted rather freely from one end to the other end [137].

In order to apply these porphyrin arrays for a variety of applications, it is highly desirable to fabricate arrays with a thiol or carboxylic acid group, which will allow for a chemical bond with the metal surface. In this respect, the free end *meso*-position of the *meso-meso* linked porphyrin arrays is quite attractive. Thus the author surveyed the reactivity of the end *meso*-position and developed useful and complete conversion into *meso*-mercaptophenyl porphyrin arrays.

6-2. Fabrication of *meso-meso* Linked Porphyrin Arrays

Compared to the chain elongation steps, the purification issue is more serious for modifications of the porphyrin arrays. For example, separation of **ZnBr_2** from **Zn** was practically impossible over the preparative GPC because of small difference in molecular weight of products, and serious tailing of the long arrays on silica gel or alumina column precluded the separation of these products. This obstacle has been circumvented by the quantitative NBS bromination of the array. This is also a remarkable finding, in that macromolecules in general tend to become less reactive upon the increase of their size compared to small molecules [138]. The NBS bromination proceeded in a quantitative manner at least up to **Z64**, in which there are only two free *meso*-positions against 512 free pyrrolic β-positions that are all potentially susceptible to NBS bromination. Nevertheless, the NBS bromination occurred exclusively only at both *meso*-positions, hence fabricating synthetic handles just at the edges of rod-like long molecules.

As means to attach functional groups, the author selected Pd-catalyzed Suzuki-Miyaura arylation of *meso*-halogenated porphyrins with an arylboronic acid on the basis of several successful precedents [125]. However, usual thiol protective groups such as acetyl and benzoyl groups were found not to tolerate under coupling basic conditions. To avoid this, a diphenylmethy group was selected as a protective group [139].

Synthetic scheme of *meso*-thiophenylated porphyrin arrays is shown in Scheme 6-2. 4-Bromobenzenethiol (**25**) was protected with 1,1-diphenylmethanol (**26**) with the aid of TFA to form sulfide **27**, which was transformed into boronate **28** by Pd-catalyzed reaction with an equivalent of bis(pinacolato)diboron [140].

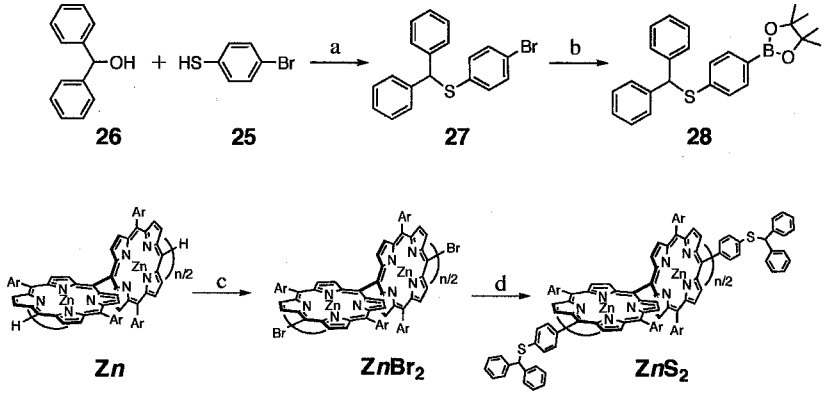

Scheme 6-2. Ar = 3,5-dioctyloxyphenyl. (a) TFA, CH_2Cl_2, (b) bispinacolate diboron, KOAc, $PdCl_2$(dppf), DMF, (c) NBS, pyridine, $CHCl_3$, (d) **28**, $Pd(PPh_3)_4$, Cs_2CO_3, toluene, DMF.

Regio-selective *meso,meso'*-dibromination of **Z2** was performed with 2.2 equiv. *N*-bromosuccinimide (NBS) to give Zn^{II} *meso,meso'*-dibromoporphyrin **Z2Br$_2$** quantitatively. This bromination was similarly effective for **Z3**, **Z4**, **Z6**, **Z8**, **Z12**, **Z16**, **Z24**, **Z48**, and **Z64** to afford Zn^{II} *meso,meso'*-dibromo porphyrin arrays **Z3Br$_2$** (95%), **Z4Br$_2$** (87%), **Z6Br$_2$** (78%), **Z8Br$_2$** (83%), **Z12Br$_2$** (92%), **Z16Br$_2$** (84%), **Z24Br$_2$** (89%), **Z48Br$_2$** (91%), and **Z64Br$_2$** (87%), respectively, with high regioselectivity at *meso*-position, despite increasing pyrrolic *β*-positions in longer arrays, which are potentially susceptible to NBS bromination. It is worthy to note that the present NBS bromination proceeded quantitatively for all the **Z*n*** examined, which allowed for isolation of pure **Z*n*Br$_2$** by passing through a short silica gel column without purification over GPC column.

Suzuki-Miyaura arylation of **Z6Br$_2$** with 10 equiv. of **28** (10mol% $Pd(PPh_3)_4$, 3 equiv. Cs_2CO_3, DMF/toluene, at 80°C, for 4 h) gave thiolated Zn^{II} porphyrin arrays **Z6S$_2$** in 90% yield. Similarly, **Z12Br$_2$**, **Z24Br$_2$**, **Z48Br$_2$**, and **Z64Br$_2$** were effectively arylated under the same conditions to furnish **Z12S$_2$** (85%), **Z24S$_2$** (79%), **Z48S$_2$** (81%), and **Z64S$_2$** (91%), respectively. Here again, the conversion of **Z*n*Br$_2$** to **Z*n*S$_2$** was nearly quantitative and almost pure **Z*n*S$_2$** products were isolated by simple precipitation of product. These products were also characterized by the MALDI-TOF mass and ^{1}H NMR measurements. Figure 6-1 illustrates the comparison of the ^{1}H NMR spectra of **Z64**, **Z64Br$_2$**, and **Z64S$_2$**. Single signal for H^m in the spectrum of **Z64** is missing in those of **Z64Br$_2$** and **Z64S$_2$**, and doublet signal for H^1 is low-field shifted in the spectrum of **Z64Br$_2$** as an influence of the *meso*-substituted bromine and high-field shifted in **Z64S$_2$** as an influence of the *meso*-substituted aryl group. The protecting groups in **Z*n*S$_2$** can be cleaved by subjecting them into 2.5% phenol/TFA (*w*/*v*) solution for certain time to provide *meso,meso'*-phenylthiol modified *meso-meso* linked porphyrin arrays **Z*n*SH$_2$** (Scheme 6-3).

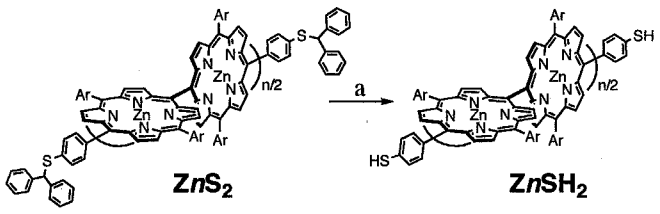

Scheme 6-3. Ar = 3,5-dioctyloxyphenyl. (a) i) PhOH, TFA, ii) $Zn(OAc)_2$, $CHCl_3$, MeOH, iii) dithiothreitol, THF.

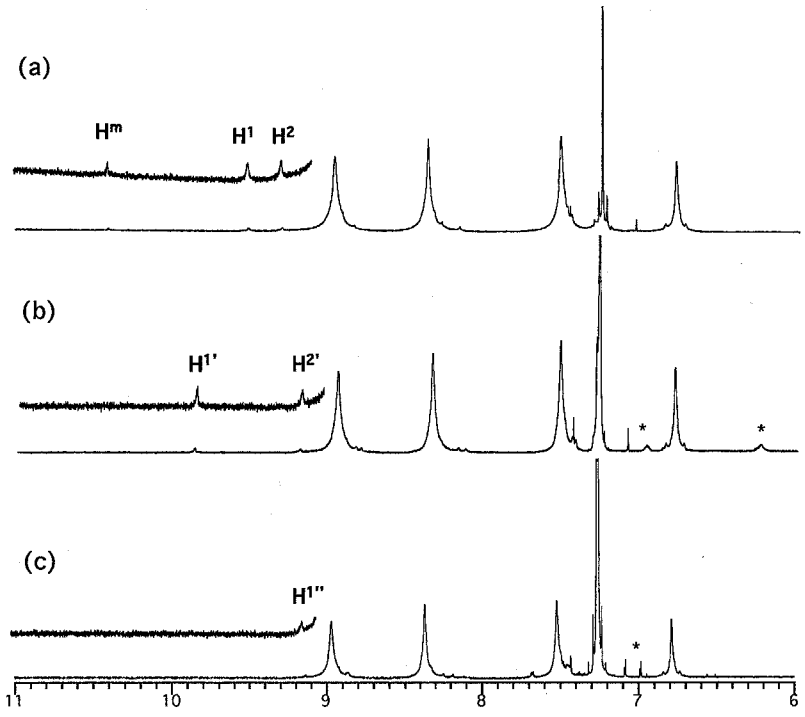

Figure 6-1. ^{1}H-NMR spectra of **Z64** , **Z64Br$_2$**, and **Z64S$_2$** in $CDCl_3$.

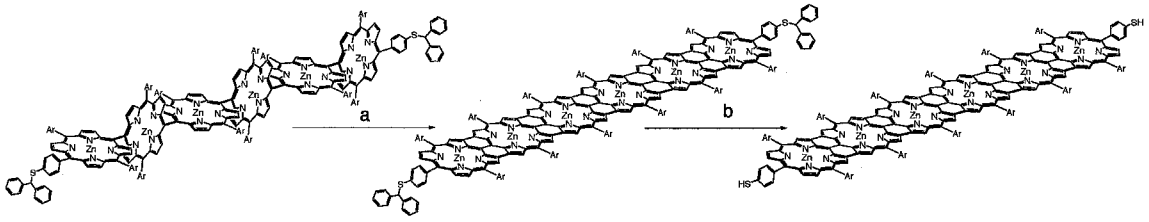

Scheme 6-4. Ar = 3,5-dioctyloxyphenyl. (a) DDQ, $Sc(OTf)_3$, (b) i) PhOH, TFA, ii) $Zn(OAc)_2$, $CHCl_3$, MeOH, iii) dithiothreitol, THF.

Finally, **Z6S$_2$** was treated with DDQ-$Sc(OTf)_3$ to form a functionalized porphyrin tape **T6S$_2$**, which was transformed into thiolated porphyrin tape **T6SH$_2$** (Scheme 6-4).

6-3. Measurement of Molecular Scale Electronic Conductivities

The electrical conductivity measurements through single or, at most, a few porphyrin arrays were preliminary performed. Two extreme types of porphyrin arrays to investigate the influence of electronic interactions between the adjacent porphyrin molecules on the electrical transport properties were prepared. One is directly *meso-meso* linked Zn^{II} porphyrin arrays **Z24SH$_2$**. The other one is completely flat, tape-shaped Zn^{II} porphyrin arrays **T6SH$_2$**.

To measure the electrical transport properties of porphyrin arrays directly, two kinds of Au/Ti nano-gap electrodes were prepared. For the orthogonal porphyrin array with the length of about 20 nm, nano-gap electrodes with a spacing of about 20 nm were fabricated by electron-beam lithography and a double-angle evaporation technique onto degenerately doped silicon substrate with a top SiO_2 layer of 0.5 μm. On the other hand, for the fused porphyrin array with ca. 5 nm in its length, the Au/Ti nano-gap electrodes with a spacing of less than 5 nm were prepared by utilizing the electromigration-induced break-junction technique [141]. Electrical contact between porphyrin arrays and metal electrodes was made by spontaneous assembly method. To porphyrin solution (1.0 ml) was add the electrode tip. The sample was dried under nitrogen purging and characterized using a semiconductor characterization system (Keithley 4200). All electrical transport measurements were performed under atmosphere.

Figure 6-2 displays the *I-V* curve measured at room temperature for **Z24SH$_2$** trapped between two nano-gap electrodes. It exhibits the semi-conductor-like behavior. From the slope of *I-V* curves, the room-temperature resistance is estimated to be ~2000 MΩ.

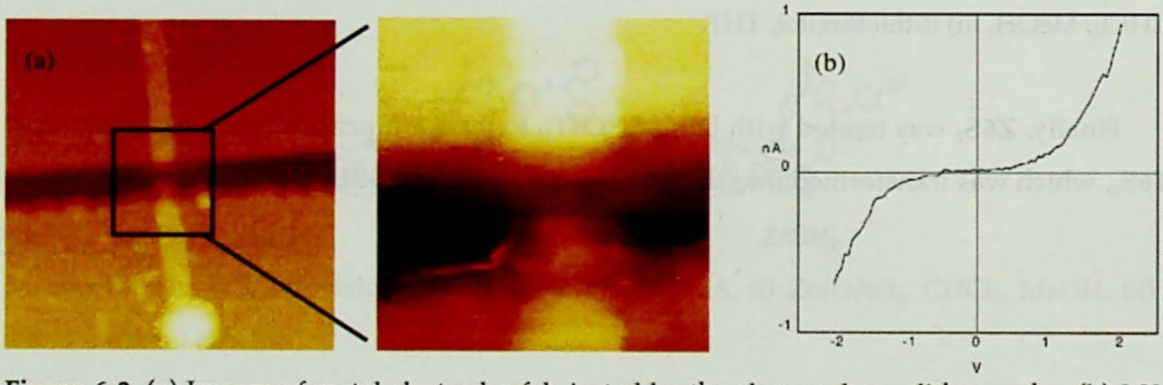

Figure 6-2. (a) Images of metal electrodes fabricated by the electron-beam lithography. (b) *I-V* curves measured at room temperature on **Z24SH$_2$** trapped between two metal electrodes.

Figure 6-3 shows the *I-V* curves measured at room temperature for **T6SH$_2$**. Compared with **Z24SH$_2$**, a higher conductivity and a smaller voltage gap were found. The room-temperature resistance estimated from the slope of the *I-V* curve is about 0.15 MΩ, which is smaller than that of **Z24SH$_2$**. These results indicate that the stronger π-electron conjugation results in better electrical conduction.

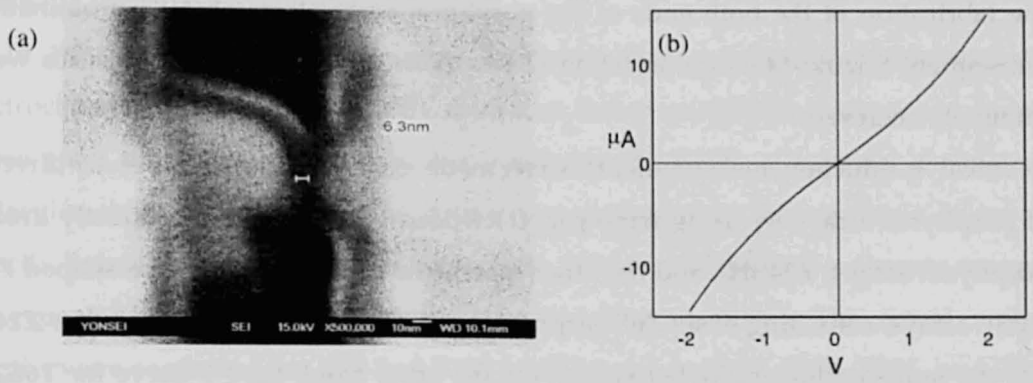

Figure 6-3. (a) Images of metal electrodes fabricated by the electromigration-induced break-junction technique (b) *I-V* curves measured at room temperature on **T6SH$_2$** trapped between two metal electrodes.

6-4. Summary

Functionalization of both ends of porphyrin array is an important step for their applications. When the fabrication of porphyrin arrays is possible with a thiol-containing group, resultant fabricated arrays can be used for covalent attachment on gold surface.

The fabrication of the both ends of the porphyrin arrays through NBS bromination and subsequent Suzuki-Miyaura arylation (**Z*n*** to **Z*n*Br$_2$** to **Z*n*S$_2$**) up to **Z64** series were quantitatively achieved.

Electrical conduction measurements were made on two extreme types of directly linked porphyrin arrays by using nano-gap electrodes. One type is the directly linked Zn^{II} porphyrin arrays, **Z24SH$_2$**, and the other type is the completely flat, tape-shaped Zn^{II} porphyrin arrays, consisting of six Zn^{II} porphyrin units (**T6SH$_2$**). The *I-V* curve for **Z24S$_2$** exhibits the semi-conducter-like behavior. On the other hand, the *I-V* curve for **T6S$_2$** is nearly symmetric, leading to the higher conductivity and the smaller band gap. These results illustrate that the stronger π-electron conjugation in **T6SH$_2$**, as compared with that of **Z24SH$_2$**, results in better electrical conduction.

These both-ends fabricated porphyrin arrays should be quite useful in a variety of embryonic fields including molecular wire, sensor, and molecular electronics.

Summary of This Thesis

The broadly defined porphyrin research area is one of the most stimulating and rewarding for scientists in the field of chemistry, physics, biology and medicine. The beautifully constructed porphyrinoid ligand provides the chromophore for a multitude of iron, magnesium, and cobalt complexes, which are primary metabolites and without which life itsself could not be maintained.

In this Thesis, the synthesis, the structural characteristics, and the optical and electrochemical properties of directly *meso-meso* linked porphyrin arrays were described. These giant molecules are of particular interest in the fields of material chemistry and molecular electronic devices. The author has succeeded in the synthesis of *meso-meso* directly linked zinc(II) porphyrin arrays up to 1024-mer (**Z1024**) in a discrete manner by the repeated Ag^I salt promoted *meso-meso* coupling reaction. The actual molecular lengths were confirmed for **Z48** and **Z128** by STM and for **Z96, Z128, Z256,** and **Z512** by AFM. The fabrication of the both ends of the porphyrin arrays through NBS bromination and subsequent Suzuki-Miyaura arylation (**Z*n*** to **Z*n*Br$_2$** to **Z*n*S$_2$**) up to **Z64** series. In solution, the arrays **Z*n*** are considered to take overall linear rod-like structures but with substantial conformational flexibility as judged from their ^{1}H NMR spectra, diffusion coefficients, eluting behaviors on GPC-HPLC, and UV-vis and fluorescence spectra. The conformational flexibility has also been realized through the single-molecular SPM images on a Cu(111) surface and the single molecular AFM images on HOPG and Al_2O_3 surfaces.

As an extension, an oxidation reaction (DDQ and $Sc(OTf)_3$) allows effective transformation of *meso-meso* linked porphyrin arrays to *meso-meso*, *β-β*, *β-β*, triply-linked porphyrin arrays. Fascinating tape-shaped flat porphyrin arrays thus prepared promise for their remarkable properties arising from fully π-conjugated electronic systems, and hence encouraging potential conversion of a photonic wire to an electronic wire.

The chemistry described here opens a new area for nano-scaled and sub-micro-scaled functional materials.

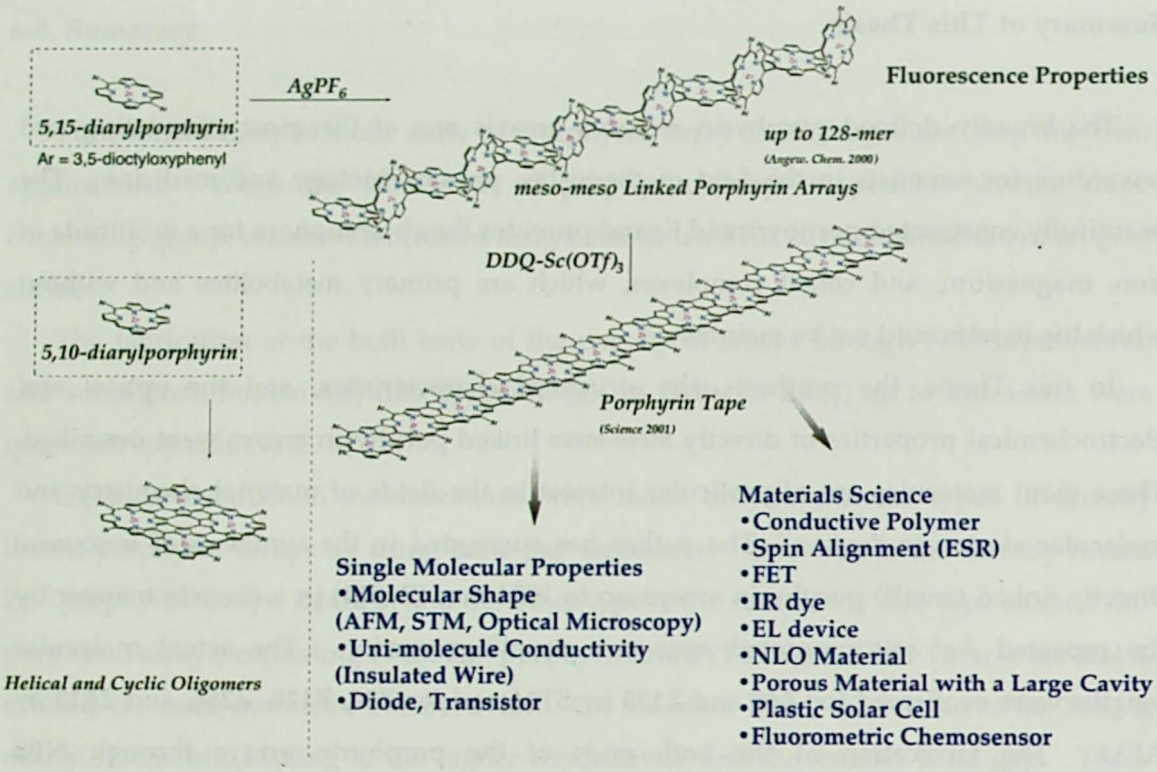
5,15-diarylporphyrin
Ar = 3,5-dioctyloxyphenyl
$AgPF_6$
Fluorescence Properties
up to 128-mer
(Angew. Chem. 2000)
meso-meso Linked Porphyrin Arrays
$DDQ\text{-}Sc(OTf)_3$
5,10-diarylporphyrin
Porphyrin Tape
(Science 2001)
Helical and Cyclic Oligomers
Single Molecular Properties
•Molecular Shape
(AFM, STM, Optical Microscopy)
•Uni-molecule Conductivity
(Insulated Wire)
•Diode, Transistor
Materials Science
•Conductive Polymer
•Spin Alignment (ESR)
•FET
•IR dye
•EL device
•NLO Material
•Porous Material with a Large Cavity
•Plastic Solar Cell
•Fluorometric Chemosensor

Experimental Section

General Procedure.

All reagents and solvents were of the commercial reagent grade and were used without further purification except where noted. Dry CH_2Cl_2 and $CHCl_3$ were obtained by refluxing and distilling over CaH_2. ^{1}H-NMR spectra were recorded on a JEOL ALPHA-500 and ECA-600 spectrometers, and chemical shifts were reported in the delta scale relative to internal standard of $CHCl_3$ (δ = 7.26 ppm). The spectroscopic grade tetrahydrofuran (THF) and toluene were used as solvents for all experiments. UV-visible absorption spectra were recorded on a Shimadzu UV-2400PC spectrometer. Steady-state fluorescence emission spectra were recorded on a Shimadzu RF-5300PC spectrometer. Mass spectra were recorded on a JEOL HX-110 spectrometer, using positive-FAB ionization method with accelerating voltage 10 kV and a 3-nitrobenzylalcohol matrix, or on a Shimadzu/KRATOS KOMPACT MALDI4 spectrometer, using positive-MALDI-TOF method with a 9-nitro anthracene matrix. Redox potentials were measured by the method of cyclic voltammetry and differential pulse voltammetry on a BAS electrochemical analyzer model 660. GPC-HPLC was performed on JAIGEL 2.5H-AF, 3H-AF, 4H-AF, and 5H-AF columns in series with JASCO HPLC system using multiwavelength detector MD-915. Recycling preparative GPC-HPLC was carried out on JAI LC-908 using preparative JAIGEL-2.5H, 3H, 4H, and 5H columns. Preparative separations were performed by silica gel flash column chromatography (Merck Kieselgel 60H Art.7736), silica gel gravity column chromatography (Wako gel C-200) and preparative size exclusion chromatography (BioRad Bio-Beads S-X1 packed in chloroform in a 4.0 x 100 cm HPLC column; flow rate 3.8 mL min^{-1}).

Single-Crystal Diffraction Analysis.

Data were collected on a Rigaku R-axis imaging plate refined by full-matrix least-squares procedures with anisotropic thermal parameters for the non-hydrogen atoms. The hydrogen atoms were calculated in ideal positions. Solution and structures were performed using the Crystal Structure, crystallographic software package of Molecular Structure Corporation. Crystallographic details are summarized in Table 1. Compounds **H1**: Crystals were obtained by vapor diffusion of EtOH into a CH_2Cl_2 solution of **H1**, and the data crystal was a red prism of dimensions 0.7 x 0.2 x 0.1 mm

($C_{64}H_{86}N_4O_4$). **ZP3**: Crystals were obtained by vapor diffusion of MeOH into a CH_2Cl_2 solution of **ZP3**, and the data crystal was a red prism of dimensions 0.3 x 0.2 x 0.1 mm ($C_{101}H_{72}N_{12}O_6Zn_3Cl_4$).

STM and AFM Measurement Conditions.

For STM measurements, Cu(100) or Cu(111) were used as a substrate. Clean flat surfaces of Cu(100) were obtained from a single crystal by Ar^+ sputtering and annealing (550°C) cycles, while those of Cu(111) were made on a cleaved mica surface by thermal evaporation. The arrays were dissolved into proper solvent ($CHCl_3$ or CH_2Cl_2) to ca. 10^{-5} mol L^{-1} in concentration. They were deposited by spraying ca. 0.5 μl of the solution onto the substrate in high vacuum (10^{-6} mbar) using the pulse injection method, which is adequate for the arrays too large to be thermally evaporated. In-situ STM imaging was performed in constant height mode at room temperature in ultra high vacuum (< 10^{-10} mbar) with a home-build STM by using an electrochemical etched Pt/Ir tip. For AFM measurements, the arrays were deposited by dropping the dilute $CHCl_3$ solution (ca. 10^{-5} mol L^{-1}) onto the tilted sapphire substrate $Al_2O_3(0001)$ and blown it off by air under ambient condition. AFM imaging was performed in an intermittent contact mode under ambient condition with a commercially available AFM (Nanoscope III, Digital Instruments Ltd.) with Si cantilevers (resonant frequency f = 300 kHz).

Methyl 3,5-dihydroxybenzoate (3). 3,5-Dihydroxybenzoic acid (**2**) (25.00 g, 162 mmol) was dissolved in methanol (500 mL). Conc. sulfuric acid (7 mL) was added to this mixture, and the solution was refluxed overnight, and then methanol was evaporated. The residue was dissolve in ethyl acetate and washed with water. The organic layer was separated and dried over anhydrous Na_2SO_4, and evaporated. The methyl ester **2** that was precipitated during evaporation was collected by filtration, and washed with hexane to give white crystals of **2**. Yield 26.02 g (155 mmol, 95%); mp 163.5-164.0°C; ^{1}H-NMR (DMSO) δ 9.61 (s, 2H, OH), 6.80 (d, J = 2 Hz, 2H, Ar-2,6-H), 6.43 (t, J = 2 Hz, 1H, Ar-4-H), 3.78 (s, 3H, Me); IR (KBr) 3383 + 3319 (br, m, OH), 1695 (s, C=O), 1169 (m, C-O) cm^{-1}.

Methyl 3,5-dioctyloxybenzoate (4). The methyl ester **3** (11.87 g, 70.7 mmol) was dissolved in acetone (300 mL). To this solution was added potassium carbonate (24.4 g, 177 mmol) and octylbromide (25.6 mL, 148 mmol). The mixture was heated under reflux for 2 days. The precipitates in formal were filtered, and the filtrate was concentrated by a rotary evaporator. To the resultant residue was added CH_2Cl_2 (100 mL), and water

(300 mL) was finally poured into this reaction mixture. The organic layer was separated. The aqueous layer was further extracted with CH_2Cl_2 (100 mL). The combined organic layer was washed with brine, dried over anhydrous Na_2SO_4, and evaporated. Unreacted octylbromide was distilled off under reduced pressure. The product was separated by silica gel chromatography (CH_2Cl_2). Yield 22.87 g (58 mmol, 83%); ^{1}H-NMR ($CDCl_3$) δ 7.16 (d, J = 2 Hz, 2H, Ar-2,6-H), 6.64 (t, J = 2 Hz, 1H, Ar-4-H), 3.97 (t, J = 7 Hz, 4H, octyloxy), 3.89 (s, 3H, Me), 1.77 (t-t, J = 7 Hz, 4H, octyloxy), 1.43 (m, 4H, octyloxy), 1.29 (m, 16H, octyloxy), and 0.88 (t, J = 7 Hz, 6H, octyloxy). Anal. Calcd. for $C_{24}H_{40}O_4$: C, 73.43; H, 10.27. Found: C, 73.29; H, 10.57.

3,5-Dioctyloxybenzyl alcohol (5). Lithium aluminum hydride (2.73 g, 72 mmol) was suspended in dry THF (100 mL) and then cooled to 0°C under nitrogen. The methyl ester **4** (40 g, 100 mmol) was dissolved in dry THF (200 mL), and this was added dropwise to above mentioned $LiAlH_4$/THF suspension at 0°C under nitrogen. After the mixture was stirred for 1 h, water was carefully added dropwise. The solid was deposited during addition of water and removed by filtration under reduced pressure. The filtrate was extracted with diethyl ether, and the organic layer was separated, washed with brine, dried over anhydrous sodium sulfate, and evaporated. Colorless crystal. Yield 34.17 g (94 mmol, 92%); ^{1}H-NMR ($CDCl_3$) δ 6.50 (d, J = 2 Hz, 2H, Ar-2,6-H), 6.38 (t, J = 2 Hz, 1H, Ar-4-H), 4.61 (d, J = 6 Hz, 2H, benzyl), 3.97 (t, J = 7 Hz, 4H, octyloxy), 1.78 (t-t, J = 7 Hz, 4H, octyloxy), 1.61 (t, J = 6 Hz, 1H, OH), 1.43 (m, 4H, octyloxy), 1.29 (m, 16H, octyloxy), and 0.89 (t, J = 7 Hz, 6H, octyloxy); FAB MS m/z 364.5, calcd for $C_{23}H_{40}O_3$ m/z 364.3. Anal. Calcd. for $C_{23}H_{40}O_3$: C, 75.77; H, 11.06. Found: C, 75.49; H, 10.83.

3,5-Dioctyloxybenzaldehyde (6). Alcohol **5** (33 g, 90 mmol) was dissolved in dry CH_2Cl_2 (200 mL). Sodium acetate (14.7 g, 180 mmol) was suspended in this solution, and the resultant suspension was cooled to 0°C. Pyridinium chlorochromate (PCC) (29 g, 200 mmol) was carefully added to the suspension at 0°C. After stirring for 2 h diethyl ether was added to the reaction mixture, and the liquid phase was separated by decantation. The residual gummy solid was washed with diethyl ether several times. The combined liquid phase was passed though a florisil short column. Diethyl ether was evaporated. The product was crystallized during evaporation. Colorless oil. Yield 30 g (81 mmol, 91%); ^{1}H-NMR ($CDCl_3$) δ 9.90 (s, 1H, CHO), 6.98 (d, J = 2 Hz, 2H, Ar-2,6-H), 6.70 (t, J = 4 Hz, 1H, Ar-4-H), 3.99 (t, J = 7 Hz, 4H, octyloxy), 1.80 (t-t, J = 7 Hz, 4H, octyloxy), 1.43 (m, 4H, octyloxy), 1.29 (m, 16H, octyloxy), and 0.89 (t, J = 7 Hz, 6H, octyloxy); FAB MS m/z 362.4, calcd for $C_{23}H_{38}O_3$ m/z 362.3. Anal. Calcd. for $C_{23}H_{38}O_3$: C, 76.20; H, 10.56. Found:

C, 76.02; H, 10.76.

Bis(2-pyrryl)methane (**7**) was prepared by the method reported by Lee *et al.* [66]. A solution of formalin (12 mL, 0.14 mol) and pyrrole (50 mL, 0.72 mol) was stirred for 15 min at 50°C then carefully added TFA (1.1 ml, 0.014 mol). After the work-up, **7** (5.23 g, 26%) was obtained.

5,15-Bis(3,5-dioctyloxyphenyl)porphyrin H1. A solution of **7** (1.00 g, 6.85 mmol) and 3,5-dioctyloxybenzaldehyde **6** (2.48 g, 6.85 mmol) in dry CH_2Cl_2 (1.3 L) was stirred under Ar, the flask was shielded from light. Trifluoroacetic acid (0.328 mL, 4.26 mmol) was added via syringe, and the solution was stirred for 2-3 h at room temperature. DDQ (2.32 g, 10.3 mmol) was added to the solution, and the resulting solution was stirred for an additional 2-3 h. After the reaction mixture was neutralized by triethylamine and passed over Alumina column to remove polymeric materials, the solvent was removed by a rotary evaporator and the residue was purified by a silica gel flash column chromatography with CH_2Cl_2/hexane. The product was recrystallized from CH_2Cl_2-EtOH. Yield; 1.47 g, 44%. This reaction scheme was repeated for 10 times, resulting in the making of 15 g porphyrin. ^{1}H NMR ($CDCl_3$) δ 10.30 (s, 2H, *meso*), 9.38 (d, J = 5 Hz, 4H, β), 9.19 (d, J = 5 Hz, 4H, β), 7.43 (d, J = 3 Hz, 4H, Ar), 6.92 (t, J = 3 Hz, 2H, Ar), 4.12 (t, J = 7 Hz, 8H, octyloxy), 1.89 (t-t, J = 7 Hz, 8H, octyloxy), 1.51 (t-t, J = 7 Hz, 8H, octyloxy), 1.38-1.27 (m, 32H, octyloxy), 0.87 (t, J = 7 Hz, 12H, octyloxy), and -3.15 (s, 2H, N-H); FAB MS *m/z* 974.6, calcd for $C_{64}H_{86}N_4O_4$ *m/z* 974.7; Anal. Calcd. for $C_{64}H_{86}N_4O_4$: C, 78.81; H, 8.89; N, 5.74. Found: C, 78.62; H, 8.89; N, 5.73; UV-vis (THF) λ_{max} 407, 501, 537, 574, and 630 nm; Fluorescence (THF, λ_{ex} = 413 nm) λ_{em} 631 and 696 nm.

Z1. ^{1}H NMR ($CDCl_3$) δ 10.31 (s, 2H, *meso*), 9.43 (d, J = 5 Hz, 4H, β), 9.26 (d, J = 5 Hz, 4H, β), 7.43 (d, J = 3 Hz, 4H, Ar), 6.92 (t, J = 3 Hz, 2H, Ar), 4.15 (t, J = 7 Hz, 8H, octyloxy), 1.89 (t-t, J = 7 Hz, 8H, octyloxy), 1.51 (t-t, J = 7 Hz, 8H, octyloxy), 1.39-1.27 (m, 32H, octyloxy), and 0.87 (t, J = 7 Hz, 12H, octyloxy); FAB MS *m/z* 1036.4, calcd for $C_{64}H_{84}N_4O_4Zn$ *m/z* 1036.6; Anal. Calcd. for $C_{64}H_{84}N_4O_4Zn$: C, 74.00; H, 8.15; N, 5.39. Found: C, 73.75; H, 8.21; N, 5.16; UV-vis (THF) λ_{max} (ε) [nm ($cm^{-1}M^{-1}$)] 413 (645000) and 543 (22000); Fluorescence (THF, λ_{ex} = 413 nm) λ_{em} 584 and 634 nm.

General Procedure for *Meso-meso* Coupling Reaction of Zn^{II} 5,15-bis(3,5-dioctyloxyphenyl)porphyrin arrays *Zn*.

The reaction vessel containing a solution of Zn^{II} 5,15-bis(3,5-dioctyloxyphenyl) porphyrin array in dry $CHCl_3$ was covered with foil. A stock solution of $AgPF_6$ in dry

CH_3CN (0.127 M) was added to that solution, and the resulting mixture was stirred at 30°C or room temperature, while the progress of the reaction was monitored by the analytical GPC-HPLC. The reaction was stopped by adding water and the reaction mixture was dried over anhydrous Na_2SO_4. A solution of $Zn(OAc)_2$ in methanol was added, and the solution was stirred at refluxed temperature for 1-2 h. Then it was washed successively with water, and saturated $NaHCO_3$ solution, and dried over anhydrous Na_2SO_4. The solvent was removed by a rotary evaporator. The product separation was performed on a preparative size exclusion column (a medium-pressure size-exclusion column (SEC) chromatography for **Z2**, **Z3**, and **Z4**, and recycling preparative GPC-HPLC for larger arrays).

Z2. A round-bottomed flask was charged with **Z1** (570 mg, 0.55 mmol) and dry $CHCl_3$ (160 mL). A stock solution of $AgPF_6$ (4.78 mL, 0.66 mmol) in acetonitrile was added at once. The reaction mixture was stirred for 10 h at 30°C. After the usual work-up, the oligomers ware separated by a preparative size exclusion column (SEC). Fractions of 2-mer and 3-mer ware separated, and the solvent was removed by a rotary evaporator. Recrystallization from $CHCl_3$/EtOH gave red-blown solids of **Z2** (138 mg, 24%). ^{1}H NMR ($CDCl_3$) δ 10.38 (s, 2H, *meso*), 9.49 (d, J = 5 Hz, 4H, β), 9.28 (d, J = 5 Hz, 4H, β), 8.82 (d, J = 5 Hz, 4H, β), 8.10 (d, J = 5 Hz, 4H, β), 7.42 (d, J = 3 Hz, 8H, Ar), 6.92 (t, J = 3 Hz, 4H, Ar), 4.06 (t, J = 7 Hz, 16H, octyloxy), 1.80 (t-t, J = 7 Hz, 16H, octyloxy), 1.44 (t-t, J = 7 Hz, 16H, octyloxy), 1.32-1.21 (m, 64H, octyloxy), and 0.81 (t, J = 7 Hz, 24H, octyloxy); MALDI-TOF-MS m/z 2076, calcd for $C_{128}H_{166}N_8O_8Zn_2$ m/z 2075.1; Anal. Calcd. for $C_{128}H_{166}N_8O_8Zn_2$ (H_2O): C, 73.43; H, 8.09; N, 5.35; Found: C, 73.23; H, 8.13; N, 5.34; UV-vis (THF) λ_{max} (ε) [nm ($cm^{-1}M^{-1}$)] 418 (270000), 452 (250000), and 560 (60000); Fluorescence (THF, λ_{ex} = 413 nm) λ_{em} 657 nm.

Z3. ^{1}H NMR ($CDCl_3$) δ 10.40 (s, 2H, *meso*), 9.50 (d, J = 5 Hz, 4H, β), 9.29 (d, J = 5 Hz, 4H, β), 8.89 (d, J = 5 Hz, 4H, β), 8.80 (d, J = 5 Hz, 4H, β) 8.24 (d, J = 5 Hz, 4H, β) 8.12 (d, J = 5 Hz, 4H, β), 7.45 (d, J = 3 Hz, 8H, Ar), 7.38 (d, J = 3 Hz, 4H, Ar), 6.84 (t, J = 3 Hz, 4H, Ar), 6.67 (t, J = 3 Hz, 2H, Ar), 4.09 (t, J = 7 Hz, 16H, octyloxy), 3.95 (t, J = 7 Hz, 8H, octyloxy), 1.82 (t-t, J = 7 Hz, 16H, octyloxy), 1.69 (t-t, J = 7 Hz, 8H, octyloxy), 1.46 (t-t, J = 7 Hz, 16H, octyloxy), 1.33-1.13 (m, 104H, octyloxy), 0.81 (t, J = 7 Hz, 24H, octyloxy) and 0.72 (t, J = 7 Hz, 12H, octyloxy); MALDI-TOF-MS m/z 3114, calcd for $C_{192}H_{248}N_{12}O_{12}Zn_3$ m/z 3112; UV-vis (THF) λ_{max} (nm) 414, 476, and 571; Fluorescence (THF, λ_{ex} = 413 nm) λ_{em} 632 and 669 nm.

Z4. A round-bottomed flask was charged with **Z2** (90 mg, 0.043 mmol) and dry

$CHCl_3$ (60 mL). A stock solution of $AgPF_6$ (0.26 mL, 0.033 mmol) was added at once. The reaction mixture was stirred for 5 h at room temperature. After the usual work up, the separation over SEC and recrystallization from $CHCl_3$/MeOH gave a pure **Z4** (24 mg, 27%). ^{1}H NMR ($CDCl_3$) δ 10.40 (s, 2H, *meso*), 9.51 (d, J = 5 Hz, 4H, β), 9.30 (d, J = 5 Hz, 4H, β), 8.90 (d, J = 5 Hz, 4H, β), 8.88 (d, J = 5 Hz, 4H, β), 8.82 (d, J = 5 Hz, 4H, β), 8.28 (d, J = 5 Hz, 4H, β), 8.25 (d, J = 5 Hz, 4H, β), 8.14 (d, J = 5 Hz, 4H, β), 7.46 (d, J = 3 Hz, 8H, Ar), 7.43 (d, J = 3 Hz, 8H, Ar), 6.85 (br, 4H, Ar), 6.71 (br, 4H, Ar), 4.10 (t, J = 7 Hz, 16H, octyloxy), 4.00 (t, J = 7 Hz, 16H, octyloxy), 1.83 (t-t, J = 7 Hz, 16H, octyloxy), 1.73 (t-t, J = 7 Hz, 16H, octyloxy), 1.47 (t-t, J = 7 Hz, 16H, octyloxy), 1.38-1.16 (m, 144H, octyloxy), 0.82 (t, J = 7 Hz, 24H, octyloxy), and 0.75 (t, J = 7 Hz, 24H, octyloxy); MALDI-TOF-MS *m/z* 4146, calcd for $C_{256}H_{330}N_{16}O_{16}Zn_4$ *m/z* 4148; UV-vis (THF) λ_{max} (ε) [nm ($cm^{-1}M^{-1}$)] 414 (440000), 488 (410000) and 576 (140000); Fluorescence (THF, λ_{ex} = 413 nm) λ_{em} 639 and 666 nm.

Z5. ^{1}H NMR ($CDCl_3$) δ 10.41 (s, 2H, *meso*), 9.52 (d, J = 5 Hz, 4H, β), 9.31 (d, J = 5 Hz, 4H, β), 8.95-8.91 (m, 12H, β), 8.85 (d, J = 5 Hz, 4H, β), 8.35-8.32 (m, 8H, β), 8.28 (d, J = 5 Hz, 4H, β), 8.17 (d, J = 5 Hz, 4H, β), 7.48 (d, J = 2 Hz, 12H, Ar), 7.45 (d, J = 2 Hz, 8H, Ar), 6.85 (br, 4H, Ar), 6.76 (br, 2H, Ar) 6.72 (br, 4H, Ar), 4.11-4.01 (m, 40H, octyloxy), 1.85-1.72 (m, 40H, octyloxy), 1.49-1.17 (m, 200H, octyloxy), 0.83 (t, J = 7 Hz, 20H, octyloxy), and 0.78-0.74 (m, 40H, octyloxy); MALDI-TOF-MS *m/z* 5183, calcd for $C_{320}H_{412}N_{20}O_{20}Zn_5$ *m/z* 6221; UV-vis (THF) λ_{max} (nm) 414, 494 and 580; Fluorescence (THF, λ_{ex} = 413 nm) λ_{em} 640 nm.

Z6. ^{1}H NMR ($CDCl_3$) δ 10.42 (s, 2H, *meso*), 9.52 (d, J = 5 Hz, 4H, β), 9.31 (d, J = 5 Hz, 4H, β), 8.95-8.91 (m, 16H, β), 8.85 (d, J = 5 Hz, 4H, β), 8.35-8.32 (m, 12H, β), 8.28 (d, J = 5 Hz, 4H, β), 8.17 (d, J = 5 Hz, 4H, β), 7.48 (d, J = 2 Hz, 8H, Ar), 7.47 (d, J = 3 Hz, 8H, Ar), 7.45 (d, J = 2 Hz, 8H, Ar), 6.85 (br, 4H, Ar), 6.76 (br, 4H, Ar) 6.72 (br, 4H, Ar), 4.11-4.01 (m, 48H, octyloxy), 1.85-1.72 (m, 48H, octyloxy), 1.49-1.17 (m, 240H, octyloxy), 0.83 (t, J = 7 Hz, 24H, octyloxy), and 0.78-0.74 (m, 48H, octyloxy); MALDI-TOF-MS *m/z* 6214, calcd for $C_{384}H_{494}N_{24}O_{24}Zn_6$ *m/z* 6221; UV-vis (THF) λ_{max} (nm) 414, 498 and 582; Fluorescence (THF, λ_{ex} = 413 nm) λ_{em} 640 nm.

Z7. ^{1}H NMR ($CDCl_3$) δ 10.41 (s, 2H, *meso*), 9.53 (d, J = 5 Hz, 4H, β), 9.31 (d, J = 5 Hz, 4H, β), 8.95-8.91 (m, 20H, β), 8.85 (d, J = 5 Hz, 4H, β), 8.35-8.32 (m, 16H, β), 8.28 (d, J = 5 Hz, 4H, β), 8.17 (d, J = 5 Hz, 4H, β), 7.51-7.46 (m, 28H, Ar), 6.86 (br, 4H, Ar), 6.77 (br, 6H, Ar), 6.73 (br, 4H, Ar), 4.11-4.02 (m, 56H, octyloxy), 1.83-1.73 (m, 56H, octyloxy), 1.48-1.20 (m, 280H, octyloxy), 0.83 (t, J = 7 Hz, 21H, octyloxy), and 0.80-0.74 (m, 63H, octyloxy); MALDI-TOF-MS *m/z* 7253, calcd for $C_{448}H_{576}N_{28}O_{28}Zn_7$ *m/z* 7259; UV-vis (THF) λ_{max} (nm)

414, 500 and 583; Fluorescence (THF, λ_{ex} = 413 nm) λ_{em} 642 nm.

Z8. A stock solution of $AgPF_6$ in CH_3CN (0.047 mL, 0.006 mmol) was added to a solution of **Z4** (31 mg, 0.0075 mmol) in $CHCl_3$ (40 mL), and stirred for 3 h at room temperature. After the usual work-up, the separation over a recycling preparative GPC-HPLC and recrystallization from $CHCl_3$/MeOH gave a pure **Z8** (7 mg, 22%). ^{1}H NMR ($CDCl_3$) δ 10.42 (s, 2H, *meso*), 9.53 (d, J = 5 Hz, 4H, β), 9.31 (d, J = 5 Hz, 4H, β), 8.95-8.91 (m, 24H, β), 8.85 (d, J = 5 Hz, 4H, β), 8.35-8.32 (m, 20H, β), 8.28 (d, J = 5 Hz, 4H, β), 8.17 (d, J = 5 Hz, 4H, β), 7.51-7.46 (m, 32H, Ar), 6.86 (br, 4H, Ar), 6.77 (br, 8H, Ar), 6.73 (br, 4H, Ar), 4.11-4.02 (m, 64H, octyloxy), 1.83-1.73 (m, 64H, octyloxy), 1.48-1.20 (m, 320H, octyloxy), 0.83 (t, J = 7 Hz, 24H, octyloxy), and 0.80-0.74 (m, 72H, octyloxy); MALDI-TOF-MS m/z 8303, calcd for $C_{512}H_{658}N_{32}O_{32}Zn_8$ m/z 8296; UV-vis (THF) λ_{max} (ε) [nm ($cm^{-1}M\varepsilon$)] 414 (745000), 502 (735000) and 585 (430000); Fluorescence (THF, λ_{ex} = 413 nm) λ_{em} 640 nm.

Z10. ^{1}H NMR ($CDCl_3$) δ 10.41 (s, 2H, *meso*), 9.53 (br, 4H, β), 9.31 (br, 4H, β), 8.96-8.92 (m, 32H, β), 8.85 (d, J = 5 Hz, 4H, β), 8.36-8.33 (m, 28H, β), 8.29 (d, J = 5 Hz, 4H, β), 8.17 (d, J = 5 Hz, 4H, β), 7.52-7.46 (m, 40H, Ar), 6.87 (br, 4H, Ar), 6.78 (br, 12H, Ar), 6.74 (br, 4H, Ar), 4.12-4.07 (m, 80H, octyloxy), 1.86-1.74 (m, 80H, octyloxy), 1.50-1.19 (m, 400H, octyloxy), and 0.85-0.75 (m, 120H, octyloxy); MALDI-TOF-MS m/z 10351, calcd for $C_{640}H_{822}N_{40}O_{40}Zn_{10}$ m/z 10369; UV (THF) λ_{max} (nm) 414, 505 and 586; Fluorescence (THF, λ_{ex} = 413 nm) λ_{em} 642 nm.

Z12. ^{1}H NMR ($CDCl_3$) δ 10.41 (s, 2H, *meso*), 9.52 (br, 4H, β), 9.31 (br, 4H, β), 8.96-8.92 (m, 40H, β), 8.85 (d, J = 5 Hz, 4H, β), 8.36-8.33 (m, 36H, β), 8.28 (d, J = 5 Hz, 4H, β), 8.17 (d, J = 5 Hz, 4H, β), 7.52-7.46 (m, 48H, Ar), 6.86 (br, 4H, Ar), 6.79 (br, 16H, Ar), 6.73 (br, 4H, Ar), 4.07 (m, 96H, octyloxy), 1.86-1.76 (m, 96H, octyloxy), 1.50-1.19 (m, 480H, octyloxy), and 0.85-0.75 (m, 144H, octyloxy); MALDI-TOF-MS m/z 12416, calcd for $C_{768}H_{986}N_{48}O_{48}Zn_{12}$ m/z 12443; UV ($CHCl_3$) λ_{max} (nm) 414, 507 and 587; Fluorescence ($CHCl_3$, λ_{ex} = 413 nm) λ_{em} 642 nm.

Z16. A stock solution of $AgPF_6$ in CH_3CN (0.012 mL, 0.0015 mmol) was added to a solution of **Z8** (18 mg, 2.2 mmol) in $CHCl_3$ (20 mL), and stirred for 12 h at room temperature. After the usual work-up, the separation over a recycling preparative GPC-HPLC and recrystallization from $CHCl_3$/MeOH gave a pure **Z16** (5 mg, 27%). ^{1}H NMR ($CDCl_3$) δ 10.42 (s, 2H, *meso*), 9.53 (br, 4H, β), 9.31 (br, 4H, β), 8.97-8.85 (m, 60H, β), 8.37-8.17 (m, 60H, β), 7.52-7.46 (m, 64H, Ar), 6.86-6.73 (br, 32H, Ar), 4.07 (m, 128H, octyloxy), 1.84-1.78 (m, 128H, octyloxy), 1.44-1.20 (m, 640H, octyloxy), and 0.85-0.75 (m, 192H, octyloxy); MALDI-TOF-MS m/z 16620, calcd for $C_{1024}H_{1314}N_{64}O_{64}Zn_{16}$ m/z 16590;

UV-vis (THF) λ_{max} (ε) [nm ($cm^{-1}M^{-1}$)] 414 (1 300 000), 508 (1 380 000) and 587 (950 000); Fluorescence (THF, λ_{ex} = 413 nm) λ_{em} 642 nm.

Z20. ^{1}H NMR ($CDCl_3$) δ 10.41 (s, 2H, *meso*), 9.52 (br, 4H, β), 9.31 (br, 4H, β), 8.96-8.84 (m, 76H, β), 8.36-8.16 (m, 76H, β), 7.52-7.45 (m, 80H, Ar), 6.86-6.73 (m, 40H, Ar), 4.07 (m, 160H, octyloxy), 1.79 (m, 160H, octyloxy), 1.44-1.21 (m, 800H, octyloxy), and 0.84-0.75 (m, 240H, octyloxy); MALDI-TOF-MS *m/z* 20769, calcd for $C_{1280}H_{1642}N_{80}O_{80}Zn_{20}$ *m/z* 20736; UV-vis ($CHCl_3$) λ_{max} (nm) 414, 506 and 585; Fluorescence ($CHCl_3$, λ_{ex} = 413 nm) λ_{em} 641 nm.

Z24. ^{1}H NMR ($CDCl_3$) δ 10.41 (s, 2H, *meso*), 9.52 (br, 4H, β), 9.30 (br, 4H, β), 8.97-8.84 (m, 92H, β), 8.37-8.16 (m, 92H, β), 7.52-7.45 (m, 96H, Ar), 6.86-6.73 (m, 48H, Ar), 4.07 (m, 192H, octyloxy), 1.79 (m, 192H, octyloxy), 1.44-1.21 (m, 960H, octyloxy), and 0.84-0.74 (m, 288H, octyloxy); MALDI-TOF-MS *m/z* 24465, calcd for $C_{1536}H_{1970}N_{96}O_{96}Zn_{24}$ *m/z* 24884; UV-vis ($CHCl_3$) λ_{max} (nm) 414, 506 and 585; Fluorescence ($CHCl_3$, λ_{ex} = 413 nm) λ_{em} 641 nm.

Z32. $AgPF_6$ (0.014 mL of 0.138 M stock solution in dry CH_3CN, 0.0019 mmol) was added to a solution of **Z16** (40 mg, 0.0024 mmol) in $CHCl_3$ (20 mL), and stirred for 4 h at room temperature. Again $AgPF_6$ solution (0.014 mL) was added and the mixture was stirred for more 5 h. After the usual work-up, the separation over a recycling preparative GPC-HPLC and recrystallization from $CHCl_3$/MeOH gave a pure **Z32** (10 mg, 25%). ^{1}H NMR ($CDCl_3$) δ 10.42 (s, 2H, *meso*), 9.52 (br, 4H, β), 9.31 (br, 4H, β), 8.97-8.85 (m, 124H, β), 8.38-8.17 (m, 124H, β), 7.53-7.46 (m, 128H, Ar), 6.86-6.73 (br, 64H, Ar), 4.08 (m, 256H, octyloxy), 1.80 (m, 256H, octyloxy), 1.46-1.21 (m, 1280H, octyloxy), and 0.85-0.75 (m, 384H, octyloxy); MALDI-TOF-MS *m/z* 33790, calcd for $C_{2048}H_{2626}N_{128}O_{128}Zn_{32}$ *m/z* 33178; UV-vis (THF) λ_{max} (ε) [nm ($cm^{-1}M^{-1}$)] 414 (2690000), 509 (3070000) and 588 (220000); Fluorescence (THF, λ_{ex} = 413 nm) λ_{em} 642 nm.

Z40. ^{1}H NMR ($CDCl_3$) δ 10.42 (s, 2H, *meso*), 9.52 (br, 4H, β), 9.31 (br, 4H, β), 8.97-8.85 (m, 156H, β), 8.37-8.16 (m, 156H, β), 7.52-7.46 (m, 160H, Ar), 6.86-6.73 (m, 80H, Ar), 4.07 (m, 320H, octyloxy), 1.80 (m, 320H, octyloxy), 1.44-1.22 (m, 1600H, octyloxy), and 0.88-0.75 (m, 480H, octyloxy); MALDI-TOF-MS *m/z* 41177, calcd for $C_{2560}H_{3282}N_{160}O_{160}Zn_{40}$ *m/z* 41470; UV-vis ($CHCl_3$) λ_{max} (nm) 414, 507 and 586; Fluorescence ($CHCl_3$, λ_{ex} =413 nm) λ_{em} 641 nm.

Z48. ^{1}H NMR ($CDCl_3$) δ 10.42 (s, 2H, *meso*), 9.52 (br, 4H, β), 9.31 (br, 4H, β), 8.97 (m, 188H, β), 8.37-8.16 (m, 188H, β), 7.52-7.46 (m, 192H, Ar), 6.86-6.73 (m, 96H, Ar), 4.07 (m, 384H, octyloxy), 1.80 (m, 384H, octyloxy), 1.45-1.22 (m, 1920H, octyloxy), and 0.87-0.75 (m, 576H, octyloxy); MALDI-TOF-MS *m/z* 49447, calcd for $C_{3072}H_{3938}N_{192}O_{192}Zn_{48}$ *m/z* 49764;

UV-vis ($CDCl_3$) λ_{max} (nm) 413, 508 and 586; Fluorescence ($CHCl_3$, λ_{ex} =413 nm) λ_{em} 640 nm.

Z64. $AgPF_6$ (0.004 mL of 0.138 M stock solution in dry CH_3CN, 0.0005 mmol) was added to a solution of **Z32** (18 mg, 0.0005 mmol) in $CHCl_3$ (3 mL), and stirred for 7 h at room temperature. After the usual work-up, the separation over a recycling preparative GPC-HPLC and recrystallization from $CHCl_3$/MeOH gave a pure **Z64** (3.7 mg, 22%). ^1H NMR ($CDCl_3$) δ 10.42 (s, 2H, *meso*), 9.52 (br, 4H, β), 9.31 (br, 4H, β), 8.97 (m, 252H, β), 8.38-8.17 (m, 252H, β), 7.53 (m, 256H, Ar), 6.86-6.74 (br, 128H, Ar), 4.07 (m, 512H, octyloxy), 1.80 (m, 512H, octyloxy), 1.45-1.22 (m, 2560H, octyloxy), and 0.85-0.75 (m, 768H, octyloxy); MALDI-TOF-MS *m/z* 66258, calcd for $C_{4096}H_{5250}N_{256}O_{256}Zn_{64}$ *m/z* 66350; UV-vis (THF) λ_{max} (nm) 414, 510 and 589; Fluorescence (THF, λ_{ex} = 413 nm) λ_{em} 642 nm.

Z96. ^1H NMR ($CDCl_3$) δ 10.42 (s, 2H, *meso*), 9.52 (br, 4H, β), 9.31 (br, 4H, β), 8.97 (m, 380H, β), 8.37-8.16 (m, 380H, β), 7.52 (m, 384H, Ar), 6.79 (br, 192H, Ar), 4.07 (m, 768H, octyloxy), 1.80 (m, 768H, octyloxy), 1.45-1.22 (m, 3840H, octyloxy), and 0.88-0.76 (m, 1152H, octyloxy); MALDI-TOF-MS *m/z* 99050, calcd for $C_{6144}H_{7874}N_{384}O_{384}Zn_{96}$ *m/z* 99503; UV-vis ($CHCl_3$) λ_{max} (nm) 413, 508 and 586; Fluorescence ($CHCl_3$, λ_{ex} = 413 nm) λ_{em} 641 nm.

Z128. ^1H NMR ($CDCl_3$) δ 10.40 (s, 2H, *meso*), 9.52 (br, 4H, β), 9.30 (br, 4H, β), 8.96 (m, 508H, β), 8.36 (m, 508H, β), 7.52 (m, 512H, Ar), 6.79 (br, 256H, Ar), 4.06 (m, 1024H, octyloxy), 1.79 (m, 1024H, octyloxy), 1.44-1.22 (m, 5120H, octyloxy), and 0.81-0.78 (m, 1536H, octyloxy); MALDI-TOF-MS *m/z* 130295, calcd for $C_{8192}H_{10498}N_{512}O_{512}Zn_{128}$ *m/z* 132702; UV-vis (THF) λ_{max} (nm) 414, 511 and 589; Fluorescence (THF, λ_{ex} = 413 nm) λ_{em} 642 nm.

Z256. ^1H NMR ($CDCl_3$) δ 10.42 (s, 2H, *meso*), 9.53 (br, 4H, β), 9.31 (br, 4H, β), 8.97 (m, 1020H, β), 8.37 (m, 1020H, β), 7.52 (m, 1024H, Ar), 6.79 (br, 512H, Ar), 4.06 (m, 2048H, octyloxy), 1.79 (m, 2048H, octyloxy), 1.44-1.22 (m, 10240H, octyloxy), and 0.81-0.78 (m, 3072H, octyloxy); UV-vis (THF) λ_{max} (nm) 414, 511 and 589; Fluorescence (THF, λ_{ex} = 413 nm) λ_{em} 642 nm.

Z384. UV-vis (THF) λ_{max} (nm) 414, 511 and 589; Fluorescence (THF, λ_{ex} = 413 nm) λ_{em} 642 nm.

Z512. UV-vis (THF) λ_{max} (nm) 414, 511 and 589; Fluorescence (THF, λ_{ex} = 413 nm) λ_{em} 642 nm.

H2. **Z2** was dissolved in a mixture of CH_2Cl_2 and 3 N HCl. The resulting solution was stirred for 1 h at room temperature, poured into water, and extracted with CH_2Cl_2. The organic layer was separated off, and the combined extracts were washed with water,

saturated aqueous $NaHCO_3$, water, and dried over anhydrous Na_2SO_4. The solvent was evaporated and the product was recrystallized from CH_2Cl_2/MeOH to give **H2**. ^1H NMR ($CDCl_3$) δ 10.34 (s, 2H, *meso*), 9.42 (d, J = 5 Hz, 4H, β), 9.18 (d, J = 5 Hz, 4H, β), 8.72 (d, J = 5 Hz, 4H, β), 8.03 (d, J = 5 Hz, 4H, β), 7.39 (d, J = 3 Hz, 8H, Ar), 6.80 (t, J = 3 Hz, 4H, Ar), 4.06 (t, J = 7 Hz, 16H, octyloxy), 1.79 (t-t, J = 7 Hz, 16H, octyloxy), 1.44 (t-t, J = 7 Hz, 16H, octyloxy), 1.32-1.21 (m, 64H, octyloxy), 0.80 (t, J = 7 Hz, 24H, octyloxy), and -2.44 (s, 4H, inner-NH); FAB-MS m/z 1947.2, calcd for $C_{128}H_{170}N_8O_8$ m/z 1947.3; UV-vis ($CHCl_3$) λ_{max} (nm) 413, 445, 519, 588, and 644; Fluorescence ($CHCl_3$, λ_{ex} = 413 nm) λ_{em} 650 and 711 nm.

H3. ^1H NMR ($CDCl_3$) δ 10.36 (s, 2H, *meso*), 9.44 (d, J = 5 Hz, 4H, β), 9.21 (d, J = 5 Hz, 4H, β), 8.81 (d, J = 5 Hz, 4H, β), 8.72 (d, J = 5 Hz, 4H, β) 8.20 (d, J = 5 Hz, 4H, β) 8.09 (d, J = 5 Hz, 4H, β), 7.43 (d, J = 2 Hz, 8H, Ar), 7.35 (d, J = 2 Hz, 4H, Ar), 6.84 (t, J = 2 Hz, 4H, Ar), 6.67 (br, 2H, Ar), 4.10 (t, J = 7 Hz, 16H, octyloxy), 3.96 (t, J = 7 Hz, 8H, octyloxy), 1.84 (t-t, J = 7 Hz, 16H, octyloxy), 1.70 (t-t, J = 7 Hz, 8H, octyloxy), 1.46-1.13 (m, 120H, octyloxy), 0.82 (t, J = 7 Hz, 24H, octyloxy), 0.73 (t, J = 7 Hz, 12H, octyloxy), -1.65 (s, 2H, inner-NH), -2.40 (s, 4H, inner-NH); MALDI-TOF-MS m/z 2917, calcd for $C_{192}H_{254}N_{12}O_{12}$ m/z 2922; UV-vis ($CHCl_3$) λ_{max} (nm) 410, 469, 528, and 596; Fluorescence ($CHCl_3$, λ_{ex} = 413 nm) λ_{em} 661 and 724 nm.

H4. ^1H NMR ($CDCl_3$) δ 10.37 (s, 2H, *meso*), 9.44 (d, J = 5 Hz, 4H, β), 9.21 (d, J = 5 Hz, 4H, β), 8.82-8.81 (m, 8H, β), 8.75 (d, J = 5 Hz, 4H, β), 8.26 (d, J = 5 Hz, 4H, β), 8.22 (d, J = 5 Hz, 4H, β), 8.11 (d, J = 5 Hz, 4H, β), 7.44 (d, J = 3 Hz, 8H, Ar), 7.40 (d, J = 3 Hz, 8H, Ar), 6.84 (br, 4H, Ar), 6.71 (br, 4H, Ar), 4.10 (t, J = 7 Hz, 16H, octyloxy), 4.00 (t, J = 7 Hz, 16H, octyloxy), 1.83 (t-t, J = 7 Hz, 16H, octyloxy), 1.73 (t-t, J = 7 Hz, 16H, octyloxy), 1.47 (t-t, J = 7 Hz, 16H, octyloxy), 1.38-1.16 (m, 144H, octyloxy), 0.82 (t, J = 7 Hz, 24H, octyloxy), 0.75 (t, J = 7 Hz, 24H, octyloxy), -1.62 (s, 4H, inner-NH), and -2.39 (s, 4H, inner-NH); MALDI-TOF-MS m/z 3894, calcd for $C_{256}H_{338}N_{16}O_{16}$ m/z 3894; UV-vis ($CHCl_3$) λ_{max} (nm) 411, 480, 535, and 596; Fluorescence ($CHCl_3$, λ_{ex} = 413 nm) λ_{em} 665 and 726 nm.

H6. ^1H NMR ($CDCl_3$) δ 10.37 (s, 2H, *meso*), 9.45 (d, J = 5 Hz, 4H, β), 9.22 (d, J = 5 Hz, 4H, β), 8.85-8.83 (m, 16H, β), 8.76 (d, J = 5 Hz, 4H, β), 8.29-8.28 (m, 12H, β), 8.23 (d, J = 5 Hz, 4H, β), 8.12 (d, J = 5 Hz, 4H, β), 7.45 (m, 16H, Ar), 7.41 (d, J = 3 Hz, 8H, Ar), 6.85 (t, J = 2 Hz, 4H, Ar), 6.76 (t, J = 2 Hz, 4H, Ar) 6.72 (t, J = 2 Hz, 4H, Ar), 4.12-4.01 (m, 48H, octyloxy), 1.85-1.72 (m, 48H, octyloxy), 1.49-1.17 (m, 240H, octyloxy), 0.83 (t, J = 7 Hz, 24H, octyloxy), 0.78-0.74 (m, 48H, octyloxy), -1.57 (s, 4H, inner-NH), -1.60 (s, 4H, inner-NH), and -2.38 (s, 4H, inner-NH); MALDI-TOF-MS m/z 5839, calcd for $C_{384}H_{506}N_{24}O_{24}$ m/z 5841; UV-vis ($CHCl_3$) λ_{max} (nm) 412, 489, 541, 599, and 656; Fluorescence ($CHCl_3$, λ_{ex} = 413 nm) λ_{em} 667

and 727 nm.

5,15-Diphenylporphyrin. A solution of 2,2'-dipyrrylmethane (1.15 g, 7.84 mmol) and benzaldehyde (0.796 mL, 7.84 mmol) in freshly distilled CH_2Cl_2 (1.5 L) was stirred under N_2, and the flask was shielded from light. Trifluoroacetic acid (0.376 mL, 4.88 mmol) was added via syringe, and the solution was stirred for 3 h at room temperature. DDQ (2.67 g, 11.75 mmol) was added to the solution, and the resulting solution was stirred for an additional 2 h. After the reaction mixture was neutralized by triethylamine and passed over Alumina column to remove polymeric materials, the solvent was removed by a rotary evaporator and the residue was purified by a silica gel column chromatography with CH_2Cl_2. The product was recrystallized from CH_2Cl_2-*n*-hexane. Yield; 705 mg, 39%. ^{1}H NMR ($CDCl_3$) δ 10.32 (s, 2H, *meso*), 9.40 (d, J = 5 Hz, 4H, β), 9.09 (d, J = 5 Hz, 4H, β), 8.28 (m, 4H, Ar), 7.82 (m, 6H, Ar), and -3.10 (s, 2H, N-H); FAB MS *m/z* 462.2, calcd for $C_{32}H_{22}N_4$ *m/z* 462.2.

ZP3. A round-bottomed flask was charged with **ZP1** (100 mg, 0.19 mmol) and dry $CHCl_3$ (100 mL). A stock solution of $AgPF_6$ (1.80 mL, 0.23 mmol) in acetonitrile was added at once. The reaction mixture was stirred for 10 h at 30°C. After the usual work-up, the oligomers ware separated by a preparative size exclusion column. Fractions of 2-mer and 3-mer ware separated, and the solvent was removed by a rotary evaporator. Recrystallization from $CHCl_3$/MeOH gave red-blown solids. **ZP2**: ^{1}H NMR ($CDCl_3$) δ 10.35 (s, 2H, *meso*), 9.47 (d, J = 5 Hz, 4H, β), 9.12 (d, J = 5 Hz, 4H, β), 8.64 (d, J = 5 Hz, 4H, β), 8.23 (m, 8H, Ar), 8.02 (d, J = 5 Hz, 4H, b), 7.67 (m, 12H, Ar). **ZP3**; 1H NMR ($CDCl_3$) δ 10.37 (s, 2H, *meso*), 9.49 (d, J = 5 Hz, 4H, β), 9.15 (d, J = 5 Hz, 4H, β), 8.72 (d, J = 5 Hz, 4H, β), 8.63 (d, J = 5 Hz, 4H, β), 8.28 (m, 8H, Ar), 8.18 (m, 8H, Ar + β), 8.07 (d, J = 5 Hz, 4H, β), 7.71 (m, 12H, Ar), 7.55 (m, 6H, Ar).

5-Bromo-10,20-bis(3,5-dioctyloxyphenyl)porphyrin 8. ^{1}H NMR ($CDCl_3$) δ 10.15 (s, 1H, *meso*), 9.74 (d, J = 5 Hz, 2H, β), 9.27 (d, J = 5Hz, 2H, β), 9.08 (m, 4H, β), 7.38 (d, J = 3 Hz, 4H, Ar), 6.93 (t, J = 3 Hz, 2H, Ar), 4.15 (t, J = 7 Hz, 8H, octyloxy), 1.89 (t-t, J = 7 Hz, 8H, octyloxy), 1.55-1.26 (m, 40H, octyloxy), and 0.88 (t, J = 7 Hz, 12H, octyloxy); FAB MS *m/z* 1054.53, calcd for $C_{64}H_{85}Br_1N_4O_4$ 1054.57.

5-Bromo-10,20-bis(3,5-dioctyloxyphenyl)porphyrinate zinc(II). ^{1}H NMR ($CDCl_3$) δ 9.90 (s, 1H, *meso*), 9.73 (d, J = 5 Hz, 2H, β), 9.17 (d, J = 5 Hz, 2H, β), 9.12 (d, J = 5 Hz, 2H, β), 9.08 (d, J = 5 Hz, 2H, β), 7.30 (d, J = 3 Hz, 4H, Ar), 6.77 (t, J = 3 Hz, 2H, Ar), 4.05 (t, J = 7 Hz, 8H, octyloxy), 1.86 (t-t, J = 7 Hz, 8H, octyloxy), 1.55-1.26 (m, 40H, octyloxy), and 0.90 (t, J = 7 Hz, 12H, octyloxy); FAB MS *m/z* 1116.6, calcd for $C_{64}H_{83}Br_1N_4O_4Zn_1$ 1116.5.

5-Bromo-10,20-bis(3,5-dioctyloxyphenyl)porphyrinate nickel(II) 10. ^{1}H NMR ($CDCl_3$) δ 9.75 (s, 1H, *meso*), 9.55 (d, J = 5 Hz, 2H, β), 9.07 (d, J = 5 Hz, 2H, β), 8.95-8.93 (m, 4H, β), 7.16 (d, J = 2 Hz, 4H, Ar), 6.77 (t, J = 2 Hz, 2H, Ar), 4.08 (t, J = 7 Hz, 8H, octyloxy), 1.85 (t-t, J = 7 Hz, 8H, octyloxy), 1.52-1.26 (m, 40 H, octyloxy), and 0.87 (t, J = 7 Hz, 12H, octyloxy); FAB MS m/z 1108.4, calcd for $C_{64}H_{83}Br_1N_4O_4Ni_1$ 1108.5.

5-(4,4,5,5-Tetramethyl-1,3,2-dioxaborolan-2-yl)-10,20-bis(3,5-dioctyloxyphenyl) porphyrinate zinc(II) 9. ^{1}H NMR ($CDCl_3$) δ 10.28 (s, 1H, *meso*), 9.96 (d, J = 5 Hz, 2H, β), 9.41 (d, J = 5 Hz, 2H, β), 9.27 (d, J = 5 Hz, 2H, β), 9.22 (d, J = 5 Hz, 2H, β), 7.44 (d, J = 3 Hz, 4H, Ar), 6.93 (t, J = 3 Hz, 2H, Ar), 4.16 (t, J = 7 Hz, 8H, octyloxy), 1.89 (m, 20H, octyloxy + Me), 1.55-1.26 (m, 40H, octyloxy), and 0.90 (t, J = 7 Hz, 12H, octyloxy); FAB MS m/z 1162.6, calcd for $C_{70}H_{95}B_1N_4O_6Zn_1$ 1162.7.

Zn^{II}-free base hybrid diporphyrin ZH. Bromoporphyrin **8** (8.0 mg, 0.008 mmol), porphyrin boronate **9** (10 mg, 0.008 mmol), Cs_2CO_3 (4 mg, 0.012 mmol), and Pd(PPh3)4 (1 mg, 0.0008 mmol) were dissolved in a mixture of dry DMF (0.5 mL) and dry toluene (1 mL). The solution was deoxygenated via three freeze-pump-thaw degas cycles, and the resulting mixture was heated at 80°C for 3 h under Ar. At the endpoint, the reaction was quenched with water and extracted with ether. The organic layer was dried over anhydrous Na2SO4, passed through short silica gel column, and evaporated. The product separation was performed on a recycling preparative GPC-HPLC. Yield; 10 mg, 62%. ^{1}H NMR ($CDCl_3$) δ 10.38 (s, 1 H, *meso*), 10.32 (s, 1H, *meso*), 9.48 (d, J = 5 Hz, 2H, β), 9.41 (d, J = 5 Hz, 2H, β), 9.26 (d, J = 5 Hz, 2H, β), 9.17 (d, J = 5 Hz, 2H, β), 8.81 (d, J = 5 Hz, 2H, β), 8.69 (d, J = 5 Hz, 2H, β), 8.12 (d, J = 5 Hz, 2H, β), 7.98 (d, J = 5 Hz, 2H, β), 7.40 (d, J = 2 Hz, 4H, Ar), 7.39 (d, J = 5 Hz, 2H, Ar), 6.79 (t, J = 2 Hz, 4H, Ar), 4.05 (t, J = 7 Hz, 16H, octyloxy), 1.15-1.83 (m, 96H, octyloxy), 0.79 (t, J = 7 Hz, 24H, octyloxy), and -2.43 (s, 2H, NH); FAB MS m/z: 2009.24, calcd for $C_{128}H_{168}N_8O_8Zn$ 2009.23; UV-vis (THF) λ_{max} 417, 445, 513, 555, 591, and 650 nm; Fluorescence (THF, λ_{ex} = 413 nm) λ_{em} 647 and 712 nm.

Zn^{II}-Ni^{II} hybrid diporphyrin ZN. Bromoporphyrinate Ni^{II} **10** (12 mg, 0.010 mmol), porphyrin boronate **9** (12 mg, 0.010 mmol), Cs_2CO_3 (5 mg, 0.015 mmol), and $Pd(PPh_3)_4$ (1 mg, 0.0008 mmol) were dissolved in a mixture of dry DMF (0.5 mL) and dry toluene (1 mL). The mixture was reacted according to the conditions described above for 3 h. Yield; 12 mg, 57%. ^{1}H NMR ($CDCl_3$) δ 10.36 (s, 1H, *meso*), 9.98 (s, 1H, *meso*), 9.46 (d, J = 5 Hz, 2H, β), 9.24 (d, J = 5 Hz, 2H, β), 9.23 (d, J = 5 Hz, 2H, β), 9.07 (d, J = 5 Hz, 2H, β), 8.82 (d, J = 5 Hz, 2H, β), 8.64 (d, J = 5 Hz, 2H, β), 8.11 (d, J = 5 Hz, 2H, β), 8.01 (d, J = 5 Hz, 2H, β), 7.39 (d, J = 2 Hz, 4H, Ar), 7.22 (d, J = 2 Hz, 2H, Ar), 6.81 (t, J = 2 Hz, 2H, Ar), 6.74 (t, J =

2 Hz, 2H, Ar), 4.06 (t, J = 7 Hz, 8H, octyloxy), 4.01 (t, J = 7 Hz, 8H, octyloxy), 1.83-1.74 (m, 16 H, octyloxy), 1.46-1.20 (m, 80H, octyloxy), and 0.82-0.78 (m, 24H, octyloxy); MALDI-TOF-MS *m/z*: 2068.6, calcd for $C_{128}H_{166}N_8O_8Zn_1Ni_1$ 2069.2; UV-vis (THF) λ_{max} 416, 444, 522, 557, and 592 nm.

Linear-shaped hybrid triporphyrin 13. 5,15-Dibromo-10,20-diphenylporphyrin **11** (2.4 mg, 0.004 mmol), porphyrin boronate **12** (5.0 mg, 0.008 mmol), Cs_2CO_3 (4 mg, 0.012 mmol), and $Pd(PPh_3)_4$ (1 mg, 0.0008 mmol) were dissolved in a mixture of dry DMF (0.5 mL) and dry toluene (0.5 mL). The solution was reacted according to the conditions described above for 3 h. The product separation was performed on a recycling preparative GPC-HPLC to give **13** (2.6 mg, 45%). ^{1}H NMR ($CDCl_3$) δ 10.38 (s, 2 H, *meso*), 9.49 (d, J = 5 Hz, 4H, β), 9.15 (d, J = 4 Hz, 4H, β), 8.76 (d, J = 4 Hz, 4H, β), 8.58 (d, J = 5 Hz, 4H, β), 8.28-8.27 (m, 12H, β + Ar), 8.21-8.19 (m, 4H, Ar), 8.07 (d, J = 5 Hz, 4H, β), 7.72-7.71 (m, 12H, Ar), 7.57-7.56 (m, 4H, Ar), and -1.60 (s, 2H, NH); MALDI-TOF-MS *m/z*: 1510, calcd for $C_{96}H_{58}N_{12}Zn_2$ 1510.4; UV-vis (THF) λ_{max} 416, 467, 521, 558, 599, and 657 nm; Fluorescence (THF, λ_{ex} = 556 nm) λ_{em} 665 and 727 nm.

Linear-shaped Zinc^{II} triporphyrin 14. ^{1}H NMR ($CDCl_3$) δ 10.42 (s, 2 H, *meso*), 9.52 (d, J = 4 Hz, 4H, β), 9.18 (d, J = 4 Hz, 4H, β), 8.78 (d, J = 5 Hz, 4H, β), 8.69 (d, J = 5 Hz, 4H, β), 8.30-8.26 (m, 12H, β + Ar), 8.23-8.20 (m, 4H, Ar), 8.16 (d, J = 5 Hz, 4H, β), 7.72-7.71 (m, 12H, Ar), and 7.56-7.52 (m, 4H, Ar); MALDI-TOF-MS *m/z*: 1574, calcd for $C_{96}H_{56}N_{12}Zn_3$ 1572.3; UV-vis (THF) λ_{max} 412, 475, 570, and 611 nm; Fluorescence (THF, λ_{ex} = 411 nm) λ_{em} 639 nm.

Bent-shaped hybrid triporphyrin 16. 5,10-Dibromo-15,20-diphenylporphyrin **15** (2.4 mg, 0.004 mmol), porphyrin boronate **12** (5.0 mg, 0.008 mmol), Cs_2CO_3 (4 mg, 0.012 mmol), and $Pd(PPh_3)_4$ (1 mg, 0.0008 mmol) were dissolved in a mixture of dry DMF (0.5 mL) and dry toluene (0.5 mL). The solution was reacted according to the conditions described above for 3 h. The product separation was performed on a recycling preparative GPC-HPLC to give **16** (2.7 mg, 46%). ^{1}H NMR ($CDCl_3$) δ 10.32 (s, 2H, *meso*), 9.42 (d, J = 5 Hz, 4H, β), 9.08 (d, J = 5 Hz, 4H, β), 8.97 (s, 2H, β), 8.72 (d, J = 5 Hz, 4H, β), 8.62 (d, J = 5 Hz, 2H, β), 8.31-8.27 (m, 8H, β + Ar), 8.24-8.23 (m, 4H, Ar), 8.13 (d, J = 6 Hz, 4H, Ar), 8.07 (d, J = 5 Hz, 2H, β), 7.72-7.62 (m, 20H, β + Ar), and -1.60 (s, 2H, NH); MALDI-TOF-MS *m/z*: 1509, calcd for $C_{96}H_{58}N_{12}Zn_2$ 1510.4; UV-vis (THF) λ_{max} 416, 447, 521, 556, 602, and 660 nm; Fluorescence (THF, λ_{ex} = 556 nm) λ_{em} 664 and 728 nm.

Bent-shaped Zinc^{II} triporphyrin 17. ^{1}H NMR ($CDCl_3$) δ 10.31 (s, 2 H, *meso*), 9.42 (d, J = 5 Hz, 4H, β), 9.08 (d, J = 5 Hz, 4H, β), 9.06 (s, 2H, β), 8.72 (d, J = 5 Hz, 2H, β), 8.70 (d, J = 5 Hz, 4H, β), 8.31-8.29 (m, 4H, Ar), 8.26-8.23 (m, 8H, β + Ar), 8.15 (d, J = 5 Hz, 2H, β), 8.13 (d,

J = 8Hz, 4H, Ar), 7.74 (s, 2H, *β*), and 7.71-7.63 (m, 18H, Ar); MALDI-TOF-MS *m/z*: 1574, calcd for $C_{96}H_{56}N_{12}Zn_3$ 1572.3; UV-vis (THF) λ_{max} 411, 456, 569, and 613 nm; Fluorescence (THF, λ_{ex} = 411 nm) λ_{em} 632 and 669 nm.

***meso-meso* Linked hybrid porphyrin octamer 19 and heptamer 20.** *meso,meso'*-Dibromo-hexa-Zn^{II}-porphyrin **Z6Br$_2$** was prepared from **Z6** and NBS in 80% yield. **Z6Br$_2$** (5.0 mg, 0.78 μ mol), porphyrin boronate **18** (1.7 mg, 1.6 μmol), Cs_2CO_3 (0.8 mg, 0.0024 mmol), and $Pd(PPh_3)_4$ (0.2 mg) were dissolved in a mixture of dry DMF (0.5 mL) and dry toluene (0.5 mL). The solution was deoxygenated via three freeze-pump-thaw degas cycles, and the resulting mixture was heated at 80°C for 3 h under Ar. At the endpoint, the reaction was quenched with water and extracted with ether. The organic layer was dried over anhydrous Na_2SO_4, passed through short silica gel, and evaporated. The product separation was performed on a recycling preparative GPC-HPLC to give **19** (0.70 mg, 11 %) and **20** (1.8 mg, 32 %). **19**: ^{1}H NMR ($CDCl_3$) δ 10.36 (s, 2H, *meso*), 9.45 (d, *J* = 5 Hz, 4H, *β*), 9.22 (d, *J* = 5 Hz, 4H, *β*), 8.94-8.91 (m, 20H, *β*), 8.86 (d, *J* = 5 Hz, 4H, *β*), 8.82 (d, *J* = 5 Hz, 4H, *β*), 8.35-8.32 (m, 20H, *β*), 8.21 (d, *J* = 5 Hz, 4H, *β*), 8.18 (d, *J* = 5 Hz, 4H, *β*), 7.50-7.49 (m, 16H, Ar), 7.45 (d, *J* = 2 Hz, 8H, Ar), 7.44 (d, *J* = 2 Hz, 8H, Ar), 6.85 (t, *J* = 2 Hz, 4H, Ar), 6.76 (m, 8H, Ar), 6.73 (t, *J* = 2 Hz, 4H, Ar), 4.11-4.01 (m, 64H, octyloxy), 1.85-1.17 (m, 384H, octyloxy), 0.90-0.74 (m, 96H, octyloxy), and -2.36 (s, 4H, NH); MALDI-TOF-MS *m/z*: 8167, calcd for $C_{512}H_{662}N_{32}O_{32}Zn_6$ 8169; UV-vis (THF) λ_{max} 411, 502, and 584 nm; Fluorescence (THF, λ_{ex} = 411 nm) λ_{em} 650 and 712 nm. **20**: ^{1}H NMR ($CDCl_3$) δ 10.41 (s, 1H, *meso*), 10.36 (s, 1H, *meso*), 9.52 (d, *J* = 5 Hz, 2H, *β*), 9.45 (d, *J* = 5 Hz, 2H, *β*), 9.31 (d, *J* = 5 Hz, 2H, *β*), 9.22 (d, *J* = 5 Hz, 2H, *β*), 8.95-8.91 (m, 18H, *β*), 8.86 (d, *J* = 5 Hz, 2H, *β*), 8.84 (d, *J* = 5 Hz, 2H, *β*), 8.81 (d, *J* = 4 Hz, 2H, *β*), 8.35-8.33 (m, 16H, *β*), 8.28 (d, *J* = 5 Hz, 2H, *β*), 8.21 (d, *J* = 5 Hz, 2H, *β*), 8.18 (d, *J* = 5 Hz, 2H, *β*), 8.17 (d, *J* = 5 Hz, 2H, *β*), 7.49-7.45 (m, 56H, Ar), 6.85 (m, 4H, Ar), 6.76 (m, 6H, Ar), 6.72 (t, *J* = 2 Hz, 4H, Ar), 4.11-4.01 (m, 56H, octyloxy), 1.85-1.18 (m, 336H, octyloxy), 0.84-0.74 (m, 84H, octyloxy), and -2.35 (s, 2H, NH); MALDI-TOF-MS *m/z*: 7198, calcd for $C_{448}H_{578}N_{28}O_{28}Zn_6$ 7196; UV-vis (THF) λ_{max} 413, 499, and 583 nm; Fluorescence (THF, λ_{ex} = 411 nm) λ_{em} 650 and 708 nm.

5-[4-(4,4,5,5-Tetramethyl-1,3,2-dioxaborolan-2-yl)phenyl]-15-(3,5-dioctyloxyphenyl) porphyrin 21. 4-(4,4,5,5-Tetramethyl-1,3,2-dioxaborolan-2-yl)benzaldehyde was prepared from 4-formylphenylboronic acid and 2,3-dimethyl-2,3-butandiol (pinacol, 1.2 equiv) by using a Dean-Stark trap apparatus in 92% yield. A solution of 2,2'-dipyrrylmethane (1.40 g, 9.50 mmol), 3,5-dioctyloxybenzaldehyde (1.74 g, 4.75 mmol), and the boronate-appended benzaldehyde (1.10 g, 4.75 mmol) in dry CH_2Cl_2 (1.5 L) was stirred

under N_2, and shielded from light. Trifluoroacetic acid (TFA) (0.460 mL, 5.60 mmol) was added *via* syringe, and the solution was stirred for 3 h at room temperature. DDQ (3.78 g, 16.6 mmol) was added to the solution, and the resulting solution was stirred for an additional 3 h. After the reaction mixture was neutralized by triethylamine and passed over a short silica gel column to remove polymeric materials, the solvent was removed by a rotary evaporator and the residue was separated by silica gel column chromatography with CH_2Cl_2/*n*-hexane. The first fraction was 5,15-bis(3,5-dioctyloxy- phenyl)porphyrin and the second fraction was the desired porphyrin **21**. The product was recrystallized from CH_2Cl_2-MeOH. Yield; 541 mg, 13%. ^{1}H NMR ($CDCl_3$) δ 10.30 (s, 2 H, *meso*), 9.38 (d, J = 5 Hz, 4H, β), 9.19 (d, J = 4 Hz, 2H, β), 9.07 (d, J = 5 Hz, 2H, β), 8.30 (d, J = 8 Hz, 2H, Ar), 8.26 (d, J = 8 Hz, 2H, Ar), 7.43 (d, J = 3 Hz, 1H, Ar), 6.93 (t, J = 3 Hz, 2H, Ar), 4.16 (t, J = 7 Hz, 4H, octyloxy), 1.90 (t-t, J = 7 Hz, 4H, octyloxy), 1.38-1.27 (m, 20H, octyloxy), 0.88 (t, J = 7 Hz, 6H, octyloxy), and -3.11 (s, 2H, N-H); FAB MS *m/z* 844.1, calcd for $C_{54}H_{65}B_1N_4O_4$ *m/z* 844.5.

5,15-Dibromo-10-[4-(4,4,5,5-tetramethyl-1,3,2-dioxaborolan-2-yl)phenyl]-20-(3,5-dioctyloxyphenyl)porphyrin zinc(II) 22. The porphyrin **21** (200 mg, 0.237 mmol) was dissolved in a mixture of $CHCl_3$ (100 mL) and pyridine (0.5 mL). NBS (0.480 mmol) was added to this solution and the resulting solution was stirred for 2 h at 0°C. The mixture was poured into water and extracted with $CHCl_3$. The combined organic extracts were dried over anhydrous Na_2SO_4. A saturated solution of $Zn(OAc)_2$ in MeOH was added to the solution, and the resulting mixture was stirred for 2 h. The mixture was poured into water and extracted with $CHCl_3$. After the combined organic extracts were dried over Na_2SO_4, the solvent was removed by a rotary evaporator and the residue was purified by silica gel column chromatography with CH_2Cl_2. The product was recrystallized from $CHCl_3$-MeOH. Yield; 232 mg, 92%. ^{1}H NMR ($CDCl_3$) δ 9.70 (m, J = 5 Hz, 4H, β), 9.05 (d, J = 5 Hz, 2H, β), 8.91 (d, J = 5 Hz, 2H, β), 8.21 (d, J = 8 Hz, 2H, Ar), 8.17 (d, J = 8 Hz, 2H, Ar), 7.32 (d, J = 3 Hz, 2H, Ar), 6.90 (t, J = 3 Hz, 1H, Ar), 4.13 (t, J = 7 Hz, 4H, octyloxy), 1.88 (t-t, J = 7 Hz, 4H, octyloxy), 1.38-1.26 (m, 20H, octyloxy), and 0.87 (t, J = 7 Hz, 6H, octyloxy); FAB MS *m/z* 1064.25, calcd for $C_{54}H_{61}B_1Br_2N_4O_4Zn$ *m/z* 1064.24.

5-[4-(4,4,5,5-Tetramethyl-1,3,2-dioxaborolan-2-yl)phenyl]-10,20-bis(phenylethynyl)-15-(3,5-dioctyloxyphenyl)porphyrin zinc(II) 23. The bromoporphyrin **22** (200 mg, 0.19 mmol) and phenylacetylene (153 mg, 1.50 mmol) were dissolved in a mixture of dry toluene (20 mL) and triethylamine (4 mL) and this solution was purged with Ar for 30 min. $Pd(PPh_3)_2Cl_2$ (30 mg) and CuI (12 mg) were added and the resulting solution was

heated at 50°C for 3 h under Ar. After the reaction mixture was filtered, the filtrate was separated by chromatography on a silica gel column (eluant CH_2Cl_2/n-hexane) to give **23**. The product was recrystallized from CH_2Cl_2-MeOH. Yield; 132 mg, 64%. ^{1}H NMR ($CDCl_3$) δ 9.70 (d, J = 5 Hz, 2H, β), 9.69 (d, J = 5 Hz, 2H, β), 9.04 (d, J = 5 Hz, 2H, β), 8.89 (d, J = 5 Hz, 2H, β), 8.22 (m, 4H, Ar), 7.95 (d, J = 8 Hz, 4H, Ph), 7.52 (t, J = 7 Hz, 4H, Ph), 7.44 (t, J = 8 Hz, 2H, Ph), 7.36 (d, J = 3 Hz, 2H, Ar), 6.89 (t, J = 3 Hz, 1H, Ar), 4.14 (t, J = 7 Hz, 4H, octyloxy), 1.89 (t-t, J = 7 Hz, 4H, octyloxy), 1.51-1.28 (m, 20H, octyloxy), and 0.86 (t, J = 7 Hz, 6H, octyloxy); FAB MS m/z 1106.6, calcd for $C_{70}H_{71}B_1N_4O_4Zn$ m/z 1106.5; UV-vis (THF) λ_{max} 448 and 648 nm.

General Procedure for Preparation of Z*n*A via Palladium-Catalyzed Cross-Coupling.

Brominated *meso-meso* linked Zn^{II} 5,15-bis(3,5-dioctyloxyphenyl)porphyrin arrays **Z*n*Br** , porphyrin boronate **23**, Cs_2CO_3 (1.5 equiv for 3), and $Pd(PPh_3)_4$ (10mol% for the bromoporphyrin) were dissolved in a mixture of dry DMF and toluene. The solution was deoxygenated three times via freeze-pump-thaw degas cycles, and the resulting mixture was heated at 80-90°C for 3 h under Ar. At the endpoint, the reaction was quenched with water and extracted with ether. The organic layer was dried over anhydrous Na_2SO_4, passed through a short silica gel column, and evaporated. The product separation was performed on a preparative size exclusion column. Larger oligomers elute first then smaller oligomers were separated. Selected physical properties and detailed isolation procedures are presented below.

Z1A. A round-bottomed flask was charged with **23** (11 mg, 0.0099 mmol), 5-bromo-10,20-bis(3,5-dioctyloxyphenyl)porphyrin (5.0 mg, 0.0041 mmol), Cs_2CO_3, Pd-catalyst, dry toluene (2 mL) and dry DMF (1 mL). After the usual work-up, the oligomers were separated by an SEC. Fractions of 2-mer and 1-mer were separated, and the solvent was removed by a rotary evaporator. The desired product was a dark green solid in 77% yield. ^{1}H NMR ($CDCl_3$) δ 10.32 (s, 1H, *meso*), 10.00 (d, J = 5 Hz, 2H, β), 9.84 (d, J = 5 Hz, 2H, β), 9.47-9.45 (m, 4H, β), 9.42 (d, J = 5 Hz, 2H, β), 9.35 (d, J = 5 Hz, 2H, β), 9.30 (d, J = 5 Hz, 2H, β), 9.11 (d, J = 5 Hz, 2H, β), 8.66 (d, J = 8 Hz, 2H, Ar), 8.61 (d, J = 8 Hz, 2H, Ar), 8.11 (d, J = 7 Hz, 4H, Ph), 7.61 (t, J = 7 Hz, 4H, Ph), 7.54-7.51 (m, 6H, Ar + Ph), 7.42 (d, J = 3 Hz, 2H, Ar), 6.97 (t, J = 3 Hz, 2H, Ar), 6.94 (t, J = 3 Hz, 1H, Ar), 4.21-4.19 (m, 12H, octyloxy), 1.93-1.90 (m, 12H, octyloxy), 1.51-1.27 (m, 60H, octyloxy), and 0.87 (t, J = 7 Hz, 18H, octyloxy); MALDI-TOF MS m/z 2020.7, calcd for $C_{128}H_{142}N_8O_6Zn_2$ m/z 2019.0; UV-vis

(THF) λ_{max} 419, 448, 550, 590 and 650 nm; Fluorescence (THF, λ_{ex} = 550 nm) λ_{em} 654, and 716 nm.

Z2A. (76%) ^{1}H NMR ($CDCl_3$) δ 10.40 (s, 1H, *meso*), 10.01 (d, J = 5 Hz, 2H, β), 9.86 (d, J = 5 Hz, 2H, β), 9.52 (d, J = 5 Hz, 2H, β), 9.50 (d, J = 5 Hz, 2H, β), 9.45 (d, J = 5 Hz, 2H, β), 9.35 (d, J = 5 Hz, 2H, β), 9.28 (d, J = 5 Hz, 2H, β), 9.13 (d, J = 5 Hz, 2H, β), 8.86 (d, J = 5 Hz, 2H, β), 8.84 (d, J = 5 Hz, 2H, β), 8.75 (d, J = 8 Hz, 2H, Ar), 8.66 (d, J = 8 Hz, 2H, Ar), 8.18 (d, J = 5 Hz, 2H, β), 8.12-8.10 (m, 6H, β + Ph), 7.61 (t, J = 7 Hz, 4H, Ph), 7.54 (t, J = 8 Hz, 2H, Ph), 7.50 (d, J = 3 Hz, 4H, Ar), 7.44 (d, J = 3 Hz, 4H, Ar), 7.43 (d, J = 3 Hz, 2H, Ar), 6.95 (t, J = 3 Hz, 1H, Ar), 6.85 (t, J = 3 Hz, 2H, Ar), 6.82 (t, J = 3 Hz, 2H, Ar), 4.19 (t, J = 7 Hz, 4H, octyloxy), 4.10 (m, 16H, octyloxy), 1.92 (t, J = 7 Hz, 4H, octyloxy), 1.81 (t-t, J = 7 Hz, 16H, octyloxy), 1.51-1.22 (m, 100H, octyloxy), 0.88 (t, J = 7 Hz, 6H, octyloxy) and 0.80 (t, J = 7 Hz, 24H, octyloxy); MALDI-TOF MS m/z 3056.7, calcd for $C_{192}H_{224}N_{12}O_{10}Zn_3$ m/z 3055.5; UV-vis (THF) λ_{max} 423, 448, 465, 564, 604 and 649 nm; Fluorescence (THF, λ_{ex} = 564 nm) λ_{em} 655 and 716 nm.

Z3A. (37%) ^{1}H NMR ($CDCl_3$) δ 10.40 (s, 1H, *meso*), 10.00 (d, J = 5 Hz, 2H, β), 9.87 (d, J = 5 Hz, 2H, β), 9.54 (d, J = 5 Hz, 2H, β), 9.51 (d, J = 5 Hz, 2H, β), 9.48 (d, J = 5 Hz, 2H, β), 9.38 (d, J = 5 Hz, 2H, β), 9.30 (d, J = 5 Hz, 2H, β), 9.14 (d, J = 5 Hz, 2H, β), 8.93 (d, J = 5 Hz, 2H, β), 8.91 (d, J = 5 Hz, 2H, β), 8.86 (d, J = 5 Hz, 2H, β), 8.82 (d, J = 5 Hz, 2H, β), 8.77 (d, J = 8 Hz, 2H, Ar), 8.69 (d, J = 8 Hz, 2H, Ar), 8.28 (d, J = 5 Hz, 2H, β), 8.26 (d, J = 5 Hz, 2H, β), 8.23 (d, J = 5 Hz, 2H, β), 8.15-8.12 (m, 6H, β + Ph), 7.64 (t, J = 7 Hz, 4H, Ph), 7.55 (t, J = 8 Hz, 2H, Ph), 7.54 (d, J = 3 Hz, 4H, Ar), 7.46 (d, J = 3 Hz, 4H, Ar), 7.43 (d, J = 3 Hz, 2H, Ar), 7.41 (d, J = 3 Hz, 4H, Ar), 6.96 (t, J = 3 Hz, 1H, Ar), 6.90 (t, J = 3 Hz, 2H, Ar), 6.85 (t, J = 3 Hz, 2H, Ar), 6.69 (t, J = 3 Hz, 2H, Ar), 4.20 (t, J = 7 Hz, 4H, octyloxy), 4.15-4.09 (m, 16H, octyloxy), 3.98 (t, J = 7 Hz, 8H, octyloxy), 1.93 (t-t, J = 7 Hz, 4H, octyloxy), 1.84 (t-t, J = 7 Hz, 16H, octyloxy), 1.71 (t-t, J = 7 Hz, 8H, octyloxy), 1.55-1.15 (m, 140H, octyloxy), and 0.92-0.72 (m, 42H, octyloxy); MALDI-TOF MS m/z 4094.9, calcd for $C_{256}H_{306}N_{16}O_{14}Zn_4$ m/z 4092.9; UV-vis (THF) λ_{max} 418, 448, 480, 573 and 649 nm; Fluorescence (THF, λ_{ex} = 560 nm) λ_{em} 655 and 715 nm.

Z6A. (10%) ^{1}H NMR ($CDCl_3$) δ 10.41 (s, 1H, *meso*), 10.03 (d, J = 5 Hz, 2H, β), 9.87 (d, J = 5 Hz, 2H, β), 9.56 (d, J = 5 Hz, 2H, β), 9.52 (d, J = 5 Hz, 2H, β), 9.48 (d, J = 5 Hz, 2H, β), 9.40 (d, J = 5 Hz, 2H, β), 9.30 (d, J = 5 Hz, 2H, β) 9.14 (d, J = 5 Hz, 2H, β), 8.96-8.90 (m, 18H, β), 8.84 (d, J = 5 Hz, 2H, β), 8.78 (d, J = 8 Hz, 2H, Ar), 8.69 (d, J = 8 Hz, 2H, Ar), 8.35-8.31 (m, 14H, β), 8.28 (d, J = 5 Hz, 2H, β), 8.26 (d, J = 5 Hz, 2H, β), 8.16 (d, J = 5 Hz, 2H, β), 8.13 (d, J = 8 Hz, 4H, Ph), 7.64 (t, J = 7 Hz, 4H, Ph), 7.56 (d, J = 3 Hz, 4H, Ar), 7.55 (t, J = 8 Hz, 2H,

Ph), 7.49-7.48 (m, 16H, Ar), 7.45 (d, J = 3 Hz, 4H, Ar), 7.43 (d, J = 3 Hz, 2H, Ar), 6.96 (t, J = 3 Hz, 1H, Ar), 6.90 (t, J = 3 Hz, 2H, Ar), 6.85 (t, J = 3 Hz, 2H, Ar), 6.77-6.72 (m, 8H, Ar), 4.20-4.04 (m, 52H, octyloxy), 1.89-1.19 (m, 312H, octyloxy), and 0.91-0.74 (m, 78H, octyloxy); MALDI-TOF MS *m/z* 7203.8, calcd for $C_{448}H_{552}N_{28}O_{26}Zn_7$ *m/z* 7203.2; UV-vis (THF) λ_{max} 417, 448, 499, 582 and 649 nm; Fluorescence (THF, λ_{ex} = 560 nm) λ_{em} 654 and 717 nm.

Z12A. (34%) ^{1}H NMR ($CDCl_3$) δ 10.41 (s, 1H, *meso*), 10.03 (d, J = 5 Hz, 2H, β), 9.87 (d, J = 5 Hz, 2H, β), 9.56 (d, J = 5 Hz, 2H, β), 9.52 (d, J = 5 Hz, 2H, β), 9.48 (d, J = 5 Hz, 2H, β), 9.40 (d, J = 5 Hz, 2H, β), 9.30 (d, J = 5 Hz, 2H, β), 9.14 (d, J = 5 Hz, 2H, β), 8.96-8.90 (m, 42H, β), 8.84 (d, J = 5 Hz, 2H, β), 8.78 (d, J = 8 Hz, 2H, Ar), 8.69 (d, J = 8 Hz, 2H, Ar), 8.35-8.31 (m, 38H, β), 8.28 (d, J = 5 Hz, 2H, β), 8.26 (d, J = 5 Hz, 2H, β), 8.16 (d, J = 5 Hz, 2H, β), 8.13 (d, J = 8 Hz, 4H, Ph), 7.64 (t, J = 7 Hz, 4H, Ph), 7.56-7.48 (m, 52H, Ar), 6.96 (t, J = 3 Hz, 1H, Ar), 6.90 (t, J = 3 Hz, 2H, Ar), 6.85 (t, J = 3 Hz, 2H, Ar), 6.77-6.72 (m, 20H, Ar), 4.20-4.04 (m, 100H, octyloxy), 1.89-1.19 (m, 600H, octyloxy), and 0.91-0.74 (m, 150H, octyloxy); MALDI-TOF MS *m/z* 13423, calcd for $C_{832}H_{1044}N_{52}O_{50}Zn_{13}$ *m/z* 13423.9; UV-vis (THF) λ_{max} 415, 448, 506, 586 and 649 nm; Fluorescence (THF, λ_{ex} = 560 nm) λ_{em} 654 and 717 nm.

Z24A. (28%) ^{1}H NMR ($CDCl_3$) δ 10.42 (s, 1H, *meso*), 10.04 (d, J = 5 Hz, 2H, β), 9.87 (d, J = 5 Hz, 2H, β), 9.56 (d, J = 5 Hz, 2H, β), 9.52 (d, J = 5 Hz, 2H, β), 9.48 (d, J = 5 Hz, 2H, β), 9.40 (d, J = 5 Hz, 2H, β), 9.30 (d, J = 5 Hz, 2H, β), 9.14 (d, J = 5 Hz, 2H, β), 8.96-8.90 (m, 90H, β), 8.84 (d, J = 5 Hz, 2H, β), 8.78 (d, J = 8 Hz, 2H, Ar), 8.69 (d, J = 8 Hz, 2H, Ar), 8.35-8.31 (m, 86H, β), 8.28 (d, J = 5 Hz, 2H, β), 8.26 (d, J = 5 Hz, 2H, β), 8.16 (d, J = 5 Hz, 2H, β), 8.13 (d, J = 8 Hz, 4H, Ph), 7.64 (t, J = 7 Hz, 4H, Ph), 7.56-7.48 (m, 100H, Ar), 6.96 (t, J = 3 Hz, 1H, Ar), 6.90 (t, J = 3 Hz, 2H, Ar), 6.85 (t, J = 3 Hz, 2H, Ar), 6.77-6.72 (m, 44H, Ar), 4.20-4.04 (m, 196H, octyloxy), 1.89-1.19 (m, 1176H, octyloxy), and 0.91-0.74 (m, 294H, octyloxy); MALDI-TOF MS *m/z* 25862, calcd for $C_{1600}H_{2028}N_{100}O_{98}Zn_{25}$ *m/z* 25865.1; UV-vis (THF) λ_{max} 415, 448, 509, 588 and 649 nm; Fluorescence (THF, λ_{ex} = 560 nm) λ_{em} 654 and 717 nm.

ZnBr_2. *Meso-meso* linked porphyrin arrays was dissolved in a mixture of $CHCl_3$ and pyridine (0.5%). NBS (2.2 equiv.) was added to this solution and the resulting solution was stirred for 2 h. The mixture was poured into water and extracted with $CHCl_3$. After the combined organic extract was dried over Na2SO4 and passed through a short silica gel column, the solvent was removed by a rotary evaporator. The product was recrystallized from $CHCl_3$-MeOH.

Z2Br_2. (quant). ^{1}H NMR ($CDCl_3$) δ 9.81 (d, J = 5 Hz, 4H, β), 9.13 (d, J = 5 Hz, 4H, β),

8.71 (d, J = 5 Hz, 4H, β), 8.01 (d, J = 5 Hz, 4H, β), 7.34 (d, J = 3 Hz, 8H, Ar), 6.77 (t, J = 3 Hz, 4H, Ar), 4.02 (t, J = 7 Hz, 16H, octyloxy), 1.78 (t-t, J = 7 Hz, 16H, octyloxy), 1.43 (t-t, J = 7 Hz, 16H, octyloxy), 1.32-1.10 (m, 64H, octyloxy), and 0.80 (t, J = 7 Hz, 24H, octyloxy); MALDI-TOF-MS m/z 2232.4, calcd for $C_{128}H_{164}N_8O_8Zn_2Br_2$ m/z 2233.0.

Z3Br$_2$. (95%). ^{1}H NMR ($CDCl_3$) δ 9.87 (d, J = 5 Hz, 4H, β), 9.19 (d, J = 5 Hz, 4H, β), 8.81 (d, J = 5 Hz, 4H, β), 8.79 (d, J = 5 Hz, 4H, β) 8.16 (d, J = 5 Hz, 4H, β) 8.14 (d, J = 5 Hz, 4H, β), 7.39 (d, J = 3 Hz, 8H, Ar), 7.37 (d, J = 3 Hz, 4H, Ar), 6.82 (t, J = 3 Hz, 4H, Ar), 6.68 (t, J = 3 Hz, 2H, Ar), 4.08 (t, J = 7 Hz, 16H, octyloxy), 3.95 (t, J = 7 Hz, 8H, octyloxy), 1.81 (t-t, J = 7 Hz, 16H, octyloxy), 1.69 (t-t, J = 7 Hz, 8H, octyloxy), 1.45 (t-t, J = 7 Hz, 16H, octyloxy), 1.33-1.13 (m, 104H, octyloxy), 0.81 (t, J = 7 Hz, 24H, octyloxy) and 0.72 (t, J = 7 Hz, 12H, octyloxy); MALDI-TOF-MS m/z 3267, calcd for $C_{192}H_{246}N_{12}O_{12}Zn_3Br_2$ m/z 3270.

Z4Br$_2$. (87%). ^{1}H NMR ($CDCl_3$) δ 9.88 (d, J = 5 Hz, 4H, β), 9.20 (d, J = 5 Hz, 4H, β), 8.88 (d, J = 5 Hz, 4H, β), 8.84 (d, J = 5 Hz, 4H, β), 8.81 (d, J = 5 Hz, 4H, β), 8.27 (d, J = 5 Hz, 4H, β), 8.19 (d, J = 5 Hz, 4H, β), 8.16 (d, J = 5 Hz, 4H, β), 7.41 (d, J = 3 Hz, 8H, Ar), 7.40 (d, J = 3 Hz, 8H, Ar), 6.83 (br, 4H, Ar), 6.71 (br, 4H, Ar), 4.09 (t, J = 7 Hz, 16H, octyloxy), 3.99 (t, J = 7 Hz, 16H, octyloxy), 1.82 (t-t, J = 7 Hz, 16H, octyloxy), 1.72 (t-t, J = 7 Hz, 16H, octyloxy), 1.47 (t-t, J = 7 Hz, 16H, octyloxy), 1.38-1.15 (m, 144H, octyloxy), 0.82 (t, J = 7 Hz, 24H, octyloxy), and 0.74 (t, J = 7 Hz, 24H, octyloxy); MALDI-TOF-MS m/z 4310, calcd for $C_{256}H_{328}N_{16}O_{16}Zn_4Br_2$ m/z 4307.

Z6Br$_2$. (78%) ^{1}H NMR ($CDCl_3$) δ 9.88 (d, J = 5 Hz, 4H, β), 9.20 (d, J = 5 Hz, 4H, β), 8.94-8.91 (m, 12H, β), 8.86 (d, J = 5 Hz, 4H, β), 8.82 (d, J = 5 Hz, 4H, β), 8.34-8.31 (m, 12H, β), 8.21 (d, J = 5 Hz, 4H, β), 8.18 (d, J = 5 Hz, 4H, β), 7.48 (d, J = 2 Hz, 8H, Ar), 7.44 (d, J = 3 Hz, 8H, Ar), 7.42 (d, J = 2 Hz, 8H, Ar), 6.83 (br, 4H, Ar), 6.76 (br, 4H, Ar) 6.73 (br, 4H, Ar), 4.11-4.00 (m, 48H, octyloxy), 1.85-1.72 (m, 48H, octyloxy), 1.49-1.17 (m, 240H, octyloxy), 0.83 (t, J = 7 Hz, 24H, octyloxy), and 0.78-0.72 (m, 48H, octyloxy); MALDI-TOF-MS m/z 6381, calcd for $C_{384}H_{492}N_{24}O_{24}Zn_6Br_2$ m/z 6380.

Z8Br$_2$. (83%). ^{1}H NMR ($CDCl_3$) δ 9.89 (d, J = 5 Hz, 4H, β), 9.21 (d, J = 5 Hz, 4H, β), 8.95-8.91 (m, 20H, β), 8.86 (d, J = 5 Hz, 4H, β), 8.82 (d, J = 5 Hz, 4H, β), 8.35-8.31 (m, 20H, β), 8.21 (d, J = 5 Hz, 4H, β), 8.18 (d, J = 5 Hz, 4H, β), 7.50-7.49 (m, 16H, Ar), 7.44 (d, J = 3 Hz, 8H, Ar), 7.42 (d, J = 3 Hz, 8H, Ar), 6.84 (br, 4H, Ar), 6.77 (br, 8H, Ar), 6.73 (br, 4H, Ar), 4.10-4.02 (m, 64H, octyloxy), 1.85-1.73 (m, 64H, octyloxy), 1.48-1.20 (m, 320H, octyloxy), 0.83 (t, J = 7 Hz, 24H, octyloxy), and 0.80-0.71 (m, 72H, octyloxy).

Z12Br$_2$. (92%) ^{1}H NMR ($CDCl_3$) δ 9.86 (d, J = 5 Hz, 4H, β), 9.18 (d, J = 5 Hz, 4H, β), 8.90-8.86 (m, 36H, β), 8.80 (d, J = 5 Hz, 4H, β), 8.77 (d, J = 5 Hz, 4H, β), 8.29-8.24 (m, 36H, β),

8.13 (d, J = 5 Hz, 4H, β), 8.07 (d, J = 5 Hz, 4H, β), 7.50-7.48 (m, 32H, Ar), 7.43 (d, J = 3 Hz, 8H, Ar), 7.41 (d, J = 3 Hz, 8H, Ar), 6.84 (br, 4H, Ar), 6.77 (br, 16H, Ar), 6.73 (br, 4H, Ar), 4.06 (m, 96H, octyloxy), 1.84-1.76 (m, 96H, octyloxy), 1.50-1.19 (m, 480H, octyloxy), and 0.85-0.75 (m, 144H, octyloxy).

Z16Br$_2$. (84%). ^{1}H NMR ($CDCl_3$) δ 9.88 (d, J = 5 Hz, 4H, β), 9.02 (d, J = 5 Hz, 4H, β), 8.96 (m, 52H, β), 8.86 (d, J = 5 Hz, 4H, β), 8.82 (d, J = 5 Hz, 4H, β), 8.36 (m, 52H, β), 8.21 (d, J = 5 Hz, 4H, β), 8.17 (d, J = 5 Hz, 4H, β), 7.52-7.42 (m, 64H, Ar), 6.85 (d, J = 3 Hz, 4H, Ar), 6.78 (br, 24H, Ar), 6.73 (d, J = 3 Hz, 4H, Ar), 4.06 (m, 128H, octyloxy), 1.84-1.78 (m, 128H, octyloxy), 1.44-1.20 (m, 640H, octyloxy), and 0.85-0.75 (m, 192H, octyloxy).

Z24Br$_2$. (89%). ^{1}H NMR ($CDCl_3$) δ 9.87 (d, J = 5 Hz, 4H, β), 9.19 (d, J = 5 Hz, 4H, β), 8.95-8.80 (m, 92H, β), 8.35-8.15 (m, 92H, β), 7.50-7.41 (m, 96H, Ar), 6.83-6.72 (m, 48H, Ar), 4.06 (m, 192H, octyloxy), 1.77 (m, 192H, octyloxy), 1.42-1.23 (m, 960H, octyloxy), and 0.84-0.72 (m, 288H, octyloxy).

Z48Br$_2$. (91%). ^{1}H NMR ($CDCl_3$) δ 9.88 (d, J = 5 Hz, 4H, β), 9.20 (d, J = 5 Hz, 4H, β), 8.95-8.80 (m, 188H, β), 8.35-8.15 (m, 188H, β), 7.50-7.41 (m, 192H, Ar), 6.83-6.72 (m, 96H, Ar), 4.06 (m, 384H, octyloxy), 1.77 (m, 384H, octyloxy), 1.42-1.24 (m, 1920H, octyloxy), and 0.84-0.71 (m, 576H, octyloxy).

Z64Br$_2$. (87%). ^{1}H NMR ($CDCl_3$) δ 9.87 (br, 4H, β), 9.19 (br, 4H, β), 8.93-8.80 (m, 252H, β), 8.32-8.11 (m, 252H, β), 7.50 (m, 256H, Ar), 6.77 (br, 128H, Ar), 4.08 (m, 512H, octyloxy), 1.80 (m, 512H, octyloxy), 1.45-1.22 (m, 2560H, octyloxy), and 0.85-0.77 (m, 768H, octyloxy).

27. 4-Bromobenzenethiol (**25**) (920 mg, 5.0 mmol) was dissolved in a mixture of TFA (9 ml) and CH_2Cl_2 (2 ml) and stirred for 15 min under Ar at room temperature. To the solution was added benzhydrol (**26**) (945 mg, 5.0 mmol). After 5 min, the precipitate was collected and purified over a silica gel column (CH_2Cl_2/hexane = 1/4). The product was given as white crystal (1.48 g, 83%). ^{1}H NMR ($CDCl_3$) δ 7.37 (d, J = 8 Hz, 4H, Ar), 7.30-7.19 (m, 8H, Ar), 7.06 (d, J = 8 Hz, 2H, Ar), and 5.48 (s, 1H, benzyl). FAB MS m/z 402.3, calcd for $C_{32}H_{22}N_4$ m/z 402.2.

28. **26** (178 mg, 0.5 mmol) was mixed with bispinacolate diboron (125 mg, 0.5 mmol), KOAc (125 mg), and $PdCl_2$(dppf) (12 mg) in DMF (2 ml). The mixture was degassed 3 times by freeze-pump thaw cycles and stirred at 80°C for 6 h. Then the mixture was washed with water, and organic layer was extracted with ether, dried over Na_2SO_4 and evaporated. The residue was separated by a silica gel column (benzene). The boronate was obtained as a white solid (96 mg, 48%). ^{1}H NMR ($CDCl_3$) δ 7.59 (d, J = 8 Hz, 2H, Ar), 7.42 (d, J = 8 Hz, 4H, Ar), 7.29 (t, J = 8 Hz, 4H, Ar), 7.21 (t, J = 8 Hz, 2H, Ar), 7.19 (d, J = 8

Hz, 2H, Ar), 5.64 (s, 1H, benzyl), and 1.30 (s, 12H, Me). FAB MS *m/z* 402.3, calcd for $C_{32}H_{22}N_4$ *m/z* 402.2.

ZnS_2. Bromo porphyrin **ZnBr_2** was mixed with boronate **28** (10 equiv), Cs_2CO_3 (15 equiv), and $Pd(PPh_3)_4$ (10 mol%) in a mixed solvent of toluene (1 ml) and DMF (1 ml). The mixture was degassed 3 times by freeze-pump thaw cycles and stirred at 80°C for 5 h. Then the mixture was washed with water, extracted with $CHCl_3$, dried over Na_2SO_4 and evaporated. After passed through a short silica gel column, the residue was loaded in GPC (THF) to remove unreacted **28**. The porphyrin fraction was collected and the solvent was evaporated. The residue was recrystallized with $CHCl_3$/Methanol.

Z6S_2. (90%). ^{1}H NMR ($CDCl_3$) δ 9.14 (d, J = 5 Hz, 4H, β), 8.93-8.91 (m, 16H, β), 8.86-8.85 (m, 4H, β), 8.34-8.31 (m, 12H, β), 8.24 (d, J = 5 Hz, 4H, β), 8.18 (d, J = 5 Hz, 4H, β), 8.12 (d, J = 8 Hz, 4H, Ph), 7.68-7.67 (m, 12H, Ph + Ar), 7.48 (m, 16H, Ph + Ar), 7.44 (d, J = 3 Hz, 8H, Ar), 7.42 (d, J = 2 Hz, 8H, Ar), 7.38 (t, J = 8 Hz, 4H, Ph), 6.83 (br, 4H, Ar), 6.75 (br, 4H, Ar) 6.72 (br, 4H, Ar), 4.10-4.01 (m, 48H, octyloxy), 1.82-1.72 (m, 48H, octyloxy), 1.48-1.17 (m, 240H, octyloxy), 0.82 (t, J = 7 Hz, 24H, octyloxy), and 0.78-0.74 (m, 48H, octyloxy); MALDI-TOF-MS *m/z* 6381, calcd for $C_{384}H_{492}N_{24}O_{24}Zn_6Br_2$ *m/z* 6380.

Z12S_2. ^{1}H NMR ($CDCl_3$) δ 9.06 (d, J = 5 Hz, 4H, β), 8.89-8.79 (m, 48H, β), 8.85 (d, J = 5 Hz, 4H, β), 8.29-8.25 (m, 38H, β), 8.17 (d, J = 5 Hz, 4H, β), 8.11 (d, J = 5 Hz, 4H, β), 8.06 (d, J = 8 Hz, 4H, Ph), 7.61-7.59 (m, 12H, Ph + Ar), 7.45-7.28 (m, 60H, Ph + Ar), 6.77 (br, 4H, Ar), 6.71 (br, 16H, Ar), 6.66 (br, 4H, Ar), 5.84 (s, 2H, benzyl), 4.07 (m, 96H, octyloxy), 1.86-1.76 (m, 96H, octyloxy), 1.50-1.19 (m, 480H, octyloxy), and 0.85-0.75 (m, 144H, octyloxy).

Z24S_2. (79%). ^{1}H NMR ($CDCl_3$) δ 9.11 (d, J = 5 Hz, 4H, β), 8.95-8.84 (m, 96H, β), 8.35 (m, 88H, β), 8.22 (d, J = 5 Hz, 4H, β), 8.17 (d, J = 5 Hz, 4H, β), 8.12 (d, J = 8 Hz, 4H, Ph), 7.65 (m, 12H, Ph + Ar), 7.45-7.41 (m, 108H, Ph + Ar), 6.83-6.72 (m, 48H, Ar), 5.89 (s, 2H, benzyl), 4.06 (m, 192H, octyloxy), 1.77 (m, 192H, octyloxy), 1.42-1.23 (m, 960H, octyloxy), and 0.84-0.72 (m, 288H, octyloxy).

Z48S_2. (79%). ^{1}H NMR ($CDCl_3$) δ 9.11 (br, 4H, β), 8.95-8.84 (m, 192H, β), 8.35 (m, 184H, β), 8.24 (d, J = 5 Hz, 4H, β), 8.19 (d, J = 5 Hz, 4H, β), 8.15 (d, J = 8 Hz, 4H, Ph), 7.65 (m, 12H, Ph + Ar), 7.45-7.41 (m, 204H, Ph + Ar), 6.83-6.72 (m, 96H, Ar), 5.89 (s, 2H, benzyl), 4.06 (m, 384H, octyloxy), 1.77 (m, 384H, octyloxy), 1.42-1.23 (m, 1920H, octyloxy), and 0.84-0.72 (m, 576H, octyloxy).

Z64S*J*. (91%). ^{1}H NMR ($CDCl_3$) δ 9.15 (br, 4H, β), 8.97-8.87 (m, 256H, β), 8.37-8.20 (m, 252H, β), 8.13 (br, 4H, Ph), 7.67 (d, J= 7 Hz, 12H, Ph + Ar), 7.52 (m, 268H, Ar), 6.79 (br, 128H, Ar), 5.92 (s, 2H, benzyl), 4.08 (m, 512H, octyloxy), 1.80 (m, 512H, octyloxy), 1.45-1.22

(m, 2560H, octyloxy), and 0.85-0.77 (m, 768H, octyloxy).

References and Notes

[1] Cyanobacterial PS I (*Synechococcus elongatus*): Jordan, P.; Fromme, P.; Witt, H. T.; Klukas, O.; Saenger, W.; Krauß, N. *Nature* **2001**, *411*, 909.

[2] Cyanobacterial PS II (*Synechococcus elongates*): Zouni, A.; Witt, H. T.; Kern, J.; Fromme, P.; Krauß, N.; Saenger, W.; Orth, P. *Nature* **2001**, *409*, 739.

[3] Cyanobacterial PS I (*Synechococcus* sp.): Krauß, N.; Hinrichs, W.; Witt, I.; Fromme, P.; Pritzkow, W.; Dauter, Z.; Betzel, C.; Wilson, K. S.; Witt, H. T.; Saenger, W. *Nature* **1993**, *361*, 326.

[4] Purple bacterial RC (*Rhodopseudomonas viridis*): Deisenhofer, J.; Epp, O.; Miki, K.; Huber, R.; Michel, H. *J. Biol. Chem.* **1984**, *180*, 385.

[5] Purple bacterial RC (*Rhodopseudomonas viridis*): Deisenhofer, J.; Epp, O.; Miki, K.; Huber, R.; Michel, H. *Nature* **1985**, *318*, 618.

[6] Purple bacterial RC (*Rhodopseudomonas sphaeroides*): Allen, J. P.;Feher, G.; Yeates, T. O.; Komiya, H.; Rees, D. C. *Proc. Natl. Acad. Sci. USA* **1988**, *85*, 8487.

[7] Purple bacterial RC (*Rhodopseudomonas sphaeroides vs Rhodopseudomonas sphaeroides*): Allen, J. P.; Feher, G; Yeates, T. O.; Komiya, H.; Rees, D. C. *Proc. Natl. Acad. Sci. USA* **1986**, *83*, 8589.

[8] van Grondelle, R,; Dekker, J. P.; Gillbro, T.; Sundström, V. *Biochim. Biophys. Acta* **1994**, *1187*, 1.

[9] Purple bacterial LH2 (*Rhodopseudomonas acidophila*): McDermott, G.; Prince, S. M.; Freer, A. A.; Hawthornthwaite-Lawless, A. M.; Papiz, M. Z.; Cogdell, R. J.; Isaacs, N. W. *Nature* **1995**, *374*, 517.

[10] Bacteriochlorophyll protein (*Chlorobium limicola*): Fenna, R. E.; Matthews, B. W. *Nature* **1975**, *258*, 573.

[11] Purple bacterial LH1 (*Rhodospirillum rubrum*): Karrasch, S.;Bullough, P. A.; Ghosh, R. *EMBO J.* **1995**, *14*, 631.

[12] Purple bacterial RC-LH1 (*Rhodopseudomonas palustris*): Roszak, A. W.; Howard, T. D.; Southall, J.; Gardiner, A. T.; La, C. J.; Isaacs, N. W.; Cogdell, R. J. *Nature* **2003**, *302*, 1969.

[13] Wasielewski, M. R. *Chem. Rev.* **1992**, *92*, 435.

[14] Gust, D.; Moore, T. A.; Moore, A. L. *Acc. Chem. Res.* **1993**, *26*, 198.

[15] Gust, D.; Moore, T. A.; Moore, A. L. *Acc. Chem. Res.* **2001**, *34*, 40.

[16] Holten, D.; Bocian, D.; Lindsey, J. S. *Acc. Chem. Res.* **2002**, *35*, 57.

[17] Burrell, A. K.; Officer, D. L.; Plieger, P. G.; Reid, D. C. W. *Chem. Rev.* **2001**, *101*, 2751.

[18] Osuka, A.; Marumo, S.; Mataga, N.; Taniguchi, S.; Okada, T.; Yamazaki, I.; Nishimura, Y.; Ohno, T.; Nozaki, K. *J. Am. Chem. Soc.* **1996**, *118*, 155.

[19] Osuka, A.; Noya, G.; Taniguchi, S.; Okada, T.; Nishimura, Y.; Yamazaki, I.; Mataga, N. *Chem. Eur. J.* **2000**, *6*, 33.

[20] Osuka, A.; Nakajima, S.; Okada, T.; Taniguchi, S.; Nozaki, K.; Ohno, T.; Yamazaki, I.; Nishimura, Y.; Mataga, N. *Angew. Chem. Int. Ed. Engl.* **1996**, *35*, 92.

[21] Baldwin, J. E.; Crossley, M. J.; Debernadis, J. *Tetrahedron* **1982**, *38*, 685.

[22] Osuka, A.; Shimidzu, H. *Angew. Chem. Int. Ed. Engl.* **1997**, *36*, 135.

[23] Yoshida, N.; Shimidzu, H.; Osuka, A. *Chem. Lett.* **1998**, 55.

[24] Susumu, K.; Shimidzu, T.; Tanaka, K.; Segawa, H. *Tetrahedron Lett.* **1996**, *37*, 8399.

[25] Khoury, R. G.; Jaquinod, L.; Smith, K. M. *Chem. Commun.* **1997**, 1957.

[26] Wojaczynski, J.; Latos-Grazynski, L.; Chmielewski, P. J.; Van Calcar, P.; Balch, A. L. *Inorg. Chem.* **1999**, *38*, 3040.

[27] Senge, M. O.; Feng, X. *Tetrahedron Lett.* **1999**, *40*, 4165.

[28] Shi, X.; Liebeskind, L. S. *J. Org. Chem.* **2000**, *65*, 1655

[29] Ogawa, T.; Nishimoto, Y.; Yoshida, N.; Ono, N.; Osuka, A. *Chem. Commun.* **1998**, 337.

[30] For general references on porphyrins, Kadish, K. M.; Smith, K. M.; Guilard R., Eds. *The Porphyrin Handbook*; Vols.1-10; Academic Press, New York, 1999. Vol.11-20; Academic Press, New York, 2003.

[31] Balzani, V.; Credi, A.; Raymo, F. M.; Stoddart, J. F. *Angew. Chem. Int. Ed.* **2000**, *39*, 3348.

[32] (a) Nagata, T.; Osuka, A.; Maruyama, K. *J. Am. Chem. Soc.* **1990**, *112*, 68. (b) Osuka, A.; Tanabe, N.; Zhang, R.-P.; Maruyama, K. *Chem. Lett.* **1993**, 1505. (c) Osuka, A.; Tanabe, N.; Nakajima, S.; Maruyama, K. *J. Chem. Soc. Perkin Trans. 2* **1996**, 199.

[33] Covalently linked cyclic porphyrin dodecamer: Peng, X.; Aratani, N.; Takagi, A.; Matsumoto, T.; Kawai, T.; Hwang, I.-W.; Ahn, T. K.; Kim, D.; Osuka, A. *J. Am. Chem. Soc.* **2004**, *126*, 4468.

[34] Non-covalently linked cyclic porphyrin arrays: (a) Takahashi, R.; Kobuke, Y. *J. Am. Chem. Soc.* **2003**, *125*, 2372. (b) Kuramochi, Y.; Satake, A.; Kobuke, Y. *J. Am. Chem. Soc.* **2004**, *126*, 8668.

[35] (a) Dubowchik, G. M.; Hamilton, A. D. *J. Chem. Soc. Chem. Commun.* **1987**, 293. (b) Li, J.; Ambroise, A.; Yang, S. I.; Diers, J. R.; Seth, J.; Wack, C. R.; Bocian, D. F.; Holten, D.; Lindsey, J. S. *J. Am. Chem. Soc.* **1999**, *121*, 8927. (c) Mongin, O.; Schuwey, A.; Vallot,

M.-A.; Gossauer, A. *Tetrahedron Lett.* **1999**, *40*, 8347. (d) Mongin, O.; Papamicaël, C.; Hoyler, N.; Gossauer, A. *J. Org. Chem.* **1998**, *63*, 5568. (e) Anderson H. L. and Sanders, J. K. M. *J. Chem. Soc., Chem. Commun.* **1989**, 1714. (f) Anderson, S.; Anderson, H. L.; Sanders, J. K. M. *Acc. Chem. Res.* **1993**, *26*, 469. (g) Sugiura, K.; Fujimoto, Y.; Sakata, Y. *Chem. Commun.* **2000**, 1105. (g) Kato, A.; Sugiura, K.-i.; Miyasaka, H.; Tanaka, H.; Kawai, T.; Sugimoto, M.; Yamashita, M. *Chem. Lett.* **2004**, *33*, 578.

[36] (a) Mak, C. C.; Bampos, N.; Sanders, J. K. M. *Angew. Chem. Int. Ed.* **1998**, *37*, 3020. (b) Sugiura, K.-i.; Tanaka, H.; Matsumoto, T.; Kawai, T.; Sakata, Y. *Chem. Lett.* **1999**, 1193. (c) Choi, M.-S.; Aida, T.; Yamazaki, T.; Yamazaki, I. *Chem. Eur. J.* **2002**, *8*, 2667. (d) Choi, M.-S.; Aida, T.; Yamazaki, T.; Yamazaki, I. *Angew. Chem. Int. Ed.* **2001**, *40*, 3194.

[37] (a) Collman, J. P.; Denisevich, P.; Konai, Y.; Marrocco, M.; Koval, C.; Anson, F. C. *J. Am. Chem. Soc.* **1980**, *102*, 6027. (b) Fillers, J. P.; Ravichandran, K. G.; Abdalmuhdi, I.; Tulinksi, A.; Chang, C. K. *J. Am. Chem. Soc.* **1986**, *108*, 417. (c) Osuka, A.; Nakajima, S.; Nagata, T.; Maruyama, K.; Toriumi, T. *Angew. Chem. Int. Ed. Engl.* **1991**, *30*, 582.

[38] (a) Cho, H. S.; Rhee, H.; Song, J. K.; Min, C.-K.; Takase, M.; Aratani, N.; Cho, S.; Osuka, A.; Joo, T.; Kim, D. *J. Am. Chem. Soc.* **2003**, *125*, 5849. (b) Officer, D. L.; Burrell, A. K.; Reid, D. C. W. *Chem. Commun.* **1996**, 1657. (c) Kuciauskas, D.; Liddell, P. A.; Lin, S.; Johnson, T. E.; Weghorn, S. J.; Lindsey, J. S.; Moore, A. L.; Moore, T. A.; Gust, D. *J. Am. Chem. Soc.* **1999**, *121*, 8604.

[39] Wind-mill like porphyrin arrays: (a) Nakano, A.; Osuka, A.; Yamazaki, I.; Yamazaki, T.; Nishimura, Y. *Angew. Chem. Int. Ed.* **1998**, *37*, 3023. (b) Nakano, A.; Osuka, A.; Yamazaki, T.; Nishimura, Y.; Akimoto, S.; Yamazaki, I.; Itaya, A.; Murakami, M.; Miyasaka, H. *Chem. Eur. J.* **2001**, *7*, 3134.

[40] Grid like porphyrin arrays: Nakano, A.; Yamazaki, T.; Nishimura, Y.; Yamazaki, I.; Osuka, A. *Chem. Eur. J.* **2000**, *6*, 3254.

[41] Martin, R. E.; Diederich, F. *Angew. Chem. Int. Ed.* **1999**, *38*, 1350. (b) Tour, J. M. *Chem. Rev.* **1996**, *96*, 537. (c) Schwab, P. F. H.; Levin, M. D.; Michl, J. *Chem. Rev.* **1999**, *99*, 1863. (d) Cornil, J.; Beljonne, D.; Calbert, J.-P.; Brédas, J.-L. *Adv. Mater.* **2001**, *13*, 1053. (e) Kraft, A.; Grimsdale, A. C.; Holmes, A. B. *Angew. Chem. Int. Ed.* **1998**, *37*, 402. (f) Moore, J. S. *Acc. Chem. Res.* **1997**, *30*, 402. (g) McQuade, D. T.; Pullen, A. E.; Swager, T. M. *Chem. Rev.* **2000**, *110*, 2537. (h) Watson, M. D.; Fechtenkötter, A.;

Müllen, K. *Chem. Rev.* **2001**, *101*, 1267. (i) Zhao, D.; Moore, J. S. *Chem. Commun.* **2003**, 807. (j) Li, W.-S.; Jiang, D.-L.; Aida, T. *Angew. Chem. Int. Ed.* **2004**, *43*, 2943. (k) Diederich, F. *Chem. Commun.* **2001**, 219.

[42] Tour, J. M. *Acc. Chem. Res.* **2000**, *33* 791.

[43] Joachim, C.; Gimzewski, J. K.; Aviram, A. *Nature* **2000**, *408* 541.

[44] Aratani, N.; Osuka, A.; Kim, Y. H.; Jeong, D. H.; Kim, D. *Angew. Chem. Int. Ed.* **2000**, *39*, 1458.

[45] Kim, Y. H.; Jeong, D. H.; Kim, D.; Jeoung, S. C.; Cho, H. S.; Kim, S. K.; Aratani, N.; Osuka, A. *J. Am. Chem. Soc.* **2001**, *123*, 76.

[46] Aratani, N.; Osuka, A. *Org. Lett.* **2001**, *3*, 4213

[47] Aratani, N.; Cho H. S.; Ahn, T. K.; Cho, S.; Kim, D.; Sumi, H.; Osuka, A. *J. Am. Chem. Soc.* **2003**, *125*, 9668

[48] Aratani, N.; Takagi, A.; Yanagawa, Y.; Matsumoto, T.; Kawai, T.; Yoon, Z. S.; Kim, D.; Osuka, A. manuscript in preparation.

[49] (a) Chiang, C. K.; Fincher, Jr., C. R.; Park, Y. W.; Heeger, A. J.; Shirakawa, H.; Louis, E. J.; Gau, S. C.; MacDiarmid, A. G. *Phys. Rev. Lett.* **1977**, *39*, 1098. (b) McGehee, M. D.; Heeger, A. J. *Adv. Mater.* **2000**, *12*, 1655. (c) Brabec, C. J.; Saricific, N. S.; Hummelen, J. C. *Adv. Funct. Mater.* **2001**, *11*, 15.

[50] Grubisic, Z.; Remmp, P.; Benoit, H. *J. Polym. Sci., Polym. Lett.* **1967**, *5*, 753.

[51] Kovacic P. M.; Jones, B. *Chem. Rev.* **1987**, *87*, 357.

[52] (a) Wegner, G. *Angew. Chem., Int. Ed. Engl.* **1981**, *20*, 361. (b) Speight, J. G.; Kovacicand, P.; Koch, F. W. *J. Macromol. Sci. Rev. Macromol. Chem.* **1971**, *C5(2)*, 295.

[53] (a) Yamamoto, T. *Bull. Chem. Soc. Jpn.*, **1999**, *72*, 621. (b) Fichou, D. *Handbook of Oligo- and Polythiophenes*; Wiley-VCH: Weinheim, 1999.

[54] Tour, J. M. *Adv. Mater.* **1994**, *6*, 190.

[55] Yamakawa, H. *Modern Theory of Polymer Solutions*; Harper & Row: New York, 1971.

[56] Liess, P.; Hensel, V.; Schlüter, A. D. *Liebigs Ann.* **1996**, 1037.

[57] Hensel, V.; Schlüter, A. D. *Chem. Eur. J.* **1999**, *5*, 421.

[58] Stalmach, U.; Kolshorn, H.; Brehm, I.; Meier, H. *Liebigs Ann.* **1996**, 1449.

[59] Jones II, L.; Schumm, J. S.; Tour, J. M. *J. Org. Chem.* **1997**, *62*, 1388.

[60] Huang, S.; Tour, J. M. *J. Org. Chem.* **1999**, *64*, 8898.

[61] Cravino, A.; Sariciftci, N. S. *J. Mater. Chem.* **2002**, *12*, 1931.

[62] (a) Roncali, J. *Acc. Chem. Res.* **2000**, *33*, 147. (b) Roncali, J. *Chem. Rev.* **1997**, *97*, 173. (c) Jestin, I.; Frere, P.; Blanchard, P.; Roncali, J. *Angew. Chem. Int. Ed.* **1998**, *37*, 942.

[63] (a) Tachibana, M.; Tanaka, S.; Yamashita, Y.; Yoshizawa, K. *J. Phys. Chem. B* **2002**, *106*, 3549. (b) Tanaka, S.; Yamashita, Y. *Synth. Met.* **1995**, *69*, 599.

[64] (a) Izumi, T.; Kobashi, S.; Takimiya, K.; Aso, Y.; Otsubo, T. *J. Am. Chem. Soc.* **2003**, *125*, 5286. (b) Otsubo, T.; Aso, Y.; Takimiya, K. *Bull. Chem. Soc. Jpn.* **2001**, *74*, 1789. (c) Inouchi, K.; Kobashi, S.; Takimiya, K.; Aso, Y.; Otsubo, T. *Org. Lett.* **2002**, *4*, 2533.

[65] The longest molecule in publication (up to Dec 2004): Li, W.-S.; Jiang, D.-L.; Aida, T. *Angew. Chem. Int. Ed.* **2004**, *43*, 2943.

[66] (a) Crezy, P. S.; Smith, G. A.; *Aust. J. Chem.* **1969**, *22*, 239. (b) Wang, Q. M.; Bruce, D. W. *Synlett*, **1995**, 1267. (c) Littler, B. J.; Miller, M. A.; Hung, C.-H.; Wagner, R. W.; O'Shea, D. F.; Boyle, P. D. ;Lindsey, J. S. *J. Org. Chem.* **1999**, *64*, 1391. (d) Screen, T. E. O.; Lawton, K. B.; Wilson, G. S.; Dolney, N.; Ispasoiu, R.; Goodson III, T.; Martin, S. J.; Bradley D. D. C.; Anderson, H. L. *J. Mater. Chem.* **2001**, *11*, 312. (e) Ka, J.-W.; Lee, C.-H. *Tetrahederon Lett.* **2000**, *41*, 4609.

[67] (a) Lindsey, J. S.; Schreiman, I. C.; Hsu, H. C.; Kearney, P. C.; Marguerettaz, A. M. *J. Org. Chem.* **1987**, *52*, 827. (b) DiMagno, S. G.; Lin, V. S.-Y.; Therien, M. J. *J. Org. Chem.* **1993**, *58*, 5983.

[68] Yoshida, N.; Aratani, N.; Osuka, A. *Chem. Commun.* **2000**, 197.

[69] Nakano, A.; Shimidzu, H.; Osuka, A. *Tetrahedron Lett.* **1998**, *39*, 9489.

[70] (a) Pearson D. L.; Schumm, J. S.; Tour, J. M. *Macromolecules*, **1994**, *27*, 2348. (b) Schumm, J.; Pearson, D. L.; Tour, J. M. *Angew. Chem., Int. Ed. Engl.* **1994**, *33*, 1360.

[71] X-ray crystal structure of *meso-meso* linked Cu(II) diporphyrin was reported. Yoshida, N.; Ishizuka, T.; Osuka, A.; Jeong, D. H.; Cho, H. S.; Kim, D.; Matsuzaki, Y.; Nagami, A.; Tanaka, K. *Chem. Eur. J.* **2003**, **9**, 58. Other examples of X-ray crystal structures of singly directly linked diporphyrins, see ref [25] and (a) Deng, Y.; Chang, C. K.; Nocera, D. G. *Angew. Chem. Int. Ed.* **2000**, *39*, 1066. (b) Nakamura, Y.; Aratani, N.; Tsuda, A.; Osuka, A.; Furukawa, K.; Kato, T. *J. Porphyrins Phthalocyanines* **2003**, **7**, 264. (c) Tsuda, A.; Furuta, H.; Osuka, A. *J. Am. Chem. Soc.* **2001**, *123*, 10304.

[72] (a) Aurivillius, B.; Carter, R. E.; *J. Chem. Soc., Perkin* 2 **1978**, 1033. (b) Nishino, M.; Hirota, H. *Tetrahedron* **1989**, *45*, 7201. (c) Takahashi, H.; Tsuboyama, S.; Umezawa, Y.; Honda, K.; Nishio, M. *Tetrahedron* **2000**, *56*, 6185. (d) Nishio, M. *CrystEngComm* **2004**, *6*, 130.

[73] Binnig, G.; Rohrer, H.; Gerber, Ch.; Weibel, E. *Phys. Rev. Lett.* **1982**, *49*, 57.

[74] (a) Mena-Osteritz, E.; Meyer, A.; Langeveld-Voss, B. M. W.; Janssen, R. A. J.; Meijer, E. W.; Bäuerle, P. *Angew. Chem. Int. Ed.* **2000**, *39*, 2679. (b) Anderson, H. L. *Angew.*

Chem. Int. Ed. **2000**, *39*, 2451.

[75] (a) Jung, T. A.; Schlittler, R. R.; Gimzewski, J. K.; Tang, H.; Joachim, C. *Science* **1996**, *271*, 181. (b) Gimzewski, J. K.; Joachim, C. *Science* **1999**, *283*, 1683.

[76] (a) Bampos, N.; Woodburn, C. N.; Welland, M. E.; Sanders, J. K. M. *Angew. Chem. Int. Ed.* **1999**, *38*, 2780. (b) Sugiura, K.-i.; Matsumoto, T.; Ohkouchi, S.; Naitoh, Y.; Kawai, T.; Takai, Y.; Ushiroda, K.; Sakata, Y. *Chem. Commun.* **1999**, 1957.

[77] Tanaka, H.; Nakagawa T.; Kawai, T. *Surf. Sci.*, **1996**, *364*, L575.

[78] (a) Takagi, A.; Yanagawa, Y.; Tsuda, A; Aratani, N.; Matsumoto, T.; Osuka, A.; Kawai, T. *Chem. Commun.* **2003**, 2986.

[79] (a) Kasha, M. *Rev. Mod. Phys.* **1959**, *31*, 162. (b) Kasha, M.; Rawls, H. R.; El-Bayoumi, M. A. *Pure Appl. Chem.* **1965**, *11*, 371. (c) MacRae, E. G.; Kasha, M. In *Physical Processes in Radiation Biology*, Augenstein, L.; Mason, R.; Rosenberg, B. Eds.; Academic Press: New York, 1964; pp 23. (d) Kasha, M. *Radiat. Res.* **1963**, *20*, 55.

[80] (a) Cho, H. S.; Song, N. W.; Kim, Y. H.; Jeoung, S. C.; Hahn, S.; Kim, D.; Kim, S. K.; Yoshida, N.; Osuka, A. *J. Phys. Chem. A* **2000**, *104*, 3287.

[81] Bakalis, L. D.; Knoester, J. *J. Phys. Chem. B* **1999**, *103*, 6620.

[82] Gouterman, M. In *The Porphyrins*, Dolphin D. Ed. Academic Press, New York, 1978, Vol. 3, p 1.

[83] Ohta, N.; Iwaki, Y.; Ito, T.; Yamazaki, I.; Osuka, A. *J. Phys. Chem. B* **1999**, *103*, 11242.

[84] Seybold, P. G.; Gouterman, M. *J. Mol. Spectro.* **1969**, *31*, 1.

[85] Song, N.; Cho, H. S.; Yoon, M.-C.; Aratani, N.; Osuka, A.; Kim, D. *Bull. Korean Chem. Soc.* **2002**, *23*, 271

[86] Kim, Y. R.; Share, P.; Pereira, M.; Sarisky, M.; Hochstrasser, R. M. *J. Chem. Phys.* **1983**, *91*, 7557.

[87] Lakowicz, J. R. In *Principles of Fluorescence Spectroscopy*, Plenum Press, New York and London, 1983.

[88] Kobayashi, H.; Kaizu, Y. In *Porphyrins: Excited States and Dynamics*; Gouterman, M.; Rentizepis, P.; Straub, K. D. Eds. American Chemical Society Symposium Series 321; American Chemical Society: Washington, DC, 1986, p105.

[89] Pullerits, T.; Chachisvilis, M.; Sundström, V. *J. Phys. Chem.* **1996**, *100*, 10787.

[90] van Oijen, A. M.; Ketelaars, M.; Köhler, J.; Aartsma, T. J.; Schmidt, J. *Science* **1999**, *285*, 400.

[91] De Boer, S.; Wiersma, D. A. *Chem. Phys. Lett.* **1990**, *165*, 45.

[92] Kasha, M. *Discuss. Faraday Soc.* **1950**, *9*, 14.

[93] Fajer, J.; Borg, D. C.; Forman, A.; Dolphin, D.; Felton, R. H. *J. Am. Chem. Soc.* **1970**, *92*, 3451.

[94] Ohya-Nishiguchi, H. *Bull. Chem. Soc. Jpn.* **1979**, *52*, 2064.

[95] Ogawa, T.; Nishimoto, Y.; Yoshida, N.; Ono, N. Osuka, A. *Angew. Chem. Int. Ed.* **1999**, *38*, 176.

[96] Kamo, M.; Tsuda, A.; Nakamura, Y.; Aratani, N.; Furukawa, K.; Kato, T.; Osuka, A. *Org. Lett.* **2003**, *5*, 2079.

[97] Pardo, E.; Faus,J.; Julve, M.; Lloret, F.; Muñoz, M. C.; Cano, J.; Ottenwaelder, X.; Journaux, Y.; Carrasco, R.; Blay, G.; Fernández, I.; Ruiz-García, R. *J. Am. Chem. Soc.* **2003**, *125*, 10770.

[98] Tanaka, K.; Tengeiji, A.; Kato, T.; Toyama, N.; Shionoya, M. *Science* **2003**, *299*, 1212.

[99] (a) Segawa, H.; Senshu, Y.; Nakazaki, J.; Susumu, K. *J. Am. Chem. Soc.* **2004**, *126*, 1354. (b) Segawa, H.; Machida, D.; Senshu, Y.; Nakazaki, J.; Hirokawa, K. Wu, F. *Chem. Commun.* **2002**, 3032

[100] Johnson, Jr. C. S.; *Prog. Nucl. Magn. Reson. Spectrosc.* **1999**, *34*, 203.

[101] (a) Olenyuk, B.; Levin, M. D.; Whiteford, J. A.; Shield, J. E.; Stang, P. J. *J. Am. Chem. Soc.* **1999**, *121*, 10434. (b) Otto, W. H.; Keefe, M. H.; Splan, K. E.; Hupp, J. T.; Larive, C. K. *Inorg. Chem.* **2002**, *41*, 6172.

[102] Jeon, W. S.; Ziganshina, A. Y.; Lee, J. W.; Ko, Y. H.; Kang, J.-K.; Lee, C.; Kim, K. *Angew. Chem. Int. Ed.* **2003**, *42*, 4097.

[103] Aratani, N.; Osuka, A.; Cho, H. S.; Kim, D. *J. Photochem. Photobio. C: Photochem. Rev.* **2002**, *3*, 25.

[104] Cho, H. S.; Jeong, D. H.; Yoon, M.-C.; Kim, Y. H.; Kim, Y.-R.; Kim, D.; Jeoung, S. C.; Kim, S. K.; Aratani, N.; Shinmori, H.; Osuka, A. *J. Phys. Chem. A* **2001**, *105*, 4200.

[105] Hyslop, A. G.; Kellett, M. A.; Iovine, P. M.; Therien, M. J. *J. Am. Chem. Soc.* **1998**, *120*, 12676.

[106] Taniguchi, S.; Hasegawa, H.; Nishimura, M.; Takahashi, M. *Synlett*, **1999**, 73.

[107] Nakamura, Y.; Hwang, I.-W.; Aratani, N.; Ahn, T. K.; Ko, D. M.; Takagi, A.; Kawai, T.; Matsumoto, T.; Kim, D.; Osuka, A. *J. Am. Chem. Soc.* **2005**, *127*, 236.

[108] For a review: (a) Grave, C.; Schlüter, A. D. *Eur. J. Org. Chem.* **2002**, 3075. (b) Prautzsch, V.; Ibach, S.; Vögtle, F. *J. Inclusion Phenom. Macrocyclic Chem.* **1999**, *33*, 427.

[109] Mayor, M.; Lehn, J.-M. *J. Am. Chem. Soc.* **1999**, *121*, 11231.

[110] Hensel, V.; Schlüter, A. D. *Chem. Eur. J.* **1999**, *5*, 421.

[111] Krömer, J.; Rios-Carreras, I.; Fuhrmann, G.; Munsch, C.; Wunderlin, M.;

Debaerdemaeker, T.; Mena-Osteritz, E.; Bäuerle, P. *Angew. Chem. Int. Ed.* **2000**, *39*, 3481.

[112] Seidel, D.; Lynch, V.; Sessler, J. L. *Angew. Chem. Int. Ed.* **2002**, *41*, 1422.

[113] Mayor, M.; Didschies, C. *Angew. Chem. Int. Ed.* **2003**, *42*, 3176.

[114] Lévy, L. P.; Dolan, G.; Dunsmuir, J.; Bouchiat, H. *Phys. Rev. Lett.* **1990**, *64*, 2074.

[115] (a) Holzwarth, A. R.; Griebenow, K.; Shaffner, K. *J. Photochem. Photobiol. A: Chem.* **1992**, *65*, 61. (b) Hildebrandt, P.; Tamiaki, H.; Holzwarth, A. R.; Shaffner, K. *J. Phys. Chem.* **1994**, *98*, 2192.

[116] (a) Gantt, E. *Int. Rev. Cytol.* **1980**, *66*, 45. (b) Yamazaki, I.: Mimuro, M.; Tamai, N.; Yamazaki, T.; Fujita, Y. *Photochem. Photobiol.* **1984**, *39*, 233. (c) Holzwarth, A. R.; Wendler, J.; Suter, G. W. *Biophys. J.* **1987**, *51*, 1.

[117] Tamiaki, H.; Miyatake, T.; Tanikaga, R.; Holzwarth, A. R.; Shaffner, K. *Angew. Chem., Int. Ed. Engl.* **1996**, *35*, 772.

[118] (a) van Grondelle, R.; Dekker, J. P.; Gillbro, T.; Sundström, V. *Biochim. Biophys. Acta* **1994**, *1187*, 1. (b) Pullerits, T.; Sundström, V. *Acc. Chem. Res.* **1996**, *29*, 381.

[119] (a) Sumi, H. *J. Phys. Chem. B* **1999**, *103*, 252. (b) Sumi, H. J. *Luminesc.* **2000**, *87-89*, 71. (c) Sumi, H. *Chem. Record* **2001**, *1*, 480.

[120] (a) Mukai, K.; Abe, S.; Sumi, H. *J. Phys. Chem. B*, **1999**, *103*, 6096. (b) Mukai, K.; Abe, S.; Sumi, H. J. *Luminesc.* **2000**, *87-89*, 818. (c) Scholes, G. D.; Fleming, G. R. *J. Phys. Chem. B*, **2000**, *104*, 1854. (d) Scholes, G. D.; Jordanides, X. J.; Fleming, G. R. *J. Phys. Chem. B*, **2001**, *105*, 1640.

[121] Van Patten, P. G.; Shreve, A. P.; Lindsey, J. S.; Donohoe, R. *J. Phys. Chem. B* **1998**, *102*, 4209.

[122] (a) Sonogashira, K.; Tohda, Y.; Hagihara, N. *Tetrahedron Lett.* **1975**, *16*, 4467. (b) Lindey, J. S.; Prathapan, S.; Johnson, T. E.; Wagner, R. W. *Tetrahedron* **1994**, *50*, 8941.

[123] Nakano, A.; Yasuda, Y.; Yamazaki, T.; Akimoto, S.; Yamazaki, I.; Miyasaka, H.; Itaya, A.; Murakami, M.; Osuka, A. *J. Phys. Chem. A*, **2001**, *105*, 4822.

[124] (a) Miyaura, N.; Suzuki, A. *Chem. Rev.* **1995**, *95*, 2457.

[125] (a) Zhou, X.; Chan, K. S. *J. Org. Chem.* **1998**, *63*, 99. (b) Shultz, D. A.; Lee, H.; Kumar, R. K.; Gwaltney, K. P. *J. Org. Chem.* **1999**, *64*, 9124. (c) Mizutani, T.; Wada, K.; Kitagawa, S. *J. Am. Chem. Soc.* **2001**, *123*, 6459. (d) Yu, L.; Lindsey, J. S. *Tetrahedron* **2001**, *57*, 9285.

[126] (a) Förster, T. *Ann. Phys.* **1948**, *2*, 55. (b) Förster, T. *Discuss. Faraday Soc.* **1959**, *27*, 7.

[127] Bakalis, L. D.; Knoester, J. *J. Phys. Chem. B*, **1999**, *103*, 6620.

[128] Kakitani, T.; Kimura, A. *J. Phys. Chem. A*, **2002**, *106*, 2173.

[129] Ha, J. H.; Cho, H. S.; Song, J. K.; Kim, D.; Aratani, N.; Osuka, A. *ChemPhysChem*, **2004**, *5*, 57.

[130] (a) Chang, J. C. *J. Chem. Phys.* **1977**, *67*, 3901. (b) Warshel, A.; Parson, W. W. *J. Am. Chem. Soc.* **1987**, *109*, 6143. (c) Parson, W. W.; Warshel, A. *J. Am. Chem. Soc.* **1987**, *109*, 6152. (d) Nagae, H.; Kakitani, T.; Katoh, T.; Mimuro, M. *J. Chem. Phys.* **1993**, *98*, 8012. (e) Alden, R. G.; Johnson, E.; Nagarajan, V.; Parson, W. W.; Law, C. J.; Cogdell, R. G. *J. Phys. Chem. B*, **1997**, *101*, 4667. (f) Krueger, B. P.; Scholes, G. D.; Fleming, G. R. *J. Phys. Chem. B*, **1998**, *102*, 5378.

[131] (a) Kim, D.; Osuka, A. *Acc. Chem. Res.* **2004**, *37*, 735. (b) Kim, D. Osuka, A. *J. Phys. Chem. A*, **2003**, *107*, 8791.

[132] (a) Crossley, M. J.; Burn, P. L. *J. Chem. Soc., Chem. Commun.* **1987**, 39. (b) Crossley, M. J.; Burn, P. L. Langford, S. J.; Prashar, K. J. *J. Chem. Soc., Chem. Commun.* **1995**, 1921. (c) Kobayashi, N.; Numao, M.; Kondo, R.; Nakajima, S.; Osa, T. *Inorg. Chem.* **1991**, *30*, 2241. (d) Jaquinod, L.; Siri, O.; Khoury, R. G.; Smith, K. M. *Chem. Commun.* **1998**, 1261. (e) Vicente, M. G. H.; Cancilla, M. T.; Lebrilla, C. B.; Smith, K. M. *Chem. Commun.* **1998**, 2355. (f) Paolesse, R.; Jaquinod, L.; Della, S.; Nurco, D. J.; Prodi, L.; Montalti, M.; Natale, C. D.; D'Amico, A.; Carlo, A. D.; Lugli, P.; Smith, K. M. *J. Am. Chem. Soc.* **2000**, *122*, 11295.

[133] Tsuda, A.; Nakano, A.; Furuta, H.; Yamochi, H.; Osuka, A. *Angew. Chem. Int. Ed.* **2000**, *39*, 558.

[134] Sugiura, K.-i.; Matsumoto, T.; Ohkouchi, S.; Naitoh, Y.; Kawai, T.; Takai, Y.; Ushiroda, K.; Sakata, Y. *Chem. Commun.* **1999**, 1957.

[135] (a) Tsuda, A.; Furuta, H.; Osuka, A. *Angew. Chem. Int. Ed.* **2000**, *39*, 2549. (b) Tsuda, A.; Furuta, H.; Osuka, A. *J. Am. Chem. Soc.* **2001**, *123*, 10304.

[136] Tsuda, A.; Osuka, A. *Science* **2001**, *293*, 79.

[137] Cho, H. S.; Jeong, D. H.; Cho, S.; Kim, D.; Matsuzaki, Y.; Tanaka, K.; Tsuda, A.; Osuka, A. *J. Am. Chem. Soc.* **2002**, *124*, 14642.

[138] (a) Pearson, D. L.; Tour, J. M. *J. Org. Chem.* **1997**, *62*, 1376. (b) Sumi, N.; Nakanishi, H.; Ueno, S.; Takimiya, K.; Aso, Y.; Otsubo, T. *Bull. Chem. Soc. Jpn.* **2001**, *74*, 979.

[139] Photaki, I.; T.-Papadimitriou, J.; Sakarellos, C.; Mazarakis, P.; Zervas, L. *J. Chem. Soc. C*, **1965**, 2683.

[140] (a) Ishiyama, T.; Murata, M.; Miyaura, N. *J. Org. Chem.* **1995**, *60*, 7508. (b) Murata, M.; Watanabe, S.; Masuda, Y. *J. Org. Chem.* **1997**, 62, 6458. (c) Murata, M.; Oyama,

T.; Watanabe, S.; Masuda, Y. *J. Org. Chem.* **2000**, *65*, 164.

[141] Park, H.; Lim, A. K. L.; Alivisatos, A.; Park, J.; McEuen, P. L. *Appl. Phys. Lett.* **1999**, *75*, 301.

List of Publications

Original Papers

1. Yoshida, N.; Aratani, N.; Osuka, A. "Poly(Zinc(II)-5,15-Porphyrinylene) from Silver(I)-promoted Oxidation of Zinc(II)-5,15-Diarylporphyrins", *Chem. Commun.* **2000**, 197-198.
2. Aratani, N.; Osuka, A.; Kim, Y. H.; Jeong, D. H.; Kim, D. "Extremely Long, Discrete *meso-meso*-Coupled Porphyrin Arrays", *Angew. Chem., Int. Ed.* **2000**, *39*, 1458-1462.
3. Kim, Y. H.; Jeong, D. H.; Kim, D.; Jeoung, S. C.; Cho, H. S.; Kim, S. K.; Aratani, N.; Osuka, A. "Photophysical Properties of Long Rodlike *meso-meso*-Linked Zinc(II) Porphyrins Investigated by Time-resolved Laser Spectroscopic Methods", *J. Am. Chem. Soc.* **2001**, *123*, 76.
4. Min, C. K.; Joo, T.; Yoon, M.-C.; Kim, C. M.; Hwang, Y. N.; Kim, D.; Aratani, N.; Yoshida, N.; Osuka, A. "Transient Absorption Anisotropy Study of Ultrafast Energy Transfer in Porphyrin Monomer, its Direct *meso-meso* Coupled Dimer and Trimer", *J. Chem. Phys.* **2001**, *114*, 6750-6758.
5. Cho, H. S.; Jeong, D. H.; Yoon, M.-C.; Kim, Y. H.; Kim, Y.-R.; Kim, D.; Jeoung, S. C.; Kim, S. K.; Aratani, N.; Shinmori, H.; Osuka, A. "Excited-State Energy Transfer Processes in Phenylene- and Biphenylene- Linked and Directly-Linked Zinc(II) and Free-base Hybrid Diporphyrins", *J. Phys. Chem. A*, **2001**, *105*, 4200.
6. Nakano, A.; Aratani, N.; Furuta, H.; Osuka, A. "Directly Linked Dehydropurpurin-Porphyrin Dyads from Ag(I)-promoted Oxidation of *meso*-Phenylethynyl Substituted Zinc(II) Porphyrins", *Chem. Commun.* **2001**, 1920-1921.
7. Aratani, N.; Osuka, A. "Synthesis of *meso-meso* Linked Hybrid Porphyrin Arrays by Pd-catalyzed Cross-coupling Reaction", *Org. Lett.* 2001, 3, 4213-4216.
8. Ohta, N.; Iwaki, Y.; Osuka, A.; Aratani, N. "Excitation Dynamics and its Electric Field Dependence of *meso,meso*-Linked Porphyrin Arrays in a Polymer Film", *Intern J Modern Phys B*, **2001**, *15*, 3588-3592
9. Song, N. .W; Cho, H. S.; Yoon, M.-C.; Aratani, N.; Osuka, A.; Kim, D. "Energy Relaxation Dynamics of Excited Triplet States of Directly Linked Zn(II)porphyrin Arrays", *Bull. Korean Chem. Soc.* **2002**, *23*, 271-276.
10. Jeong, D.; Yoon, M.-C.; Jang, S. M.; Kim, D.; Cho, D. W.; Yoshida, N.; Aratani, N.; Osuka, A. "Resonance Raman Spectroscopic Investigation of Directly Linked Zinc(II)

Porphyrin Linear Arrays", *J. Phys. Chem. A*, **2002**, *106*, 2359-2368.

11. Miyahara, T.; Nakatsuji, H.; Hasegawa, J.; Osuka, A.; Aratani, N.; Tsuda, A. "Ground and Excited States of Linked and Fused Zinc Porphyrin Dimers: Symmetry Adapted Cluster (SAC)-Configuration Interaction (CI) Study", *J. Chem. Phys.* **2003** *117*, 11196-11207.
12. Cho, H. S.; Rhee, H.; Song, J. K.; Min, C.-K.; Takase, M.; Aratani, N.; Cho, S.; Osuka, A.; Joo, T.; Kim, D. "Excitation Energy Transport Processes of Porphyrin Monomer, Dimer, Cyclic Trimer, and Hexamer Probed by Ultrafast Fluorescence Anisotropy Decay", *J. Am. Chm. Soc.* **2003**, *125*, 5849-5860.
13. Kamo, M.; Tsuda, A.; Nakamura, Y.; Aratani, N.; Furukawa, K.; Kato, T.; Osuka, A. "Metal-Dependent Regioselective Oxidative Coupling of 5,10,15-Triarylporphyrins with DDQ-$Sc(OTf)_3$ and Formation of an Oxo-quinoidal Porphyrin", *Org. Lett.* **2003**, *5*, 2079-2082.
14. Yamazaki, I.; Aratani, N.; Akimoto, S.; Yamazaki, T.; Osuka, A. "Observation of Quantum Coherence for Recurrence Motion of Exciton in Anthracene Dimers in Solution", *J. Am. Chem. Soc.* **2003**, *125*, 7192-7193.
15. Aratani, N.; Cho, H. S.; Ahn, T. K.; Cho, S.; Kim, D.; Sumi, H.; Osuka, A. "Efficient Excitation Energy Transfer in Long *meso-meso* Linked Zn(II) Porphyrin Arrays Bearing a 5,15-Bisphenylethynylated Zn(II) Porphyrin Acceptor", *J. Am. Chem. Soc.* **2003**, *125*, 9668-9681.
16. Yoon, D. H.; Lee, S. B.; Yoo, K.-Y.; Kim, J.; Lim, J. K.; Aratani, N.; Tsuda, A.; Osuka, A.; Kim, D. "Electrical Conduction through Linear Porphyrin Arrays", *J. Am. Chem. Soc.* **2003**, *125*, 11062-11064.
17. Nakamura, Y.; Aratani, N.; Tsuda, A.; Osuka, A.; Furukawa, K.; Kato, T. "Oxidative Direct Coupling of Metalloporphyrins", *J. Porphyrins Phthalocyanines*, **2003**, *7*, 264-269.
18. Takagi, A.; Yanagawa, Y.; Tsuda, A; Aratani, N.; Matsumoto, T.; Osuka, A.; Kawai, T. "STM Images of Individual Porphyrin Hexamers; *meso-meso* Singly Linked Orthogonal Hexamer and *meso-meso*, *β-β*, *β-β* Triply-Linked Planar Hexamer on Cu(100) Surface", *Chem. Commun.* **2003**, 2986-2987.
19. Ha, J.-H.; Cho, H. S.; Song, J. K.; Kim. D.; Aratani, N.; Osuka, A. "Excitonic Coupling Strength and Coherence Length in the Singlet and Triplet Excited States of *meso-meso* Directly Linked Zn(II)porphyrin Arrays", *ChemPhysChem*, **2004**, *5*, 57-67.
20. Tanaka, Y.; Hoshino, W.; Shimizu, S.; Youfu, K.; Aratani, N.; Maruyama, N.; Fujita,

S.; Osuka, A. "Thermal Splitting of Bis-Cu(II) Octaphyrin(1.1.1.1.1.1.1.1) into Two Cu(II) Porphyrins", *J. Am. Chem. Soc.* **2004**, *126*, 3046-3047.

21. Peng, X.; Aratani, N.; Takagi, A.; Matsumoto, T.; Kawai, T.; Hwang, I.-W.; Ahn, T. K.; Kim, D.; Osuka, A. "A Dodecameric Porphyrin Wheel", *J. Am. Chem. Soc.* **2004**, *126*, 4468-4469.
22. Peng, X.; Nakamura, Y.; Aratani, N.; Kim, D.; Osuka, A. "1,4-Phenylene-bridged *meso-meso* Linked Diporphyrin Array", *Tetrahedron Lett.* **2004**, *45*, 4981-4984.
23. Nakamura, Y.; Hwang, I.-W.; Aratani, N.; Ahn, T. K.; Ko, D. M.; Takagi, A.; Kawai, T.; Matsumoto, T.; Kim, D.; Osuka, A. "Directly *meso-meso* Linked Porphyrin Rings: Synthesis, Characterization, and Efficient Excitation Energy Hopping", *J. Am. Chem. Soc.* **2005**, 127, 237-246.

Accounts and Reviews

1. Aratani, N.; Osuka, A. "Monodisperse Giant Porphyrin Arrays", *Macromole. Rapid Commun.* **2001**, *22*, 725-740.
2. Aratani, N.; Osuka, A. "A New Strategy for Construction of Covalently Linked Giant Porphyrin Arrays with One, Two, and Three Dimensionally Arranged Architectures", *Bull. Chem. Soc. Jpn.* **2001**, *74*, 1361-1379.
3. Aratani, N.; Tsuda, A.; Osuka, A. "Discrete Giant Porphyrin Arrays: Challenges to Molecular Size, Length and the Extent of Electronic π-Conjugation", *Synlett*, **2001**, 1663-1674.
4. Aratani, N.; Osuka, A.; Cho, H. S.; Kim, D. "Photochemistry of Covalently-Linked Multi-Porphyrinic Systems", *J. Photochem. Photobiol. C: Photochem. Rev.* **2002**, *3*, 25-52.
5. Aratani, N.; Osuka, A. "'超' 分子エレクトロニクス", *高分子*、**2003**, *52*, 570.
6. Aratani, N.; Osuka, A. "Directly Linked Porphyrin Arrays", *Chem. Record*, **2003**, *3*, 225-234.
7. Aratani, N.; Osuka, A. "メゾ-メゾ結合ポルフィリン多量体および縮環ポルフィリン多量体の光物性", *光化学協会誌*、**2004**, *35*, 94-101.
8. Yamazaki, I.; Akimoto, S.; Aratani, N.; Osuka, A. "Observation of Coherent Recurrence Motion of Excitons in Anthracene Dimers", *Bull. Chem. Soc. Jpn*, **2004**, *77*, 1959-1971.

Chapter in Book

1. Tsuda, A.; Yoshida, N.; Nakano, A.; Aratani, N.; Osuka, A. "Directly Linked and Fused Oligoporphyrin Arrays", in *Advanced Macromolecular and Supramolecular Materials and Processes*, Kurt E. Geckeler Ed. Kluwer Academic Publishers: New York, 2003, 115-123.
2. Aratani, N.; Osuka, A. "ポルフィリン超分子の分子設計・合成戦略", 超分子科学, 中嶋直敏　編著、V 部 24 章 243-252.

Acknowledgement

The author wishes to express his gratitude to Professor Atsuhiro Osuka at Graduate School of Science, Kyoto University, for his invaluable guidance and encouragement throughout this study.

The author is deeply grateful to Professor Hiroyuki Furuta at Graduate School of Engineering, Kyushu University, Professor Hiroshi Shinokubo at Graduate School of Science, Kyoto University, and Dr. Hideyuki Shinmori, Yamanashi University, for their helpful discussions and suggestions during the course of this work.

The author also wishes to thank Professor Dongho Kim and his group members at Yonsei University, for measurements of various spectroscopies and their invaluable discussions.

The author greatfully acknowledges to Professor Takuya Matsumoto, Professor Tomoji Kawai, Dr. Akihiko Takagi, and Mr. Yoshiki Yanagawa at the Institute of Scientific and Industrial Research, Osaka University, for STM measurements.

The author desires to express his sincere thanks to Professor Iwao Yamazaki at Graduate School of Engineering, Hokkaido University, and Professor Hitoshi Sumi, for their insightful suggestion.

The author is deeply grateful to Dr. Tomoya Ishizuka and Dr. Hiromitsu Maeda, for their continuous encouragement.

The author thanks all the members of organic chemistry of molecular assembly laboratory.

Finally, the author wishes to thank his parents for their patience and heartful encouragement.